

JSCSEN 87(4)401–543(2022)

ISSN 1820-7421(Online)

Journal of the Serbian Chemical Society

e
l
e
c
t
r
o
n
i
c

VOLUME 87

No 4

BELGRADE 2022



Available on line at



www.shd.org.rs/JSCS/

The full search of JSCS
is available through

DOAJ DIRECTORY OF
OPEN ACCESS
JOURNALS
www.doaj.org

The **Journal of the Serbian Chemical Society** (formerly Glasnik Hemijskog društva Beograd), one volume (12 issues) per year, publishes articles from the fields of chemistry. The **Journal** is financially supported by the **Ministry of Education, Science and Technological Development of the Republic of Serbia**.

Articles published in the **Journal** are indexed in **Clarivate Analytics products: Science Citation Index-Expanded™** – accessed via **Web of Science®** and **Journal Citation Reports®**.

Impact Factor announced 2021: **1.240; 5-year Impact Factor: 1.144.**

Articles appearing in the **Journal** are also abstracted by: **Scopus, Chemical Abstracts Plus (CAplus™), Directory of Open Access Journals, Referativni Zhurnal (VINITI), RSC Analytical Abstracts, EuroPub, Pro Quest and Asian Digital Library.**

Publisher:

Serbian Chemical Society, Karnegijeva 4/III, P. O. Box 36, 1120 Belgrade 35, Serbia
tel./fax: +381-11-3370-467, E-mails: **Society** – shd@shd.org.rs; **Journal** – jscs@shd.org.rs
Home Pages: **Society** – <http://www.shd.org.rs/>; **Journal** – <http://www.shd.org.rs/JSCS/>
Contents, Abstracts and full papers (from Vol 64, No. 1, 1999) are available in the electronic form at the Web Site of the **Journal** (<http://www.shd.org.rs/JSCS/>).

Internet Service:

Former Editors:

Nikola A. Pušin (1930–1947), **Aleksandar M. Leko** (1948–1954),
Panta S. Tutundžić (1955–1961), **Miloš K. Mladenović** (1962–1964),
Dorđe M. Dimitrijević (1965–1969), **Aleksandar R. Despić** (1969–1975),
Slobodan V. Ribnikar (1975–1985), **Dragutin M. Dražić** (1986–2006).

Editor-in-Chief:

BRANISLAV Ž. NIKOLIĆ, Serbian Chemical Society (E-mail: jscs-ed@shd.org.rs)

Deputy Editor:

DUŠAN SLADIĆ, Faculty of Chemistry, University of Belgrade

Sub editors:

Organic Chemistry

DEJAN OPSENICA, Institute of Chemistry, Technology and Metallurgy, University of Belgrade

Biochemistry and Biotechnology

JÁNOS CSANÁDI, Faculty of Science, University of Novi Sad

Inorganic Chemistry

OLGICA NEDIĆ, INEP – Institute for the Application of Nuclear Energy, University of Belgrade

Theoretical Chemistry

MILOŠ ĐURAN, Serbian Chemical Society

Physical Chemistry

IVAN JURANIĆ, Serbian Chemical Society

Electrochemistry

LJILJANA DAMJANOVIĆ-VASILIĆ, Faculty of Physical Chemistry, University of Belgrade

Analytical Chemistry

SNEŽANA GOJKOVIĆ, Faculty of Technology and Metallurgy, University of Belgrade

Polymers

SLAVICA RAŽIĆ, Faculty of Pharmacy, University of Belgrade

Thermodynamics

BRANKO DUNJIĆ, Faculty of Technology and Metallurgy, University of Belgrade

Chemical Engineering

MIRJANA KIJEVČANIN, Faculty of Technology and Metallurgy, University of Belgrade

Materials

TATJANA KALUDEROVIĆ RADOIČIĆ, Faculty of Technology and Metallurgy, University of Belgrade

Metallic Materials and Metallurgy

RADA PETROVIĆ, Faculty of Technology and Metallurgy, University of Belgrade

Environmental and Geochemistry

ANA KOSTOV, Mining and Metallurgy Institute Bor, University of Belgrade

History of and Education in Chemistry

VESNA ANTIĆ, Faculty of Agriculture, University of Belgrade

English Language Editors:

DRAGICA TRIVIĆ, Faculty of Chemistry, University of Belgrade

Technical Editors:

LYNNE KATSIKAS, Serbian Chemical Society

Journal Manager & Web Master:

VLATKA VAJS, Serbian Chemical Society

Office:

JASMINA NIKOLIĆ, Faculty of Technology and Metallurgy, University of Belgrade

VLADIMIR PANIĆ, ALEKSANDAR DEKANSKI, VUK FILIPOVIĆ, Institute of Chemistry, Technology and Metallurgy, University of Belgrade

ALEKSANDAR DEKANSKI, Institute of Chemistry, Technology and Metallurgy,

University of Belgrade

VERA ĆUŠIĆ, Serbian Chemical Society

Editorial Board

From abroad: **R. Adžić**, Brookhaven National Laboratory (USA); **A. Casini**, University of Groningen (The Netherlands); **G. Cobb**, Baylor University (USA); **D. Douglas**, University of British Columbia (Canada); **G. Inzelt**, Etvos Lorand University (Hungary); **N. Katsaros**, NCSR “Demokritos”, Institute of Physical Chemistry (Greece); **J. Kenny**, University of Perugia (Italy); **Ya. I. Korenman**, Voronezh Academy of Technology (Russian Federation); **M. D. Lechner**, University of Osnabrueck (Germany); **S. Macura**, Mayo Clinic (USA); **M. Spiteller**, INFU, Technical University Dortmund (Germany); **M. Stratakis**, University of Crete (Greece); **M. Swart**, University de Girona (Cataluna, Spain); **G. Vunjak-Novaković**, Columbia University (USA); **P. Worsfold**, University of Plymouth (UK); **J. Zagal**, Universidad de Santiago de Chile (Chile).

From Serbia: **B. Abramović**, **V. Antić**, **V. Beškoski**, **J. Csanadi**, **Lj. Damjanović-Vasić**, **A. Dekanski**, **V. Dondur**, **B. Dunjić**, **M. Duran**, **S. Gojković**, **I. Gutman**, **B. Jovančević**, **I. Juranić**, **T. Kaluderović**, **Radiočić**, **L. Katsikas**, **M. Kijevčanin**, **A. Kostov**, **V. Leovac**, **S. Milonjić**, **V.B. Mišković-Stanković**, **O. Nedić**, **B. Nikolić**, **J. Nikolić**, **D. Opsićica**, **V. Panić**, **M. Petkovska**, **R. Petrović**, **I. Popović**, **B. Radak**, **S. Ražić**, **D. Sladić**, **S. Sovilj**, **S. Šerbanović**, **B. Solaja**, **Z. Tešić**, **D. Trivić**, **V. Vajs**.

Subscription: The annual subscription rate is **150.00 €** including postage (surface mail) and handling. For Society members from abroad rate is **50.00 €**. For the proforma invoice with the instruction for bank payment contact the Society Office (E-mail: shd@shd.org.rs) or see JSCS Web Site: <http://www.shd.org.rs/JSCS/>, option Subscription.

Godišnja pretplata: Za članove SHD: **2.500,00 RSD**, za penzionere i studente: **1000,00 RSD**, a za ostale: **3.500,00 RSD**; za organizacije i ustanove: **16.000,00 RSD**. Uplate se vrše na tekući račun Društva: **205-13815-62**, poziv na broj **320**, sa naznakom “pretplata za JSCS”.

Nota: Radovi čiji su svi autori članovi SHD prioritetno se publikuju.

Odlukom Odbora za hemiju Republičkog fonda za nauku Srbije, br. 66788/1 od 22.11.1990. godine, koja je kasnije potvrđena odlukom Saveta Fonda, časopis je uvršten u kategoriju međunarodnih časopisa (M-23). Takođe, aktom Ministarstva za nauku i tehnologiju Republike Srbije, 413-00-247/2000-01 od 15.06.2000. godine, ovaj časopis je proglašen za publikaciju od posebnog interesa za nauku. **Impact Factor** časopisa objavljen 2021. godine iznosi **1,240**, a petogodišnji **Impact Factor 1,144**.



Journal of the Serbian Chemical Society

JSCS-info@shd.org.rs • www.shd.org.rs/JSCS

J. Serb. Chem. Soc. Vol. 87, No. 4 (2022)

CONTENTS*

<i>T. Dodevska, D. Hadzhiev, I. Shterev and Y. Lazarova:</i> Application of biosynthesized metal nanoparticles in electrochemical sensors (Review).....	401
Biochemistry and Biotechnology	
<i>J. Jović, J. Hao and Lj. Mojović:</i> Examination and optimization of lignocellulolytic activity of <i>Stereum gausapatum</i> F28 on beechwood sawdust supplemented with molasses stillage.....	437
Inorganic Chemistry	
<i>B. Dražić, M. Antonijević-Nikolić, M. Marinović-Cincović, V. Živković-Radovanović, B. Borović and S. B. Tanasković:</i> New copper(II) cyclam complexes with amino-carboxylate co-ligands: Synthesis, characterization, and <i>in vitro</i> antiproliferative and antibacterial studies	451
Theoretical Chemistry	
<i>S. D. Stojanović and M. V. Zlatović:</i> Investigations on the role of cation–π interactions in active centres of superoxide dismutase	465
Physical Chemistry	
<i>D. S. Belić, M. M. Vojnović, M. M. Ristić, X. Urbain and P. Defrance:</i> Rate coefficients for electron-impact dissociation of O ₃ ⁺ to singly charged fragments	479
Materials	
<i>M. Pavlović, J. Nikolić, Lj. Andrić, D. Todorović, K. Božić and S. Drmanić:</i> Synthesis of the new lost foam refractory coatings based on talc.....	491
Chemical Engineering	
<i>S. Li, G. Chen, C. Fan and J. Luo:</i> Microextraction of lanthanum using a rotating micro-channel extractor.....	505
Geochemistry	
<i>S. Pržulj, A. Radović, M. Kašanin-Grubin, D. Pešević, S. Stojadinović, B. Jovančićević and G. Veselinović:</i> Distribution and provenance of heavy metals in sediments of the Vrbas River, Bosnia and Herzegovina	519
Hystory of and Education in Chemistry	
<i>L. R. Ralevic, B. I. Tomasevic and D. D. Trivic:</i> Internet pages for asynchronous online and face-to-face learning about solutions and dissolution.....	531

Published by the Serbian Chemical Society
Karnegijeva 4/III, P.O. Box 36, 11120 Belgrade, Serbia
Printed by the Faculty of Technology and Metallurgy
Karnegijeva 4, P.O. Box 35-03, 11120 Belgrade, Serbia

* For colored figures in this issue please see electronic version at the Journal Home Page:
<http://www.shd.org.rs/JSCS/>



REVIEW

Application of biosynthesized metal nanoparticles in electrochemical sensors

TOTKA DODEVSKA*, DOBRIN HADZHEV, IVAN SHTEREV
and YANNA LAZAROVA

*Department of Organic Chemistry and Inorganic Chemistry, University of Food Technology,
26 Maritsa Boulevard, Plovdiv 4002, Bulgaria*

(Received 21 May, revised 17 August, accepted 1 October 2021)

Abstract: Recently, the development of eco-friendly, cost-effective and reliable methods for synthesis of metal nanoparticles has drawn a considerable attention. The so-called green synthesis, using mild reaction conditions and natural resources as plant extracts and microorganisms, has established as a convenient, sustainable, cheap and environmentally safe approach for synthesis of a wide range of nanomaterials. Over the past decade, biosynthesis is regarded as an important tool for reducing the harmful effects of traditional nanoparticle synthesis methods commonly used in laboratories and industry. This review emphasizes the significance of biosynthesized metal nanoparticles in the field of electrochemical sensing. There is increasing evidence that green synthesis of nanoparticles provides a new direction in designing of cost-effective, highly sensitive and selective electrode-catalysts applicable in food, clinical and environmental analysis. The article is based on 157 references and provided a detailed overview on the main approaches for green synthesis of metal nanoparticles and their applications in designing of electrochemical sensor devices. Important operational characteristics including sensitivity, dynamic range, limit of detection, as well as data on stability and reproducibility of sensors have also been covered.

Keywords: biosynthesis; green synthesis; nanomaterials; nanotechnology; modified electrodes; review.

CONTENTS

1. INTRODUCTION
2. GREEN SYNTHESIS OF METAL/METAL OXIDE NANOPARTICLES USING PLANTS
3. GREEN SYNTHESIS OF METAL/METAL OXIDE NANOPARTICLES USING MICROORGANISMS

*Corresponding author. E-mail: dodevska@mail.bg
<https://doi.org/10.2298/JSC200521077D>

4. ELECTROCHEMICAL SENSORS BASED ON BIOSYNTHESIZED METAL/METAL OXIDE NANOPARTICLES

- 4.1. *Electrochemical sensors based on biosynthesized AgNPs*
- 4.2. *Electrochemical sensors based on biosynthesized AuNPs*
- 4.3. *Electrochemical sensors based on other biosynthesized metal and metal oxide nanoparticles*

5. CONCLUSIONS AND FUTURE PERSPECTIVES

1. INTRODUCTION

Nowadays green nanotechnology has remained at the forefront of scientific research due to its outstanding approaches and applications. Green nanotechnology involves the application of green chemistry principles to the design of valuable and sustainable nanosized materials in a more environmentally benign approach.¹

The unique properties of nanomaterials such as catalytic potential,² optoelectrical properties,³ magnetic behavior⁴ and biological activity⁵ are the main factors determining their extremely wide applications in various fields of science, technology and industry. Nanosized materials are widely used as catalysts⁶ and nanoelectronic components,⁷ in the composition of antibiotics, antiseptics and disinfectants,⁸ in drug delivery,⁹ food and material packaging,¹⁰ targeted delivery of pharmaceuticals,¹¹ development of biosensors,¹² etc.

The main challenge in the development of catalytically active nano-sized materials is to prepare nanoparticles that are highly active, selective, stable, robust, and inexpensive. Classical synthesis of metal nanoparticles (MNPs) most commonly involves chemical reduction of metal ions from solutions of their salts in the presence of organic or inorganic reducing agent such as ethylene glycol, dimethylformamide and sodium borohydride (NaBH₄), followed by addition of a stabilizing agent.¹³ The reagents used are usually expensive and toxic substances which could generate hazardous by-products harmful to health and environment.¹⁴ Therefore, there is a growing concern to develop new, alternative and sustainable methods for MNPs preparation. Research on the possibilities of using biological systems (plants, bacteria, fungi, algae) to obtain stable MNPs and metal oxide NPs has been particularly intense in recent years. The so-called green synthesis has received more attention as a cost effective and valuable alternative for environmentally safe and energy-efficient production of nanoparticles with desired properties.^{2,15–19} Unlike chemical and physical processes, bio-inspired synthetic methods restrict the use of sophisticated instruments, toxic chemicals and energy (high temperature, pressure, irradiation). Green synthesis of MNPs involves the use of plant extracts or microorganisms for the bioreduction of metal ions into their zero-valent elemental form. Biomolecules such as proteins, sugars, flavonoids, alkaloids, polyphenols, etc. (Fig. 1) act as reducing and capping agents. Regarding the process of metal oxide NPs synthesis in a

green way, researchers suggest that specific biomolecules react with the metal ions to reduce or to form complexes. The resulting product is subjected to thermal treatment to get final metal oxide NPs. Therefore, different mechanisms of metal oxide NPs formation were proposed considering the ability of the active compounds in reducing and chelating the metal ions.

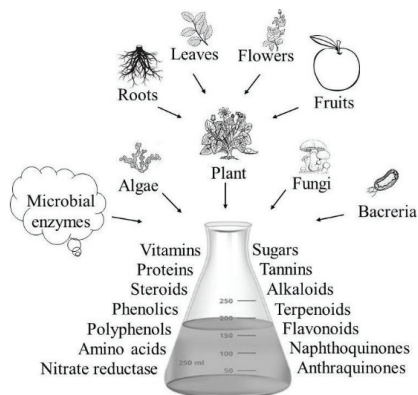


Fig. 1. Schematic illustration of the natural sources used to synthesize NPs in a green way.

Biological systems differ in their capabilities to supply MNPs, hence the production process highly varies depending on the choice of green material. The plant extracts are considered to be more suitable compared to microorganisms for green synthesis of MNPs. Plant extract mediated synthesis of MNPs is preferable due to its economic and ecological effectiveness – easily available plant material, aqueous solvents and normal conditions are used for the synthesis of nanoparticles in a simple one-step procedure. Extensive research shows that the plant-assisted synthesis is relatively fast and suitable for large-scale production of stable MNPs. At the same time, delicate, complicated and meticulous preparation steps are required for microbial synthesis of MNPs. Organisms such as bacteria and fungi need to be cultured or propagated in order to obtain sufficient starting materials. Thus, synthesis protocols include prior procedures such as microorganism isolation and identification, growth optimization and culture preparation. Other challenges are the slow reduction process (ranging from hour to days) and poor understanding of the mechanisms controlling the shape and dispersity of microbial synthesized MNPs. In addition, development of new green synthesis methods based on the use of waste products from agriculture and food-processing is one of the current research areas that has attracted a great deal of attention over the past years.² These waste derived MNPs have found a variety of applications in biotechnology, however, data on their applications in sensor technologies are still limited.

Current review features recent trends in electrode catalysts based on metal and metal oxide NPs synthesized by using plant extracts and microorganisms.

Even though research on the applications of biosynthesized nanoparticles in electrochemical sensors is actually at a really early stage, there are already promising opportunities for development of novel sensing platforms. Most relevant biosynthesis approaches, successful integration strategies, selected sensing applications and future prospects of these biosynthesized nanomaterials for the design of advanced sensor platforms are also highlighted.

2. GREEN SYNTHESIS OF METAL/METAL OXIDE NANOPARTICLES USING PLANTS

Due to the abundance of biomass and the diversity of species, plants are most suitable for large-scale biosynthesis and they are preferred for green synthesis of MNPs.^{20–22} Plant leaf extracts are the most common choice for bio-inspired synthesis of MNPs but the use of seeds, bark, fruits, tubers and root extracts has also been reported.^{20,23,24} It was established that experimental conditions such as temperature,^{25–27} pH,^{27,28} concentration and quantity of extract^{27,29,30} and/or metal ions,^{26,27} and contact time²⁷ affect the efficiency and rate of the process of metal reduction and nanoparticles with desired shape and size could be produced. Researchers suggested that various compounds such as amino acids, citric acid, heterocyclic compounds, flavonoids, polyphenols, terpenoides, enzymes, peptides, polysaccharides, saponins, tannins were responsible for reduction of metal ions and subsequent stabilization of the produced nanoparticles.^{4, 32–41}

Green synthesis of MNPs based on the reduction of precious and non-precious transition metals including silver, gold, palladium, platinum and copper using plant extracts has been investigated by some authors.^{20,21,25} Silver nanoparticles (AgNPs) and gold nanoparticles (AuNPs) are the most common ones used for chemical, electrochemical, biomedical and environmental applications.⁴²

Owing to their high surface-to-volume ratio and unique physicochemical properties, AgNPs possess various important characteristics: high catalytic activity, electrical and thermal conductivity, as well as broad-spectrum bioactivities.^{43,44} In medicine AgNPs have received tremendous attention for their excellent antimicrobial, antibacterial and anticancer potential. Antimicrobial properties of AgNPs caused the use of these nanomaterials in cosmetics, military, packaging, *etc.*

A large number of research groups have been reported completely green, feasible, renewable and inexpensive approaches for synthesis of stable AgNPs. A new, simplified and rapid methodologies for green synthesis of AgNPs using *Azadirachta indica*,⁴⁵ *Crotalaria retusa*⁴⁶ and *Terminalia arjuna*⁴⁷ plant extracts as reducing and stabilizing agents have been proposed. Experimental data show that the so-synthesized nanoparticles exhibit high catalytic activity as well as excellent antimicrobial properties against Gram-negative and Gram-positive bacteria. The extract of some grape by-products such as stalks, leaves, stems, seeds and dried fruits have been successfully used for synthesis of AgNPs,⁴⁸ bimetallic

Fe/Pd⁴⁹ and Fe₃O₄/Ag⁵⁰ nanoparticles. Recent studies on the chemical composition of grapes have revealed that the main components are polar compounds soluble in hot water with a high content of tannins and polyphenolic compounds.⁵¹ This suggests that the grape extract will also contain polyphenolic compounds that could act as reducing and stabilizing agents in the formation of nanoparticles.

AuNPs have drawn the attention of researchers because of their extensive applications in areas such as electronics, catalysis, sensing/biosensing, medicine, controlled drug delivery, etc. Intensive studies have revealed that AuNPs possess potential to serve as building blocks for plasmonic devices, as well as being used as catalysts and antimicrobials against a wide range of microorganisms.^{31,52} To date, a number of methods for synthesis of AuNPs including physical, electrochemical, photochemical and liquid chemical reduction have been developed. Krishnaswamy *et al.* have reported a single step green synthesis of AuNPs using agricultural wastes materials such as grape seed, skin and stalk.⁵³ Various methodologies for biosynthesis of AuNPs from plant extracts also have been reported – *Ginkgo biloba*,⁵⁴ sunflower (*Helianthus annuus*), *Chilopsis linearis*, *Medicago sativa*, *Brassica juncea*,⁵⁵ leaves of *Sphaeranthus indicus* and various parts from plants (bark, stem, root, etc.)⁵⁶ have been used to synthesize AuNPs.

Palladium nanoparticles (PdNPs) have broad application in heterogeneous catalysis due to their excellent catalytic/electrocatalytic ability, high surface-to-volume ratio and high surface energy. Recently, it has been reported that PdNPs could be synthesized by using extracts of *Filicium decipiens*⁵⁷ and *Hippophae rhamnoides Linn.*⁵⁸

Research teams have reported production of nanoparticles of metal oxides (CuO and ZnO) using *Centella asiatica*⁵⁹ and aloe leaf,⁶⁰ respectively. Reddy has reported on a new green method for the synthesis of CuO nanoparticles (CuONPs) using *Calotropis procera*.⁶¹ CuONPs are widely used as catalysts due to their excellent photocatalytic properties.⁶² Ghidan *et al.*⁶³ also have described successful biosynthesis of CuONPs using *Punica granatum* bark extract, and Ijaz *et al.*⁶⁴ propose a method for synthesis of CuONPs from fresh leaves of *Abutilon indicum*.

Zinc oxide nanoparticles (ZnONPs) have aroused great interest due to their low cost, attractive properties and important role as semiconductor materials, in development of catalysts, ceramic resistors, gas sensors and energy-saving materials.⁶⁵ Due to their antimicrobial and antibacterial potential ZnONPs are widely used in medicine.^{66,67} Matinise *et al.* have reported an eco-friendly method for the synthesis of ZnONPs using Moringa *Oleifera* extract.⁶⁸ Mechanisms of formation of the ZnONPs via the chemical reaction of the zinc nitrate precursor with the bioactive compounds of the Moringa *Oleifera* are proposed. The electrochemical analysis proved that ZnONPs have high electrochemical activity

without any modifications and therefore are considered as a potential candidate in electrochemical applications. Nava *et al.* also have used zinc nitrate as a source of the zinc ions and different peels extracts, from *Lycopersicon esculentum* (tomato), *Citrus sinensis* (orange), *Citrus paradisi* (grapefruit) and *Citrus aurantiifolia* (lemon), for the green synthesis of ZnONPs.⁶⁹ The proposed formation mechanism is based on the chemical characteristics of the flavonoids, limonoids and carotenoids that present in the peel extracts. These biomolecules are believed to chelate Zn²⁺ and form metal coordinated complexes that are further thermally treated to form ZnONPs. Authors have analyzed the effect of the extract used on the surface morphology of the resulting ZnONPs, and tested the efficiency of ZnONPs in the photocatalytic degradation of methylene blue under UV irradiation. The presented results highlight that the chemical composition of the extract has a significant effect on the size and shape distribution of nanoparticles, which further is directly associated with their catalytic activity.

3. GREEN SYNTHESIS OF METAL/METAL OXIDE NANOPARTICLES USING MICROORGANISMS

A variety of microorganisms are utilized in nanoparticle synthesis. Prokaryotic bacteria, actinomycetes, yeasts, fungi and algae have been broadly employed for biosynthesis of metal/metal oxide nanoparticles. Bacterial synthesis of MNPs is accepted due to the relative ease of manipulation of bacteria.⁴¹ Some examples of bacterial strains that have been widely used for synthesis of bioreduced AgNPs with different morphology are: *Escherichia coli*, *Lactobacillus casei*, *Bacillus cereus*, *Aeromonas* sp. SH10 *Phaeocystis antarctica*, *Pseudomonas proteolytica*, *Bacillus amyloliquefaciens*, *Bacillus indus*, *Bacillus cecembensis*, *Enterobacter cloacae*, *Geobacter spp.*, *Arthrobacter gangotriensis*, *Corynebacterium Sp. SH09* and *Shewanella oneidensis*.⁷⁰ From bacterial strains such as *Candida guilliermondii*,⁷¹ *Pseudomonas denitrificans*,⁷² *Pseudomonas fluorescens* 417,⁷³ *Staphylococcus epidermidis*⁷⁴ and *Bacillus stearothermophilus*⁷⁵ spherical AuNPs with a diameter between 5 and 80 nm have been successfully synthesized.⁷⁶ AgNPs and AuNPs of various shapes (spherical and triangular) have also been synthesized using algal strains such as *Pithophora oedogonia*,⁷⁷ *Ecklonia cava*,⁷⁸ *Chondrus crispus* and *Spyrogyra insignis*⁷⁹ and *Sargassum wightii* Greville.⁸⁰

Fungi-mediated biosynthesis of metal/metal oxide nanoparticles is also a very efficient process for the production of monodispersed nanoparticles with well-defined morphologies.⁷⁰ Fungi act as good biological agents for the synthesis of nanoparticles of metals and metal oxides due to the presence of a variety of intracellular enzymes.⁸¹ Compared to bacteria, fungi could be a source for a large amount production of nanoparticles.⁸² The probable mechanism for the formation of MNPs is enzymatic reduction in the cell wall or inside the fungal cell. A variety of fungal species are used to synthesize metal/metal oxide nano-

particles such as AgNPs, AuNPs, TiO₂NPs, ZnONPs.⁷⁰ Successful synthesis of nanomaterials via yeast also has been reported by numerous research groups.⁷⁰

4. ELECTROCHEMICAL SENSORS BASED ON BIOSYNTHESIZED METAL/METAL OXIDE NANOPARTICLES

Research on electrochemical sensors attracts lots of current interest because of their promising applications in food industry, ecology, medicine, pharmacy, etc. Electrochemical sensor systems offer advantages of a cost-effective, rapid, highly sensitive, selective, compact and convenient to handling method for quantitative detection of the target analyte. These devices provide the opportunity for an accurate and susceptible automation analysis, and are a promising alternative of the conventional analytical techniques where time-consuming procedures for sample pre-treatment and expensive instruments are required. Variety of electroanalytical techniques including cyclic voltammetry (CV), constant potential amperometry (Amp.), differential pulse voltammetry (DPV), square wave voltammetry (SWV), linear sweep voltammetry (LSV) and stripping voltammetry are available and applicable for electroanalysis. Advantages of these techniques over classical detection methods such as spectroscopy and chromatography are their accuracy, reliability, ease of use and low cost.

The general principle of electrochemical detection is illustrated in Fig. 2.

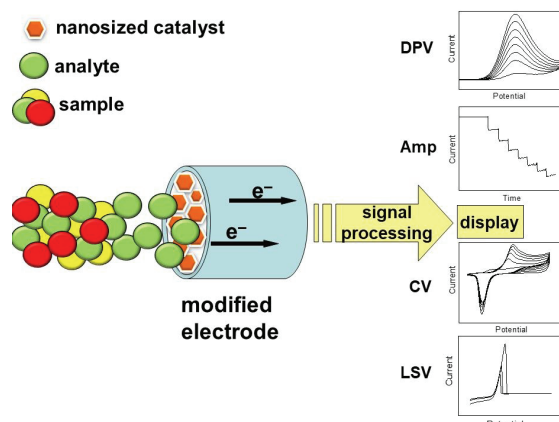


Fig. 2. Illustrative representation of electrochemical detection.

The analyte reacts at the surface of the sensing electrode (modified working electrode) involving either an oxidation or reduction mechanism. This reaction is catalyzed by the electrode material specifically developed for the analyte of interest. The current generated in the process is converted into a signal that could be amplified, processed and displayed easily by modern electrical instruments. By analyzing the magnitude of the electrical signal, we can obtain information about the concentration of the substance being analyzed.

The experimental setup used for electrochemical analysis consists of conventional three-electrode cell including working electrode (WE), reference electrode (RE) and counter electrode (CE), potentiostat and personal computer (Fig. 3). The working electrode is the electrode at which the reaction of interest occurs; as a reference electrode Ag/AgCl or saturated calomel electrode is usually used; an inert conducting material (Pt) is used as a counter electrode. During experiments, charge flow (current) occurs between the working electrode and the counter electrode while the potential of the working electrode is measured with respect to the reference electrode.

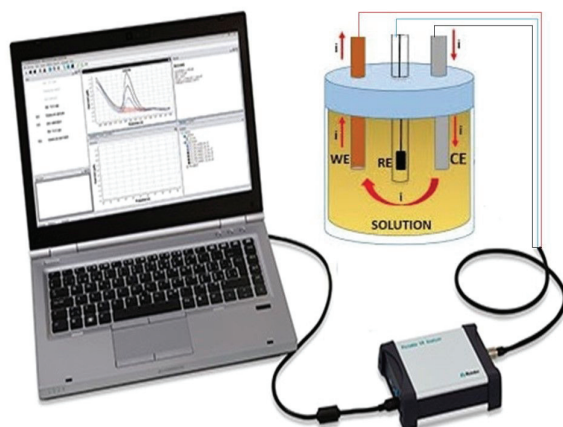


Fig. 3. Experimental setup used for electrochemical analysis.

In electrochemical sensors design, in order to enhance the effective electrode surface and to increase the sensitivity, various nanomaterials such as carbon nanoparticles, metal/metal oxide nanoparticles, nanosized alloys and binary nanocomposites are used for the functionalization of electrode surface as a direct active layer.^{83–85} As a result, modified electrodes have extremely high catalytic efficiency due to the reduced overpotentials and faster electron transfer kinetics.

Therefore, the importance of developing nanostructured highly active and selective electrode-catalysts applicable for quality and safety assessment of foods, for environmental monitoring, pharmaceutical analysis and clinical diagnostics, has received considerable attention nowadays.^{86–91}

Physical, chemical and electrochemical methods including laser ablation, high energy ball milling, reactive sputtering, thermal salt decomposition, sol-gel method, electrodeposition, *etc*, have been developed to obtain nanosized metal or metal oxide particles. Although each one of the methods mentioned above had its merits, there are considerable disadvantages in terms of preparation and cost – multi-step time-consuming methodologies and requirement of sophisticated equipment. In this connection, recently biosynthetic approaches has received

great attention due to their capability to design alternative, environmentally friendly, safer, energy efficient and less toxic routes towards synthesis. The green synthesis of nanosized materials has found a wide range of applications in the field of electrochemical sensors/biosensors, revolutionizing this field.^{92–94}

Fig. 4 shows the basic steps in the preparation of electrode modified with biosynthesized MNPs. In summary: 1) plant extract was mixed with the metal salt solution; 2) bio compounds reduce metal from positive oxidation state to zero oxidation state; 3) the working surface of electrode was modified through a drop-wise of the resulting colloidal solution.

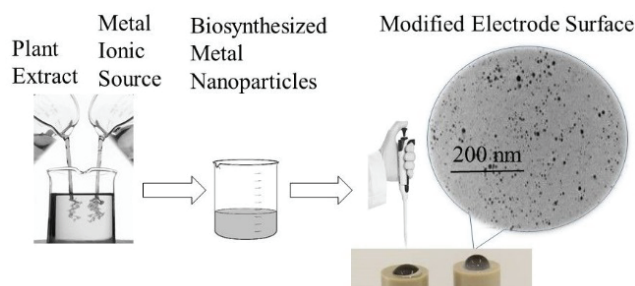


Fig. 4. Scheme of the basic steps in the preparation of electrode modified with biosynthesized MNPs.

In the next part of this review article we have summarized and discussed the recent progress, current challenges and future perspectives in green synthesis of different metal/metal oxide nanoparticles and their applications in the development of new electrode-catalysts for electroanalytical purposes.

The most commonly used metal nanoparticles as electron-transfer mediators are AgNPs and AuNPs due to their chemical stability, unique physicochemical properties, good conductivity and electrocatalytic activity. Relatively simple procedures for synthesis of AgNPs and AuNPs, facile electrode modification with AgNPs and AuNPs as well as their key role in reducing the overpotentials of electrocatalytic reactions make them extremely attractive to research groups.⁹⁵

4.1. Electrochemical sensors based on biosynthesized AgNPs

Nowadays, considerable attention has been paid to the detection of hydrogen peroxide (H_2O_2) owing to its wide applications. H_2O_2 is used in industrial wastewater treatment, as a disinfectant in medicine, as an oxidant and bleaching agent in textile, paper, pharmaceutical and cosmetic industries. Due to its inherent bactericidal properties H_2O_2 is also used as a sterilizing agent in milk and dairy production^{96,97} and in food aseptic packaging.⁹⁸ Reliable and rapid quantification of H_2O_2 is also important in various biological, medical and clinical studies since H_2O_2 is one of the by-products of enzyme-catalyzed reactions occurring in living organisms. H_2O_2 acts as a precursor in the formation of highly reactive and

potentially harmful hydroxyl radicals and it is one of the most important markers of oxidative stress. Excessive accumulation of H₂O₂ in the body causes various diseases such as cardiovascular disorders, Alzheimer's, DNA fragmentation, tissue damage and cancer.

A number of research groups have confirmed remarkable electrocatalytic activity of AgNPs for H₂O₂ reduction and successfully have employed AgNPs-modified electrodes as sensing interface to construct enzyme-free H₂O₂ electrochemical sensors.^{99–104} In the cited articles electrode surface modification with AgNPs has been performed applying chemical or electrochemical methods in order to enhance the rate of electron transfer and to decrease the required high overpotential – the major barrier for effective electrochemical detection of H₂O₂ at ordinary solid electrodes.

Salazar *et al.* have investigated the catalytic activity of electrode modified with biosynthesized AgNPs in the reaction of electroreduction of H₂O₂.¹⁰⁵ They have presented a simple one-step eco-friendly strategy to obtain silver nanoparticle-modified reduced graphene oxide nanocomposites (rGO/AgNPs) using green tea extract for reducing both Ag⁺ and graphene oxide sheets. TEM image and the size distribution for AgNPs confirmed the quasi-spherical shape of the AgNPs with an average size of about 25 nm (a size range distribution from 5 to 60 nm). Glassy carbon (GC) electrode was conveniently modified with rGO/AgNPs nanocomposite and electrochemical tests were carried out to study the electrocatalytic properties of the rGO/AgNPs/GC sensor towards H₂O₂ reduction. Basic analytical parameters such as selectivity, sensitivity, limit of quantification and limit of detection, time of response and stability of modified electrode in 0.1 M PBS under optimized conditions (pH 8.0; applied potential of –0.4 V vs. Ag/AgCl, 3 M) were also studied. It was determined that the electrode has a sensitivity of 236 μA mM⁻¹ cm⁻² ($R^2 = 0.999$) in the concentration range from 0.002 to 20 mM, rapid response (~2 s) and detection limit of 0.73 μM H₂O₂ estimated on the criterion signal-to-noise $S/N = 3$. After 7 months storage it was established that rGO/AgNPs/GC has no significant loss of sensitivity. The selectivity of the modified electrode was tested against different biological interferences including dopamine, glutamate, glucose and ascorbic acid with promising results. In addition, the applicability of this sensor for H₂O₂ detection in real samples was confirmed in antiseptic solutions, commercial milk and urine.

Tagetes erecta (Marigold) flowers extract has been used for production of AgNPs in a green route.¹⁰⁶ Characterization of biosynthesized nanoparticles was done using different methods: ultraviolet-visible spectroscopy (UV–Vis), field emission scanning electron microscopy (FESEM), elemental dispersive X-ray spectroscopy (EDX), Fourier transform infrared spectroscopy (FTIR), X-ray diffraction (XRD) and X-ray photoelectron spectroscopy (XPS). The UV–Vis studies showed the occurrence of an absorption band at 430 nm which is specific

for AgNPs. FESEM analysis indicated that the biosynthesized AgNPs have a homogenous size distribution. The XRD patterns reflected that the particles are crystalline in nature, with a face-centered cubic structure. Using AgNPs and chitosan (CS), modified pencil graphite electrode (PGE) was fabricated by drop-casting method and the as-prepared hybrid material PGE/AgNPs/CS was used for supercapacitor and electrochemical sensing applications. It has been shown that PGE/AgNPs/CS electrode provided remarkable catalytic activity towards electrochemical reduction of H₂O₂. Quantitative analysis of H₂O₂ was performed in supporting electrolyte 0.1 M HCl/KCl (pH 2.0) using cyclic voltammetry (CV) and a linear graph was obtained in the concentration range of 1.0–10.0 μM (limit of detection was found to be 0.52 μM). Furthermore, the sensor was applied to real sample analysis. The results obtained suggested that the proposed electrochemical device can be used for traces analysis of H₂O₂ in cosmetic products.

Since the industrially steam distillation of essential oil crops never leads to complete extraction of the aroma substances, the essential oil industry wastes have a potential for extraction of residual volatile polar metabolites. The waste is rich in non-volatile polar metabolites (flavonoids, organic acids, carbohydrates, amino acids, etc.) and some of these compounds have also reduction properties and could influence the synthesis and stabilization of AgNPs. Dodevska *et al.*¹⁰⁷ have reported for the first time utilization of *Rosa damascena* waste for synthesis of AgNPs and applicability of the nanoparticles for development of electrochemical sensors for H₂O₂ and vanillin detection. The process of AgNPs synthesis takes place in one-stage and it is based on the utilization of abundant and cheap waste materials. The authors stated that the main functional groups involved in the AgNPs formation were aromatic hydroxyl groups and carbonyl groups and substances such as phenolic acids, flavonoids, proteins, terpenes, carbohydrates, etc. having important role in reduction of Ag⁺. Furthermore, proteins, polysaccharides and carboxylic acids additionally participated in the process by capping the *in situ* generated nanoparticles. The data suggested that the ethanolic extracts have higher content of phenolic acids and flavonoids than water extracts. On the other hand, the water extracts were rich in carbohydrates (including reducing sugars), proteins and pectic substances (as suggested by the presence of uronic acids). TEM micrographs showed that using water extract of *Rosa damascena* AgNPs were obtained as sphere-like particles with an average size calculated to be 25.8±11.5 nm. Biosynthesized AgNPs were deposited onto a spectroscopic graphite (Gr) electrode and the electroactive layer was stabilized by applying thin film of chitosan onto the modified electrode surface. Chitosan is commercially available natural polymer and preferable material in designing sensors/biosensors. It is a linear amine-rich polysaccharide, biocompatible polymer distinguished by its ability to form flexible, strength, highly adhesive membranes. In electrochemical sensors chitosan is commonly used to enhance the stability of

nanoparticles. The coverage of chitosan on the biosynthesized AgNPs not only protected the nanoparticles against aggregation, but also stabilized surface properties of AgNPs while enhancing their catalytic activity. The electrochemical performance of the modified electrode AgNPs/CS/Gr was studied by means of CV, DPV and chronoamperometry at pH 7.0 and its applicability for amperometric detection of H₂O₂ and vanillin was investigated. Vanillin (4-hydroxy-3-methoxybenzaldehyde) has a specific aroma, pronounced antioxidant and antimicrobial properties and it is one of the most commonly used food supplements. For adults the permissible daily intake of vanillin is less than 10 mg kg⁻¹ (the addition of vanillin in baby formula and infant food is not permitted). The overweight content of vanillin in food products, as the excessive ingestion via the dietary intake has potential toxic effect – symptoms of a vanillin overdose can include nausea, vomiting and headache; in cases of severe intoxication vanillin can cause irreversible damage to the liver and kidneys. Therefore, the development of novel analytical techniques have been employed for fast and reliable quantitative detection of vanillin. Electrochemical studies suggested that graphite electrode modified with AgNPs, biosynthesized using *Rosa damascena* waste, possesses a stable response to vanillin up to 0.5 mM with a detection limit of 8.4 μM at an applied potential of 0.58 V (vs. Ag/AgCl, 3 M KCl). The developed electrode exhibited a sensitive and reproducible response for quantitative determination of H₂O₂ at applied potentials from -0.2 to -0.3 V. Constant potential amperometry measurements at -0.3 V showed highly sensitive response to H₂O₂ up to 6.6 mM. Electrochemical studies with AgNPs synthesized using flower aqueous extracts of *Achillea millefolium* and *Lavandula angustifolia* wastes as reducing agents, which is a novel simple approach, inexpensive and eco-friendly in nature, also were reported.⁹⁴ The representative electron micrographs of AgNPs showed that the nanoparticles grew very tiny with spherical shape. From the presented histograms it can be seen the size distribution of AgNPs and their mean sizes were 2.8 nm for AgNPs/*Achillea millefolium* and 3.1 nm for AgNPs/*Lavandula angustifolia*, respectively. Selected area electron diffraction (SAED) pattern represents the (111), (220) and (222) crystal planes of the cubic structure of AgNPs in both samples. Biosynthesized AgNPs were deposited onto a spectroscopic graphite surface, applying two different procedures, and stabilized using chitosan to build new electrocatalysts. The electrochemical performance of the modified electrodes was studied by means of CV and chronoamperometry in neutral medium and their applicability for amperometric quantitative determination of H₂O₂ was demonstrated. The modified electrodes showed a remarkable activity at applied potentials of -0.3 and -0.2 V vs. Ag/AgCl, 3 M KCl, rapid, stable and reproducible amperometric response. It was stated that amperometry at constant potential of -0.3 V is distinguished by extremely high sensitivity (533.5 μA mM⁻¹ cm⁻²) up to 4.3 mM H₂O₂. In order to study the selectivity, the amp-

erometric response was examined in the presence of common interfering species such as nitrate, glucose, uric acid, ascorbic acid and citric acid. The authentic record of the electrode signal clearly shows that the tested species had no effect on the H_2O_2 detection – no response was observed in the presence of the above mentioned substances and the current response for H_2O_2 , registered after adding the substances, corresponds to the one determined in the calibration study. These results demonstrate that the modified electrode has good selectivity for H_2O_2 and reveal the application potential of the so-biosynthesized AgNPs for sensing of H_2O_2 in real samples.

Potassium and sodium nitrates (KNO_2 , NaNO_2) are listed as permitted food additives (E249, E250). KNO_2 and NaNO_2 show important bacteriostatic and bacteriocidal activity against several spoilage bacteria and foodborne pathogens in meat products and are widely used as preservatives in the preparation of cured meat products.¹⁰⁸ Nitrite ions not only have a pronounced antimicrobial activity, but also act as a color fixative and inhibits lipid oxidation, thereby slowing meat spoiling. In addition, nitrite ion concentration is one of the most important indicators determining the quality of drinking water – according to the recommendation of the World Health Organization^{109,110} the acceptable NO_2^- content is 0.2 mg L⁻¹; according to European Community regulation^{111,112} the maximum permissible nitrite content of drinking water is 0.1 mg L⁻¹. Consumption of foods with excessive nitrite content poses a serious threat to human health. A number of clinical studies have shown that nitrite intake is associated with higher relative risk of breast cancer, gastric cancer, renal cell carcinoma, adult glioma, colorectal cancer, esophageal cancer and thyroid cancer.¹¹³ Therefore, the importance of improved analytical methods for determination of nitrite in drinking water, cured food and environmental systems has received considerable attention. Nitrite ion is an electroactive and can be quantified electrochemically. In comparison with the conventional analytical techniques, electrochemical analysis has been considered as a fast, low-cost and effective way due to its intrinsic simplicity and high sensitivity.¹¹⁴

A promising electrochemical sensor for accurate, sensitive and selective detection of nitrates is developed by Shivakumar *et al.*¹¹⁵ The authors reported on a facile, cost effective, green synthesis method of silver nanospheres (AgNS) by using pre-hydrolyzed liquor (PHL) from the *Nilgiri* wood generated from pulp industry without any pre-treatment. The synthesis was performed at room temperature within 3 h. The presented XRD pattern of AgNS evidences face centered cubic crystalline structure of metallic silver; the average crystallite size of AgNS calculated from Scherrer equation was found to be ~30 nm. It was suggested that hemicelluloses present in PHL were responsible for the reduction of silver ions and stabilization of AgNS. The GC electrode modified with biosynthesized AgNS has been shown to exhibit excellent electrocatalytic activity in nitrite oxid-

ation – extremely low detection limit ($0.031 \mu\text{M}$) and high electrode sensitivity of $580 \mu\text{A mM}^{-1} \text{cm}^{-2}$ in the concentration range from 0.1 to $8.0 \mu\text{M}$. It is noteworthy that after 30 days storage the presented electrode retains up to 98 % of its initial activity.

Ascorbic acid (AA), known as vitamin C, is a naturally occurring organic compound with antioxidant properties – it is one of the strongest reductants and free radical scavengers in living cells that is suggested to decrease oxidative damage and lowering the risk of certain chronic diseases. The antioxidant activity of AA is the main reason to be frequently used in food industry to prevent unwanted changes in the color and aroma of foods. The use of AA in meat products, with the addition of nitrites, is important for the activity of reduction dependent upon nitrousmetamyoglobin-Fe (III) converted into nitrousmetamyoglobin-Fe (II), which maintains the colour of the product most brilliant.¹¹⁶ Additives based on AA are widely used in the production of food and beverages (jam, candy, fruit juices, fish and meat products, beer, etc.). AA is used as well as in cosmetics as a skin conditioning agent and in pharmaceutical industry as a diet supplement in various forms.¹¹⁴ The wide and effective therapeutic potential of AA in dermatology also has been proven. Vitamin C plays a key role in maintaining skin health, provides protection against UV-induced photodamage, participates in the formation of skin barrier lipids and collagen in the dermis, as well as in the modulation of cell signal pathways of cell growth and differentiation. Numerous clinical studies and *in-vitro* data support the use of topically applied AA for photoprotection, antiaging, anti-inflammatory and skin-lightening uses. A topical AA treatment of the epidermal surface suppressed UVB-induced cell death, apoptosis, DNA damage, reactive oxygen species (ROS) production, and the inflammatory response by downregulating tumour necrosis factor- α (TNF- α) expression and release.¹¹⁷

Under normal physiological conditions, melanin is produced by the epidermal melanocytes in response to UV-irradiation. An excessive production of melanin causes dermatological problems such as freckles, age spot and melasma. These skin pigmentation disorders can be caused by various factors such as an excessive sun exposure, hormonal imbalance during pregnancy or menopause, side effects from certain medications. Emerging evidence has indicated that AA has therapeutic effects on facial hyperpigmentation, as it reduces melanin synthesis. AA suppresses the catalytic activity of tyrosinase, the rate-limiting enzyme in melanin biosynthesis.¹¹⁸ Although the antipigmentary and skin-protective mechanisms of AA still need to be clarified, AA has been used widely as skin-lightening, anti-aging, anti-oxidant and anti-inflammatory agent in commercially available cosmetics (creams, lotions, dental care products, *etc.*).

Due to the important role of AA, recently there is a significant research interest to develop electrochemical sensors for detection of AA content in various

samples including foods, drugs, cosmetics and biological fluids.^{114,119} In this regard crystalline silver face-centered cubic phase, spherical in shape, with mean particle size about 5.3–10.2 nm was synthesized using onion extracts.¹²⁰ The authors of this study believe that high phenolic content of the water extract of onion is responsible for production and stabilization of AgNPs. It was suggested that the formation of AgNPs was related to the reaction temperature, pH, duration, as well as concentrations of silver nitrate solution and onion extract. Modified carbon paste electrode (AgNPs/CPE) was prepared using the AgNPs phyto-synthesized at optimal conditions (5 mM AgNO₃, 17 wt. % onion extract, temperature 35 °C, pH 10 and 18 h reaction time). The effect of synthesized AgNPs on AA electrooxidation was investigated by SWV. Voltammograms show that the peak current at 0.48 V remains linear in the concentration range 0.4 to 450 μM AA; detection limit was calculated to be 0.1 μM AA. The real sample analysis reveals the practical applicability of AgNPs/CPE for AA detection in fruit and vegetable juices.

Electrochemical sensor for dopamine (DA) based on biosynthesized AgNPs was developed by Sreenivasulu *et al.*¹²¹ Dopamine (4-(2-aminoethyl)benzene-1,2-diol) is a neurotransmitter that affects numerous physiological processes and plays an important and diverse role in brain function. Dopamine molecule is biomarker for diseases such as Parkinson's, depression, schizophrenia and some brain tumors. Reliable detection of dopamine is important in research and clinical disease diagnosis and various types of electrochemical sensors have been developed due to its electroactive nature. Sreenivasulu *et al.* have used aqueous root extract of *Mimosa pudica* for facile and stable biosynthesis of AgNPs. The formation of AgNPs were identified using UV–Vis spectrophotometer and thoroughly characterized by using XRD, FTIR, SEM, EDAX and TEM. TEM analysis showed that the synthesized AgNPs have a spherical shape and average sizes from 35.0 to 42.5 nm. Amperometric studies revealed that the AgNPs-assembled-GC electrode possesses high sensitivity, low limit of detection (0.5 μM) and an excellent dynamic range (10–60 μM) for quantitative detection of DA. The authors stated that these results are comparable with those obtained by chemically modified GC electrodes previously reported in the literature.

Nitrobenzene (NB) is widely used as a precursor for aniline, pesticides, herbicides, insecticides, azo dyes, explosives, and drugs. Acute (short-term) and chronic (long-term) inhalation, oral, and dermal exposure of humans to NB result in effects on the blood, central nervous system, liver and kidney. Prolonged exposure may cause headache, nausea, fatigue, dizziness, impaired vision, cyanosis and anemia. Unfortunately, a huge amount of NB was excreted into water, soil and sediments from industries. Therefore, the timely and accurate detection of NB is an important concern in public and environmental protection. Different analytical methods have been used for detection of NB and electrochemical methods are

considered simpler and more sensitive than available chromatographic and spectrophotometric methods.¹²² Shivakumar *et al.* have described eco-friendly synthesis of AgNPs using *Eucalyptus* extract as a reducing and stabilizing agent.¹²³ A GC electrode was modified with the so-synthesized nanoparticles and AgNPs/GC was tested for quantitative detection of NB. Two electrochemical techniques – CV and DPV were used to study the electrochemical behaviour of AgNPs/GC. The modified electrode exhibited good electrocatalytic activity in the reaction of electroreduction of NB – linear current response in the concentration range 5 to 40 µM, sensitivity of 2.262 µA µM⁻¹ cm⁻², detection limit of 0.027 µM and good selectivity. Stability studies were carried out by running the CV of the modified electrode in the presence of 1 mM NB on the day of preparation and every alternate day up to 20 days. The authors stated that the sensor exhibited great storage stability retaining up to 92.8 % of preliminary current at the end of tested period. The practical applicability of developed electrode material to detect selectively NB in tap water and lake water was tested and satisfactory results were obtained.

In order to improve selectivity, sensitivity and detection limit for determination of NB, Karthik *et al.* have modified GC electrode with sphere-like AgNPs biosynthesized using *Camellia japonica* leaves.¹²⁴ The fabricated electrocatalyst AgNPs/GC have been shown to have ability to detect NB with an excellent selectivity, extremely low limit of detection (0.012 µM) and a wide linear range (up to 2.593 mM). The AgNPs/GC showed excellent selectivity towards the NB detection – the results from selectivity test showed that the addition of potentially interfering species (common metal ions, some anions and nitroaromatic containing substances) into the system in 500-fold concentration relative to the analyte does not affect the electrode signal. This result is remarkable given the fact that other nitroaromatic compounds usually significantly affect the peak current response of NB owing to their similar structural activity. The practical applicability of this catalyst for selective quantitative analysis of NB in real samples was tested successfully in contaminated waste water. The sensor device is simple, cost effective and portable and can be applied in a number of industrial and research measurements. An electrochemical sensor for NB based on reduced graphene oxide (rGO) and AgNPs, biosynthesized using *Justicia glauca* leaf extract, has been developed.¹²⁵ The modified rGO/AgNPs/GC electrode showed good efficiency for selective quantitative determination of NB, compared to other modified electrodes – the electrode signal retained its linearity in the concentration range from 0.5 to 900 µM, the sensitivity was determined as 0.836 µA µM⁻¹ cm⁻² with a detection limit of 0.261 µM NB. In addition, the reduction peak current response to 100 µM NB was examined up to 52 days by CV and rGO/AgNPs/GC was stored in phosphate buffer solution (PBS) when not in use. The modified electrode retained about 90.15 % of its initial current response after 52

days, which indicates the excellent storage stability of the sensor. The authors have reported that the fabricated sensor showed a satisfactory reproducibility with *RSD* of 3.8 % for determination of NB using 5 different sensors. The good recovery results and *RSDs* of the developed sensor obtained in waste water samples proved the practical applicability towards the determination of NB in real samples.

Bastos-Arrieta *et al.* have demonstrated that biosynthesized AgNPs may be useful in developing catalysts for electrochemical sensing of some heavy metal ions.¹²⁶ Heavy metal toxicity has proven to be a major threat and there are serious health risks associated with it.¹²⁷ Toxicity of heavy metals is due to accumulation in tissues, metabolic interference, mutagenesis and carcinogenesis. Arsenic, cadmium, mercury, chromium, lead and nickel induce oxidative stress, DNA damage, cell aging and cell death processes, resulting in increase the risk of cancer and cancer-related diseases.¹²⁸ Bastos-Arrieta *et al.* reported on synthesis of AgNPs by using an aqueous extract of grape stalk waste as a reducing and capping agent, thus leading to a reagent-free procedure and valorisation of agri-food waste.¹²⁶ Various factors affecting the AgNPs synthesis such as temperature, contact time, extract/metal solution volume ratio and pH have been studied. AgNPs with an average diameter of 27.7 ± 0.6 nm were selected to proof their suitability for sensing purposes. Screen-printed carbon nanofiber electrode modified with biosynthesized AgNPs (AgNPs–SPCNFE) was tested for the simultaneous stripping voltammetric determination of Pb(II) and Cd(II). The good reproducibility, high sensitivity and low limits of detection (around $2.7 \mu\text{g L}^{-1}$ for both metal ions) make this electrocatalyst a promising sensing element in electrochemical sensor device for a fast and reliable simultaneous detection of Pb(II) and Cd(II).

Table I summarizes electrochemical sensors based on biosynthesized AgNPs. Important operational characteristics including sensitivity, dynamic range, limit of detection, as well as data on stability and reproducibility of sensors were presented.

4.2. Electrochemical sensors based on biosynthesized AuNPs

In nanotechnology AuNPs have attracted much attention due to their remarkable properties including high mechanical stability, unique tunable optical and distinct electronic properties, high electrical conductivity, strong binding affinity to thiols, and catalytic activity. Adhering to the principles of green chemistry, Mohd Taib *et al.* have described a new method for synthesis of AuNPs, using water extract of *Hibiscus sabdariffa* leaves (*H. sabdariffa* L.) as both reductant and stabilizer.¹³⁶ The proposed procedure is reliable, environmentally friendly and cost-effective compared to other conventional synthesis methods. The authors suggested that chlorogenic acid (an ester of caffeic acid and quinic acid) in *H. sabdariffa* L. extract is the major compound involved in the reduction of Au^{3+} to Au.

TABLE I. Operational characteristics of electrochemical sensors based on biosynthesized AgNPs; Amp. (amperometry); CV (cyclic voltammetry); DPV (differential pulse voltammetry); DPASV (differential pulse anodic stripping voltammetry); SWV (square wave voltammetry); SWASV (square wave anodic stripping voltammetry); LOD (limit of detection); AgNS (silver nanospheres); CS (chitosan); GC (glassy carbon); Gr (graphite); GO (graphene oxide); rGO (reduced graphene oxide); SPCNFE (screen-printed carbon nanofiber electrode); CPE (carbon paste electrode); NB (nitrobenzene); AA (ascorbic acid); DA (dopamine)

Modified electrode	Reducing agent	Method (E / V)	Analyte	Sensitivity, $\mu\text{A mM}^{-1} \text{cm}^{-2}$ (linear range) (LOD)	Stability (RSD)
AgNPs/CS/Gr ⁹⁴	<i>Achillea millefolium</i>	Amp. (-0.3 ^a)	H_2O_2	533.5 (up to 4.3×10^{-3} M) (-) (6.8 %)	–
AgNPs/CS/Gr ⁹⁴	<i>Lavandula angustifolia</i>	Amp. (-0.3 ^a)	H_2O_2	374.7 (up to 3.5×10^{-3} M) (-) (–)	–
AgNPs/CS/PGE ¹⁰⁶	<i>Tagetes erecta</i>	CV (-0.55 ^a)	H_2O_2	0.129 mA μM^{-1} (1.0–10.0 μM) (0.52 μM)	4 weeks (1.4 %)
rGO/AgNPs/GC ¹⁰⁵	<i>Green tea</i>	Amp. (-0.4 ^a)	H_2O_2	236 (0.002–20.0 mM) (0.73 μM)	7 weeks (3.6 %)
AgNPs/CS/Gr ¹⁰⁷	<i>Rosa damascena</i>	Amp. (-0.3 ^a)	H_2O_2	115.2 (up to 6.6 mM) (-) (6.7 %)	–
AgNPs/Gr ¹⁰⁷	<i>Rosa damascena</i>	Amp. (-0.3 ^a)	H_2O_2	214.7 (up to 3.9 mM) (-) (6.7 %)	–
AgAu/rGO/GC ¹²⁹	<i>Azadirachta indica</i>	Amp. (-0.4 ^a)	H_2O_2	– (0.1–5.0 mM) (1.0 μM)	– (–)
rGO/AgNPs/GC ¹³⁰	<i>Plectranthus amboinicus</i>	Amp. (-0.32 ^a)	H_2O_2	– (1.0–800 μM) (0.312 μM)	– (–)
AgNPs/GO/GC ¹³¹	<i>Callicarpa maingayi</i>	Amp. (-0.32 ^a)	H_2O_2	– (5.0–700 μM) (0.6 μM)	– (–)
AgNPs/GC ¹³²	<i>Bacillus subtilis</i>	Amp. (-0.35 ^b)	H_2O_2	236 (0.05–120 mM) (8.0 μM)	30 days (3.1 %)
AgNS/GC ¹¹⁵	<i>Nilgiri wood</i>	Amp. (0.86 ^a)	NO_2^-	580 (0.1–8.0 μM) (0.031 μM)	30 days (3.6 %)
AgNPs/GC ¹³³	<i>Piper betle</i>	Amp. (1.0 ^a)	NO_2^-	1642.27 (1.0–6000 μM) (0.046 μM)	30 days (3.3 %)
AgNPs/GO/GC ¹³⁴	AA	SWASV (-0.6 ^a)	As^{3+}	180.5 $\mu\text{A } \mu\text{M}^{-1}$ (13.33–375.19 nM) (0.24 nM)	90 days (–)
AgNPs/SPCNFE ¹²⁶	Grape stalk waste	DPASV (-0.42 ^a)	Pb^{2+}	62 nA $\mu\text{g}^{-1} \text{L}$ (8.9–100.4 $\mu\text{g L}^{-1}$) (2.7 $\mu\text{g L}^{-1}$)	– (–)
AgNPs/SPCNFE ¹²⁶	Grape stalk waste	DPASV (-0.55 ^a)	Cd^{2+}	46 nA $\mu\text{g}^{-1} \text{L}$ (9.5–37.9 $\mu\text{g L}^{-1}$) (2.8 $\mu\text{g L}^{-1}$)	– (–)
AgNPs/CPE ¹²⁰	Onion	SWV (0.45 ^a)	AA	– (0.4–450 μM) (0.1 μM)	– (–)
AgNPs/GC ¹²¹	<i>Mimosa pudica</i>	DPV (0.1 ^a)	DA	– (10.0–60 μM) (0.5 μM)	– (–)
AgNPs/GC ¹³⁵	<i>Ocimum tenuiflorum</i>	Amp. (0.55 ^a)	glucose	895.8 (1.0–8.9 mM) (0.0048 μM)	10 days (1.15 %)
rGO/AgNPs/GC ¹²⁵	<i>Justicia glauca</i>	DPV (-0.458 ^a)	NB	0.836 $\mu\text{A } \mu\text{M}^{-1} \text{cm}^{-2}$ (0.5–900 μM) (0.261 μM)	52 days (3.8 %)

TABLE I. Continued

Modified electrode	Reducing agent	Method (<i>E</i> / V)	Analyte	Sensitivity, $\mu\text{A mM}^{-1} \text{cm}^{-2}$ (linear range) (<i>LOD</i>)	Stability (<i>RSD</i>)
AgNPs/GC ¹²⁴	<i>Camellia japonica</i>	Amp. (-0.42 ^a)	NB	- (0.05–21.0 μM) (23.0–2593 μM) (0.012 μM)	- (-)
AgNPs/GC ¹²³	<i>Eucalyptus</i>	DPV (-0.78 ^a)	NB	2.262 $\mu\text{A } \mu\text{M}^{-1} \text{cm}^{-2}$ (5.0–40.0 μM) (0.027 μM)	20 days (-)
AgNPs/CS/Gr ¹⁰⁷	<i>Rosa damascena</i>	Amp. (-0.3 ^a)	vanillin	56.8 (up to 0.5 mM) (8.4 μM)	- (-)

^aReference electrode: Ag/AgCl, 3 M KCl (0.200 V vs. SHE); ^breference electrode: saturated calomel electrode (SCE, 0.242 V vs. SHE)

Previous reports on AuNPs-synthesis have shown that the caffeic acid moiety of chlorogenic acid was essential to reduce Au^{3+} . TEM analysis confirmed that the so-biosynthesized AuNPs were formed with a narrow distribution and an average particle size of 7 ± 2 nm. A glassy carbon electrode modified with the AuNPs was tested as a catalyst in electrooxidation of nitrite. AuNPs/GC showed good electrocatalytic activity in the target reaction – sensitivity was calculated to be $917\pm30 \mu\text{A mM}^{-1} \text{cm}^{-2}$ in the concentration range from 0.37 to 10 mM and detection limit of 0.11 mM (*S/N* = 3). The stability, reproducibility and repeatability of AuNPs/GC electrode were investigated by voltammetric measurements. After 21 days storage the prepared electrode possesses around 80 % of its initial response. An analysis for ten sequential prepared electrodes showed *RSD* of 4.27 % which confirmed the repeatability of AuNPs/GC. The sensor-to-sensor reproducibility was investigated by measuring the current responses of five diverse electrodes prepared independently by the same procedure. The results showed that the response produced by different electrodes had a good reproducibility with *RSD* of 4.21 % and authors concluded that the sensor fabrication methodology was reliable.

Emmanuel *et al.* have presented a green procedure for synthesis of AuNPs using *Acacia nilotica* twig bark extract at room temperature.¹³⁷ The synthesis protocol shows that the formation of gold particles is within 10 min, which implies a higher reaction rate. The size of biosynthesized AuNPs was calculated using Debye–Scherrer equation which showed that the nanoparticles were in the average size of 30 nm. The AuNPs modified glassy carbon electrode exhibited excellent reduction ability towards NB compared to the unmodified electrode. The developed sensor AuNPs/GC displayed a wide linear response from 0.1 to 600 μM with high sensitivity ($1.01 \mu\text{A } \mu\text{M}^{-1} \text{cm}^{-2}$) and a low detection limit of 0.016 μM in DPV mode. The modified electrode demonstrated exceptional selectivity in the presence of ions, phenolic and biologically active compounds. In

addition, the AuNPs/GC exhibited an outstanding recovery results towards NB in various real water samples.

Electrochemical sensor for quantitative detection of hydrazine – another environmentally hazardous pollutant, was devepoled by Karthik *et al.*¹³⁸ Their study envisages easy and innovative method for green synthesis of AuNPs on GC electrode; the fabricated modified electrode was used for the detection of hydrazine by using sensitive amperometric method. Hydrazine is an inorganic base, which is an important reagent in the production of polymer foams, pesticides, insecticides, pharmaceuticals, etc. Hydrazine is also used as rocket fuel – it is a high volumetric energy density liquid fuel (at room temperature and atmospheric pressure) that contains 12.6 wt. % of hydrogen. However, hydrazine is a highly toxic compound with mutagenic and carcinogenic effects. Serious effects on the reproductive system are observed in animals after hydrazine inhalation. Therefore, rapid and precise detection of hydrazine is of great importance. Karthik *et al.* have used *Cerasus serrulata* (*C. serrulata*) leaves extract for green synthesis of AuNPs. TEM images confirmed that biosynthesized AuNPs were spherical in shape and approximately in the range of 5 to 25 nm. DFT studies revealed that the coumarin present in the *C. serrulata* leaves extract demonstrated greater reducing and stabilizing properties compared to the properties of other compounds like butylhydroxytoluene and hydrocoumarin present in the extract. The electrochemical results showed remarkable electrocatalytic activity of the AuNPs-modified GC electrode towards oxidation of hydrazine. AuNPs/GC exhibited a wide linear range from 5 nM to 272 µM with a low detection limit of 0.05 µM. The fabricated electrode showed good selectivity towards the sensitive determination of hydrazine even in the presence of 1000-fold and 150-fold excess concentration of common ions and biological interferents (ascorbic acid, uric acid and dopamine), respectively. Thus the proposed electrode seems to be a potential candidate for developing a simple, rapid and cost-effective electrochemical sensor for hydrazine detection.

For the first time Karthik *et al.* report in electrochemical chloramphenicol (CAP) sensor using plant extract derived AuNPs.¹³⁹ CAP is an effective broad-spectrum antibiotic that has been widely used to treat mammalian, poultry, aquatic and bee diseases around the world. However, CAP is associated with numerous toxic and fatal side effects in human, especially bone marrow suppression, aplastic anemia and agranulocytosis. Therefore, development of fast, simple and reliable methods for CAP monitoring in food samples are extremely important in food quality control. Karthik *et al.* have presented a simple and rapid green synthesis using *Bischofia javanica Blume* leaves as reducing agent for the preparation of AuNPs. The biosynthesis procedure requires less than 40 s to reduce gold salts to AuNPs. They have used graphene oxide (GO) as support to anchor and stabilize AuNPs which also avoids aggregation. The successful formation of

the AuNPs/GO composite was revealed by morphological, elemental, spectroscopic and electrochemical methods. The green synthesized AuNPs/GO delivered high conductivity, surface area and porosity. AuNPs/GO composite film modified electrode has shown excellent electrocatalytic ability to CAP. The amperometric sensing platform possesses a sensitivity of $3.81 \mu\text{A} \mu\text{M}^{-1} \text{cm}^{-2}$ in the range of $1.5 \mu\text{M}$ – $2.95 \mu\text{M}$; LOD of the sensor was calculated as $0.25 \mu\text{M}$ CAP. The amperometric measurements proved that the modified electrode has a good anti-interference ability, a fast response (the current reached 95 % steady-state current within 5 s of CAP injection), satisfactory repeatability (RSD for five repeatable measurements was calculated to be 3.18 %) and reproducibility of the procedure (five different AuNPs/GO modified electrodes showed RSD 3.83 %). The long-term storage stability of the electrode was also reasonable – 92.15 % of the initial response current was retained over 15 days. The real sample analysis tested in milk, powdered milk, honey and eye drops samples validates excellent practical feasibility of AuNPs/GO modified electrode to determine CAP content in food and pharmaceutical samples.

Table II provides an overview of the electrochemical sensors based on biosynthesized AuNPs.

TABLE II. Operational characteristics of electrochemical sensors based on biosynthesized AuNPs; SPE (screen-printed electrode); CAP (chloramphenicol). Other abbreviations are the same as Table I

Modified electrode	Reducing agent	Method (E / V)	Analyte	Sensitivity (linear range) (LOD)	Stability (RSD)
AuNPs/CPE ¹⁴⁰	Glycerol	SWV (0.65 ^b)	NO_2^-	$0.268 \mu\text{A L mol}^{-1}$ (0.2 – $15 \mu\text{M}$) ($0.2 \mu\text{M}$)	60 days (4.0 %)
AuNPs/GC ¹³⁶	<i>Hibiscus sabdariffa</i>	Amp. (0.8 ^a)	NO_2^-	917 (370 – $10000 \mu\text{M}$) ($110 \mu\text{M}$)	21 days (4.21 %)
rGO/AuNPs/GC ¹⁴¹	<i>Abelmoschus esculentus</i>	SWASV (−0.791 ^a)	Cd^{2+}	$19.05 \mu\text{A} \mu\text{M}^{-1} \text{cm}^{-2}$ (5 – $10 \mu\text{M}$) (31.81nM)	– (–)
rGO/AuNPs/GC ¹⁴¹	<i>Abelmoschus esculentus</i>	SWASV (−0.54 ^a)	Pb^{2+}	$47.7 \mu\text{A} \mu\text{M}^{-1} \text{cm}^{-2}$ (5 – $10 \mu\text{M}$) (12.69nM)	– (–)
rGO/AuNPs/GC ¹⁴¹	<i>Abelmoschus esculentus</i>	SWASV (−0.064 ^a)	Cu^{2+}	$22.10 \mu\text{A} \mu\text{M}^{-1} \text{cm}^{-2}$ (5 – $10 \mu\text{M}$) (27.42nM)	– (–)
rGO/AuNPs/GC ¹⁴¹	<i>Abelmoschus esculentus</i>	SWASV (0.228 ^a)	Hg^{2+}	$29.28 \mu\text{A} \mu\text{M}^{-1} \text{cm}^{-2}$ (5 – $10 \mu\text{M}$) (20.70nM)	– (–)
AuNPs/SPE ⁷⁷	<i>Pithophora oedogonia</i>	Amp. (0.77 ^a)	Carbendazim	– (0.05 – $25 \mu\text{M}$) ($0.0029 \mu\text{M}$)	– (–)
AuNPs/GC ¹³⁸	<i>Cerasus serrulata</i>	Amp. (0.24 ^a)	Hydrazine	– (0.005 – $272 \mu\text{M}$) ($0.05 \mu\text{M}$)	– (–)
AuNPs/GC ¹³⁷	<i>Acacia nilotica</i>	DPV (−0.7 ^a)	NB	$1.01 \mu\text{A} \mu\text{M}^{-1} \text{cm}^{-2}$ (0.1 – $600 \mu\text{M}$) ($0.016 \mu\text{M}$)	8 days (2.1 %)

TABLE II. Continued

Modified electrode	Reducing agent	Method (E / V)	Analyte	Sensitivity (linear range) (LOD)	Stability (RSD)
AuNPs/GO/GC ¹³⁹	<i>Bischofia javanica</i>	Amp. (-0.45 ^a)	CAP	3.81 $\mu\text{A} \mu\text{M}^{-1} \text{cm}^{-2}$ (1.5–2.95 μM) (0.25 μM)	15 days (3.18 %)
AuNPs/GC ¹⁴²	Peanut seeds	CV (-0.3 ^a)	Sudan IV	– (10–80 μM) (4.0 μM)	20 cycles (–)

4. 3. Electrochemical sensors based on other biosynthesized metal and metal oxide nanoparticles

Copper nanoparticles (CuNPs) are particularly attractive because of high natural abundance of copper, low cost and the practical and straightforward multiple ways of preparing Cu-based nanomaterials.¹⁴³ Cu-based materials can promote and undergo a variety of reactions due to accessible oxidation states of copper which enable reactivity *via* both one- and two-electron pathways. Recently, copper oxide nanostructures have been given more attention as promising electrode materials for supercapacitors, gas sensors, electrochemical sensors and anode materials for lithium ion batteries. Many researchers have found that the electrochemical performance of CuO/Cu₂O composites has been improved due to their stable multiple oxidation states and integration of their catalytic capabilities. A simple, low cost, stable and sensitive electrochemical sensor based on biosynthesized copper oxide nanoparticles (CuO/Cu₂O NPs) was developed for formaldehyde detection.¹⁴⁴ Momeni *et al.* have successfully synthesized CuO/Cu₂O nanoparticles using Gum Arabic (highly branched complex polysaccharide, non-toxic and hydrophilic with abundant hydroxyl and carboxyl groups) as a stabilizing and capping agent. The CuO/Cu₂O NPs modified carbon ionic liquid electrode (CuO/Cu₂O/CILE) was designed and its catalytic activity was investigated towards formaldehyde oxidation in alkaline medium. Formaldehyde is one of the most widely used chemicals – it acquires applications in different areas, such as resin, adhesive and plastic industry, fuel cells and electroless plating industry, agriculture and food manufacturing, as an industrial disinfectant and a preservative agent in medical labs, *etc.* However, a number of studies have suggested that formaldehyde exposure is associated with certain types of cancer, particularly myeloid leukemia.¹⁴⁵ In the commented article the results showed that CuO/Cu₂O/CILE electrode possesses good electrocatalytic activity in the target reaction with a linear current response in the range from 0.1 to 110 mM formaldehyde and a detection limit of 10 μM . The authors have proven the good reproducibility and stability of modified electrode. The long term stability of CuO/Cu₂O/CILE electrode was tested by storing the electrode at room temperature for one month and the current response retained 94 % of its initial response. A simple and green route for synthesis of CuO/Cu₂O NPs together with enhanced electrocatalytic

activity toward formaldehyde oxidation show that the CuO/Cu₂O/CILE is one of the most promising systems for detection of formaldehyde.

Copper oxide nanoparticles (CuONPs) were synthesized using *Caesalpinia bonduc* seed extract *via* a green synthetic pathway and were evaluated for electrochemical detection of riboflavin (vitamin B2).¹⁴⁶ Riboflavin is a water-soluble vitamin needed for the proper functioning of human organs, such as it plays an essential role in the sequence of protein, carbohydrate and fat metabolism. The lack of vitamin B2 leads to skin disorders and eye lesions. At the same time excess of riboflavin in the human body is dangerous because leads to damage to DNA and tissues. Riboflavin cannot be produced by the human body – it is provided through dietary supplements and pharmaceutical products. Therefore, it is essential to monitor vitamin B2 *in situ* in real food and pharmaceutical samples. Sukumar *et al.* have reported on the development of modified paraffin-impregnated graphite electrode CuONPs/PIG as a suitable sensor for the determination of nanomolar concentration of vitamin B2 with an observed linear range of 3.13–56.3 nM and a limit of detection of 1.04 nM. The electrode showed satisfactory stability over a period of 4 months – 95 % residual activity was recorded after 80 days and 80 % after 120 days, respectively. The practical applicability of CuONPs/PIG was checked with real samples – egg yolk, milk powder and commercially available B-complex tablets. The concentration of vitamin B₂ was evaluated by the standard addition method, and the recovery values range from 99 to 99.75 %. The results showed high recovery and the authors stated that this method could be extended for further practical applications.

Kumar *et al.* have demonstrated a facile and eco-friendly approach for the simultaneous reduction of graphene oxide as well as copper acetate to prepare Cu₂O decorated reduced GO (rGO/Cu₂O).¹⁴⁷ In this work an easily available and naturally occurring mango bark (*M. indica*) extract has been used as the reducing agent instead of hazardous and toxic chemicals. Fourier transform infrared and X-ray photoelectron spectroscopy have been performed to confirm the removal of oxygen functional groups from the surface of GO and the X-ray diffraction pattern reveals the formation of Cu₂ONPs. The electrocatalytic behaviour of the resultant rGO/Cu₂O composite has been carried by CV and constant potential amperometry. The utility of rGO/Cu₂O as an electrochemical sensor towards H₂O₂ detection was shown; the sensitivity and limit of detection were found to be 7.435 $\mu\text{A }\mu\text{M}^{-1}$ and 42.35 nM, respectively.

Amanulla *et al.* have reported the development of a sensitive and selective amperometric sensor for H₂O₂, using for the first time biosynthesized iron nanoparticles (FeNPs).¹⁴⁸ A simple and facile green process was used for the synthesis of FeNPs decorated rGO nanocomposite using *Ipomoea pestigridis* leaf extract as a reducing and stabilizing agent. The physicochemical results confirmed the successful formation of rGO/FeNPs composite; TEM images showed

that the FeNPs were evenly distributed on rGO surface with an average diameter of 28 ± 4 nm. The nanocomposite rGO/FeNPs was further modified on GC electrode and used for H_2O_2 sensing. CV data reveal that rGO/FeNPs nanocomposite has an excellent behavior to H_2O_2 electroreduction when compared to the response of FeNPs and rGO modified electrodes. Amperometry was further used to quantify selectively H_2O_2 using rGO/FeNPs nanocomposite: the electrode response at an applied potential of -0.5 V (vs. Ag/AgCl) was linear over the concentration range from 0.1 μM to 2.15 mM and exceptionally fast (2 s). The limit of detection and sensitivity of the proposed sensor were estimated as 0.056 μM and 0.2085 $\mu\text{A } \mu\text{M}^{-1} \text{ cm}^{-2}$, respectively. The practical ability of the fabricated sensor was examined in commercial contact lens solution, human serum and urine samples.

Selenium nanoparticles (SeNPs) synthesis has been achieved by either physical or chemical methods, which suffer from drawback like high pressure, low yields and longer growth times which cannot be regarded as an eco-friendly process. Prasad *et al.* have developed an eco-friendly and simple method for SeNPs synthesis using a selenium-resistant bacterium identified as *Bacillus pumilus* sp. BAB-3706 cell-free extract.¹⁴⁹ A working electrode was modified by coating the surface of indium tin oxide (ITO) with resulting colloidal SeNPs (size 10–80 nm). The proposed sensor SeNPs/ITO exhibited good electrocatalytical activity towards the reduction of H_2O_2 and low detection limit. Hence, microbial SeNPs can be a promising source for the development of electrochemical sensor system for H_2O_2 .

Among various metallic nanoparticles, platinum (Pt) and palladium (Pd) nanoparticles are the most widely studied due to their extremely high catalytic/electrocatalytic activity. Due to their extensive applications in sensors, biosensors and catalysts, production of PtNPs and PdNPs through environment friendly methods has a significant role. In this regard, Momeni *et al.* have presented green synthesis of PdNPs using natural and low-cost crude extract derived from the marine alga *Sargassum bovinum*.⁹³ TEM study confirmed the monodispersed and octahedral shape of PdNPs within the size ranges 5–10 nm. Electrocatalytic performance of the so-biosynthesized PdNPs towards reduction of H_2O_2 was investigated. PdNPs-modified carbon ionic liquid electrode (PdNPs/CILE) was developed as a nonenzymatic sensor for the determination of hydrogen peroxide. Amperometric measurements at potential of -0.2 V (vs. Ag/AgCl) showed that PdNPs/CILE has an excellent stability and it is a reliable sensor for the detection of H_2O_2 in a wide range of 5.0 μM – 15.0 mM with a sensitivity of 284.35 mA $\text{mM}^{-1} \text{ cm}^{-2}$ and a detection limit of 1.0 μM H_2O_2 . The method is reliable – *RSD* of current response to 1 mM H_2O_2 of five separate electrodes made with different CILE pastes was calculated to be 3.2 %, and a single electrode using five consecutive determinations showed average *RSD* of less than 2.5 %. The authors concluded that the interesting performances of the electrode coupled with its simple,

effective and green preparation procedure of PdNPs synthesis, without any surfactants and templates, make it a promising electrochemical sensing platform.

Rapid and eco-friendly synthesis of platinum nanoparticles (PtNPs) using aqueous leaves extract of *Quercus glauca* has been reported for first time for detection of hydrazine.¹⁵⁰ The prepared PtNPs were spherical in shape and size from 5–15 nm. The electrocatalytic performance of modified electrode PtNPs/GC for hydrazine has been studied by CV and amperometric techniques. Cyclic voltammogram of PtNPs/GC showed a sharp peak at a very lower onset oxidation potential of –0.3 V. The fabricated hydrazine sensor showed excellent selectivity, low detection limit of 7 nM, wide linear range from 0.01 to 283 μM and a sensitivity of 1.704 μA μM^{–1} cm^{–2}. The sensor was successfully used for the detection of hydrazine in spiked water samples.

Manganese oxide nanoparticles (MnONPs) of different sizes were synthesized in aqueous medium using clove, *i.e.*, *Syzygium aromaticum* extract (CE) as reducing and stabilizing agent. MnONPs with size ~4 nm were used for the electrochemical sensing of *p*-nitrophenol – a toxic pollutant released by textile and leather industries, iron and steel production, pharmaceutical manufacturing, rubber processing, production of electrical and electronic components.¹⁵¹ Acute inhalation or ingestion of *p*-nitrophenol in humans leads to headache, drowsiness, nausea and cyanosis (result of methemoglobinemia). Endocrine disrupting effect and hypothalamic pituitary gonadal toxicity of *p*-nitrophenol on animals have been documented recently.¹⁵² *p*-Nitrophenol exposure disrupted steroidogenesis during the ovarian development in female rats, reduced testosterone synthesis, caused morphological changes in testes, and ultimately decreased semen quality in the roosters.^{153,154}

The MnONPs, prepared using CE-based green chemistry approach, were useful for *p*-nitrophenol sensing. MnONPs-modified gold electrode detected *p*-nitrophenol with good sensitivity (0.16 μA μM^{–1} cm^{–2}) and detection limit of 15.65 μM.

An overview on the main operational parameters of electrodes modified with biosynthesized metal NPs or metal oxide NPs is presented in Table III.

TABLE III. Operational characteristics of electrochemical sensors based on other biosynthesized metal NPs and metal oxide NPs; UA (uric acid); MGPE (modified graphite paste electrode); EGCG (epigallocatechin gallate); CILE (carbon ionic liquid electrode); PIG (paraffin-impregnated graphite electrode); ITO (indium tin oxide); BCA (butyl carbitol acetate). Other abbreviations are the same as Table I

Modified electrode	Reducing agent	Method (E / V)	Analyte	Sensitivity (linear range) (LOD)	Stability (RSD)
PdNPs/CILE ⁹³	<i>Sargassum bovinum</i>	Amp. (–0.2 ^a)	H ₂ O ₂	284.35 (5.0–15000 μM) (1.0 μM)	(2.5 %)

TABLE III. Continued

Modified electrode	Reducing agent	Method (<i>E</i> / V)	Analyte	Sensitivity (linear range) (<i>LOD</i>)	Stability (<i>RSD</i>)
rGO/FeNPs/GC ¹⁴⁸	<i>Ipomoea pes-tigridis</i>	Amp. (-0.5 ^a)	H ₂ O ₂	0.2085 μA μM ⁻¹ cm ⁻² (0.1–2150 μM) (0.056 μM)	— (3.6 %)
SeNPs/ITO ¹⁴⁹	<i>Bacillus pumilus</i>	Amp. (-1.0 ^b)	H ₂ O ₂	16.54 (5.0–600 mM) (3.0 μM)	— (–)
Cu ₂ O/rGO ¹⁴⁷	<i>M. indica</i>	Amp. (-0.2 ^a)	H ₂ O ₂	7.435 μA μM ⁻¹ (0.2–3.6 μM) (42.35 nM)	15 days (–)
PdAg/CPE ¹⁵⁵	Fungi	DPV (0.3 ^a)	UA	– (up to 273.0 nM) (5.543 nM)	— (–)
Cu/Cu ₂ O/CuONPs/GC ¹⁵	<i>Pomegranate</i>	CV (-0.3 ^a)	Ethanol	0.049 μA mM ⁻¹ (0.5–2.0 μM) (0.09 μM)	— (–)
CuO/Cu ₂ O/CILE ¹⁴⁴	Gum Arabic	CV (0.4 ^a)	Formaldehyde	186.0 (0.1–110 mM) (10 μM)	30 days (4.6 %)
CoONPs/CPE ¹⁵⁷	Gelatin	CV (-0.34 ^a)	Glucose	609.04 mM ⁻¹ cm ⁻² (7.0–1000.0 μM) (5.3 μM)	4 weeks (2.9 %)
PtNPs/GC ¹⁵⁰	<i>Quercus glauca</i>	Amp. (-0.18 ^a)	Hydrazine	1.704 μA μM ⁻¹ cm ⁻² (0.01–283.0 μM) (7 nM)	— (–)
MnONPs/BCA/Au ¹⁵¹	<i>Syzygium aromaticum</i>	DPV (-0.69 ^a)	p-Nitrophenol	0.16 μA μM ⁻¹ cm ⁻² (200.0–550.0 μM) (15.65 μM)	— (–)
CuONPs/PIG ¹⁴⁶	<i>Caesalpinia bonduc</i>	SWV (0.03)	Riboflavin	– (3.13–56.3 nM) (1.04 nM)	120 days (–)

5. CONCLUSIONS AND FUTURE PERSPECTIVES

Over the past decade intensive research on the possibility of using plant extracts or microorganisms to produce stable metal nanoparticles with pronounced antibacterial and antitumor activity, as well as studies focused on biosynthesized nanoparticles as catalytically active components in the development of new electrocatalysts, have been observed. There is convincing evidence that green synthesis of metal and metal oxide nanoparticles has a potential to provide a new direction in the fabrication of cheap and highly effective electrocatalysts applicable in food, clinical, pharmaceutical and environmental analysis. In this review we have been summarized the main approaches for biosynthesis of metal nanoparticles and their use in the construction of novel electrochemical sensor platforms. It was shown that the biosynthesized metal nanoparticles produced by plants and microorganisms are successfully applied in designing of electrochemical sensors for detection of broad spectrum of analytes.

Currently, researchers have focused their attention on detection of biomolecules involved in the synthesis of metal nanoparticles as well as on understanding the principles/pathways and mechanisms of nanoparticle biosynthesis. Since the properties of nanomaterials strongly depend on their size and shape, efforts should also be focused on optimizing the experimental conditions to yield stable and reproducible size-controlled biosynthesis of nanoparticles. Therefore, researchers should refine the biological mediated synthesis protocols to ensure increasing the sustainability of the processes involved in the production of nanoparticles. Scalability of the production method also is a necessary – appropriate technologies need to be developed for safe and efficient production of these novel nanomaterials on a commercially sustainable scale while maintaining a satisfactory size distribution.

In terms of electrochemical sensing applications selectivity and reproducibility of the electrode signal in real complex matrices, as well as long-term stability of the modified material are extremely important. The experimental data show that the modified with biosynthesized nanoparticles surfaces still remain challenging as they are not often as reproducible and stable as one would hope. Further research needs to be done to address these issues and to improve the electrode performance. Consequently the emphasis should be on achieving a higher operational and storage stability of the electrode-catalysts modified with biosynthesized metal/metal oxide nanoparticles. Expectations in this area are also related with broadening the spectrum of target analytes, as well as development of surface modification methods capable of enhancing the electrode sensitivity and selectivity.

In summary, the significant development of electrochemical sensor platforms based on biosynthesized nanomaterials is giving rise to new impetus of generating novel sustainable bio-based technologies for analysis and securing the environmental and food safety.

ИЗВОД

ПРИМЕНА БИОСИНТЕТИСАНИХ МЕТАЛНИХ НАНОЧЕСТИЦА У ЕЛЕКТРОХЕМИЈСКИМ СЕНЗОРИМА

TOTKA DODEVSKA, DOBRIN HADZHIEV, IVAN SHTEREV и YANNA LAZAROVA

Department of Organic Chemistry and Inorganic Chemistry, University of Food Technology, 26 Maritsa Boulevard, Plovdiv 4002, Bulgaria

У новије време развој еколошки прихватљивих, исплативих и поузданих метода синтезе металних наночестица привлачи значајну пажњу. Такозване зелене синтезе, које користе благе реакционе услове и природна средства као што су биљни екстракти и микроорганизми, успостављене су као погодан, одржив, јефтин и еколошки безбедан приступ синтези разноврсних наноматеријала. Током протекле деценије биосинтеза се наметнула као значајна метода којом се смањују штетни ефекти традиционалних метода синтезе наночестица које су уобичајене у лабораторијама и индустрији. Овај прегледни

рад наглашава значај биосинтетисаних металних наночестица у области електрохемијских сензора. Све је више доказа да зелена синтеза наночестица пружа нови правац у дизајнирању исплативих, високо осетљивих и селективних катализатора за електроде које се примењују у анализи хране, као и у клиничким анализама и заштити животне средине. Рад је базиран на 157 литературних навода и даје детаљан преглед главних приступа зеленој синтези металних наночестица и њиховој примени у електрохемијским сензорима. Такође су обухваћене значајне радне карактеристике укључујући осетљивост, динамички опсег, границу детекције, као и податке о стабилности и репродуктивности сензора.

(Примљено 21. маја, ревидирано 17. августа, прихваћено 1. октобра 2021)

REFERENCES

1. J. A. Dahl, B. L. S. Maddux, J. E. Hutchison, *Chem. Rev.* **107** (2007) 2228 (<https://doi.org/10.1021/cr050943k>)
2. G. Kratošová, V. Holíšová, Z. Konvičková, A. P. Ingle, S. Gaikwad, K. Škrlová, A. Prokop, M. Rai, D. Plachá, *Biotechnol. Adv.* **37** (2019) 154 (<https://doi.org/10.1016/j.biotechadv.2018.11.012>)
3. C. C. Bonatto, L. P. Silva, *Ind. Crop Prod.* **58** (2014) 46 (<http://dx.doi.org/10.1016/j.indcrop.2014.04.007>)
4. M. Yehia, Sh. Labib, S. M. Ismail, *Physica, B* **446** (2014) 49 (<http://dx.doi.org/10.1016/j.physb.2014.04.032>)
5. V. K. Sharma, R. A. Yngard, Y. Lin, *Adv. Colloid Interface Sci.* **145** (2009) 83 (<http://dx.doi.org/10.1016/j.cis.2008.09.002>)
6. R. Narayanan, M. A. El-Sayed, *J. Phys. Chem., B* **109** (2005) 12663 (<https://doi.org/10.1021/jp051066p>)
7. G. P. Wiederrecht, G. A. Wurtz, J. Hranisavljevic, *Nano Lett.* **4** (2004) 2121 (<http://dx.doi.org/10.1021/nl0488228>)
8. M. Rai, A. Yadav, A. Gade, *Biotechnol. Adv.* **27** (2009) 76 (<http://dx.doi.org/10.1016/j.biotechadv.2008.09.002>)
9. S. C. McBain, H. H. P. Yiu, J. Dobson, *Int. J. Nanomedicine* **3** (2008) 169 (<https://doi.org/10.2147/IJN.S1608>)
10. E. S. Kozlova, T. E. Nikiforova, *Russ. J. Appl. Chem.* **88** (2015) 638 (<http://dx.doi.org/10.1134/S1070427215040151>)
11. A. Yu. Olenin, G. V. Lisichkin, *Russ. J. Appl. Chem.* **91** (2018), 1393 (<http://dx.doi.org/10.1134/S107042721809001X>)
12. M. Holzinger, A. Le Goff, S. Cosnier, *Front. Chem.* **2** (2014) 63 (<https://www.frontiersin.org/article/10.3389/fchem.2014.00063>)
13. C. J. Murphy, T. K. Sau, A. M. Gole, C. J. Orendorff, J. Gao, L. Gou, S. E. Hunyadi, T. Li, *J. Phys. Chem., B* **109** (2005) 13857 (<http://dx.doi.org/10.1021/jp0516846>)
14. P. G. Jamkhande, N. W. Ghule, A. H. Bamer, M. G. Kalaskar, *J. Drug Deliv. Sci. Technol.* **53** (2019) 101174 (<https://doi.org/10.1016/j.jddst.2019.101174>)
15. D. Sharma, S. Kanchi, K. Bisetty, *Arab. J. Chem.* **12** (2019) 3576 (<https://doi.org/10.1016/j.arabjc.2015.11.002>)
16. S. Jadoun, R. Arif, N. K. Jangid, R. K. Meena, *Environ. Chem. Lett.* **19** (2021) 355 (<https://doi.org/10.1007/s10311-020-01074-x>)

17. A. Gour, N. K. Jain, *Artif. Cells Nanomed. Biotechnol.* **47** (2019) 844 (<https://doi.org/10.1080/21691401.2019.1577878>)
18. S. Rajawat, M. S. Qureshi, *Arab. J. Sci. Eng.* **39** (2014) 563 (<http://dx.doi.org/10.1007/s13369-013-0879-4>)
19. L. P. Silva, I. G. Reis, C. C. Bonatto, *Green Processes for Nanotechnology*, V. A. Basiuk, E. V. Basiuk (Eds.), Springer, Berlin, 2015 (http://dx.doi.org/10.1007/978-3-319-15461-9_9)
20. S. Iravani, *Green Chem.* **13** (2011) 2638 (<http://dx.doi.org/10.1039/c1gc15386b>)
21. A. Corciova, B. Ivanescu, *J. Serb. Chem. Soc.* **83** (2018) 515 (<https://doi.org/10.2298/JSC170731021C>)
22. A. K. Jha, K. Prasad, K. Prasad, A. R. Kulkarni, *Colloids Surfaces, B* **73** (2009) 219 (<http://dx.doi.org/10.1016/j.colsurfb.2009.05.018>)
23. M. Rai, A. Yadav, A. Gade, *Crit. Rev. Biotechnol.* **28** (2008) 277 (<http://dx.doi.org/10.1080/07388550802368903>)
24. O. V. Kharissova, H. V. Rasika Dias, B. I. Kharisov, B. O. Perez, V. M. J. Pere, *Trends Biotechnol.* **31** (2013) 240 (<http://dx.doi.org/10.1016/j.tibtech.2013.01.003>)
25. J. Y. Song, B. S. Kim, *Bioprocess. Biosyst. Eng.* **32** (2009) Article 79 (<http://dx.doi.org/10.1007/s00449-008-0224-6>)
26. S. P. Dubey, M. Lahtinen, M. Sillanpää, *Process. Biochem.* **45** (2010) 1065 (<http://dx.doi.org/10.1016/j.procbio.2010.03.024>)
27. A. D. Dwivedi, K. Gopal, *Colloids Surfaces, A* **369** (2010) 27 (<http://dx.doi.org/10.1016/j.colsurfa.2010.07.020>)
28. V. Armendariz, I. Herrera, J. R. Peralta-Videa, M. Jose-Yacaman, H. Troiani, P. Santiago, J. L. Gardea-Torresdey, *J. Nanopart. Res.* **6** (2004) 377 (<https://doi.org/10.1007/s11051-004-0741-4>)
29. S. L. Smitha, D. Philip, K. G. Gopchandran, *Spectrochim. Acta, A* **74** (2009) 735 (<https://doi.org/10.1016/j.saa.2009.08.007>)
30. D. Philip, *Spectrochim. Acta, A* **77** (2010) 807 (<http://dx.doi.org/10.1016/j.saa.2010.08.008>)
31. S. P. Dubey, M. Lahtinen, M. Sillanpää, *Colloids Surfaces, A* **364** (2010) 34 (<http://dx.doi.org/10.1016/j.colsurfa.2010.04.023>)
32. Y. Shao, Y. Jin, S. Dong, *J. Chem. Commun.* **9** (2004) 1104 (<http://dx.doi.org/10.1039/b315732f>)
33. S. Shiv Shankar, A. Ahmad, R. Pasricha, M. Sastry, *J. Mater. Chem.* **13** (2003) 1822 (<http://dx.doi.org/10.1039/B303808B>)
34. S. K. Sivaraman, I. Elango, S. Kumar, V. Santhanam, *Curr. Sci.* **97** (2009) 1055 (<https://scholar.google.com/scholar?oi=bibs&cluster=2564938837098274102&btnI=1&hl=bg>)
35. J. Huang, Q. Li, D. Sun, Y. Lu, Y. Su, X. Yang, H. Wang, Y. Wang, W. Shao, N. He, J. Hong, C. Chen, *Nanotechnology* **18** (2007) 105104 (<http://dx.doi.org/10.1088/0957-4484/18/10/105104>)
36. K. B. Narayanan, N. Sakthivel, *Adv. Colloid Interface Sci.* **169** (2011) 59 (<http://dx.doi.org/10.1016/j.cis.2011.08.004>)
37. Y. N. Tan, J. Y. Lee, D. I. Wang, *J. Am. Chem. Soc.* **132** (2010) 5677 (<http://dx.doi.org/10.1021/ja907454f>)
38. Y. Park, Y. N. Hong, A. Weyers, Y. S. Kim, R. J. Linhardt, *IET Nanobiotechnol.* **5** (2011) 69 (<http://dx.doi.org/10.1049/iet-nbt.2010.0033>)

39. K. D. Arunachalam, S. K. Annamalai, S. Hari, *Int. J. Nanomedicine* **8** (2013) 1307 (<http://dx.doi.org/10.2147/IJN.S36670>)
40. X. Huang, H. Wu, S. Pu, W. Zhang, X. Liao, B. Shi, *Green Chem.* **13** (2011) 950 (<http://dx.doi.org/10.1039/c0gc00724b>)
41. K. N. Thakkar, S. S. Mhatre, R. Y. Parikh, *Nanomed. Nanotechnol. Biol. Med.* **6** (2010) 257 (<http://dx.doi.org/10.1016/j.nano.2009.07.002>)
42. M. G. Heinemann, C. H. Rosa, G. R. Rosa, D. Dias, *Trends Environ. Anal. Chem.* **30** (2021) e00129 (<https://doi.org/10.1016/j.teac.2021.e00129>)
43. S. H. Lee, B. H. Jun, *Int. J. Mol. Sci.* **20** (2019) 865 (<https://doi.org/10.3390/ijms20040865>)
44. L. Xu, Y. Y. Wang, J. Huang, C. Y. Chen, Z. X. Wang, H. Xie, *Theranostics* **10** (2020) 8996 (<https://doi.org/10.7150/thno.45413>)
45. S. Ahmed, Saifullah, M. Ahmad, B. L. Swami, S. Ikram, *J. Radiat. Res. Appl. Sci.* **9** (2016) 1 (<http://dx.doi.org/10.4172/2157-7439.1000309>)
46. S. Ahmed, Annu, K. Manzoor, S. Ikram, *J. Bionanosci.* **10** (2016) 282 (<http://dx.doi.org/10.1166/jbns.2016.1376>)
47. S. Ahmed, S. Ikram, *J. Nanomed. Nanotechnol.* **6** (2015) Article 309 (<http://dx.doi.org/10.4172/2157-7439.1000309>)
48. K. Dziwon, J. Pilit-Prociak, M. Banach, *Chemik: nauka- technika- rynek* **69** (2015) 33 (http://miesiecznikchemik.pl/wp-content/uploads/2015/02/chemik_2015_01-4.pdf)
49. F. Luo, D. Yang, Z. Chen, M. Megharaj, R. Naidu, *Sci. Total Environ.* **562** (2016) 526 (<http://dx.doi.org/10.1016/j.scitotenv.2016.04.060>)
50. S. Venkateswarlu, B. N. Kumar, B. Prathima, B. K. Anitha, N. V. V. Jyothi, *Phys., B* **457** (2015) 30 (<http://dx.doi.org/10.1016/j.physb.2014.09.007>)
51. D. Pujol, C. Liu, N. Fiol, M. À. Olivella, J. Gominho, I. Villaescusa, H. Pereira, *Crops Prod.* **50** (2013) 494 (<http://dx.doi.org/10.1016/j.indcrop.2013.07.051>)
52. S. M. Ghoreishi, M. Behpour, M. Khayatkashani, *Physica, E* **44** (2011) 97 (<http://dx.doi.org/10.1016/j.physe.2011.07.008>)
53. K. Krishnaswamy, H. Vali, V. Orsat, *J. Food Eng.* **142** (2014) 210 (<http://dx.doi.org/10.1016/j.jfoodeng.2014.06.014>)
54. J. Zha, C. Dong, X. Wang, X. Zhang, X. Xiao, X. Yang, *Optik – Int. J. Light Electron. Optics* **144** (2017) 511 (<http://dx.doi.org/10.1016/j.ijleo.2017.06.088>)
55. L. Marchiol, *Ital. J. Agron.* **7** (2012) 274 (<https://doi.org/10.4081/ija.2012.e37>)
56. S. Ahmed, Annu, S. Ikram, S. S. Yudha, *J. Photochem. Photobiol., B* **161** (2016) 141 (<http://dx.doi.org/10.1016/j.jphotobiol.2016.04.034>)
57. G. Sharmila, M. F. Fatima, S. Haries, S. Geetha, N. M. Kumar, C. Muthukumaran, *J. Mol. Struct.* **1138** (2017) 35 (<http://dx.doi.org/10.1016/j.molstruc.2017.02.097>)
58. M. Nasrollahzadeh, S. M. Sajadi, M. Maham, *J. Mol. Catal., A* **396** (2015) 297 (<http://dx.doi.org/10.1016/j.molcata.2014.10.019>)
59. H. S. Devi, T. D. Singh, *Adv. Electron. Electr. Eng.* **4** (2014) 83 (http://www.ripublication.com/aeee_spl/aeeev4n1spl_12.pdf)
60. S. Gunalan, R. Sivaraj, V. Rajendran, *J. Prog. Nat. Sci.: Mater. Int.* **22** (2012) 693 (<http://dx.doi.org/10.1016/j.pnsc.2012.11.015>)
61. K. R. Reddy, *J. Mol. Struct.* **1150** (2017) 553 (<http://dx.doi.org/10.1016/j.molstruc.2017.09.005>)

62. J. Li, F. Sun, K. Gu, T. Wu, W. Zhai, W. Li, S. Huang, *Appl. Catal., A* **406** (2011) 51 (<http://dx.doi.org/10.1016/j.apcata.2011.08.007>)
63. A. Y. Ghidan, T. M. Al-Antary, A. M. Awwad, *Environ. Nanotechnol. Monit. Manage.* **6** (2016) 95 (<http://dx.doi.org/10.1016/j.enmm.2016.08.002>)
64. F. Ijaz, S. Shahid, S. A. Khan, W. Ahmad, S. Zaman, *Trop J. Pharm. Res.* **16** (2017) 743 (<http://dx.doi.org/10.4314/tjpr.v16i4.2>)
65. S. Ahmed, Annu, S. A. Chaudhry, S. Ikram, *J. Photochem. Photobiol., B* **166** (2017) 272 (<http://dx.doi.org/10.1016/j.jphotobiol.2016.12.011>)
66. A. S. H. Hameed, C. Karthikeyan, A. P. Ahamed, N. Thajuddin, N. S. Alharbi, S. Ali Alharbi, G. Ravi, *Sci. Rep.* **6** (2016) 24312 (<http://dx.doi.org/10.1038/srep24312>)
67. A. Nasajpour, S. Mandla, S. Shree, E. Mostafavi, R. Sharifi, A. Khalilpour, S. Saghazadeh, S. Hassan, M. J. Mitchell, J. Leijten, X. Hou, A. Moshaverinia, N. Annabi, R. Adelung, Y. K. Mishra, S. R. Shin, A. Tamayol, A. Khademhosseini, *Nano Lett.* **17** (2017) 6235 (<http://dx.doi.org/10.1021/acs.nanolett.7b02929>)
68. N. Matinise, X.G. Fuku, K. Kaviyarasu, N. Mayedwa, M. Maaza, *Appl. Surf. Sci.* **406** (2017) 339 (<https://doi.org/10.1016/j.apsusc.2017.01.219>)
69. O. J. Nava, C. A. Soto-Robles, C.M. Gomez-Gutierrez, A.R. Vilchis-Nestor, A. Castro-Beltran, A. Olivas, P.A. Luque, *J. Mol. Struct.* **1147** (2017) 1 (<http://dx.doi.org/10.1016/j.molstruc.2017.06.078>)
70. J. Singh, T. Dutta, K.-H. Kim, M. Rawat, P. Samddar, P. Kumar, *J. Nanobiotechnol.* **16** (2018) Article 84 (<https://doi.org/10.1186/s12951-018-0408-4>)
71. A. Mishra, S. K. Tripathy, S.-I. Yun, *J. Nanosci. Nanotechnol.* **11** (2011) 243 (<https://doi.org/10.1166/jnn.2011.3265>)
72. A. Mewada, G. Oza, S. Pandey, M. Sharon, *J. Microbiol. Biotech. Res.* **2** (2012) 493 (<https://scholar.google.co.in/scholar?oi=bibs&cluster=14114070047215590546&btnI=1&hl=en>)
73. B. Syed, N. Prasad, S. Satisha, *J. Microsc. Ultrastruct.* **4** (2016) 162 (<http://dx.doi.org/10.1016/j.jmau.2016.01.004>)
74. B. S. Srinath, V. R. Rai, *Mater. Lett.* **146** (2015) 23 (<http://dx.doi.org/10.1016/j.matlet.2015.01.151>)
75. P. Luo, Y. Liu, Y. Xia, H. Xu, G. Xie, *Biosens. Bioelectron.* **54** (2014) 217 (<http://dx.doi.org/10.1016/j.bios.2013.11.013>)
76. N. Noah, in *Micro and Nano Technologies*, A. Shukla, S. Iravani (Eds.), Elsevier Inc., Amsterdam, 2019, p. 111 (ISBN 978-0-08-102579-6)
77. L. Li, Z. Zhang, *Int. J. Electrochem. Sci.* **11** (2016) 4550 (<http://dx.doi.org/10.20964/2016.06.13>)
78. J. Venkatesan, P. Manivasagan, S.-K. Kim, A. V. Kirithi, S. Marimuthu, A. A. Rahuman, *Bioprocess Biosyst. Eng.* **37** (2014) 1591 (<http://dx.doi.org/10.1007/s00449-014-1131-7>)
79. L. Castro, M. L. Blazquez, J. A. Muñoz, F. González, A. Ballester, *IET Nanobiotechnol.* **7** (2013) 109 (<http://dx.doi.org/10.1049/iet-nbt.2012.0041>)
80. G. Singaravelu, J. S. Arockiamary, V. G. Kumar, K. Govindaraju, *Colloids Surfaces, B* **57** (2007) 97 (<http://dx.doi.org/10.1016/j.colsurfb.2007.01.010>)
81. Y.-L. Chen, H.-Y. Tuan, C.-W. Tien, Y.-C. Hu, *Biotechnol. Prog.* **25** (2009) 1260 (<http://dx.doi.org/10.1002/btpr.199>)
82. P. Mohanpuria, N. K. Rana, S. K. Yadav, *J. Nanoparticle Res.* **10** (2008) 507 (<http://dx.doi.org/10.1007/s11051-007-9275-x>)

83. E. Asadian, M. Ghalkhani, S. Shahrokhian, *Sensors Actuators, B* **293** (2019) 183 (<https://doi.org/10.1016/j.snb.2019.04.075>)
84. J. M. George, A. Antony, B. Mathew, *Microchim. Acta* **185** (2018) Article 358 (<https://doi.org/10.1007/s00604-018-2894-3>)
85. L. Lu, X. Hu, Z. Zhu, Z. D. Li, S. Tian, Z. Chen, *J. Electrochem. Soc.* **167** (2020) Article 037512 (<http://dx.doi.org/10.1149/2.0122003JES>)
86. V. S. Manikandan, B. R. Adhikari, A. Chen, *Analyst* **143** (2018) 4537 (<http://dx.doi.org/10.1039/C8AN00497H>)
87. G. Maduraiveeran, W. Jin, *Trends Environ. Anal.* **13** (2017) 10 (<http://dx.doi.org/10.1016/j.teac.2017.02.001>)
88. R. M. Kakhki, *Russ. J. Appl. Chem.* **89** (2016) 480 (<https://link.springer.com/article/10.1134/S10704272160030204>)
89. R. Ramachandran, S. M. Chen, T. Baskar, P. Elumalai, P. Raja, T. Chen, R. Kannan, D. Kannaiyan, G. K. George, *Inorg. Chem. Front.* **6** (2019) 3418 (<http://dx.doi.org/10.1039/C9QI00602H>)
90. G. Maduraiveeran, M. Sasidharan, V. Ganesan, *Biosens. Bioelectron.* **103** (2018) 113 (<https://doi.org/10.1016/j.bios.2017.12.031>)
91. A. Joshi, K.-H. Kim, *Biosens. Bioelectron.* **153** (2020) Article 112046 (<https://doi.org/10.1016/j.bios.2020.112046>)
92. V. Shukla, R. Yadav, P. Yadav, A. C. Pandey, *J. Hazard. Mater.* **213–214** (2012) 161 (<https://doi.org/10.1016/j.jhazmat.2012.01.071>)
93. S. Momeni, I. Nabipour, *Appl. Biochem. Biotechnol.* **176** (2015) 1937 (<https://doi.org/10.1007/s12010-015-1690-3>)
94. Y. L. Lazarova, T. M. Dodevska, A. M. Slavov, D. B. Karashanova, B. G. Georgieva, *Bulg. Chem. Commun.* **51** (2019) 192 (http://www.bcc.bas.bg/BCC_Volumes/Volume_51_Special_D_2019/BCC-51-D-2019-192-197-Lazarova-40.pdf)
95. K. Murtada, V. Moreno, *J. Electroanal. Chem.* **861** (2020) Article 113988 (<http://dx.doi.org/10.1016/j.jelechem.2020.113988>)
96. N. H. Martin, A. Friedlander, A. Mok, D. Kent, M. Wiedmann, K. J. Boor, *J. Food Prot.* **77** (2014) 1809 (<https://doi.org/10.4315/0362-028X.JFP-14-074>)
97. S. Arefin, M. A. H. Sarker, M.A. Islam, Md. H. Rashid, Md. N. Islam, *J. Adv. Vet. Anim. Res.* **4** (2017) 371 (<http://doi.org/10.5455/javar.2017.d236>)
98. I. A. Ansari, A. K. Datta, *Trans IChemE* **81** (2003) 57 (<https://doi.org/10.1205/096030803765208670>)
99. X. Qin, H. Wang, X. Wang, Z. Miao, Y. Fang, Q. Chen, X. Shao, *Electrochim. Acta* **56** (2011) 3170 (<http://doi.org/10.1016/j.electacta.2011.01.058>)
100. X. Song, X. Wang, Y. Zheng, R. Ma, H. Y. Yin, *J. Nanopart. Res.* **13** (2011) 5449 (<http://doi.org/10.1007/s11051-011-0532-7>)
101. J. B. Raoof, R. Ojani, E. Hasheminejad, S. Rashid-Nadimi, *Appl. Surf. Sci.* **258** (2012) 2788 (<http://doi.org/10.1016/j.apsusc.2011.10.133>)
102. L. Zhong, S. Gan, X. Fu, F. Li, D. Han, L. Guo, L. Niu, *Electrochim. Acta* **89** (2013) 222 (<http://dx.doi.org/10.1016/j.electacta.2012.10.161>)
103. A. M. Noor, M. M. Shahid, P. Rameshkumar, N. M. Huang, *Microchim. Acta* **183** (2016) 911 (<http://dx.doi.org/10.1007/s00604-015-1679-1>)
104. Y. Yang, X. Zheng, J. Zheng, *RSC Adv.* **6** (2016) 58329 (<http://dx.doi.org/10.1039/C6RA06366G>)

105. P. Salazar, I. Fernández, M. C. Rodríguez, A. Hernandez-Creus, J. L. Gonzalez-Mora, *J. Electroanal. Chem.* **855** (2019) Article 113638 (<https://doi.org/10.1016/j.jelechem.2019.113638>)
106. M. Salve, A. Mandal, K. Amreen, K. P. Pattnaik, S. Goel, *Microchem. J.* **157** (2020) 104973 (<https://doi.org/10.1016/j.microc.2020.104973>)
107. T. Dodevska, I. Vasileva, P. Denev, D. Karashanova, B. Georgieva, D. Kovacheva, N. Yantcheva, A. Slavov, *Mater. Chem. Phys.* **231** (2019) 335 (<https://doi.org/10.1016/j.matchemphys.2019.04.030>)
108. R. B. Pegg, F. Shahidi, *Nitrite Curing of Meat*, Food & Nutrition Press Inc., Trumbull, CT, 2008 (<https://scholar.google.com/scholar?oi=bibs&cluster=4739977734055126615&btnI=1&hl=en>)
109. World Health Organization, *Guidelines for Drinking-Water Quality: Fourth Edition Incorporating the First Addendum*, WHO, Geneva, 2017 (ISBN-13: 978-92-4-154995-0)
110. P. K. Rastogi, V. Ganesan, S. Krishnamoorthi, *J. Mater. Chem., A* **2** (2014) 933 (<https://doi.org/10.1039/c3ta13794e>)
111. E. Beamonte, J. D. Bermudez, A. Casino, E. Veres, *J. Environ. Manage.* **83** (2007) 307 (<https://doi.org/10.1016/j.jenvman.2006.03.010>)
112. D. Zhang, H. Ma, Y. Chen, H. Pang, Y. Yu, *Anal. Chim. Acta* **792** (2013) 35 (<http://dx.doi.org/10.1016/j.aca.2013.07.010>)
113. M. Karwowska, A. Kononiuk, *Antioxidants (Basel)* **9** (2020) 241 (<http://dx.doi.org/10.3390/antiox9030241>)
114. T. Dodevska, I. Shterev, Y. Lazarova, *Acta Chim. Slov.* **65** (2018) 970 (<http://dx.doi.org/10.17344/acsi.2018.4672>)
115. M. Shivakumar, K. L. Nagashree, S. Manjappa, M. S. Dharmaprkash, *Electroanalysis* **29** (2017) 1434 (<http://dx.doi.org/10.1002/elan.201600775>)
116. M. Varvara, G. Bozzo, G. Celano, C. Disanto, C. N. Pagliarone, G. V. Celano, *Ital. J. Food Saf.* **5** (2016) 4313 (<http://dx.doi.org/10.4081/ijfs.2016.4313>)
117. S. Kawashima, T. Funakoshi, Y. Sato, N. Saito, H. Ohsawa, K. Kurita, K. Nagata, M. Yoshida, A. Ishigami, *Sci. Rep.* **8** (2018) 16199 (<https://doi.org/10.1038/s41598-018-34530-4>)
118. F. Miao, M.-Y. Su, S. Jiang, L.-F. Luo, Y. Shi, T.-C. Lei, *Oxidative Med. Cell. Longev.* (2019) Article ID 2084805 (<https://doi.org/10.1155/2019/2084805>)
119. K. Dhara, R. M. Debiprosad, *Anal. Biochem.* **586** (2019) 113415 (<https://doi.org/10.1016/j.ab.2019.113415>)
120. M. A. Khalilzadeh, M. Borzoo, *J. Food Drug Anal.* **24** (2016) 796 (<http://dx.doi.org/10.1016/j.jfda.2016.05.004>)
121. V. Sreenivasulu, N. Siva Kumar, M. Suguna, M. Asif, E. H. Al-Ghurabi, Z. X. Huang, Z. Zhen, *Int. J. Electrochem. Sci.* **11** (2016) 9959 (<http://dx.doi.org/10.20964/2016.12.69>)
122. R. Sakthivel, S. Palanisamy, S.-M. Chen, S. Ramaraj, V. Velusamy, P. Yi-Fan, J. M. Hall, S. K. Ramaraj, *J. Taiwan Inst. Chem. Eng.* **80** (2017) 663 (<http://dx.doi.org/10.1016/j.jtice.2017.08.047>)
123. M. Shivakumar, M. S. Dharmaprkash, S. Manjappa, K. L. Nagashree, *J. Iran. Chem. Soc.* **17** (2020) 893 (<https://doi.org/10.1007/s13738-019-01822-z>)
124. R. Karthik, M. Govindasamy, S.-M. Chen, Y.-H. Cheng, P. Muthukrishnan, S. Padmavathy, A. Elangovan, *J. Photoch. Photobiol., B* **170** (2017) 164 (<http://dx.doi.org/10.1016/j.jphotobiol.2017.03.018>)

125. C. Karuppiah, K. Muthupandi, S.-M. Chen, M. A. Ali, P. Selvakumar, A. Rajan, P. Prakash, F. M. A. Al-Hmaid, B.-S. Lou, *RSC Adv.* **5** (2015) 31139 (<http://dx.doi.org/10.1039/C5RA00992H>)
126. J. Bastos-Arrieta, A. Florido, C. Pérez-Ràfols, C. N. Serrano, N. Fiol, J. Poch, I. Villaescusa, *J. Nanomater.* **8** (2018) 946 (<http://dx.doi.org/10.3390/nano8110946>)
127. M. Jaishankar, T. Tseten, N. Anbalagan, B. B. Mathew, K. N. Beeregowda, *Interdiscip. Toxicol.* **7** (2014) 60 (<http://dx.doi.org/10.2478/intox-2014-0009>)
128. H. S. Kim, Y. J. Kim, Y. R. Seo, *J. Cancer Prev.* **20** (2015) 232 (<http://dx.doi.org/10.15430/JCP.2015.20.4.232>)
129. G. G. Kumar, K. J. Babu, K. S. Nahm, Y. J. Hwang, *RSC Adv.* **4** (2014) 7944 (<http://dx.doi.org/10.1039/c3ra45596c>)
130. Y. Zheng, A. Wang, W. Cai, Z. Wang, F. Peng, Z. Liu, L. Fu, *Enzyme Microb. Technol.* **95** (2016) 112 (<http://dx.doi.org/10.1016/j.enzmictec.2016.05.010>)
131. F. Chekin, S. Bagheri, S. Abd Hamid, *J. Chin. Chem. Soc.* **61** (2014) 631 (<http://dx.doi.org/10.1002/jccs.201300463>)
132. R. Liu, Y. Wei, J. Zheng, H. Zhang, Q. Sheng, *Chin. J. Chem.* **31** (2013) 1519 (<http://dx.doi.org/10.1002/cjoc.201300487>)
133. K. Ramachandran, D. Kalpana, Y. Sathishkumar, Y. S. Lee, K. Ravichandran, G. G. Kumar, *J. Ind. Eng. Chem.* **35** (2016) 29 (<http://dx.doi.org/10.1016/j.jiec.2015.10.033>)
134. R. A. Dar, N. G. Khare, D. P. Cole, S. P. Karna, A. K. Srivastava, *RSC Adv.* **4** (2014) 14432 (<http://dx.doi.org/10.1039/c4ra00934g>)
135. T. Dayakar, K. V. Rao, J. Park, K. K. Sadasisvuni, K. R. Rao, N. J. Rambabu, *Mater. Chem. Phys.* **216** (2018) 502 (<https://doi.org/10.1016/j.matchemphys.2018.05.046>)
136. S. H. Mohd Taib, K. Shameli, P. M. Nia, M. Etesami, M. Miyake, R. R. Ali, E. Abouzari-Lotf, Z. Izadiyan, *J. Taiwan Inst. Chem. Eng.* **95** (2019) 616 (<https://doi.org/10.1016/j.jtice.2018.09.021>)
137. R. Emmanuel, C. Karuppiah, S.-M. Chen, S. Palanisamy, S. Padmavathy, P. Prakash, *J. Hazard. Mater.* **279** (2014) 117 (<http://dx.doi.org/10.1016/j.jhazmat.2014.06.066>)
138. R. Karthik, S.-M. Chen, A. Elangovan, P. Muthukrishnan, R. Shanmugam, B.-S. Lou, *J. Colloid Interface Sci.* **468** (2016) 163 (<http://dx.doi.org/10.1016/j.jcis.2016.01.046>)
139. R. Karthik, M. Govindasamy, S.-M. Chen, V. Mani, B.-S. Lou, R. Devasenathipathy, Y.-S. Hou, A. Elangovan, *J. Colloid Interface Sci.* **475** (2016) 46 (<http://dx.doi.org/10.1016/j.jcis.2016.04.044>)
140. D. Gobelli, N. M. Correa, M. Barroso, F. Moyano, P. G. Molina, *Electroanalysis* **27** (2015) 1883 (<http://dx.doi.org/10.1002/elan.201500022>)
141. P. Gnanaprakasam, S. E. Jeena, D. Premnath, T. Selvaraju, *Electroanalysis* **28** (2016) 1885 (<http://dx.doi.org/10.1002/elan.201600002>)
142. A. Pani, T. D. Thanh, N. H. Kim, J. H. Lee, S.-Il Yun, *IET Nanobiotechnol.* **10** (2016) 431 (<http://dx.doi.org/10.1049/iet-nbt.2016.0017>)
143. M. B. Gawande, A. Goswami, F.-X. Felpin, T. Asefa, X. Huang, R. Silva, X. Zou, R. Zboril, R. S. Varma, *Chem. Rev.* **116** (2016) 3722 (<http://dx.doi.org/10.1021/acs.chemrev.5b00482>)
144. S. Momeni, F. Sedaghati, *Microchem. J.* **143** (2018) 64 (<https://doi.org/10.1016/j.microc.2018.07.035>)

145. A. Allegra, G. Spatari, S. Mattioli, S. Curti, V. Innao, R. Ettari, A. G. Allegra, C. Giorgianni, S. Gangemi, C. Musolino, *Medicina (Kaunas)* **55** (2019) Article 638 (<https://doi.org/10.3390/medicina55100638>)
146. S. Sukumar, A. Rudrasenan, D. P. Nambiar, *ACS Omega* **5** (2020) 1040 (<https://doi.org/10.1021/acsomega.9b02857>)
147. J. S. Kumar, M. Jana, P. Khanra, P. Samanta, H. Koo, N. C. Murmu, T. Kuila, *Electrochim. Acta* **193** (2016) 104 (<http://dx.doi.org/10.1016/j.electacta.2016.02.069>)
148. B. Amanulla, S. Palanisamy, S.-M. Chen, V. Velusamy, T.-W. Chiu, T.-W. Chen, S. K. Ramaraj, *J. Colloid Interface Sci.* **487** (2017) 370 (<http://dx.doi.org/10.1016/j.jcis.2016.10.050>)
149. K. S. Prasad, J. V. Vaghasiya, S. S. Soni, J. Patel, R. Patel, M. Kumari, F. Jasmani, K. Selvaraj, *Appl. Biochem. Biotechnol.* **6** (2015) 1386 (<http://dx.doi.org/10.1007/s12010-015-1814-9>)
150. R. Karthik, R. Sasikumar, S.-M. Chen, M. Govindasamy, J.V. Kumar, V. Muthuraj, *Int. J. Electrochem. Sci.* **11** (2016) 8245 (<http://dx.doi.org/10.20964/2016.10.62>)
151. V. Kumar, K. Singh, S. Panwar, S. K. Mehta, *Int. Nano Lett.* **7** (2017) 123 (<http://dx.doi.org/10.1007/s40089-017-0205-3>)
152. E. Ahmed, K. Nagaoka, M. Fayed, M. Abdel-Daim, H. Samir, G. Watanabe, *Environ. Sci. Pollut. Res.* **22** (2015) 10930 (<https://doi.org/10.1007/s11356-015-4245-9>)
153. H. Zhang, K. Taya, K. Nagaoka, M. Yoshida, G. Watanabe, *Environ. Pollut.* **229** (2017) 1 (<https://doi.org/10.1016/j.envpol.2017.04.088>)
154. S. Ren, Y. Li, C. Li, *Gen. Comp. Endocr.* **301** (2021) 113656 (<https://doi.org/10.1016/j.ygcen.2020.113656>)
155. K. Mallikarjuna, Y. V. M. Reddy, B. Sravani, B. G. Madhavi, H. Kim, S. Agarwal, V. K. Gupta, *J. Electroanal. Chem.* **822** (2018) 163 (<https://doi.org/10.1016/j.jelechem.2018.05.019>)
156. X. Fuku, M. Modibedi, M. Mathe, *SN Appl. Sci.* **2** (2020) Article 902 (<https://doi.org/10.1007/s42452-020-2704-5>)
157. F. Chekin, S. M. Vahdat, M. J. Asadi, *Russ. J. Appl. Chem.* **89** (2016) 816 (<https://doi.org/10.1134/S1070427216050219>).



Examination and optimization of lignocellulolytic activity of *Stereum gausapatum* F28 on beechwood sawdust supplemented with molasses stillage

JELENA JOVIĆ^{1*}, JIAN HAO² and LJILJANA MOJOVIĆ^{1#}

¹University of Belgrade, Faculty of Technology and Metallurgy, Department of Biochemical Engineering and Biotechnology, Karnegijeva 4, 11000 Belgrade, Serbia and ²Laboratory of Biorefinery, Shanghai Advanced Research Institute, Chinese Academy of Sciences, Pudong, Shanghai 201210, People's Republic of China

(Received 1 June, revised 26 August, accepted 16 September 2021)

Abstract: This study provides a detailed analysis of the lignocellulolytic activity of a new isolate *Stereum gausapatum* F28, a Serbian autochthonous fungi, on beechwood sawdust supplemented with cheap waste, sugar beet molasses stillage. Advanced multiple response optimization techniques were applied to improve ligninolytic and reduce hydrolytic activity as a requirement for potential biorefinery use. The applied techniques were supposed to select cultivation conditions that would give manganese peroxidase and laccase activities above 0.84 and 0.12 U g⁻¹ substrate, respectively, and cellulase and xylanase activities below 1.12 and 1.4 U g⁻¹ substrate. The optimal cultivation conditions that met the set requirements included molasses stillage concentration of 10 %, substrate moisture content of 53 %, incubation temperature of 23.5 °C, and pH 5.2. The research showed that the addition of molasses stillage had a positive effect on enzyme production and that the optimal stillage concentration differed depending on the enzyme type (for laccase it was <5 %, manganese peroxidase ≈12 %, cellulase ≈21 % and xylanase ≈16 %), which should be taken into consideration when optimizing the desired process.

Keywords: response surface method; genetic algorithm; fungi; biomass; enzymes.

INTRODUCTION

The growth of enzyme usage in industry has increased the demand for novel microbial strains that could be used for the productions of various enzymes to meet the current requirements.¹ Wood-decay fungi are recognized as organisms suitable for the production of the industrially valuable enzymes laccase (EC

* Corresponding author. E-mail: yowitch@gmx.com

Serbian Chemical Society member.

<https://doi.org/10.2298/JSC200601075J>

1.10.3.2), manganese-dependent peroxidase (MnP; EC 1.11.1.13), versatile peroxidase (VP; EC 1.11.1.16), lignin peroxidase (LiP; EC 1.11.1.14), cellulase (EC 3.2.1.4), xylanase (EC 3.2.1.8), and other hemicellulases. These fungi have been extensively examined for application in wastewater treatment, in the pretreatment of biomass to facilitate its conversion to value-added chemicals, and production of lignocellulose-degrading enzymes, which can be used in various processes in the pulp and paper industry, food and beverage, personal care, healthcare, pharmaceutical and other industries.^{2,3}

The application of fungi in the production of enzymes and other industrially and commercially valuable products from lignocellulosic waste and by-products from various industries has been emphasized in recent years. Lignocellulose has attracted attention as it is a renewable and inedible material that is generated in large amounts every year; the agro-industry alone produces about 5 billion metric tons of lignocellulosic waste per year.¹ By-products from various industries pose a danger to the environment; the demands for proper management of this waste have increased, thus enforcing the development of new technologies based on natural systems or processes to remove, purify, or convert this material into value-added products. However, for some agents, such as molasses stillage (MS) – a by-product of the alcohol industry that generates 8–15 L of MS per L of produced alcohol – adequate applications and disposal are still being sought.⁴ The potential solutions include its use as a substrate or a supplement in a lignocellulosic substrate for enhancement of fungal enzyme production (laccase, amylase, xylanase).^{5–7} Still, to recommend the use of this agent in the industry, new fungal isolates have to be examined, and particularly the influence of this agent on their enzyme production/activity.

Enzyme production and product quality can be improved using proper optimization techniques in the production process or system. Biological processes contain a large number of natural variations.⁸ Different parts of a complex network of microbial reactions are affected by various environmental/cultivation factors and factor interactions, making the formulation of appropriate conditions difficult. Increased knowledge about the examined system or process and the reliability of experimental data are prerequisites for overcoming the mentioned difficulties, which can be accomplished by appropriate experimental design and statistical evaluation of the collected results.⁸ The optimization methods can be divided into traditional (one factor at a time) and advanced (statistical/mathematical).⁸ Traditional methods are still used in the initial research to determine the composition of the appropriate medium for the production of a new metabolite or when a new organism is used in the production of an already known metabolite. Advanced methods involve the application of experimental design, in which the experimental phase enables determination of potentially influential factors and development of a predictive model that can be used to optimize factor settings

that give the best value of the response variable.⁹ The advanced methods can be used for the optimization of single or multiple responses. Optimization of a single response usually involves the application of response surface methods (RSM), such as central composite design (CCD) or Box–Behnken design (BBD), while for multiple response optimization, often used methods include desirability function and/or evolutionary algorithms (among which genetic algorithm (GA) is the most often used), or artificial neural networks.¹⁰ This research used CCD of RSM, desirability function, and GA to evaluate the influence of factors and factor interactions on the laccase, manganese peroxidase (MnP), cellulase, and xylanase activity of a fungal isolate, create predictive models, and optimize the cultivation conditions.

The aim of the present research was a detailed analysis of the lignocellulolytic activity of *S. gausapatum* F28, a novel Serbian autochthonous fungal isolate, with the purpose of application in various biotechnological processes – from enzyme production to the pretreatment of lignocellulose. The study examined the effect of MS on the lignocellulolytic activity of this fungus to assess the possibility of using this agent as a supplement to improve the production of ligninolytic or hydrolytic enzymes. The research also examined the possibility of steering the lignocellulolytic activity of this isolate into the desired direction using advanced optimization methods.

EXPERIMENTAL

Organism and substrate

This research examined an isolate *Stereum gausapatum* F28 collected in southern Serbia (previously identified using molecular methods,¹¹ its DNA sequence was deposited in the NCBI GenBank database under the accession number KY264753¹¹). The lignocellulosic substrate was beechwood sawdust obtained from a local sawmill. Sugar beet molasses stillage (MS) was a waste obtained from the local alcohol industry.

Inoculum preparation and cultivation conditions

The active culture was maintained at 30 °C on malt extract agar and every 2–3 weeks transferred to a fresh agar. The inoculum was prepared on an inoculum agar medium (the precise composition was given in a previous research⁵). Three mycelial discs, approximately 10 mm in diameter each, were taken from the edge of 7-day-old inoculum culture and transferred to 100-mL Erlenmeyer flasks containing 4.5 g dry substrate mass of the lignocellulosic substrate. The dry substrate mass was determined using the NREL/TP-510-42621 protocol.¹² The substrate moisture was adjusted using diluted MS (MS concentrations and moisture content are given in Table S-I of the Supplementary material to this paper) or distilled water. The substrate was autoclaved for 30 min before inoculation.

Enzyme extraction and assays

The enzymes were extracted with 50 mL of distilled water, which was added to Erlenmeyer flasks and subsequently shaken for 40 min at 220 rpm and 25 °C, and then filtered through a Whatman No. 1 filter paper and centrifuged at 4185g using a Z-206-A high capacity, compact centrifuge (Hermle Labortechnik GmbH, Wehingen, Germany). The extracts

were stored at 4 °C until use. Enzyme activity assays were conducted within 24 h of the extraction on a Ultrospec 3300 pro spectrophotometer, Amersham Biosciences Ltd., Little Chalfont, UK. The laccase activity was determined using the guaiacol assay, the MnP and VP activities using the Phenol Red assay and the LiP activity using Azure B. These assays were performed according to the procedures provided in the research of Jović *et al.*¹¹ Cellulase (CMCase) and xylanase activity were measured using a modified dinitrosalicylic acid (DNS) reagent method proposed by Miller following the procedure described in detail in the research by Jović *et al.*⁵

Experimental design and optimization

Response surface method. A central composite design (CCD) of the response surface method (RSM) was used to examine the influence of four factors (MS concentration, substrate moisture, temperature and pH) and factor interactions on the ligninolytic and hydrolytic activity of *S. gausapatum* F28. The factors were selected using fractional factorial design before RSM. The CCD of RSM had two blocks, *i.e.*, a factorial block that contained 2⁴ full factorial design (16 star points) and four replicates in the center point, and an axial block with eight axial points and three replicates in the center point. The response values were obtained in 31 experimental runs. The studied system was described using a second-order polynomial equation (Eq. (1)) for each examined response:

$$Y = \beta_0 + \sum \beta_i x_i + \sum \beta_{ij} x_i x_j + \sum \beta_{ii} x_{ii}^2 \quad (1)$$

where $i = 1, 2, \dots, k$ and $j = 1, 2, \dots, k$.

In Eq. (1), Y is a response, x_i/x_j are coded value of the i^{th} factor, k is the number of examined factors, and β_0 , β_i , β_{ii} and β_{ij} are the second order regression coefficients. Each factor was examined at five different levels (-2.098, -1, 0, 1, 2.098). The actual and coded values of the examined factors are given in Table S-I.

Linear regression analysis and diagnostics (R^2 value and diagnostic plots), ANOVA, and “adequate precision” (AP, calculated by Eq. (2)) were used to examine the model quality:

$$AP = (\max(\hat{Y}) - \min(\hat{Y})) / (\sqrt{(p\sigma^2/n)}) \quad (2)$$

where \hat{Y} is prediction at the run settings, p is the number of terms in the model, σ^2 is the mean square of residuals, and n is the number of runs in the design.

Optimization using desirability function and genetic algorithm. A combination of desirability function and GA was used for the optimization of the lignocellulolytic activity of *S. gausapatum* F28. Two types of individual desirability functions were used, *i.e.*, the transformation of maximization for ligninolytic activities and transformation of minimization for hydrolytic activities.

Software and statistical analysis. The software used for the design analysis was R studio version 1.3.959, and R language version 3.6.3,¹³ and R packages RSM,¹⁴ desirability¹⁵ and GA.¹⁶ The values were expressed as mean ± standard deviation. ANOVA was used for comparison of the mean values. Differences were considered significant at $p < 0.05$.

RESULTS AND DISCUSSION

S. gausapatum is the primary colonizer of oak,¹⁷ capable of producing various lignocellulose degrading enzymes. The enzymes of its lignocellulolytic system have been largely identified to date. Still, changes in its lignocellulolytic system have been insufficiently studied, both under different cultivation conditions and different incubation durations, and the information about the utilization of

waste material in lignocellulolytic enzyme production is limited. Understanding these changes could facilitate as well as improve the precision of the application of *S. gausapatum* in specific industrial processes, such as biomass conversion or enzyme production. This research examined the MnP, laccase, cellulase and xylanase activity on beechwood sawdust supplemented with MS. The LiP and VP activities were excluded as less relevant components of the lignocellulolytic system of *S. gausapatum* F28 for lignin degradation based on the screening analysis (fractional factor design), which showed that these activities were at the statistical error level, or under certain conditions completely undetectable.

Response surface method, model design, and model quality analysis

The influences of the examined factors and factor interactions on the activity of laccase, MnP, cellulase and xylanase were investigated using CCD of RSM. The CCD matrix and the predicted and measured response values of general laccase, MnP, cellulase, and xylanase activities and activities per dry substrate mass are given in Tables S-II, S-IIA, S-III and S-III A of the Supplementary material. To explain the correlation between the response variables and factors, second-order polynomial equations were created (Eqs. (S1)–(S4) in the Supplementary material) – laccase activity model (Eq. (S1)), MnP activity model (Eq. (S2)), cellulase activity model (Eq. (S3)), and xylanase activity model (Eq. (S4)).

The applied analysis of regression coefficients and model quality revealed that the generated models needed improvements, and that the effect of blocking was statistically significant in the case of the hydrolytic activities, but not in the case of ligninolytic activities. Statistically insignificant terms were removed gradually until the minimal adequate models with an improved quality and predictability were gained (Eqs. (S1)–(S4)). After each term removal, a model quality check was performed. A particular statistically-not-significant term would be retained in the equation only if the analysis revealed that its removal impaired the model quality and predictability (Tables S-IV–S-VII of the Supplementary material). The term removal reduced the R^2 -value of the models to some extent (Table S-VIII) and lowered the difference between the R^2 and the adjusted R^2 of the obtained minimal models (Table S-IX). Diagnostic plots confirmed the assumptions of the regression (linearity, normal distribution, homoscedasticity and presence/absence of influential data points). The plots are presented in Figs. S-1–S-4 of the Supplementary material, while the calculated AP-values confirmed good signal (Table S-IX), which indicated a good quality of all four minimal adequate models.

Influence of the examined factors on the ligninolytic and hydrolytic activity

The influence of factors and factor interactions on the ligninolytic and hydrolytic activities of the fungal isolate was examined and visualized using contour plots. The contour plots were created by plotting the response values against any

two independent variables while keeping the other variables at their central (0) level. It was revealed that the MS concentration and substrate moisture had the greatest influence on the ligninolytic and hydrolytic activity.

The laccase model is a min–max function with stationary points at an MS concentration of 16.6 %, a substrate moisture of 67.9 %, a temperature of 24.5 °C, and a pH of 6.4. The contour plots show that high laccase activity could be obtained at higher temperature (above 25 °C), low MS concentration (below 5 %), pH around 5.5, and substrate moisture between 70 and 80 % (Figs. S-6a and c and S-7 of the Supplementary material). Stationary points obtained for the MnP activity – an MS concentration of 12.62 %, a substrate moisture of 70 %, a temperature of 27.5 °C, and a pH of 5.6 – are points of maximum; hence, they represent the optimal cultivation conditions for MnP activity (Figs. S-6b and d and S-8). In general, lower values of temperature and substrate moisture are expected for MnP production.⁵ However, the optimal temperature depends on the fungal species or strain, and it can vary from 25 (recorded for some species such as *Trametes hirsuta*^{5,18}) to 35 °C (for species such as *Trametella trogii*¹⁸). According to the studies conducted by Humphrey and Siggers, and Herrick,^{19,20} *S. gausapatum* is a species that grows at lower temperatures. Its optimal growth temperature is around 24–25 °C, but it can grow at temperatures between 5 and 33 °C, although at maximum or minimum values of this range, it grows very little, while at 38 °C, its growth is completely inhibited. In this research, *S. gausapatum* F28 grew poorly at 33 °C, while at 37 °C, its growth was completely inhibited. Therefore, the optimal temperature for laccase production could be expected at temperatures up to 30 °C.

The optimal substrate moisture for the production of ligninolytic enzymes also depends on the fungal species. Different studies reported good ligninolytic enzyme production at a substrate moisture content between 65 to 90 %,^{21,22} while the optimal moisture content for fungal growth and biomass utilization can range from 30²² to 90 %.²¹ The level of the initial substrate moisture influences the production of ligninolytic enzyme, more specifically, the type of ligninolytic enzyme. A higher moisture level (80–90 %) is often reported as more suitable for laccase production,^{5,11,21} while a lower moisture level (50–65 %) for MnP production.^{5,21} A good production of ligninolytic enzymes is often reported at pH 5.²² MS is not extensively examined as a supplement for the production of ligninolytic enzymes. A previous study with *Trametes hirsuta* F13 showed that a high concentration of this agent (above 20 %)⁵ was required for laccase production. In the case of *S. gausapatum* F28, examined in the current research, the laccase production requires a low concentration of this agent (below 5 %), while the optimal MS concentration for MnP production obtained for *S. gausapatum* F28 (12.62 %) was close to that obtained for *T. hirsuta* F13 (14.36 %).⁵ The

optimal concentration of MS required for the production of laccase may depend on the fungal species.

According to the performed RSM analysis, only two factors had a statistically significant influence on the cellulase activity, *i.e.*, the MS concentration and the substrate moisture. The stationary points obtained for the cellulase activity model – MS concentration of 21.58 % and substrate moisture of 82.76 % – were the points of maximum and represent the optimal conditions for cellulase production (Fig. S-5d). Three factors had a statistically significant influence on the xylanase activity, *i.e.*, the MS concentration, the substrate moisture, and pH (Fig. S-5a–c). The stationary points obtained for the xylanase model were also the points of maximum, which indicates optimal cultivation conditions. These conditions included an MS concentration of 16.26 %, a substrate moisture of 70 %, and a pH of 5.6. The moisture content is a critical parameter for the production of cellulases and xylanases, and depending on the fungal species and origin of the lignocellulosic substrate, the optimal moisture content could vary from 60 to 80 %.²³ The optimal pH value also depends on the fungal species; pH values between 4 and 6.5 are often reported as optimal for the production of hydrolytic enzymes.^{23,24} Studies that examined the use of stillage in the production of fungal cellulase or xylanase are still rare. In a study conducted by Acharya *et al.*,⁷ an increase in the concentration of anaerobically treated distillery spent wash improved cellulase production by *Aspergillus ellipticus*. In the study conducted by Shahryari,⁶ the addition of tin stillage from a residual stream of the whole-wheat ethanol process positively affected the production of xylanase by *Neurospora intermedia*. The influence of MS on the fungal production of xylanase has not hitherto been reported. According to the results obtained in the current research with *S. gausapatum* F28, the addition of the appropriate MS concentration can improve the production of xylanase and cellulase. However, a higher MS concentration is required for the production of cellulase ($\approx 21\%$) than for xylanase production ($\approx 16\%$).

Optimization of the lignocellulolytic activity

The optimization process took into consideration changes in the enzyme content under different cultivation conditions and the role and importance of certain lignocellulolytic enzymes in biomass degradation. The aim was to determine cultivation conditions that would promote ligninolytic and reduce hydrolytic activities, bearing in mind the potential application in the pretreatment of lignocellulosic biomass. Variations that exist among lignocellulose of different origins and the complex structure of this material make selection and optimization of a proper pretreatment method difficult. However, some requirements, such as efficient lignin removal and recovery of a high percentage of holocellulose, apply to all pretreatment methods.²⁵ In the case of the biological process, the production

organism would need a certain amount of consumable carbohydrates to survive during the pretreatment, which further complicates process optimization.

The dominant ligninolytic activity of *S. gausapatum* F28 on beechwood sawdust supplemented with MS was MnP activity. This enzyme is crucial for the initial lignin degradation.²⁶ The optimization goal was to improve ligninolytic activity; yet, the research showed that different cultivation conditions promoted laccase or MnP activity, but not both simultaneously. However, the differences observed with *S. gausapatum* F28 were less extreme than in a previous study with *T. hirsuta* F13.⁵

The optimization took the next best approach by prioritizing MnP production and adjusting laccase production accordingly. The laccase activity values varied between 0.04 and 0.24 U g⁻¹ of dry substrate, but the most common activity values ranged between 0.11 and 0.17 U g⁻¹. Under the conditions that yielded moderate laccase activity (0.12–0.17 U g⁻¹), a fairly high MnP activity was observed (≥ 0.84 U g⁻¹). The cultivation conditions that yielded laccase activity below 0.06 U g⁻¹ were hostile for ligninolytic and hydrolytic enzymes. It was also noticed that, under the conditions that yielded laccase activity above 0.17 U g⁻¹, the recorded MnP activity was extremely low (the values were below 0.34 U g⁻¹, see Table S-II). Laccase and MnP activity values of 0.12 and 0.84 U g⁻¹, respectively, were chosen as the desired minimum activities and set as lower limits in the function of maximization. The values were selected based on the obtained results, observations, and the enzyme importance for lignin degradation.²⁶ The chosen upper limits of MnP and laccase activities were the values that, when transformed by the function of maximization, gave the highest possible value below 1 to enable the selection of a single and objective solution. The scale factor for the laccase model was set at 0.1 to slow growth toward 0.17 U g⁻¹. The scale factor for the MnP model was set at 3 to enable rapid achievement of high MnP activities.

The function of minimization was used to lower the cellulase and xylanase activity. A cellulase activity of 1.12 U g⁻¹ and a xylanase activity of 1.4 U g⁻¹ were set as the upper limits. Each of them makes about 40 % of the highest achieved corresponding activity value (Table S-II). These values were selected based on the RSM analysis as the values that would not jeopardize achieving an MnP activity above 0.84 U g⁻¹. The lower limits were chosen as values that, when transformed by the function of minimization, give the highest possible value below 1. As the production organism requires some sugar from the substrate to survive, the fast achievement of too low activity values could be counterproductive, therefore, the scale factors were set at 0.1.

The cultivation conditions selected using a GA were an MS concentration of 10 %, a substrate moisture of 53 %, a temperature of 23.5 °C, and a pH of 5.2. These conditions were expected to yield a laccase activity of 0.13 U g⁻¹, an MnP

of 1.28 U g^{-1} , a cellulase value of 0.93 U g^{-1} , and an xylanase value of 1.27 U g^{-1} . The overall desirability value was 0.568 (Fig. S-9 of the Supplementary material).

Validation of the predicted optimum and importance of molasses stillage

The optimal cultivation conditions gave the following activity values: laccase 0.17 ± 0.01 , MnP 1.05 ± 0.05 , cellulase 1.11 ± 0.05 and xylanase $1.40 \pm 0.12 \text{ U g}^{-1}$. The differences between experimental and predicted values were not statistically significant ($p > 0.05$; Fig. 1).

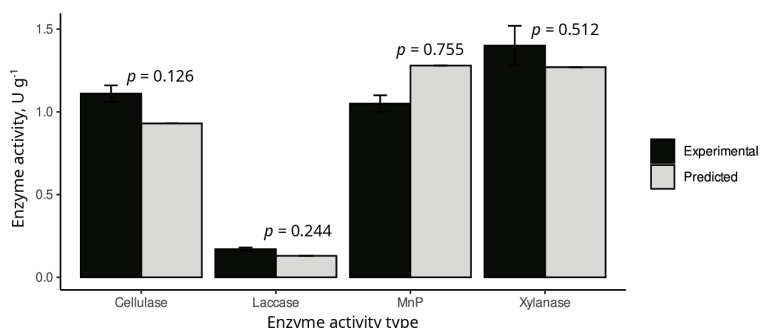


Fig. 1. Data validation, comparison of the experimental and predicted laccase, MnP, cellulase, and xylanase activity values after seven days of incubation under the optimal cultivation conditions.

The same optimal conditions, but without the addition of MS, were applied to examine the contribution of MS to the enzyme production. The results showed that the addition of MS improved laccase activity by about 18 % and MnP activity by about 55 %, which confirmed that MS could be used as a supplement for improved production of ligninolytic enzymes of *S. gausapatum* F28.

The improvement in the laccase activity was not statistically significant ($p = 0.811 > 0.05$), while the improvement in the MnP activity, which was prioritized in the optimization, was significant ($p = 0.022 < 0.05$). The achieved hydrolytic activities were low and in accordance with the set optimization conditions; although, the activity values produced in the presence of MS were similar to those obtained in its absence (Fig. 2).

Cultivation conditions change over time, which directly affects the production of enzymes of the fungal lignocellulolytic system and indirectly affects the processes in which these enzymes participate, such as biomass decomposition. In previous research, *S. gausapatum* F28 showed high efficiency in biomass decomposition but low selectivity in comparison to *T. hirsuta* F13.¹¹ That research did not investigate fluctuations and profile of lignocellulolytic activities involved in a more than 30-day long biomass treatment. However, current research examined changes in the lignocellulolytic system of *S. gausapatum* F28 to provide more

insights for a better understanding of previous results, which could help to develop methods to improve a process during an extended course of cultivation. The laccase and MnP activities decreased drastically after 18 and 33 days of incubation (Fig. 2). The laccase activities measured in the absence of MS were similar to those obtained in the presence of MS (the values were below 0.03 U g⁻¹ in both cases). By the 18th day of incubation, in the presence of MS, the MnP activity dropped to 0.39±0.02 U g⁻¹, and then, by the 33rd day, it had increased to 0.68±0.01 U g⁻¹. These activities were higher than the corresponding activities obtained without MS supplementation by ≈44 and ≈66 %, respectively. The cellulase activity increased after 18 days of incubation to 1.58±0.11 U g⁻¹ on a substrate supplemented with MS, and by the 33rd day, it had decreased by 12 % to the value of 1.41±0.22 U g⁻¹. Without MS supplementation, the cellulase activity changed only slightly, it first rose to 1.15 U g⁻¹ (18th day) and then decreased to 1.11 U g⁻¹ (33rd day). After 18 days of cultivation on the substrate supplemented with MS, the xylanase activity decreased only slightly (≈6 %), and by the 33rd day, it had dropped by an additional 19 % to 0.71 U g⁻¹. After 18 days of incubation, without MS supplementation, the xylanase activity decreased by ≈42 %, and by the 33rd day by an additional 3 % to the final value of 0.71 U g⁻¹.

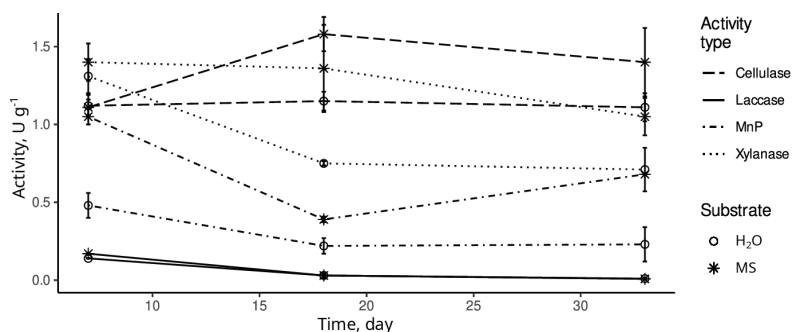


Fig. 2. Influence of MS and changes in lignocellulolytic activity during 33 days of incubation.

Potential for industrial use

Fungi that are capable to produce highly active enzymes and to withstand harsh conditions are targeted for industrial use. Most of the fungi already used in industry have been genetically modified to meet these requirements, but new organisms able to produce enzymes in higher amounts or with new characteristics are still being sought. Fungi often examined for industrial use belong to genera *Pleurotus*, *Daedaleopsis*, *Ganoderma*, *Irpex*, *Polyporus*, *Pycnoporus*, *Bjerkandera*, *Lentinus*, etc. They are examined for the production of industrial enzymes or other industrial applications such as biomass conversion to valuable chemicals, dye removal and for degradation of organic phenolic and non-phenolic compounds, or wastewater treatment. For example, Tripathi *et al.*²⁷ examined the

production of ligninolytic enzymes by *Bjerkandera adusta* and *Lentinus squarrosulus* and reported laccase activities of ≈ 5.5 and 64 U L^{-1} , and MnP activities of ≈ 215 and 370 U L^{-1} , respectively. A study conducted by Eichlerová and Baldrian²⁸ examined potential candidates for industrial use that belong to the genera *Pleurotus*, *Daedaleopsis*, *Ganoderma*, *Irpea*, *Polyporus*, *Pycnoporus*, etc. This study was focused on laccase and MnP enzyme production and fungal application in dye degradation. The enzyme activities differed depending on the fungal species and ranged from $0.04\text{--}106 \text{ U L}^{-1}$ for laccase, and $0.09\text{--}20.36 \text{ U L}^{-1}$ for MnP enzymes with the best laccase activity values obtained with *P. ostreatus* ($\approx 106 \text{ U L}^{-1}$), *Cyclocybe erebia* ($\approx 114 \text{ U L}^{-1}$), and *Abortiporus biennis* ($\approx 103 \text{ U L}^{-1}$), and the best MnP values were recorded for *Omphalina mutila* ($\approx 20 \text{ U L}^{-1}$), *Hericium erinaceus* ($\approx 17 \text{ U L}^{-1}$), and *Mycetinis alliaceus*, *Phellinus robustus*, *Inonotus obliquus* and *Fomitiporia mediterranea* each with an activity of about 16 U L^{-1} . *S. gausapatum* used in the current research showed the maximum laccase activity of 0.23 U g^{-1} (20.1 U L^{-1}) and maximum MnP activity of 1.38 U g^{-1} (123.3 U L^{-1} ; see Table S-IIA) which puts this isolate in the group of good MnP and laccase producers, and as a candidate for industrial application.

Production of enzymes depends on the substrate type and fungal isolate. Substrates with a lower amount of lignin and a higher amount of polysaccharides are more suitable for the production of hydrolytic enzymes than substrates with a higher share of lignin, such as beechwood sawdust. A study conducted by Namnuch *et al.*²⁹ examined CMCase and xylanase production by *A. flavus* KUB2 on various substrates. The best activity was obtained on sugarcane bagasse (CMCase 1.04 U mL^{-1} and xylanase 258.38 U mL^{-1}) while the lowest values were reported for production on sawdust (CMCase 0.06 U mL^{-1} and xylanase 14.07 U mL^{-1}). The maximum CMC and xylanase activities obtained with *S. gausapatum* F28 used in the current research were 1.87 U g^{-1} (166.54 L^{-1}) and 1.66 U g^{-1} (148.09 U L^{-1}), respectively, showing potential for CMC production; however, more investigation of various substrates to find the most suitable substrate for hydrolytic enzyme production is needed.

CONCLUSIONS

This research examined and optimized the lignocellulolytic system of Serbian autochthonous isolate *S. gausapatum* F28 on beechwood sawdust supplemented with MS. Advanced multiple response optimization methods were used to enhance ligninolytic and reduce hydrolytic activity. Based on the results, *S. gausapatum* F28 can grow and produce enzymes laccase, MnP, cellulase and xylanase on waste biomass (beechwood sawdust), while cheap waste, MS, can be used to improve the production of these enzymes. The optimal MS concentration is different for the production of each enzyme type. Another important cultivation factor, substrate moisture content, also differed depending on the enzyme

type. Variations in the optimal pH and temperature were less distinct and therefore less influential. *S. gausapatum* is an insufficiently researched species, but based on the results obtained for the isolate F28, its characteristics are promising for use in biorefinery or enzyme production.

SUPPLEMENTARY MATERIAL

Additional data and information are available electronically at the pages of journal website: <https://www.shd-pub.org.rs/index.php/JSCS/article/view/10808>, or from the corresponding author on request.

Acknowledgements. The Research presented in this paper was funded by the Ministry of Education, Science and Technological Development of the Republic of Serbia (Project #I-1). It is a part of Scientific and Technological Collaboration of Republic of Serbia and the People's Republic of China

ИЗВОД

ИСПИТИВАЊЕ И ОПТИМИЗАЦИЈА ЛИГНОЦЕЛУЛОЛИТИЧКЕ АКТИВНОСТИ *S. GAUSAPATUM* F28 НА ПИЉЕВИНИ БУКВЕ СА ДОДАТКОМ МЕЛАСНЕ ЦИБРЕ

ЈЕЛЕНА ЈОВИЋ¹, ЈИАН НАО² и ЉИЉАНА МОЈОВИЋ¹

¹Универзитет у Београду, Технолошко-мештаришки факултет, Кафедра за биохемијско инжењерство и биотехнологију, Карнејијева 4, 11000 Београд и ²Laboratory of Biorefinery, Shanghai Advanced Research Institute, Chinese Academy of Sciences, Pudong, Shanghai 201210, People's Republic of China

Ово истраживање детаљно анализира лигноцелулолитичку активност изолата *S. gausapatum* F28, аутотоне гљиве Србије, на пиљевини букве суплементисане јефтиним отпадом – меласном цибром пореклом од шећерне репе. Примењене су напредне технике оптимизације вишеструких одговора ради унапређења лигнинолитичке и смањења хидролитичке активности фунгалног изолата као услова за потенцијалну примену у биорадијерским поступцима. Примењеном техникама требало је да се одаберу услови култивације који би дали активности ензима манган пероксидаза и лаказа изнад 0,84 U g⁻¹, односно 0,12 U g⁻¹ супстрата, и активности целулаза и ксиланаза испод 1,12 U g⁻¹, односно 1,4 U g⁻¹ супстрата. Оптимални услови којима су испуњени постављени захтеви укључују концентрацију цибре од 10 %, влажност супстрата од 53 %, температуру инкубације од 23,5 °C и pH 5,2. Истраживање је показало да је додатак меласне цибре позитивно утицао на производњу ензима, али и да се оптимална концентрација цибре разликује за различиту врсту ензима (лаказа <5 %, манган пероксидаза ~12 %, целулаза ~21 %, ксиланаза ~16 %), на шта треба обратити пажњу приликом оптимизације жељеног процеса.

(Примљено 1. јуна, ревидирано 26. августа, прихваћено 16. септембра 2021)

REFERENCES

1. S. Bharathiraja, J. Suriya, M. Krishnan, P. Manivasagan, S.-K. Kim, in *Advances in Food and Nutrition Research*, S.-K. Kim, F. Toldrá (Eds.), Academic Press, Cambridge, MA, 2017, pp. 125–148 (<https://dx.doi.org/10.1016/bs.afnr.2016.11.003>)
2. A. P. Singh, T. Singh, *Biomass Bioenergy* **62** (2014) 198 (<https://dx.doi.org/10.1016/j.biombioe.2013.12.013>)

3. O. B. Chukwuma, M. Rafatullah, H. A. Tajarudin, N. Ismail, *Sustainability* **12** (2020) 7282 (<https://dx.doi.org/10.3390/su12187282>)
4. W. Mikucka, M. Zielińska, *Appl. Biochem. Biotechnol.* **192** (2020) 770 (<https://dx.doi.org/10.1007/s12010-020-03343-5>)
5. J. Jović, J. Hao, S. Kocić-Tanackov, L. Mojović, *Biomass Convers. Biorefinery* (2020) (<https://dx.doi.org/10.1007/s13399-020-00929-1>)
6. Z. Shahryari, M. H. Fazaelipoor, Y. Ghasemi, P. R. Lennartsson, M. J. Taherzadeh, *Molecules* **24** (2019) 721 (<https://dx.doi.org/10.3390/molecules24040721>)
7. B. K. Acharya, S. Mohana, R. Jog, J. Divecha, D. Madamwar, *J. Environ. Manage.* **91** (2010) 2019 (<https://dx.doi.org/10.1016/j.jenvman.2010.05.001>)
8. V. Singh, S. Haque, R. Niwas, A. Srivastava, M. Pasupuleti, C. K. M. Tripathi, *Front. Microbiol.* **7** (2017) (<https://dx.doi.org/10.3389/fmicb.2016.02087>)
9. D. Palhazi Cuervo, P. Goos, K. Sørensen, *Stat. Comput.* **26** (2016) 15 (<https://dx.doi.org/10.1007/s11222-014-9467-z>)
10. R. Noorossana, S. Davanloo Tajbakhsh, A. Saghaei, *Int. J. Adv. Manuf. Technol.* **40** (2009) 1227 (<https://dx.doi.org/10.1007/s00170-008-1423-7>)
11. J. Jović, A. Buntić, N. Radovanović, B. Petrović, L. Mojović, *Food Technol. Biotechnol.* **56** (2018) 354 (<https://dx.doi.org/10.17113/ftb.56.03.18.5348>)
12. A. Sluiter, B. Hames, D. Hyman, C. Payne, R. Ruiz, C. Scarlata, J. Sluiter, D. Templeton, J. Wolfe, *Biomass and Total Dissolved Solids in Liquid Process Samples, Technical Report*, National Renewable Energy Laboratory, Golden, CO, 2008, p. 9 (<https://www.nrel.gov/docs/gen/fy08/42621.pdf>)
13. R Core Team, *R: A language and environment for statistical computing*, R Foundation for Statistical Computing, Vienna, 2020 (<https://www.R-project.org>)
14. R. V. Lenth, *J. Stat. Softw.* **32** (2009) 1 (<http://dx.doi.org/10.18637/jss.v032.i07>)
15. M. Kuhn, *Desirability: function optimization and ranking via desirability functions*, R package version 2.1, 2016 (<https://CRAN.R-project.org/package=desirability>)
16. L. Scrucca, *J. Stat. Softw.* **53** (2013) 1 (<http://dx.doi.org/10.18637/jss.v053.i04>)
17. L. Boddy, D. W. Bardsley, O. M. Gibbon, *New Phytol.* **107** (1987) 143 (<https://dx.doi.org/https://doi.org/10.1111/j.1469-8137.1987.tb04888.x>)
18. E. Krumova, N. Kostadinova, J. Miteva-Staleva, G. Stoyancheva, B. Spassova, R. Abrashev, M. Angelova, *Eng. Life Sci.* **18** (2018) 692 (<https://dx.doi.org/https://doi.org/10.1002/elsc.201800055>)
19. J. A. Herrick, *Ohio J. Sci.* **39** (1939) 254 (<https://kb.osu.edu/handle/1811/3038>)
20. C. J. Humphrey, P. V. Siggers, *J. Agric. Res.* **47** (1933) 997 (<https://naldc.nal.usda.gov/download/IND43968250/PDF>)
21. G. C. dos Santos Bazanella, D. F. de Souza, R. Castoldi, R. F. Oliveira, A. Bracht, R. M. Peralta, *Folia Microbiol. (Praha)* **58** (2013) 641 (<https://dx.doi.org/10.1007/s12223-013-0253-7>)
22. P. A. Geethanjali, H. G. Gowtham, M. Jayashankar, *Bull. Natl. Res. Cent.* **44** (2020) 173 (<https://dx.doi.org/10.1186/s42269-020-00426-5>)
23. A. Kumar, *Int. J. Microbiol.* **2020** (2020) e8894215 (<https://dx.doi.org/https://doi.org/10.1155/2020/8894215>)
24. L. M. Legodi, D. La Grange, E. L. J. van Rensburg, I. Ncube, *Enzyme Res.* **2019** (2019) e1390890 (<https://dx.doi.org/https://doi.org/10.1155/2019/1390890>)
25. M. Galbe, O. Wallberg, *Biotechnol. Biofuels* **12** (2019) 294 (<https://dx.doi.org/10.1186/s13068-019-1634-1>)

26. R. Reina, H. Kellner, J. Hess, N. Jehmlich, I. García-Romera, E. Aranda, M. Hofrichter, C. Liers, *PLOS ONE* **14** (2019) e0212769 (<https://dx.doi.org/10.1371/journal.pone.0212769>)
27. A. Tripathi, R. C. Upadhyay, S. Singh, *Indian J. Microbiol.* **52** (2012) 381 (<https://dx.doi.org/10.1007/s12088-011-0232-0>)
28. I. Eichlerová, P. Baldrian, *J. Fungi* **6** (2020) 301 (<https://dx.doi.org/10.3390/jof6040301>)
29. N. Namnuch, A. Thammasittirong, S. N.-R. Thammasittirong, *Mycology* **12** (2021) 119 (<https://dx.doi.org/10.1080/21501203.2020.1806938>).

**SUPPLEMENTARY MATERIAL TO
Examination and optimization of lignocellulolytic activity of
Stereum gausapatum F28 on beechwood sawdust supplemented
with molasses stillage**

JELENA JOVIĆ¹*, JIAN HAO² and LJILJANA MOJOVIĆ¹

¹University of Belgrade, Faculty of Technology and Metallurgy, Department of Biochemical Engineering and Biotechnology, Karnegijeva 4, 11000 Belgrade, Serbia and ²Laboratory of Biorefinery, Shanghai Advanced Research Institute, Chinese Academy of Sciences, Pudong, Shanghai 201210, People's Republic of China

J. Serb. Chem. Soc. 87 (4) (2022) 437–450

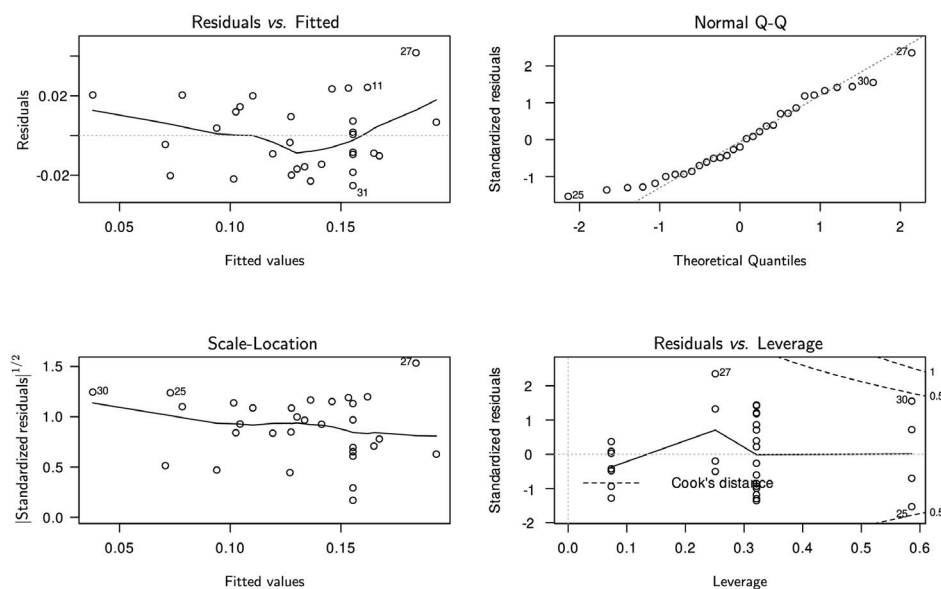


Fig. S-1. Diagnostic plots for examination of the generated laccase activity model.

*Corresponding author. E-mail: yowitch@gmx.com

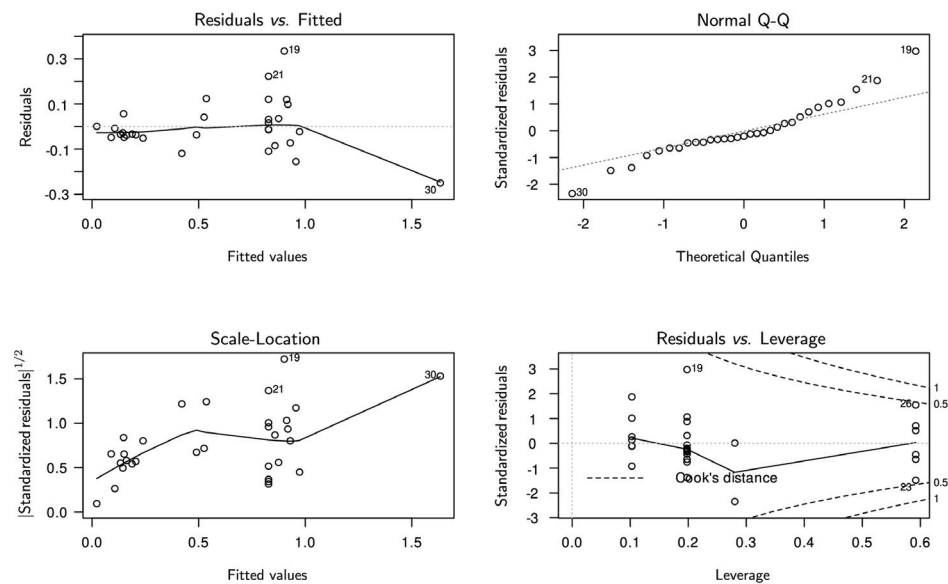


Fig. S-2. Diagnostic plots for examination of the generated MnP activity model.

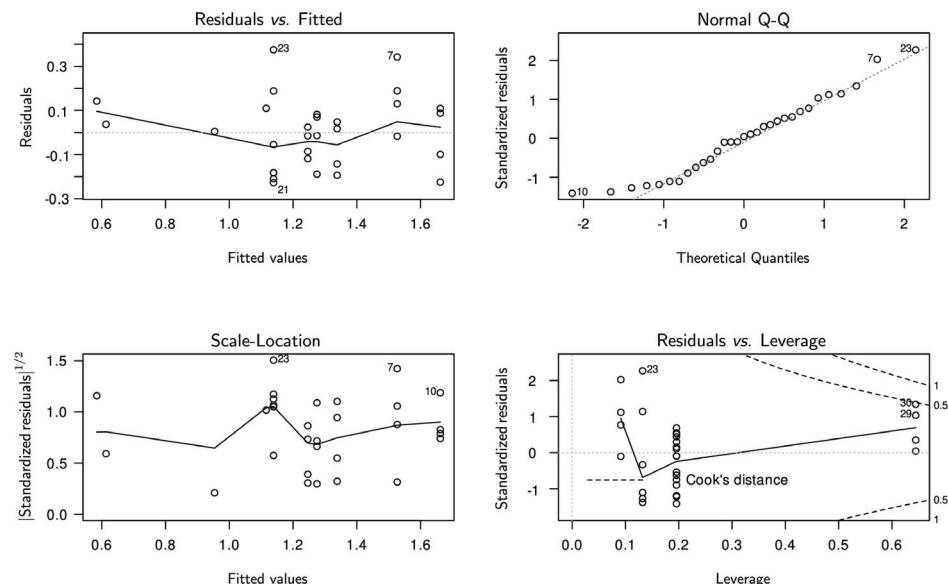


Fig. S-3. Diagnostic plots for examination of the generated cellulase activity model.

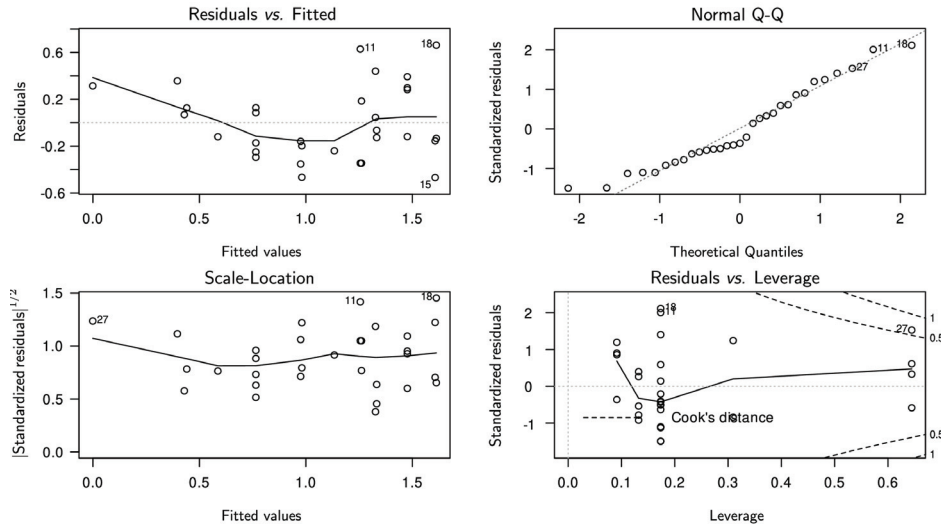


Fig. S-4. Diagnostic plots for examination of the generated xylanase activity model

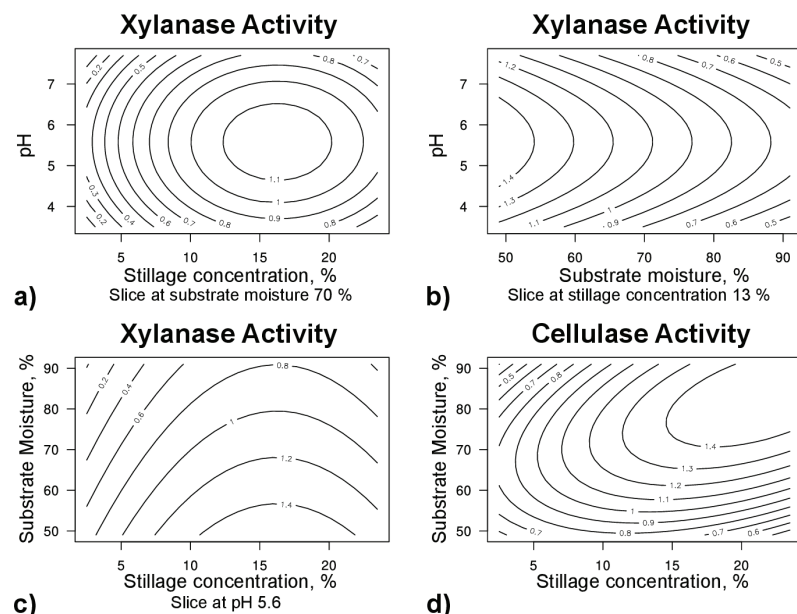


Fig. S-5. Contour plots showing the influence of a) pH and molasses stillage concentration (at a constant substrate moisture of 70 %), b) pH and substrate moisture (at a constant molasses stillage concentration of 13 %), and c) substrate moisture and MS concentration (at a constant temperature of 27 °C and pH 5.6) on the xylanase activity and the influence of substrate moisture and MS concentration on cellulase activity (at constant temperature of 27 °C and pH 5.6).

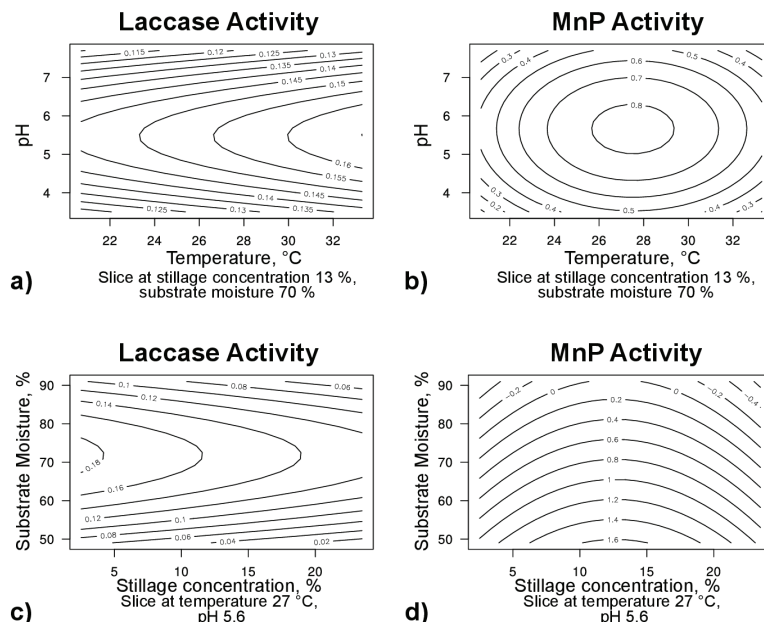


Fig. S-6. Influence of pH and temperature on a) laccase and b) MnP activity at a constant molasses stillage concentration of 13 % and a constant substrate moisture of 70 %, and influence of substrate moisture and MS concentration on c) laccase, d) MnP at a constant temperature and pH of 27 °C and 5.6, respectively.

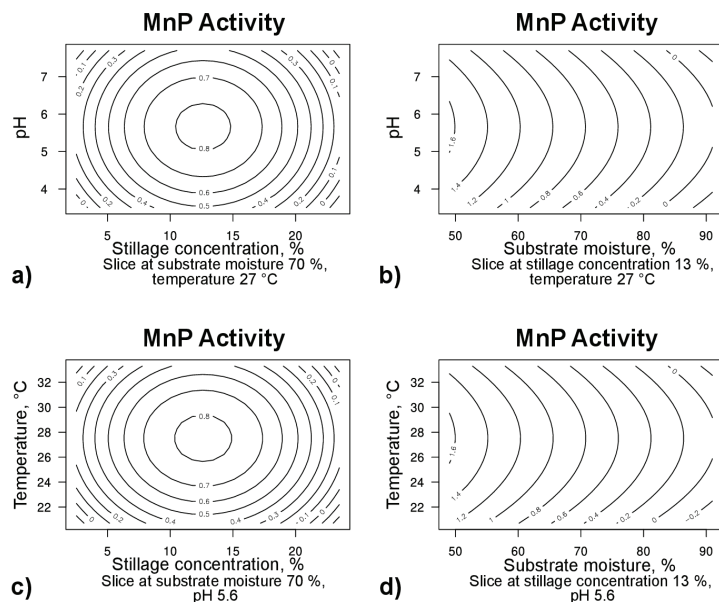


Fig. S-7. Contour plots showing the influence of a) pH and molasses stillage concentration, b) pH and substrate moisture, c) temperature and molasses stillage concentration, and d) temperature and substrate moisture on the laccase activity of *S. gausapatum* F28.

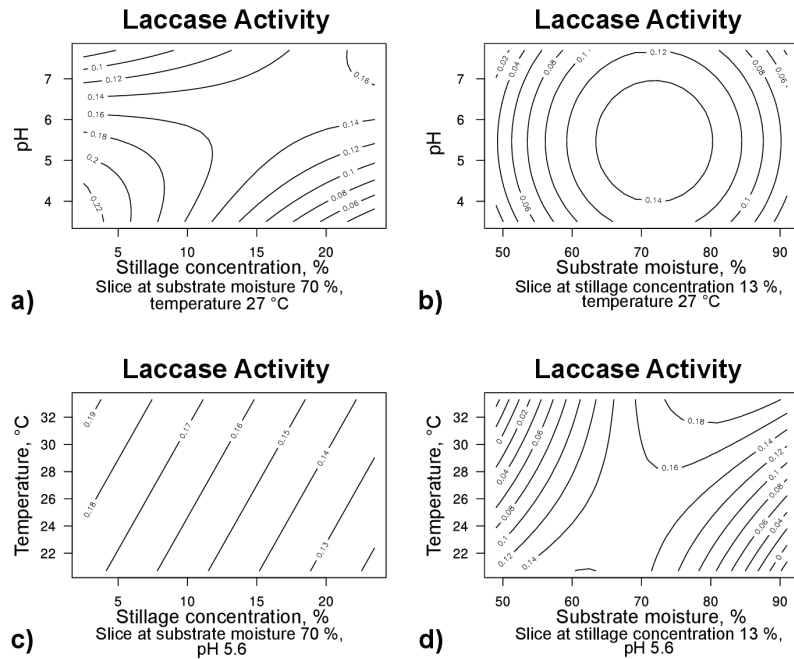


Fig. S-8. Contour plots showing the influence of a) temperature and molasses stillage concentration, b) pH and molasses stillage concentration, c) temperature and substrate moisture, and d) pH and substrate moisture on the MnP activity of *S. gausapatum* F28.

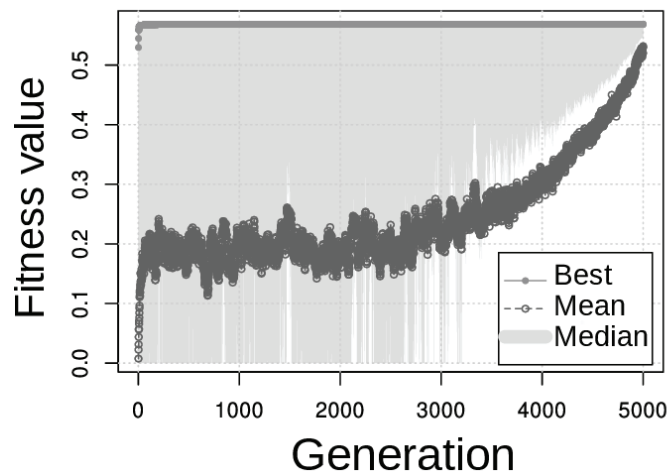


Fig. S-9. Genetic algorithm simulation.

TABLE S-I. Actual and coded values of variables.

Variable	Coded values of variables				
	- α	-1	0	1	α
Real values of variables					
MS concentration, % (<i>A</i>)	2.5	8	13	18	23.5
Substrate moisture, % (<i>B</i>)	49	60	70	80	91
Temperature, °C (<i>C</i>)	21	24	27	30	33
pH (<i>D</i>)	3.5	4.6	5.6	6.6	7.7

TABLE S-II. Central composite design matrix with coded factor values and predicted and measured response values of laccase activity (LA) and MnP activity (MA) per dry substrate mass. The data are presented in standard order of experiments. Independent variables (factors) examined in this research were molasses stillage concentration (*A*), substrate moisture (*B*), incubation temperature (*C*), and pH value (*D*). (The corresponding general enzyme activities are given in Table S-IIA)

Runs	Factor				Experimental		Predicted	
	<i>A</i>	<i>B</i>	<i>C</i>	<i>D</i>	LA, U g ⁻¹	MA, U g ⁻¹	LA, U g ⁻¹	MA, U g ⁻¹
1	-1	-1	-1	-1	0.16	1.24	0.17	0.90
2	-2.098	0	0	0	0.23	0.19	0.18	0.24
3	1	-1	-1	-1	0.12	0.77	0.10	0.86
4	2.098	0	0	0	0.12	0.20	0.13	0.15
5	-1	1	-1	-1	0.13	0.10	0.14	0.13
6	0	-2.098	0	0	0.06	1.38	0.04	1.63
7	1	1	-1	-1	0.10	0.04	0.08	0.09
8	0	2.098	0	0	0.05	0.02	0.07	0.02
9	-1	-1	1	-1	0.12	0.80	0.13	0.96
10	0	0	-2.098	0	0.17	0.30	0.15	0.42
11	1	-1	1	-1	0.07	1.03	0.07	0.91
12	0	0	2.098	0	0.16	0.66	0.16	0.54
13	-1	1	1	-1	0.20	0.15	0.19	0.19
14	0	0	0	-2.098	0.14	0.45	0.13	0.49
15	1	1	1	-1	0.11	0.12	0.13	0.14
16	0	0	0	2.098	0.11	0.57	0.12	0.53
17	-1	-1	-1	1	0.11	1.02	0.13	0.92
18	0	0	0	0	0.13	0.86	0.16	0.83
19	1	-1	-1	1	0.11	0.91	0.14	0.87
20	0	0	0	0	0.16	1.05	0.16	0.83
21	-1	1	-1	1	0.08	0.10	0.10	0.15
22	0	0	0	0	0.14	0.95	0.16	0.83
23	1	1	-1	1	0.13	0.10	0.11	0.11
24	-1	-1	1	1	0.10	0.95	0.09	0.97
25	1	-1	1	1	0.11	0.86	0.10	0.93
26	-1	1	1	1	0.18	0.17	0.15	0.20
27	1	1	1	1	0.19	0.12	0.16	0.16
28	0	0	0	0	0.16	0.82	0.16	0.83
29	0	0	0	0	0.15	0.84	0.16	0.83
30	0	0	0	0	0.15	0.81	0.16	0.83
31	0	0	0	0	0.16	0.72	0.16	0.83

TABLE S-IIA. Central composite design matrix with coded factor values and predicted and measured response values of general laccase activity (LA) and MnP activity (MA). The data are presented in standard order of experiments. Independent variables (factors) examined in this research were molasses stillage concentration (A), substrate moisture (B), incubation temperature (C), and pH value (D).

Runs	Factors				Experimental		Predicted	
	A	B	C	D	LA, U L ⁻¹	MA, U L ⁻¹	LA, U L ⁻¹	MA, U L ⁻¹
1	-1	-1	-1	-1	14	110.1	14.91	80.33
2	-2.098	0	0	0	20.1	16.7	16.39	21.3
3	1	-1	-1	-1	10.6	68.9	9.31	76.45
4	2.098	0	0	0	11	18.2	11.31	13.17
5	-1	1	-1	-1	11.3	8.82	12.59	11.87
6	0	-2.098	0	0	5.2	123.3	3.38	145.57
7	1	1	-1	-1	8.8	3.68	6.98	7.99
8	0	2.098	0	0	4.7	2.04	6.5	1.96
9	-1	-1	1	-1	10.5	71.4	11.9	85.21
10	0	0	-2.098	0	15.1	26.9	13	37.52
11	1	-1	1	-1	5.9	92	6.3	81.33
12	0	0	2.098	0	13.9	58.8	14.69	47.75
13	-1	1	1	-1	17.8	13.8	17.21	16.75
14	0	0	0	-2.098	12.2	40.4	11.36	43.65
15	1	1	1	-1	10.1	10.4	11.6	12.87
16	0	0	0	2.098	9.8	50.5	10.62	46.82
17	-1	-1	-1	1	9.6	90.6	11.38	81.84
18	0	0	0	0	11.6	76.6	13.85	73.76
19	1	-1	-1	1	10.1	81.1	12.14	77.97
20	0	0	0	0	13.9	93.6	13.85	73.76
21	-1	1	-1	1	7.1	9.1	9.05	13.38
22	0	0	0	0	12.2	84.5	13.85	73.76
23	1	1	-1	1	11.6	8.8	9.82	9.5
24	-1	-1	1	1	8.7	84.7	8.37	86.73
25	1	-1	1	1	10.2	76.4	9.14	82.85
26	-1	1	1	1	15.8	15	13.67	18.26
27	1	1	1	1	16.6	11	14.44	14.38
28	0	0	0	0	14.5	72.7	13.85	73.76
29	0	0	0	0	13.1	75.2	13.85	73.76
30	0	0	0	0	13	72.5	13.85	73.76
31	0	0	0	0	14	64	13.85	73.76

TABLE S-III. Central composite design matrix with coded factor values and predicted and measured response values of cellulase (CMCase) enzyme activity (CA) and xylanase activity (XA) per dry substrate mass. The data are presented in standard order of the experiments. Independent variables (factors) examined in this research were molasses stillage concentration (A), substrate moisture (B), incubation temperature (C), and pH value (D). (The corresponding general enzyme activities are given in Table S-IIIA)

Runs	Factors				Experimental		Predicted	
	A	B	C	D	CA, U g ⁻¹	XA, U g ⁻¹	CA, U g ⁻¹	XA, U g ⁻¹
1	-1	-1	-1	-1	1.27	1.27	1.25	1.33
2	-2.098	0	0	0	0.65	0.31	0.61	0.00
3	1	-1	-1	-1	1.14	1.48	1.34	1.61
4	2.098	0	0	0	1.23	0.47	1.12	0.59
5	-1	1	-1	-1	1.09	0.51	1.27	0.98
6	0	-2.098	0	0	0.73	0.89	0.58	1.13
7	1	1	-1	-1	1.44	0.92	1.66	1.26
8	0	2.098	0	0	0.96	0.75	0.95	0.40
9	-1	-1	1	-1	1.13	1.21	1.25	1.33
10	0	0	-2.098	0	1.51	0.59	1.14	0.77
11	1	-1	1	-1	1.35	2.27	1.34	1.61
12	0	0	2.098	0	1.33	0.47	1.14	0.77
13	-1	1	1	-1	1.34	0.78	1.27	0.98
14	0	0	0	-2.098	0.96	0.57	1.14	0.44
15	1	1	1	-1	1.77	1.45	1.66	1.26
16	0	0	0	2.098	1.08	0.50	1.14	0.43
17	-1	-1	-1	1	1.16	1.37	1.25	1.33
18	0	0	0	0	0.96	0.89	1.14	0.77
19	1	-1	-1	1	1.20	1.45	1.34	1.61
20	0	0	0	0	0.91	0.51	1.14	0.77
21	-1	1	-1	1	1.26	0.62	1.27	0.98
22	0	0	0	0	0.93	0.85	1.14	0.77
23	1	1	-1	1	1.56	0.91	1.66	1.26
24	-1	-1	1	1	1.23	1.77	1.25	1.33
25	1	-1	1	1	1.39	1.14	1.34	1.61
26	-1	1	1	1	1.36	0.82	1.27	0.98
27	1	1	1	1	1.75	1.88	1.66	1.26
28	0	0	0	0	1.51	1.76	1.53	1.48
29	0	0	0	0	1.72	1.77	1.53	1.48
30	0	0	0	0	1.66	1.36	1.53	1.48
31	0	0	0	0	1.87	1.87	1.53	1.48

TABLE S-IIIA. Central composite design matrix with coded factor values and predicted and measured response values of general cellulase (CMCase) enzyme activity (CA) and xylanase activity (XA). The data are presented in standard order of experiments. Independent variables (factors) examined in this research were molasses stillage concentration (A), substrate moisture (B), incubation temperature (C), and pH value (D).

Runs	Factors				Experimental		Predicted	
	A	B	C	D	CA, U L ⁻¹	XA, U L ⁻¹	CA, U L ⁻¹	XA, U L ⁻¹
1	-1	-1	-1	-1	113.21	112.96	111.04	118.73
2	-2.098	0	0	0	57.95	27.92	54.65	0.061
3	1	-1	-1	-1	102.02	131.76	119.25	143.69
4	2.098	0	0	0	109.19	41.61	99.42	52.28
5	-1	1	-1	-1	96.77	45.89	113.61	87.42
6	0	-2.098	0	0	64.71	79.63	52.06	101.02
7	1	1	-1	-1	128.07	81.62	148.09	112.38
8	0	2.098	0	0	85.41	67.1	84.99	35.34
9	-1	-1	1	-1	100.44	107.42	111.04	118.73
10	0	0	-2.098	0	134.89	52.84	101.48	68.18
11	1	-1	1	-1	120.73	202.69	119.25	143.69
12	0	0	2.098	0	118.28	41.87	101.48	68.18
13	-1	1	1	-1	119.85	69.81	113.61	87.42
14	0	0	0	-2.098	85.23	50.49	101.48	39.27
15	1	1	1	-1	157.8	128.84	148.09	112.38
16	0	0	0	2.098	96.6	44.32	101.48	38.23
17	-1	-1	-1	1	103.42	122.25	111.04	118.24
18	0	0	0	0	85.23	79.53	101.48	68.18
19	1	-1	-1	1	106.56	129.36	119.25	143.19
20	0	0	0	0	81.21	45.89	101.48	68.18
21	-1	1	-1	1	112.34	55.5	113.61	86.93
22	0	0	0	0	82.78	75.77	101.48	68.18
23	1	1	-1	1	139.26	81.1	148.09	111.88
24	-1	-1	1	1	109.71	157.46	111.04	118.24
25	1	-1	1	1	123.53	101.47	119.25	143.19
26	-1	1	1	1	120.9	72.74	113.61	86.93
27	1	1	1	1	155.88	167.91	148.09	111.88
28	0	0	0	0	134.54	156.73	136.04	131.56
29	0	0	0	0	152.9	158.09	136.04	131.56
30	0	0	0	0	147.66	121.002	136.04	131.56
31	0	0	0	0	166.54	166.55	136.04	131.56

TABLE S-IV. Test of significance of regression coefficients and ANOVA analysis of laccase activity model

Laccase activity model ($\hat{y}Lacc$)

Test of significance of regression coefficients

	Estimate	Std. error	t value	Pr (> t)
(Intercept)	0.1554265	0.0055548	27.9804	< 2.2×10 ⁻¹⁶ ***
A	-0.0135700	0.0041145	-3.2981	0.0032768 **
B	0.0083493	0.0041145	2.0293	0.0547024 ★★
C	0.0045173	0.0041145	1.0979	0.2841154 *
D	-0.0019613	0.0041145	-0.4767	0.6382893 ★★
A:D	0.0178854	0.0051225	3.4915	0.0020656 **
B:C	0.0213924	0.0051225	4.1762	0.0003924 ***
B ²	-0.0227264	0.0034906	-6.5107	1.504×10 ⁻⁶ ***
D ²	-0.0072959	0.0034906	-2.0902	0.0483768 *

Significant codes: *** – 0.001; ** – 0.01; * – 0.05; ★ – 0.1; * – 1

Multiple $R^2 = 0.8042$, Adjusted $R^2 = 0.733$ F-statistic: 11.29 on 8 and 22 DF, p-value = 3.264×10⁻⁶

Analysis of variance table

	Df	Sum square	Mean square	F value	Pr(>F)
FO (A, B, C, D)	4	0.0068971	0.0017243	4.1070	0.0123479
TWI (A, D)	1	0.0051182	0.0051182	12.1909	0.0020656
TWI (B, C)	1	0.0073221	0.0073221	17.4403	0.0003924
PQ (B, D)	2	0.0185985	0.0092992	22.1495	5.371×10 ⁻⁶
Residuals	22	0.0092364	0.0004198		
Lack of fit	16	0.0084268	0.0005267	3.9032	0.0505638
Pure error	6	0.0008096	0.0001349		

TABLE S-V: Test of significance of regression coefficients and ANOVA analysis of the MnP activity model

Manganese peroxidase activity model ($\hat{y}MnP$)

Test of significance of regression coefficients

	Estimate	Std. error	t value	Pr(> t)
(Intercept)	0.8277466	0.0402834	20.5481	2.680×10 ⁻¹⁶ ***
A	-0.0217628	0.0252235	-0.8628	0.397156 *
B	-0.3841607	0.0252235	-15.2303	1.662×10 ⁻¹³ ***
C	0.0273831	0.0252235	1.0856	0.288896 *
D	0.0085008	0.0252235	0.3370	0.739159 *
A ²	-0.1441678	0.0215645	-6.6854	8.062×10 ⁻⁷ ***
C ²	-0.0793849	0.0215645	-3.6813	0.001237 **
D ²	-0.0727536	0.0215645	-3.3738	0.002620 **

Significant codes: *** – 0.001; ** – 0.01; * – 1

Multiple $R^2 = 0.927$, Adjusted $R^2 = 0.9048$ F-statistic: 41.73 on 7 and 23 DF, p-value = 1.365×10⁻¹¹

Analysis of variance table

	Df	Sum square	Mean square	F value	Pr(>F)
FO(A, B, C, D)	4	3.6921	0.92303	58.4993	1.012×10 ⁻¹¹
PQ(A, C, D)	3	0.9166	0.30553	19.3638	1.728×10 ⁻⁶
Residuals	23	0.3629	0.01578		
Lack of fit	17	0.2945	0.01733	1.5202	0.3158
Pure error	6	0.0684	0.01140		

TABLE S-VI: Test of significance of regression coefficients and ANOVA analysis of cellulase activity model

Cellulase activity model (\hat{y}_{Cell})

Test of significance of regression coefficients

(Intercept)	Estimate	Std. error	t value	Pr(> t)
	1.526680	0.053576	28.4957	< 2.2×10 ⁻¹⁶ ***
Block	-0.387872	0.066581	-5.8255	5.241×10 ⁻⁶ ***
A	0.119775	0.035617	3.3629	0.002583 **
B	0.088090	0.035617	2.4733	0.020857 *
A:B	0.073709	0.044343	1.6623	0.10947 *
A ²	-0.062333	0.030216	-2.0629	0.050105 **
B ²	-0.084038	0.030216	-2.7812	0.010372 *

Significant codes: *** – 0.001; ** – 0.01; * – 0.05; ** – 0.1; * – 1

Multiple R² = 0.7303, Adjusted R² = 0.6629

F-statistic: 10.83 on 6 and 24 DF, p-value = 7.61×10⁻⁶

Analysis of variance table

	Df	Sum square	Mean square	F value	Pr(>F)
Block	1	1.06767	1.06767	33.9368	5.241×10 ⁻⁶
FO (A, B)	2	0.54823	0.27412	8.7130	0.00143
TWI (A, B)	1	0.08693	0.08693	2.7631	0.10947
PQ (A, B)	2	0.34163	0.17081	5.4294	0.01134
Residuals	24	0.75505	0.03146		
Lack of fit	3	0.18246	0.06082	2.2306	0.11449
Pure error	21	0.57259	0.02727		

TABLE S-VII. Test of significance of regression coefficients and ANOVA analysis of xylanase activity model

Xylanase activity model (\hat{y}_{Xyl})

Test of significance of regression coefficients

(Intercept)	Estimate	Std. error	t value	Pr(> t)
	1.4763510	0.1040412	14.1901	3.613×10 ⁻¹³ ***
Block	-0.7112477	0.1292971	-5.5009	1.176×10 ⁻⁵ ***
A	0.1400227	0.0691661	2.0244	0.05419 **
B	-0.1756835	0.0691661	-2.5400	0.01797 *
D	-0.0027794	0.0691661	-0.0402	0.96828 *
A ²	-0.1072887	0.0586785	-1.8284	0.07994 **
D ²	-0.0750504	0.0586785	-1.2790	0.21312 *

Significant codes: *** – 0.001; * – 0.05; ** – 0.1; * – 1

Multiple R² = 0.6538, Adjusted R² = 0.5673

F-statistic: 7.555 on 6 and 24 DF, p-value = 0.0001249

Analysis of variance table

	Df	Sum square	Mean square	F value	Pr(>F)
Block	1	3.5901	3.5901	30.2596	1.176×10 ⁻⁵
FO (A, B, D)	3	1.2519	0.4173	3.5172	0.03038
PQ (A, D)	2	0.5361	0.2681	2.2594	0.12617
Residuals	24	2.8474	0.1186		
Lack of fit	9	1.4259	0.1584	1.6719	0.18203
Pure error	15	1.4215	0.0948		

Table S-VIII. R^2 -values before and after model reduction.

Model	R^2	
	Full model	Reduced model
Laccase	0.8753	0.8042
MnP	0.9459	0.927
Cellulase	0.8201	0.7303
Xylanase	0.78	0.6538

Table S-IX. Significance, R^2 , lack of fit and AP-values of the generated laccase, MnP, cellulose, and xylanase activity models.

Model	R^2	Adjusted R^2	F-statistics	p-value	Lack of fit	AP (>4)
\hat{y}_{Lacc}	0.8042	0.733	11.29	3.264×10^{-6}	0.051	14.05
\hat{y}_{MnP}	0.927	0.9048	41.73	1.365×10^{-11}	0.3158	25.26
\hat{y}_{Cell}	0.7303	0.6629	10.83	7.61×10^{-6}	0.11449	12.79
\hat{y}_{Xyl}	0.6538	0.5673	7.555	0.0001249	0.18203	9.85

Second-order polynomial equations obtained for laccase, manganese-dependent peroxidase, cellulase, and xylanase enzyme activity:

$$\begin{aligned} \hat{y}_{Lacc} = & 0.155 - 0.014A + 0.008B + 0.005C - 0.002D + \\ & + 0.018AD + 0.021BC - 0.023B^2 - 0.007D^2 \end{aligned} \quad (S1)$$

$$\begin{aligned} \hat{y}_{MnP} = & 0.828 - 0.022A - 0.384B + 0.027C + 0.008D - 0.144A^2 - \\ & - 0.079C^2 - 0.073D^2 \end{aligned} \quad (S2)$$

$$\begin{aligned} \hat{y}_{Cell} = & 1.526 - 0.388 \text{ Block} + 0.119A + 0.088B + 0.074AB - \\ & - 0.062A^2 - 0.084B^2 \end{aligned} \quad (S3)$$

$$\begin{aligned} \hat{y}_{Xyll} = & 1.476 - 0.711 \text{ Block} + 0.140A - 0.176B - 0.003D - \\ & - 0.107A^2 - 0.075D^2 \end{aligned} \quad (S4)$$



New copper(II) cyclam complexes with aminocarboxylate co-ligands: Synthesis, characterization, and *in vitro* antiproliferative and antibacterial studies

BRANKA DRAŽIĆ^{1*}, MIRJANA ANTONIJEVIĆ-NIKOLIĆ², MILENA MARINOVIC-CINCOVIĆ³, VUKOSAVA ŽIVKOVIĆ-RADOVANOVIĆ^{4#}, BRANKA BOROVIĆ⁵ and SLAĐANA B. TANASKOVIĆ¹

¹Faculty of Pharmacy, Vojvode Stepe 450, 11000 Belgrade, Serbia, ²Academy of Applied Studies Šabac, Department for Medical, Business and Technological Studies, Hajduk Veljkova 10, 15000 Šabac, Serbia, ³Institute of Nuclear Sciences Vinča, University of Belgrade, Mike Petrovića Alasa 12-14, 11351 Vinča, Belgrade, Serbia, ⁴Faculty of Chemistry, University of Belgrade, Studentski trg 16, 11000 Belgrade, Serbia and ⁵Institute of Meat Hygiene and Technology, Kaćanskog 13, 1100 Belgrade, Serbia

(Received 7 November 2021, revised 7 March, accepted 11 March 2022)

Abstract: Two new cationic Cu(II) complexes of cyclam (1,4,8,11-tetraaza-cyclotetradecane) and aminocarboxylate coligands glycine or alanine have been synthesized. The complexes were characterized by elemental analysis (C, H and N), molar electrical conductivity, magnetic susceptibility measurement at room temperature, spectral methods (UV/Vis and Fourier transform infrared), as well as by thermogravimetric (TG) and differential thermal analysis (DTA). The analytical data of the complexes show the formation of mononuclear complexes with general formula $[\text{Cu}(\text{L})\text{cyc}](\text{ClO}_4)_2 \cdot n\text{H}_2\text{O}$, A) L = glycine, $n = 1.5$ and B) L = alanine, $n = 2.5$. The tetradeятate ligand cyclam was coordinated to metals through four N donors. The spectroscopic data suggested that the amino carboxylate ligands coordinated *via* their carboxylate ion moieties. The six-coordinate octahedral geometry around Cu(II) in both complexes was presumed. TG-DTA analysis indicated that complex B decomposed exothermally in a single step in the range of 310–400 °C. The cytotoxic activity of Cu(II) complexes and the starting ligands were tested against human cervix adenocarcinoma cell line (HeLa), human melanoma (FemX) and human colon carcinoma (LS174). The IC₅₀ values for the Cu(II) complexes were from 48.35–82.25 μM. Both complexes were tested for their antimicrobial activity against *Staphylococcus aureus*, *Bacillus subtilis*, *Escherichia coli* and the yeast *Candida albicans*.

* Corresponding author. E-mail: bdrazic@pharmacy.bg.ac.rs

Serbian Chemical Society member.

<https://doi.org/10.2298/JSC211107026D>

Keywords: copper(II) complexes; cyclam; glycine; alanine; antimicrobial and cytotoxic activity.

INTRODUCTION

The synthesis of transition metal complexes containing O- and/or N-donor ligands has become very important and attractive in the field of medical research due to the discovery of the antimicrobial and antiproliferative properties of these compounds.¹

Cyclam (1,4,8,11-tetraazacyclotetradecane, Fig. 1), as 14-membered tetraamine macrocycle, is the one of the simplest N₄-macrocycles which can strongly bind a wide range of metal ions. Some of these complexes have been used for: catalyzing different reactions, pharmacology and therapy, medical and radiopharmaceutical applications, as enzyme mimics, chemical sensors, selective metal ion recovery as well.² Medical interest has centered on clinical trials of a bicyclam for the treatment of AIDS and for stem cell mobilization, and on adducts with Tc and Cu radionuclides for diagnosis and therapy.^{3,4}

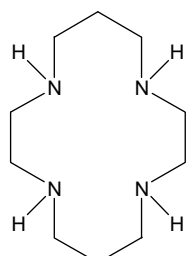


Fig. 1. 1,4,8,11-Tetraazacyclotetradecane (cyclam).

Cyclam bonds metal ions through four donor nitrogen atoms. By substituting one or more hydrogen from nitrogen with groups containing ligator atoms, numerous ligands that have the properties of both macrocyclic and non-cyclic ligands have been made. This modification of the basic macrocyclic ring changes its flexibility during the coordination of metal ions, which is a consequence of the participation of ligators from pendant groups in the coordination.

Metal cyclam complexes have a potentially rich configurational chemistry.⁴ Each of the coordinated N atoms is chiral. The metal ion can commonly be 4-, 5- or 6-coordinate. The macrocyclic 14-membered cyclam derivatives have moderately flexible structures and commonly adopt the six configurations, both trans- and cis-isomers.³

Copper is an essential trace mineral and plays a key role in such functions within the body as red blood cell production, iron absorption, the regulation of heart rate and blood pressure, and the development and maintenance of connective tissue, bones and organs. Another reason why copper is especially important for human health in pandemic conditions like the present one, is the part it

plays in immune system maintenance and activation. Copper helps to ensure a healthy supply of white blood cells, many of which are phagocytes that protect the body by engulfing bacteria, foreign particles and dying cells. Copper enzymes usually contain metal ions bound to a specific amino acid residue or directly to the amide group – carbonyl or nitrogen – in the peptide backbone, offering different coordination environments.^{5–7}

In the last two decades numerous complexes of transition metals with cyclam were synthesized. Different ways of coordination of macrocycle and its derivatives for different metal cations allows their application as antitumor, antiviral, antibacterial, antifungal or antimalarial agents.^{8–12}

The goal of this research was to define structure of the mixed Cu(II) complexes with cyclam and amino acids, glycine and alanine, as additional ligand, to screen the *in vitro* cytotoxicity of the compounds compared to the effect of commonly used drug, cis-platin against human tumor cell lines.

EXPERIMENTAL

Chemicals and materials. The chemicals: L-glycine, L-alanine, CH₃CN was used as p.a. commercial products by Merck; 1,4,8,11-tetraazacyclotetradecane (cyclam) and copper(II) perchlorate hexahydrate by Aldrich.

Preparation

(Caution! Perchlorate compounds are potentially explosive and should be prepared in small amounts and handled with care)

[Cu(gly)cyc](ClO₄)₂·1.5H₂O and [Cu(ala)cyc](ClO₄)₂·2.5H₂O, general procedure. Complexes with general formula [Cu(L)cyc](ClO₄)₂·nH₂O, A) L=glycine (gly, ⁺H₃N–CH₂–COO⁻), n = 1.5 and B) L = alanine (ala, ⁺H₃N–CH(CH₃)–COO⁻), n = 2.5 were obtained by reaction Cu(ClO₄)₂·6H₂O and cyclam with L-glycine or L-alanine.

Aqueous solution Cu(ClO₄)₂·6H₂O (111 mg, 0.30 mmol in 5 mL H₂O) was added in suspension of cyclam (61 mg, 0.30 mmol) in acetonitrile (10 mL). The violet reaction mixture was stirred at 80 °C for 30 min. Aqueous solution of glycine/alanine (34 mg/40 mg; 4.5 mmol) was added in this solution and continuously stirred at 80 °C for 90 min. The resulting reaction mixture was cooled to room temperature, filtered and left in the fridge a few days. A pink solid production was separated by filtration, and was dried in air. The product recrystallized from mixture CH₃CN:H₂O (1:1 volume ratio).

[Cu(gly)cyc](ClO₄)₂·1.5H₂O (**A**). Yield 87 %. Anal. Calcd. for C₁₂H₂₈O_{11.5}N₅CuCl₂ (FW = 560.89): C 25.92; H 5.30; N 12.06. Found: C 25.71; H 5.03; N 12.49. At temperature 20±2 °C, the complexes are well soluble in CH₃CN, DMSO, (CH₃)₂CO and DMF, and insoluble in EtOH, CH₃OH and H₂O.

[Cu(ala)cyc](ClO₄)₂·2.5H₂O (**B**). Yield 79 %. Anal. Calcd. for C₁₃H₃₂O_{12.5}N₅CuCl₂ (FW = 592.93): C 26.35; H 5.43; N 12.17. Found: C 26.34; H 5.44; N 11.82. At temperature 20±2 °C, the complexes are well soluble in CH₃CN, DMSO, (CH₃)₂CO and DMF, and insoluble in EtOH, CH₃OH and H₂O.

Measurements

The elemental analyses were performed by standard methods in the Centre for Instrumental Analyses, ICTM, University of Belgrade. The electronic absorption spectra of the

complexes and ligands in CH_3CN ($c = 10^{-3}$ M) were recorded on spectrophotometer GBC UV/Vis Cintra 20 in the range 200–900 nm. Fourier transform infrared (FTIR) spectra were recorded on Nicolet 6700 FTIR (ATR technique) in the range 400–4000 cm^{-1} . The molar conductivities were measured on conductometer Therma orion star A212 (at $20 \pm 2^\circ\text{C}$) in CH_3CN ($c = 10^{-3}$ M). The magnetic susceptibility measurements were taken at room temperature ($20 \pm 2^\circ\text{C}$) using a MSB-MKI balance (Sherwood Scientific Ltd., England). The data were corrected for diamagnetic susceptibilities using Pascal's constants.¹³

The thermal stability of the sample **B** was investigated by simultaneous non-isothermal thermo-gravimetric analysis (TG) and differential thermal analysis (DTA) using a Setaram Setsys Evolution 1750 instrument. The measurements were conducted at a heating rate of 10 $^\circ\text{C}/\text{min}$ in a dynamic argon atmosphere (flow rate was 20 mL/min) in the temperature range of 30–400 $^\circ\text{C}$. The mass of the sample was about 2 mg.

In vitro antiproliferative evaluation

Cell culture. HeLa (human adenocarcinoma), FemX (human melanoma) and LS174 (human colon carcinoma) cell lines were obtained from the American Type Culture Collection 8 (Manassas, VA, USA).

Culture medium. All cancer cell lines were maintained in RPMI-1640 (Sigma–Aldrich) medium supplemented with 10 % heat-inactivated (56 $^\circ\text{C}$) fetal bovine serum, 2 mM L-glutamine, 100 U/mL penicillin, 100 mg/mL streptomycin and 25 mM HEPES and adjusted to pH 7.2 using bicarbonate solution. Cells were cultured in a humidified chamber (37 $^\circ\text{C}$, 5 % CO_2 , 95 % air).

Other chemicals. Dimethyl sulfoxide (DMSO) (Sigma–Aldrich), sodium dodecylsulfate (SDS, Sigma–Aldrich), 3-(4,5-dimethylthiazol-2-yl)-2,5-diphenyl tetrazolium bromide (MTT, Sigma–Aldrich), fetal bovine serum (FCS, Sigma–Aldrich), cis-platin (EBewe, Pharma, Austria).

MTT assay. *In vitro* cytotoxicity of the free ligands (cyclam, glycine, alanine), complexes **A**, **B** and cis-platin were evaluated against three cancer cell lines: human cervix adenocarcinoma (HeLa), human melanoma (FemX) and human colon carcinoma (LS174). All cells were cultured in RPMI-1640 supplemented with 10 % heat-inactivated (56 $^\circ\text{C}$) fetal bovine serum, 1 % penicillin (100 IU/mL), streptomycin (100 mg/mL), L-glutamine (3 mM) and 25 mM HEPES and adjusted to pH 7.2 by bicarbonate solution. Cell lines were maintained at 37 $^\circ\text{C}$ in a 5 % CO_2 atmosphere with 95 % humidity. The compounds and cis-platin were dissolved in dimethyl sulfoxide (10 mM) and diluted to the required concentration with culture medium before use. Neoplastic HeLa cells (2000 cells per well), FemX cells (5000 cells per well) and LS174 cells (7000 cells per well) were seeded into 96-well microtiter plates, and 24 h later, after the cell adherence, five different, double diluted concentrations of the investigated compounds, were added to the wells. Final concentrations applied to target cells were 200, 100, 50, 25 and 12.5 μM . Control wells were prepared by the addition of culture medium without cells. The plates were incubated at 37 $^\circ\text{C}$ for 72 h in a 5% CO_2 . The effect of compounds on cancer cell survival was determined by the MTT test according to Mosmann,¹⁴ modification by Ohno and Abe,¹⁵ 72 h upon addition of the compounds. After the completion of the incubation, 20 μL of MTT solution (5 mg MTT/mL PBS) was added to each well. The samples were incubated for additional 4 h at 37 $^\circ\text{C}$ in 5 % CO_2 in humidified air atmosphere. Subsequently, 100 μL of 10 % SDS was added to extract the insoluble formazan formed from the conversion of the MTT dye by viable cells. The number of viable cells in each well was proportional to the intensity of the absorbance of light, which was then read in an ELISA plate reader at 570 nm. The absorbance (A) at 570 nm was measured 24 h later. To get the cell

survival (%), A of a sample with cells grown in the presence of various concentrations of the investigated extracts was divided by control optical density (the A_c of the control cells grown only in nutrient medium), and multiplied by 100. A_s of the blank was always subtracted from A of the corresponding sample with target cells.

The cell survival (S) was calculated by Eq. (1):

$$S = 100 \frac{A_t - A_s}{A_c - A_s} \quad (1)$$

where A_c is the absorbance of the control, A_t is the absorbance of the treated cells, A_s the absorbance of the blank.

All experiments were performed in triplicate. The IC_{50} value was determined as the concentration of the complex that is required to reduce the absorbance by half of the control. Cis-platin was used as standard cytotoxic agent.

Antimicrobial activity. The antimicrobial activity of the new Cu(II) complexes (**A** and **B**) were assayed using the broth-microdilution method against the following laboratory strains obtained from the American Type Culture Collection (ATCC): Gram-positive bacteria *Staphylococcus aureus* ATCC 25923 and *Bacillus subtilis* ATCC 6633, Gram-negative bacteria *Escherichia coli* ATCC 25922 and one strain of the yeast *Candida albicans* ATCC 10231. Stock solutions (10 mM) of the compounds were prepared in dimethyl sulfoxide (DMSO) and diluted to the working concentrations in fresh Müller–Hinton broth for bacteria and Sabouraud broth for *C. albicans*. Bacterial and yeast suspensions were prepared by the direct colony method. The colonies were taken directly from the plate and suspended in 5 mL of sterile 0.85 % saline. The turbidity of the initial suspension was adjusted by comparing it to 0.5 McFarland's standard. When adjusted to the turbidity of the 0.5 McFarland's standard, the bacterial suspension contained about 108 colony forming units, CFU mL⁻¹, and the suspension of yeast contained 106 CFU mL⁻¹. Ten-fold dilutions of the initial suspension were additionally prepared into Müller–Hinton broth for the bacteria and Sabouraud broth for *C. albicans*. Each dilution of complexes was poured in triplicates into a 96-well microtiter plate and inoculated with previously prepared bacterial suspension. For a negative control for each plate, only the medium was used. As a positive control of growth, wells containing only the microorganisms in the broth were used. In addition, the activity of the starting ligands was also tested. The MICs of ampicillin, and nystatin were determined in parallel experiments. In the tests, 0.05 % TTC was also added to the culture medium as a growth indicator. TTC is a redox indicator used for differentiation between metabolically active and non-active cells. The colorless compound is enzymatically reduced to red 1,3,5-triphenylformazan by cell dehydrogenases, indicating metabolic activity (red color of the medium in microtiter plate well). The bacteria growth was determined after 24 h, while the growth of *C. albicans* was determined after 48 h of incubation at 37 °C. The lowest concentration of the extract at which the microorganism does not demonstrate visible growth (MIC) was determined in broths from each well (10 mL) and inoculated in Müller–Hinton agar for 24 h at 37 °C for bacterial strains, and in Sabouraud dextrose agar for 48 h at 26 °C for the fungi. All determinations were performed in triplicate.

RESULTS AND DISCUSSION

In the reaction $\text{Cu}(\text{ClO}_4)_2 \cdot 6\text{H}_2\text{O}$ with cyclam glycine or alanine formed a mononuclear complexes with general formula $[\text{Cu}(\text{L})\text{cyc}](\text{ClO}_4)_2 \cdot n\text{H}_2\text{O}$, **A**) $\text{L} = \text{glycine}$, $n = 1.5$ and **B**) $\text{L} = \text{alanine}$, $n = 2.5$.

The analytical data corresponded to a metal–cyclam–amino acid ratio of 1:1:1 and 1.5 or 2.5 mol of water per mol of metal for complexes **A** or **B**. Data suggested a mononuclear structure for the Cu(II) complexes obtained as micro-crystalline powder. The conductivity values in CH₃CN were 330 and 340 S cm² mol⁻¹, respectively for **A** and **B**, and corresponded to 1:2 electrolytes for both complexes.¹⁶ The μ_{eff} values for the new complexes were determined at room temperature by the Gouy method. The values for **A** (1.98 μ_{B}) and **B** (2.15 μ_{B}) were in agreement with the values reported for several Cu(II) octahedral complexes ($1.9 \pm 2.2 \mu_{\text{B}}$).¹⁷

Spectral studies

UV/Vis spectroscopy. The absorption spectra in the UV and visible regions were recorded for new complexes in CH₃CN solutions. Both complexes were pink. Broad absorption bands in the visible region at 503 (ε = 172 dm³ mol⁻¹ cm⁻¹) for **A** and 508 nm (ε = 170 dm³ mol⁻¹ cm⁻¹) for **B**, corresponded to Cu(II) d–d transitions. Bands at 503 and 508 nm, can be attributed to the transition $^2\text{E}_g \rightarrow ^2\text{T}_{2g}$ and this is expected for an octahedral d⁹ configuration.¹⁸ The positions of the maxima in the absorption spectra of complexes indicated the presence of the CuN₄O₂ chromophore, being coordinated by the four N atoms of cyclam (Fig. 2a) and two O. In the visible part of the spectra of complexes Cu(II) with cyclam and various carboxylate ligands with octahedral geometry, one maximum was observed for d–d transitions at a wavelength of 505 to 546 nm.^{17,19} These spectral features are consistent with six coordinate geometry for Cu(II) complexes. Besides octahedral geometry Cu(II) complexes of square pyramid, or distorted square pyramid, geometries exhibit a band in the 550–660 nm range, whereas the corresponding trigonal bipyramidal complexes usually show a maximum at $\lambda_{\text{max}} 800$ nm with a higher energy shoulder.²⁰ It is difficult to infer the geometry of Cu(II) complexes from electronic spectra alone, as they vary with the distortion within a given coordination number, due to the plasticity of the Cu(II) coordination environment.²¹

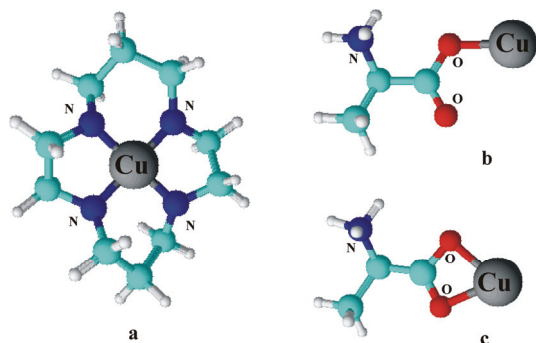


Fig. 2. a) Coordination mode of Cu(II) with 1,4,8,11-tetraazacyclotetradecane (cyclam), b) 275 and c) possible coordination modes of alanine in mononuclear complex.

Based on all the applied characterization methods it was assumed that the geometry of the both complexes is most likely octahedral.

The electronic spectra of complexes exhibited an intense intraligand transitions in the UV region: 212–279 nm (ϵ 4937–5727 $\text{dm}^3 \text{ mol}^{-1} \text{ cm}^{-1}$) for **A** and 223–288 nm (ϵ 4903–5730 $\text{dm}^3 \text{ mol}^{-1} \text{ cm}^{-1}$) for **B**,¹⁹ alongside a comparatively weaker absorption band in the visible region.²¹ Intraligand transitions were found in the spectra of ligands in the range 220–250 nm. The intraligand transitions in both complexes were slightly shifted during complexation. The value of ϵ for complexes **A** and **B** (172 and 170 $\text{dm}^3 \text{ mol}^{-1} \text{ cm}^{-1}$, respectively), was in the interval obtained for mononuclear Cu(II) cyclam complexes.²²

FTIR spectra. In the FTIR spectra of the new synthesized complexes **A** and **B**, the following bands were present: a strong bands of $\nu_s(\text{ClO}_4^-)$ and $\nu_{as}(\text{ClO}_4^-)$ which was not included in the coordination at 930 and 1063 cm^{-1} , as well as a medium sharp band from $\delta(\text{ClO}_4^-)$ at 621 cm^{-1} .²³ The infrared spectra of these complexes in comparison with free cyclam and the respective free amino acids showed characteristic band positions, shifts and intensities, which could be correlated to cyclam binding and coordination amino acid. The IR spectra of two new synthesized complexes are compared in Table I with spectra of ligands.

TABLE I. Selected FTIR absorption bands of the ligands and complexes

Compound	ν / cm^{-1}					δ / cm^{-1}	
	N–H and O–H	ClO_4^-	C–H	M–N	M–O	ClO_4^-	CH_2
Glycine	—	—	2902	—	—	—	—
Alanine	—	—	2937	—	—	—	—
Cyclam	3268	—	2867			—	1462
A	3241	1063	2878	528	436	621	1448, 1467
B	3242	1063	2880	528	436	621	1453, 1467

A stretching O–H band is observed at 3241 and 3242 cm^{-1} for the complexes **A** and **B**, respectively, together with $\nu(\text{N–H})$. This band as well as the one located at 1606 cm^{-1} indicate the presence of water in both compounds.²³ In the spectra of ligand cyc $\nu(\text{N–H})$ was found at 3268 cm^{-1} . In both complexes, $\nu(\text{N–H})$ are slightly shifted during coordination cyclam to the Cu(II). Weak broad band at 2878 (**A**) and 2880 (**B**) cm^{-1} is likely showing itself due to stretching vibration of CH, and two medium bands about 1440 and 1470 cm^{-1} from CH_2 bending vibrations.

Comparing the FTIR spectra of the complexes and amino acids in the region characteristic for $\nu(\text{NH}_3^+)$, $\delta_{as}(\text{NH}_3^+)$ and $\delta_s(\text{NH}_3^+)$, no shift was observed (Table II). It was assumed that NH_3^+ zwitter ions did not participate in coordination. However, by comparing the FTIR spectra in the region characteristic for OCO^- , a shift of $\nu_{as}(\text{OCO}^-)$ and $\nu_s(\text{OCO}^-)$ was observed. It was assumed that a carboxylate group participates in the coordination.^{24–26}

TABLE II. FTIR spectral data (cm^{-1}) for the free amino acids and their complexes

Compound	$\nu(\text{NH}_3^+)$	$\delta_{\text{as}}(\text{NH}_3^+)$	$\delta_s(\text{NH}_3^+)$	$\nu_{\text{as}}(\text{OCO}^-)$	$\nu_s(\text{OCO}^-)$
Glycine	2902	1606	1524	1594	1413
A	2939	1605	—	1485	1388
Alanine	2937	1618	1515	1590	1412
B	2939	1606	—	1485	1362

The asymmetric stretching mode of the carboxylate group of amino carboxylates ligands occurs at about 1590 cm^{-1} and the symmetric stretching mode occurs about 1410 cm^{-1} (Table II). In unidentate coordination the redistribution of electron density takes place, which shifts the asymmetric carboxylate stretch to higher wavenumbers in comparison to the uncoordinated OCO^- group. Consequently, the $\Delta\nu$ value for unidentate carboxylate coordination is higher than ionic. On the contrary, bidentate coordination shifts the position of the asymmetric carboxylate stretch to lower wavenumber in comparison to the uncoordinated group and thus lowers the value of $\Delta\nu$.

In these complexes the $\nu_{\text{as}}(\text{OCO}^-)$ and $\nu_s(\text{OCO}^-)$ shows negative shifts, which confirm the coordination of the carboxylate group, which is the case when OCO^- participates in coordination through both oxygens, or when OCO participates in H-bonds formation.^{23,24} For the complexes **A** and **B**, the difference between $\Delta\nu(\text{OCO}^-)$ is 97 or 123 cm^{-1} respectively, which is much lower than $\Delta\nu$ gly or ala (181 cm^{-1} for gly or 178 cm^{-1} for ala).

Complexes with a “pseudo-bridging” binding method have been described in the literature, where one oxygen of the carboxylate group is coordinated to the metal and the other is hydrogen bonded to another ligand even though the $\Delta\nu$ of complex is less than the $\Delta\nu$ of carboxylato ligand.²⁴

In the spectra of both complexes there are bands at 528 cm^{-1} which are originating from $\nu(\text{C}-\text{N})$ and bands at 436 cm^{-1} from $\nu(\text{C}-\text{O})$. These vibrations confirm the coordination of ligands to the central metal ions and the involvement of nitrogen atoms (from cyclam) and oxygen atoms (from OCO^- group of gly/ala) in the coordination.^{23,24}

Considering the structure of cyclam and the data obtained from the FTIR spectrum, the coordination mode of the aminocarboxylate ligand cannot be reliably determined.

Thermal analysis

The thermal decomposition of the complex **B** is shown in the Fig. 3. The complex is thermally decomposed in the range $310\text{--}400 \text{ }^\circ\text{C}$ at one step. The complex is stable up to $310 \text{ }^\circ\text{C}$ which may indicate that the water present in the complex is coordinated for Cu (II), or that it participates in the strong hydrogen bonds.¹⁷

DTA curve of this complex reveals that it decomposes at one step showing an exothermic peak at 310 °C.

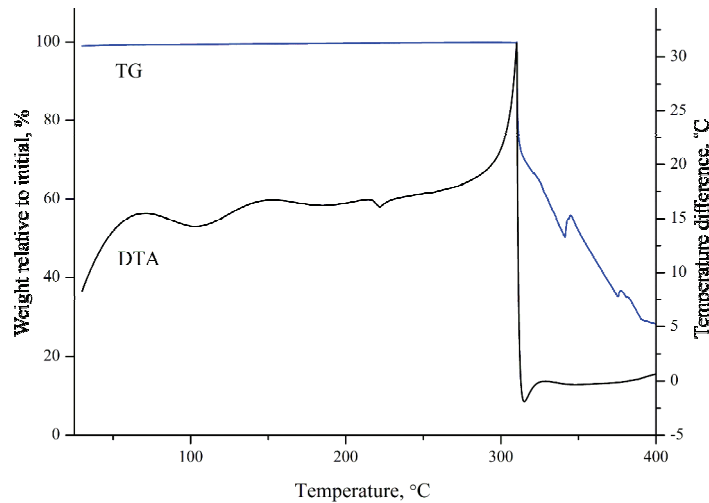


Fig. 3. Simultaneous TG-DTA of complex B.

Although TG indicates high stability of the complex up to 310 °C and possible stronger binding of the water present in the complex (in coordination with Cu (II), or building strong hydrogen bonds) based on the applied methods the coordination mode of aminocarboxylate cannot be assumed.

It can be concluded that the obtained complexes are mononuclear in which cyclam is coordinated for Cu (II); the amino acid is coordinated as a zwitter ion, *via* the OCO group; the coordination number of metals is 6 and that water molecules are present in both complexes. Based on the applied methods, it is difficult to determine the method of coordination of the carboxyl group for metal as well as the participation of water in the coordination or crystal lattice. In the further work, the obtaining of monocystalline of complexes and their analysis will give answers to these questions.

Antibacterial and antiproliferative activity

Antiproliferative activity. The *in vitro* antiproliferative activities of compounds **A**, **B**, cyclam and co-ligands were evaluated against cell lines HeLa (human adenocarcinoma), FemX (human melanoma) and LS174 (human colon carcinoma) by the MTT colorimetric assay method. The obtained IC_{50} values (the concentration of compounds that induced a 50 % decrease in cell survival) are given in Table III together with the activity of cisplatin as the referent cytostatic drug. The IC_{50} values of the complexes were in the range of 48.35–82.25

μM against the three tested cell lines, while for cisplatin, they were in the range 8.35–10.92 μM (Table III).

TABLE III. $IC_{50}\pm SD$ values (μM) after 72 h of action of the investigated complexes **A** and **B**, ligands and cisplatin on the tested cell lines, determined by the MTT test

Compound	Cell line		
	HeLa	K 562	LS 174
A	74.06 \pm 6.35	82.25 \pm 7.18	60.35 \pm 6.81
B	53.10 \pm 4.36	50.35 \pm 4.21	48.35 \pm 8.81
Cyclam, glycine, alanine	>200	>200	>200
Cis-platin	10.9 \pm 23.50	8.35 \pm 1.84	9.47 \pm 1.74

Compounds **A** and **B** showed moderate activity against all three cell lines. On the contrary, ligands did not show cytotoxic activity ($IC_{50} > 200 \mu\text{M}$) under the same conditions. Both compounds have promoted decrease in the metabolic activity of the HeLa, FemX and LS174 cells, which occurred in a dose-dependent fashion.

A number of Cu(II) chelate complexes that exhibit cytotoxic activity through cell apoptosis or enzyme inhibition have been reviewed.²⁷ Such complexes containing different ligands are effective in reducing tumor size, delaying of metastasis and significantly increasing the survival of the hosts. Chelates of curcuminoids show significant reduction of solid tumor volume in mice ($P < 0.001$), while complexes of pyridine-2-carbohidrazide derivatives inhibit the expression of c-Src, a nonreceptor tyrosine kinase, which plays a significant role in growth-mediated signaling pathway, thus showing cytotoxicity against colon cancer cell lines. Similarly, Cu(II) chelates of salclaldoxime and resorcylaldoxime²⁸ are potent antiproliferative agents, exhibiting strong cytotoxic effects by inducing cell cycle arrest and apoptosis. Their action may involve the inhibition of the enzyme topoisomerase II activity, by preventing dimer formation of the enzyme and its interaction with DNA.²⁹ Though copper is an essential cofactor for tumor angiogenesis processes, several Cu(II) binary complexes have been reported to function as proteasome inhibitors, inducing apoptosis in various types of human cancer cells. In such complexes, described as “organic copper compounds”, the metal is coordinated either to neutral heteroatomic molecules such as phenanthroline or to anionic organic ligands such as 8-hydroxyquinolate, pyrrolidine dithiocarbamate or (pyridine-2-ylmethylamino)methyl phenolate). It is noticeable that the free ligands themselves are not efficient inhibitors, and complex formation is necessary for the transportation of copper ions through the cell membrane, in order to achieve proteasome inhibition.³⁰ This seems to be the result of the increasing lipophilicity of the metal upon ligand coordination. Detailed molecular mechanisms for tumour-associated copper elevation are not completely elucidated.³¹

Antimicrobial activity. The growing resistance of microorganisms to drugs is becoming a serious threat for the suppression of microbial infections. New, more effective substances, such as coordination compounds, are still being sought to treat infections with highly resistant strains. This is also important due to the fact that cancer patients are more susceptible to bacterial infections. The Cu (II) complexes did not show activity against the Gram-(–) bacteria and the yeast *C. albicans*. Both tested complexes showed activity against Gram-(+) bacteria, *S. aureus* and *B. subtilis*. It is a consequence of the difference in the permeability of the membrane of Gram-(+) bacteria in comparison to the Gram-(–) one due to the difference in their structure. Gram-(+) bacteria are known to be more susceptible to amino acids complexes.³²

From the experimental results of the in vitro antimicrobial activities, it has been concluded that none of the preliminary tested compounds showed antifungal activity, so further investigation was focused only on bacteria. The applied method was the same as the one used in the study of antibiotics. Under the same conditions controls were inactive at concentrations up to 400 mg/ml. This indicates that the activity of the complexes, where it was found, originated from themselves. For both complexes, *MIC* values against *S. aureus* and *B. subtilis* were 200 µg mL⁻¹. The classification of antimicrobial activity of new compounds, based on *MIC* results as: good, *MIC* less than 100 µg mL⁻¹; moderate: *MIC* between 100 and 500 µg mL⁻¹; weak: *MIC* between 500 and 1000 µg mL⁻¹; and inactive when the *MIC* value is more than 1000 µg mL⁻¹ is given in the literature.³³ In this way, it was possible to evaluate the antimicrobial activity of the examined metal complexes as moderate. The examined compounds showed moderate bactericidal effect on *S. aureus* and *B. subtilis* to the other Cu(II) carboxylato complexes.³⁴

A particular geometric shape of a complex could facilitate the contact with microorganisms and rapidly inhibit their growth, if there are no steric disturbances by the ligands. The biological activity of the examined complex is also influenced by: the chelating effect, the total charge of the complex ion, the nature of the counter ion, the nature of the donor ligands, the nuclear properties of metal centres in the complex, the nature of the central metal ion and many other factors such as the solubility, the type and length of the bond between metal and ligand, etc.^{34,35}

CONCLUSION

The newly synthesized mononuclear mixed-ligand complexes of Cu(II) using the 1,4,8,11-tetraazacyclotetradecane (cyclam) and aminoacids glycine/alanine were characterized by spectral, conductometric and magnetic studies, and TG-DTA analysis. For the complexes, octahedral structure has been proposed with coordinated four nitrogen atoms from cyclam and two oxygen atoms. TG-

-DTA analysis indicates that the complexes decompose exothermally in a single step in the range of 310–400 °C. The Cu (II) complexes did not show any activity against the Gram-(–) bacteria and the yeast *C. albicans*, while they have moderate bactericidal effect on Gram-(+) bacteria: *S. aureus* and *B. subtilis*. Both compounds have promoted decrease of the metabolic activity of HeLa (human adenocarcinoma), FemX (human melanoma) and LS174 (human colon carcinoma), which occurred in a dose-dependent fashion.

Acknowledgement. This research was funded by the Ministry of Education, Science and Technological Development, Republic of Serbia through Grant Agreement with University of Belgrade-Faculty of Pharmacy, No: 451-03-68/2022-14/200161.

ИЗВОД

НОВИ КОМПЛЕКСИ БАКАР(II)-ЦИКЛАМА СА АМИНОКАРБОКСИЛАТИНМ КОЛИГАНДИМА: СИНТЕЗА, КАРАКТЕРИЗАЦИЈА И IN VITRO АНТИПРОЛИФЕРАТИВНА И АНТИБАКТЕРИЈСКА АНАЛИЗА

БРАНКА ДРАЖИЋ¹, МИРЈАНА АНТОНИЈЕВИЋ-НИКОЛИЋ², МИЛЕНА МАРИНОВИЋ-ЦИНЦОВИЋ³, ВУКОСАВА ЖИВКОВИЋ-РАДОВАНОВИЋ⁴, БРАНКА БОРОВИЋ⁵ и СЛАЂАНА Б. ТАНАСКОВИЋ¹

¹Фармацеутски факултет, Универзитет у Београду, Војводе Степе 450, 11000 Београд, ²Академија примењених стручија Шабац, Одсек за медицинске, пословно-технолошке стручије, Хајдук Вељкова 10, 15000 Шабац, ³Институј за нуклеарне науке Винча, Универзитет у Београду, Мике Пејковића Аласа 12–14, 11351 Винча, Београд, ⁴Хемијски факултет, Универзитет у Београду, Студентски трг 16, 11000 Београд и ⁵Институј за хигијену и технологију меса, Каћанској 13, 11000 Београд

Синтетисана су два нова катјонска Cu(II) комплекса са цикламом (1,4,8,11-тетраазациклотетрадекан) и аминокарбоксилатним колигандима: глицином или аланином. Комплекси су окарактерисани елементалном анализом (C, H, N), моларном електричном проводљивошћу, мерењем магнетног момента на собној температури, спектралним методама (UV/Vis и Fourier трансформисаном инфрацрвеном спектроскопијом) као и термогравиметријском (TG) и диференцијалном термијском (DTA) анализом. Аналитички подаци комплекса показују формирање мононуклеарних комплекса опште формуле $[Cu(L)cyc](ClO_4)_2 \cdot nH_2O$, A) L = глицин, n = 1,5 и B) L = аланин, n = 2,5. Тетраентатни лиганд циклам је координован са металима преко четири N донора. Спектропски подаци сугеришу да су аминокарбоксилатни лиганди координовани преко својих карбоксилатних јона. У оба комплекса претпостављена је октаедарска геометрија око Cu(II). TG-DTA анализа показује да се комплекс B егзотермно разлаже у једном кораку у опсегу од 310–400 °C. Цитотоксична активност Cu(II) комплекса и почетних лиганада је тестирана на ћелијским линијама хуманог аденокарцинома грлића материце (HeLa), хуманог меланома (FemiX) и хуманог карцинома дебelog црева (LS174). Вредности IC₅₀ за комплексе Cu(II) биле су од 48,35 до 82,25 μM. Антимикробна активност оба комплекса је тестирана према *Staphylococcus aureus*, *Bacillus subtilis*, *Escherichia coli* и *Candida albicans*.

(Примљено 7. новембра 2021, ревидирано 7. марта, прихваћено 11. марта 2022)

REFERENCES

1. L. Radovanović, J. Rogan, D. Poleti, M. Milutinović, M. V. Rodić, *Polyhedron* **112** (2016) 18 (<https://doi.org/10.1016/j.poly.2016.03.054>)

2. L. Vera-Estrada, J. Uribe-Godinez, O. Jimenez-Sandoval, *RSC Adv.* **10** (2020) 22586 (<https://doi.org/10.1039/d0ra02904a>)
3. A. Ross, J-H Choi, T. M. Hunter, C. Pannecouque, S. A Moggach, S. Parsons, E. De Clercq, P. J. Sadler, *Dalton Trans.* **41** (2012) 6408 (<https://doi.org/10.1039/c2dt30140g>)
4. X. Liang, P.J. Sadler, *Chem. Soc. Rev.* **33** (2004) 246 (<https://doi.org/10.1039/B313659K>)
5. E. I. Solomon, D. E. Heppner, E. M. Johnston, J. W. Ginsbach, J. Cirera, M. Qayyum, M. T. Kieber-Emmons, C. H. Kjaergaard, R. G. Hadt, L. Tian, *Chem. Rev.* **114** (2014) 3659 (<https://doi.org/10.1021/cr400327t>)
6. E. Faggi, R. Gavara, M. Bolte, L. Fajará, L. Juliá, L.Rodríguez, I. Alfonso, *Dalton Trans.* **44** (2015) 12700 (<https://doi.org/10.1039/C5DT01496D>)
7. Z. Mardani, K. Moeini, M. Darroudi, C. Carpenter-Warren, A. M. Z. Slawin, J. D. Woollins, *J Coord Chem.* **72** (2019) 3030 (<https://doi.org/10.1080/00958972.2019.1684477>)
8. K. Babić-Samardžija, N. Hackerman, S. P. Sovilj, V. M. Jovanović, *J. Solid State Electrochem.* **12** (2008) 155 (<http://doi.org/10.1007/s10008-007-0375-4>)
9. W. Sibert, A. H. Cory, J. G. Cory, *J. Chem. Soc., Chem. Commun.* **2** (2002) 154 (<https://doi.org/10.1039/B107899M>)
10. S. J. Paisey, P. J. Sadler, *Chem. Commun.* **3** (2004) 306 (<https://doi.org/10.1039/B312752B>)
11. X. Liang, J. A. Parkinson, M. Weishaulp, R. O. Gould, S. J. Paisey, H. Park, T. M. Hunter, C. A. Blindauer, S. Parsons, P. J. Sadler, *J. Am. Chem. Soc.* **124** (2002) 9105 (<https://doi.org/10.1021/ja0260723>)
12. M. Kubeil, K. Zarschler, J. Pietzsch, W. Kraus, P. Comba, H. Stephan, *Eur. J. Inorg. Chem.* **24** (2015) 4013 (<https://doi.org/10.1002/ejic.201500510>)
13. E. Konig, *Magnetic Properties of Coordination and Organometallic Transition Metal Compounds*, Springer-Verlag, Berlin, 1966, p. 24 (ISBN: 978-3-540-03593-0)
14. T. Mosmann, *J. Immunol. Methods* **65** (1983) 55 ([http://dx.doi.org/10.1016/0022-1759\(83\)90303-4](http://dx.doi.org/10.1016/0022-1759(83)90303-4))
15. M. Ohno, T. Abe, *J. Immunol. Methods* **145** (1991) 199 (<https://www.ncbi.nlm.nih.gov/pubmed/1765652>)
16. W. J. Geary, *Coord. Chem. Rev.* **7** (1971) 81 ([https://dx.doi.org/10.1016/S0010-8545\(00\)80009-0](https://dx.doi.org/10.1016/S0010-8545(00)80009-0))
17. N. Abdullah, Z. Arifin, E. R. T. Tiekkink, N. Sharmin, N. S. A. Tajidi, S. A. M. Hussin, *J. Coord. Chem.* **69** (2016) 862 (<http://dx.doi.org/10.1080/00958972.2016.1147032>)
18. Z. H. Chohan, M. Arif, A. M. Akhtar, C. T. Supuran, *Bioinorg. Chem. Appl.* (2006) 83131 (<https://doi.org/10.1155/BCA/2006/83131>)
19. A. B. P. Lever, *Inorganic Electronic Spectroscopy*, 2nd ed., Elsevier, Amsterdam, 1984, p. 554 (ISBN 0-444-42389-3)
20. S. S. Massoud, F. A. Mautner, R. Vicente, H. N. Sweeney, *Inorg. Chim. Acta* **359** (2006) 1489 (<https://doi.org/10.1016/j.ica.2005.10.047>)
21. B. J. Hathaway, *Copper. Coord. Chem. Rev.* **52** (1983) 87 ([https://doi.org/10.1016/0010-8545\(83\)85019-X](https://doi.org/10.1016/0010-8545(83)85019-X))
22. G. G. Mohamed, C. M. Sharaby, *Spectrochim. Acta, A* **66** (2007) 949 (<https://doi.org/10.1016/j.saa.2006.04.033>)

23. K. Nakamoto, *Infrared and Raman Spectra of Inorganic and Coordination Compounds*, Part B, 5th ed., Wiley and Sons, New York, 1997, pp. 23–26, 59–62, 83, 271 (ISSN: 0260-3594)
24. G. B. Deacon, R. J. Philips, *Coord. Chem. Rev.* **33** (1980) 227 ([https://doi.org/10.1016/S0010-8545\(00\)80455-5](https://doi.org/10.1016/S0010-8545(00)80455-5))
25. D. Lin-Vien, N. B. Colthup, W. G. Fateley, J. G. Grasselli, *The handbook of infrared and raman characteristic frequencies of organic molecules*, Academic Press, San Diego, CA, 1991 (ISBN: 9780080571164)
26. K. Nakamoto, *Infrared and Raman Spectra of Inorganic and Coordination Compounds: Part B: Applications in Coordination, Organometallic, and Bioinorganic Chemistry*, John Wiley & Sons Inc., Hoboken, NJ, 2009 (ISBN 978-0-471-74493-1)
27. L. Tripathi, P. Kumar, and A. K. Singhai, *Indian J. Cancer* **44** (2007) 62 (<https://doi.org/10.4103/0019-509X.35813>)
28. H. Elo, Z. *Naturforsch. C* **59** (2004) 609 (<https://doi.org/10.1515/znc-2004-7-828>)
29. D. Jayaraju, A. K. Kondapi, *Curr. Sci.* **81** (2001) 787 (<http://www.jstor.org/stable/24106398>)
30. S. S. Hindo, M. Frezza, D. Tomco, M. J. Heeg, L. Hryhorczuk, B. R. McGarvey, Q. P. Dou, C. N. Verani, *Eur. J. Med. Chem.* **44** (2009) 4353 (<https://doi.org/10.1016/J.Ejmec.2009.05.019>)
31. I. Iakovidis, I. Delimaris, S. M. Piperakis, *Mol. Biol. Int.* **2011** (2011) 594 (<https://doi.org/10.4061/2011/594529>)
32. E. Tacconelli, N. Magrini, *Global Priority List of Antibiotic Resistant Bacteria to Guide Research, Discovery and Development of New Antibiotics*, World Health Organization publications, Geneva, 2017, p. 1 (https://www.who.int/medicines/publications/WHO-PPL-Short_Summary_25Feb-ET_NM_WHO.pdf)
33. M. N. Patel, P. B. Pansuriya, P. A. Parmar, D. S. Gandhi, *Pharm. Chem. J.* **42** (2008) 687 (<https://dx.doi.org/10.1007/s11094-009-0214-2>)
34. C. Dendrinou-Samara, G. Psomas, C. P. Raptopoulou, D. P. Kessissoglou, *J. Inorg. Biochem.* **83** (2001) 7 ([https://doi.com/10.1016/s0162-0134\(00\)00131-8](https://doi.com/10.1016/s0162-0134(00)00131-8))
35. S. K. Sengupta, O. P. Poudey, B. K. Srivastava, V. K. Sharma, *Transition Met. Chem.* **23** (1998) 349 (<https://doi.org/10.1023/A:1006986131435>).



Investigations on the role of cation–π interactions in active centres of superoxide dismutase

SRĐAN Đ. STOJANOVIĆ¹ and MARIO V. ZLATOVIĆ^{2*}#

¹*University of Belgrade-Institute of Chemistry, Technology and Metallurgy, Department of Chemistry, Belgrade, Serbia* and ²*Faculty of Chemistry, University of Belgrade, Belgrade, Serbia*

(Received 9 January, revised 17 February, accepted 21 February 2022)

Abstract: In this study, we have analysed the influence of cation–π interactions on stability and properties of superoxide dismutase (SOD) active centres. The number of interactions formed by arginine is higher than by lysine in the cationic group, while those formed by histidine are comparatively higher in the π group. The energy contribution resulting from most frequent cation–π interactions was in the lower range of strong hydrogen bonds. The cation–π interactions involving transition metal ions as cation have energy more negative than –418.4 kJ mol^{–1}. The stabilization centres for these proteins showed that all the residues involved in cation–π interactions were important in locating one or more of such centres. The majority of the residues involved in cation–π interactions were evolutionarily conserved and might have a significant contribution towards the stability of SOD proteins. The results presented in this work can be very useful for understanding the contribution of cation–π interactions to the stability of SOD active centres.

Keywords: superoxide dismutase; cation–π interactions; catalytic site.

INTRODUCTION

Non-covalent interactions maintain an intricate balance between the rigidity and the flexibility in proteins. Understanding the balance of non-covalent interactions is vital for the stability and interactivity of biological macromolecules.¹ Cation–π interactions, as an ensemble of noncovalent attraction, play an important role in many areas ranging from molecular biology to materials design.^{2–7} In biology, consenting cations can be found in the basic side chains of proteins, as well as in many different ligands, toxins, other small molecules, or even ions that might closely interact with the protein. Similarly, the π-electron partner in a

* Corresponding author. E-mail: mario@chem.bg.ac.rs

Serbian Chemical Society member.

<https://doi.org/10.2298/JSC220109013S>

cation– π interaction can be provided either by aromatic side chains (Phe, Tyr or Trp), or by an aromatic moiety of an interacting ligand. Note that the side chain of histidine may formally act as a cation or as an aromatic group, thus requiring particular consideration.⁸ For the guanidinium moiety of arginine (a dispersed π -system itself) the side chain can interact with an aromatic through parallel (stacking) or perpendicular (T-shaped) geometries.⁹

The cation– π interaction is electrostatic in its nature, because the major contributions arise from the electrostatic attractions between cations and the quadrupole moment of the aromatics.¹⁰ This type of noncovalent interaction can be very strong, as has been showed by the solid-state studies of small-molecule crystal structures,^{11,12} and by theoretical and experimental analyses in the gas phase and in aqueous media.^{12–14} The strength of cation– π interactions ranges between 8.4 and 627.6 kJ mol^{−1},¹⁵ sometimes comparable to the strong hydrogen bonds. Its strength critically depends on the nature of aromatic system and charge of the cation.² Depending on the type of cations and the nature of the π system, it can be regulated to be weak as well. The adjustability of cation– π interaction offers a potential strategy modification of the neighbouring environment, where it is involved. Cation– π interactions are therefore considered to be an essential force in generating tertiary and quaternary protein structures induced by oligomerization and protein folding.¹⁶

Hence, we attempted to explore the nature, range, strength, and significance of the cation– π interactions in SOD proteins, which could help in understanding the protein stability and mechanism, and similarly in protein-engineering and modelling.

EXPERIMENTAL

Dataset

For this study, we used the Protein Data Bank (PDB), accessed on May 10th, 2021, at that moment listing 183,118 resolved structures.¹⁷ The selection criteria for superoxide dismutase to be included in the dataset were as follows: 1) crystal structures of proteins containing E.C. Number 1.15.1.1 (superoxide dismutase) with metal were accepted; 2) theoretical model structures and NMR structures were not included (these structures were not accepted as it was difficult to define the accuracy of the ensemble of structures in terms of displacement that was directly comparable to the X-ray diffraction studies); 3) only crystal structures with the resolution of 0.2 nm or better and a crystallographic *R*-factor of 25.0 % or lower were accepted; 4) we included only representatives having at least 30 % sequence identity. After assembling the dataset, several structures containing ligands and mutant amino acids were rejected, leaving 43 proteins that were actually used as the dataset in our analysis. Hydrogen atoms were added and optimized, where needed, using the program REDUCE,¹⁸ with default settings. REDUCE software adds hydrogen atoms to protein and/or DNA structures in standardized geometry, optimizing them to the orientations of OH, SH, NH₃⁺, Met methyls, Asn and Gln sidechain amides, and His rings. The applied software determines the best hydrogen positions by selecting the best overall score from all the possible combinations, taking into the account single scores assigned for each individual residue and for groups containing movable

protons partitioned in closed sets of local interacting networks. The PDB IDs of selected structures were as follows: 1ar5, 1cbj, 1d5n, 1hl5, 1ids, 1isa, 1kkc, 1luv, 1my6, 1qnn, 1srd, 1to4, 1unf, 1xre, 1xuq, 1y67, 1yai, 1ys0, 2aqn, 2cw2, 2goj, 2rcv, 2w7w, 3ak2, 3ce1, 3dc6, 3evk, 3f7l, 3h1s, 3js4, 3lio, 3lsu, 3mds, 3pu7, 3tqj, 4br6, 4c7u, 4f2n, 4ffk, 4yet, 5a9g, 5vf9 and 6bej.

Cation- π interaction analysis

For selecting the protein structures having various types of cation- π interactions, Discovery Studio Visualizer 2020 was used,¹⁹ with some specific criteria and geometrical feature settings. The following tests were performed to find cation- π interactions: 1) cations were considered to be atoms having a formal charge of at least +0.5 to allow the inclusion of delocalized cationic species such as lysine and arginine side chains; 2) the distance (R) between a cation and the centroid of a π ring should be less than the π -cation (max dist) cutoff (0.7 nm by default, see R in Fig. 1); 3) The angle (θ) between the cation-centroid vector and the normal to the ring plane should be less than the π -cation maximum angle (45° by default, see θ in Fig. 1). The aromatic systems include the aromatic side chains of the residues tryptophan (Trp), tyrosine (Tyr), phenylalanine (Phe), and histidine (His). All the metal ions present in the database are treated as cations, apart from the protonated basic amino acid residues lysine (Lys) and arginine (Arg). However, as His can act either as cation or as an aromatic moiety depending on its protonation state, in our study both the possibilities are considered.

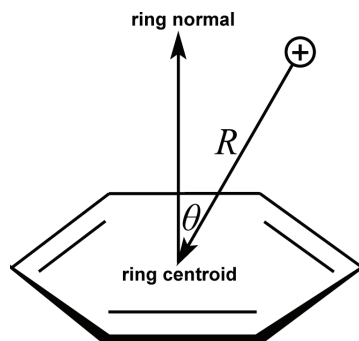


Fig. 1. Parameters for cation- π interactions: (R) the distance between the cation and the centroid; (θ) the angle between the cation-centroid vector and the normal to the ring plane. The figure was derived from parameters described in this subsection.

Computation of cation- π interaction energy

In order to apply *ab initio* methods in determining the energies of cation- π pairs on desired level of theory, with sufficient level of accuracy and still in satisfactory time frame, calculations were performed on structurally reduced model systems.²⁰ We used butan-1-amine (**1**) and 2-propylguanidine (**2**) as mimics for lysine and arginine groups, respectively. Phenylalanine was simplified to toluene (**3**), histidine to 5-methyl-1*H*-imidazole (**4**), tryptophan to 3-methyl-*H*-indole (**5**) and tyrosine was reduced to 4-methylphenol (**6**), Fig. 2.

The use of reduced model systems in calculations of specific intramolecular interaction in large systems is a well known and already proved methodology,²¹ producing accurate enough results, and still significantly reducing computation times and strength needed for them. Larger models, like whole amino acids, or parts of protein chain, will unnecessary complicate calculations and probably even bring in errors. Numerous interactions mechanisms are possible in a larger protein structure, and a single binding energy computation cannot always correctly determine which of these interactions are present and to what amount they contribute to overall stabilization. As a result, separating the involvement of the cation- π interaction and

their energy contributions from the interacting pair residues involved in other noncovalent interactions is difficult.

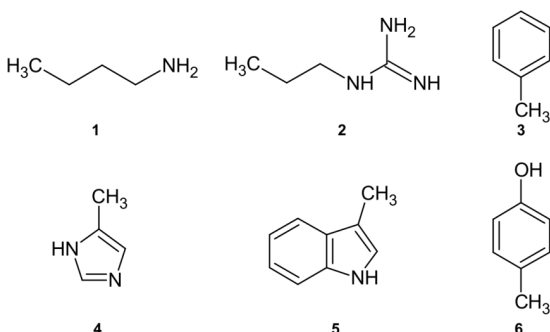


Fig. 2. Structurally reduced structures used for calculations of cation– π interaction energy. (1) instead of lysine; (2) instead of arginine; (3) instead of Phe; (4) instead of His; (5) instead of Trp; (6) instead of Tyr.

Ab initio calculations were performed by Jaguar from Schrödinger Suite 2018-1,²² using the local Møller–Plesset second-order (LMP2) method with triple zeta Dunning's correlation consistent basis set²³ and ++ diffuse functions.²⁴ All calculations were performed in vacuum. The LMP2 method applied to the study of cation– π interactions, showed to be considerably faster than the MP2 method, while the calculated interaction energies and equilibrium distances were almost identical for both methods.²⁵ Several authors found that LMP2 represents an excellent method for the calculation of interaction energies in proteins.^{26,27} Sometimes calculation results can be influenced largely by BSSE (basis set superposition error), and considering it is mandatory, making the calculation times significantly longer. Local correlation methods (such as LMP2) not only reduce the cost of the calculations, but LMP2 is also well known for reducing intramolecular BSSE.^{28–30}

The geometries of interacting structures were optimized using LMP2/cc-pVTZ(-f)++ level of theory and their single point energies calculated at LMP2/cc-pVTZ++ level. For the transition metal atoms, we used the LMP2/LACVP** for geometry optimization and LMP2//LACV3P** for energy evaluation with effective core potentials (ECPs). The LACV3P basis set is a triple-contraction of the LACVP basis set,³¹ developed and tested at Schrödinger, Inc.²² The optimized geometries were placed in space to match corresponding complexes by superimposing heavy atoms onto their respective coordinates from crystal structures and then the energies of dimeric structures produced in that way were calculated.

The cation– π interaction energies in dimers (cation– π pairs) were calculated as the difference between the energy of the complex and the sum of the energies of the monomers in their optimized geometries.

As mentioned earlier, the energies in this work were calculated in gas phase. When observing *in vitro* processes, we can expect that the water molecules and other atoms and groups from the protein structure could be present in the vicinity, influencing the binding process. To correctly describe the binding, one must be well aware of the role of solvent in the complete process of binding to the proteins. To accurately depict the enthalpy of binding and calculate the interacting energy of bonded structures, high-level quantum mechanical calculations with extended basis sets, including large number of atoms both in protein and ligand as well,

together with water molecules would be needed. But for the complete understanding of biological complexes and their behaviour, the free-energy changes (ΔG) have to be calculated using some statistical mechanics method.^{32,33} Recent theoretical studies of the long-range non-covalent interactions in protein side chains showed that the use of the dielectric continuum in order to take the account for the electronic polarization and small backbone fluctuations in proteins could sometimes lead to decrease in bonding energies for some of those interactions.³² However, a significant number of cation- π interaction pairs appear to be located in buried regions, thus minimizing the influence on cation- π interactions or direct disruption of the cation- π pairs by water molecules. However, this will exceed the main goal of this article, which is to point out the possible contribution and significance of energies of cation- π interactions to stability and orientation in proteins.

Computation of stabilization centres

Stabilization centres (SC) are defined as the clusters of residues making cooperative, non-covalent long-range interactions.³⁴ Measured as individual interactions, the stabilization forces resulting from non-covalent long-range interactions are not very strong, but since they are cooperative by their nature, in regions where they act in a group (SC) they could play an important role in maintaining the overall stability of protein structures. In order to analyse SC of interaction-forming residues, we used the SCide program.³⁵ The criteria SCide uses for determining SC are as follows: 1) two residues are in contact if there is, at least, one heavy atom–atom distance smaller than the sum of their van der Waals radii plus 0.1; 2) a contact is recognized as “long-range” interaction if the interacting residues are, at least, ten amino acids apart; 3) two residues form a stabilization centre if they are in long-range interaction and if it is possible to select one–one residues from both flanking tetrapeptides of these two residues that make, at least, seven contacts between these two triplets.³⁵

Computation of conservation of amino acid residues

The conservation of amino acid residues in each protein was computed using the ConSurf server.³⁶ This server calculates the conservation based on the comparison of the sequence of given PDB chain with the proteins deposited in Swiss–Prot database³⁷ and identifies ones that are homologous to the PDB sequence. The number of position-specific iteratives (PSI)–BLAST and the *E*-value cut-off used in all similarity searches were 1 and 0.001, respectively. All the sequences, evolutionary related to each one of the proteins in the dataset, were used in the subsequent multiple alignments. Based on these protein sequence alignments, the residues were classified into nine categories, from highly variable to highly conserved. Residues with a score of 1 are considered to be highly variable and residues with a score of 9 are considered to be highly conserved.

RESULTS AND DISCUSSION

The presence of cation- π interactions in key positions in the active site of proteins, provides scope to control the processes, which they regulate and helps in modification or design of new ligand molecules.³⁸ The quantitative understanding of drug receptor interaction with biological receptors is of prime importance in pharmacy. Therefore, the presence of cation- π interactions could be used as a means of making a difference between chemically relevant docking results and false positives. This scrutiny will assist structural biologist and medicinal chemist to design better and safer drugs.

In this study, we have analysed the influence of cation–π interactions in 43 SOD crystal structures. We have focused our study at the active centres of SOD and hence the cation–π interactions within the rest of the protein structures were not considered. The analysed protein set contains 272 cation–π interactions. We have investigated the structural stability patterns of cation–π interactions in SOD proteins in relation to other environmental preferences like preference of cation–π interaction forming residues, interaction geometries and energetic contribution of cation–π interactions, stabilization centres and conservation patterns.

Preference of cationic and aromatic residues for forming cation–π interactions

The preference of amino acid residues that are involved in cation–π interactions was analysed, and the results are presented in Table I. We observed that in these proteins, among the cationic residues involvement of, Arg in the cation–π interactions is preferred to Lys and His. The number of interactions involving His and Lys residues is almost similar. It is interesting to observe that there is a significant number of Zn²⁺–π interactions. Among the aromatic residues involved in cation–π interactions, His has the highest occurrence, and the contribution of Phe is twice to that of Trp and Tyr has the lowest occurrence. This might be because His occurs most frequently in both coordination spheres of SOD active centres of all the aromatic amino acids.^{9,20} Generally the composition of cation–π interaction forming residues is similar to other globular proteins.^{39–42}

TABLE I. Frequency of occurrence of cation–π interaction-forming residues in active centers of superoxide dismutase

Residue	Number ^a	Occurrence ^b , %
Cationic		
Lys ⁺	20	7.35
Arg ⁺	197	72.43
His ⁺	15	5.51
Zn ²⁺	40	14.71
Total	272	100
Aromatic		
His	135	49.63
Phe	79	29.04
Trp	43	15.82
Tyr	15	5.51
Total	272	100

^aThe number of times a particular amino acid occurs in an appropriate interaction; ^bpercent of amino acid occurs in an appropriate interaction

The organization of multicomponent supramolecular assemblies is often governed by multiple non-covalent interactions.⁴³ Ternary complexes are the simplest model systems where one can understand how pair of cation–π interactions mutually influences each other.^{41,44} The specific arrangement or connect-

ivity of cation- π clusters in proteins could significantly influence their structural stability. The analysis shows that around 54 % of the total interacting residues in the dataset are involved in the formation of multiple cation- π interactions. In numerous crystal structures of superoxide dismutases, we found that a cationic residue can interact with several aromatic residues. This type of interaction is marked as furcation. For example, Fig. 3 shows potentially interesting arrangement, the presence of two aromatic groups surrounding one cation. A cation group from A:Arg114 can interact with two aromatic rings of A:Phe49 and A:Phe63 simultaneously. The binding motif between a single cation and two aromatic rings, “ π -cation- π ”, plays a pivotal role in maintaining the acceptor functional structure.⁴⁵

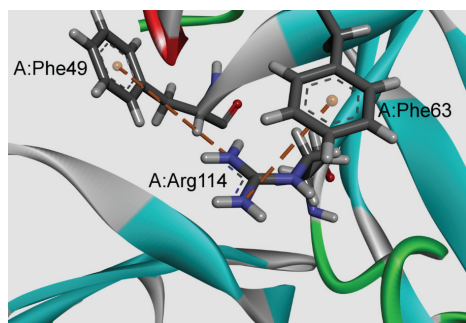


Fig. 3. Example of a multiple cation- π interactions for the cytosolic Cu/Zn SOD from *Schistosoma mansoni* (PDB code 1to4); the interactions are marked with a brown dashed lines.

Interaction geometries and energetic contribution of cation- π interactions

Fig. 4a shows the distribution of distances for cation- π interaction pairs and indicates that these pairs predominantly occur when the residues are separated 0.4 nm or more, without showing a clear geometrical preference. The most favourable distance for the cation- π interacting pairs lies in the range of 0.6–0.7 nm. The distributions of the angle between the cation and the ring plane were in angles (10 to 90° range, with a preference for higher angle values (Fig. 4b), the largest number of pairs occurring between 40 and 80°. These calculations clearly indicate that an effective cation- π interactions can occur across a wider area above the π -ring. The fluctuations are clearly a consequence of their greater flexibility and the geometrical features relating two residue-types are expected to be rather broad.

There are numerous factors that energy of cation- π interaction could depend on: size and electronic structure of the cation, nature of the π -ligand, the directionality and interplay with other noncovalent interactions.⁷ The calculated energies of the optimized cation- π interaction pairs range between -451.9 and 20.9 kJ mol⁻¹, with a most populated bin at -4.2 to -29.3 kJ mol⁻¹ (Fig. 5). The energies of the most frequent cation- π interactions examined here are in the

lower range of strong hydrogen bonds (-16.8 to -62.8 kJ mol $^{-1}$), as classified by Desiraju and Steiner.⁴⁶

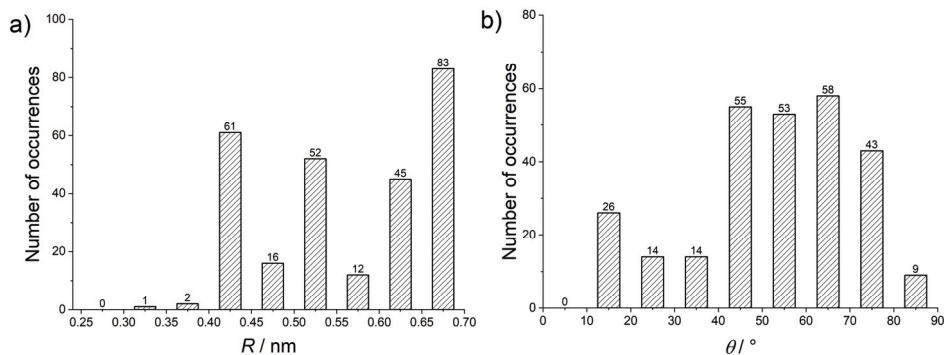


Fig. 4. Interaction geometries of cation-π interactions: a) R distance distribution, b) θ angle distribution.

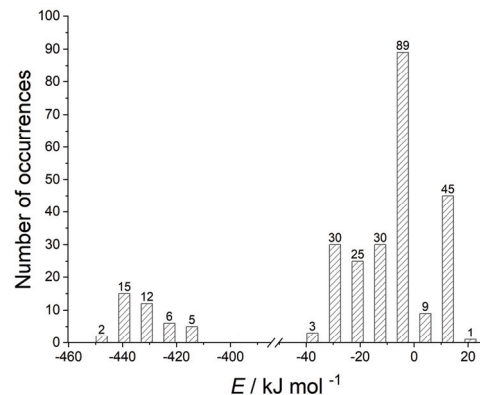


Fig. 5. Interaction energies of cation-π interactions.

The energies calculated for many of the cation-π interactions are substantially stabilizing, with roughly 20 % in this set showing positive (repulsive) predicted interaction energies. The repulsive nature of those interactions emerges from the unfavourable geometries of cation-π interactions in the crystal structures and is usually counterbalanced by other interactions.²⁰ The strongest attractive interactions (with energies more negative than -418.4 kJ mol $^{-1}$) arises for the cation-π interactions involving transition metal ions. These interactions, almost strong as covalent ones, owe their strength to the existence of d orbitals (strong electrostatic effect caused by the proximity of the metal centre). This range shows that these interactions are among the strongest noncovalent interactions, and most probably plays an important stabilizing role. In Fig. 6, we showed the structural details of the cation-π interaction involving the transition metal ions of bovine Cu/Zn SOD (PDB code 1cbj). Among amino acid the pair

$\text{His}^+ \text{--Trp}$ has strongest attractive interaction (about $-29.3 \text{ kJ mol}^{-1}$). The protonated histidine (His^+) is the cation in the cation- π interactions. The cation- π interaction energy of $\text{His}^+ \text{--Trp}$ is larger than other two interaction pairs ($\text{His}^+ \text{--Tyr}$ and $\text{His}^+ \text{--Phe}$), because of the larger aromatic system in Trp. The indole group of Trp consists of two aromatic rings: one five-membered and one six-membered. Both can take part in cation- π interactions and they can even do this simultaneously. While the cation- π interaction may be weak, they can occur frequently, rendering its overall effect on protein structure significant. Also, when a large network of interactions is considered, cooperativity could emerge, either enhancing or diminishing the overall effect.⁴³

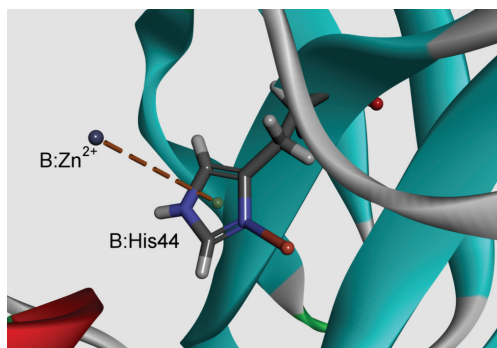


Fig. 6. Example of the cation- π interaction involving transition metal ions of bovine Cu/Zn SOD (PDB code 1cbj). The interaction is marked with a brown dashed line: B: Zn^{2+} —B:His44; $R = 0.53 \text{ nm}$, $\theta = 12.42^\circ$, $E = -436.5 \text{ kJ mol}^{-1}$.

Stabilization centres and conservation of amino acid residues

The performed structural and sequential conservation analysis showed a higher conservation of stabilization centres over protein families.³⁴ We have computed the stabilization centres for all cation- π interaction forming residues in SOD active centers. Results showed 43 % of cationic residues and 37 % of π -residues having one or more stabilization centres. From the observed results, we infer that all these residues might contribute additional stability to SOD proteins in addition to their participation in cation- π interactions.

An illustrative example of cation- π interaction involving more stabilization centres is showed in Fig. 7. A cation group from A:Arg142 interacts with π -system of A:His62. The three stabilization centres are indicated by wire-meshed surface (red labels). The residue A:Arg142 is part of A51 and A122 stabilization centres while A:His62 is part of A50 stabilization centre.

From our results we assume that most of the residues involved in cation- π interactions are evolutionarily conserved (more than 68 %, with a conservation score ≥ 6) and might have a significant contribution to the stability of SOD proteins.

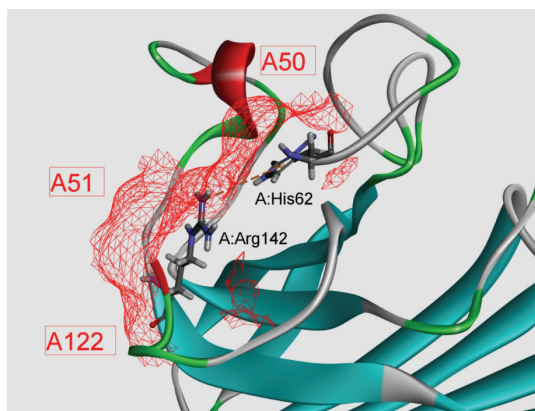


Fig. 7. Details of cation– π interaction involving more stabilization centers at active center of cytosolic Cu/Zn SOD from *Schistosoma mansoni* (PDB ID code 1to4). The cation– π interaction is marked with a brown dashed line (A:Arg142–A:His62; $R = 0.676$ nm, $\theta = 72.88^\circ$, $E = -31.2$ kJ mol $^{-1}$).

CONCLUSION

We have systematically analyzed the influence of cation– π interactions on the stability of SOD active centres. The side chain of Arg is more likely to be in cation– π interactions than Lys and His $^+$ in the cationic residues. His has the highest occurrence in this interaction, more than the other three π -residues, Phe, Tyr and Trp. From the results it can be underlined that around 54 % of the total interacting residues in the dataset are involved in the formation of multiple cation– π interactions. The distribution of distances for cation– π interactions was found to be in the distance range of 0.6–0.7 nm, and the angle distribution with a preference for higher angle values (10 to 90° range). Our results suggest the majority of the cation– π interactions will occur in energy range from −4.2 to −29.3 kJ mol $^{-1}$. The strongest interactions (with energies more negative than −418.4 kJ mol $^{-1}$) arise for the cation– π interactions involving transition metal ions. We found that all the residues found in cation– π interactions are important in locating one or more stabilization centres. In the cation– π interacting residues, 68 % of the amino acid residues that are involved in these interactions might be conserved in SOD. From all of that, we could conclude that the contribution of cation– π interactions is an important factor contributing to the structural stability of the SOD active centres that are investigated in this work.

Acknowledgment. The authors would like to thank the Ministry of Education, Science and Technological Development of Republic of Serbia (Grant No: 451-03-68/2022-14/200026 and 451-03-68/2022-14/200168) for financial support.

И З В О Д

ИСПИТИВАЊЕ УЛОГЕ КАТЈОН- π ИНТЕРАКЦИЈА У АКТИВНИМ ЦЕНТРИМА
СУПЕРОКСИД-ДИСМУТАЗА

СРЂАН Ђ. СТОЈАНОВИЋ¹ и МАРИО В. ЗЛАТОВИЋ²

¹Универзитет у Београду – Институт за хемију, технолођију и мешавине, Београд и ²Хемијски факултет, Универзитет у Београду, Београд

У овој студији смо анализирали утицај катјон- π интеракција на стабилност и особине активних центара супероксид-дисмутазе (SOD). Број интеракција које формира аргинин је већи од лизина у групи катјона, док је хистидин сразмерно већи у π групи. Енергетски допринос који је резултат најчешћих катјон- π интеракција био је у доњем опсегу јаких водоничних веза. Катјон- π интеракције које укључују јоне прелазних метала као катјон имају енергију негативнију од $-418,4 \text{ kJ mol}^{-1}$. Стабилизациони центри ових протеина показали су да су сви остаци укључени у катјон- π интеракције важни у распоређивању једног или више таквих центара. Већина остатака који су укључени у катјон- π интеракције су еволуцијски конзервирани и могли би имати значајан допринос стабилности SOD протеина. Резултати представљени у овом раду могу бити веома корисни за разумевање доприноса катјон- π интеракција стабилности активних центара SOD.

(Примљено 9. јануара, ревидирано 17. фебруара, прихваћено 21. фебруара 2022)

REFERENCES

1. K. A. Dill, *Biochemistry* **29** (1990) 7133 (<https://doi.org/10.1021/bi00483a001>)
2. J. C. Ma, D. A. Dougherty, *Chem. Rev.* **97** (1997) 1303 (<https://doi.org/10.1021/cr9603744>)
3. K. S. Kim, P. Tarakeshwar, J. Y. Lee, *Chem. Rev.* **100** (2000) 4145 (<https://doi.org/10.1021/cr990051i>)
4. R. Wintjens, J. Liévin, M. Rooman, E. Buisine, *J. Mol. Biol.* **302** (2000) 393 (<https://doi.org/10.1006/jmbi.2000.4040>)
5. J. Cheng, W. Zhu, Y. Tang, Y. Xu, Z. Li, K. Chen, H. Jiang, *Chem. Phys. Lett.* **422** (2006) 455 (<https://doi.org/10.1016/j.cplett.2006.03.005>)
6. H. Ghiassi, H. Raissi, *J. Sulfur Chem.* **36** (2015) 48 (<https://doi.org/10.1080/17415993.2014.962537>)
7. N. Kumar, A. S. Gaur, G. N. Sastry, *J. Chem. Sci.* **133** (2021) 97 (<https://doi.org/10.1007/s12039-021-01959-6>)
8. S. M. Liao, Q. S. Du, J. Z. Meng, Z. W. Pang, R. B. Huang, *Chem. Cent. J.* **7** (2013) 44 (<https://doi.org/10.1186/1752-153X-7-44>)
9. S. Stojanović, Z. Petrović, M. Zlatović, *J. Serb. Chem. Soc.* **86** (2021) 781 (<https://doi.org/10.2298/JSC210321042S>)
10. S. Mecozzi, A. P. West, D. A. Dougherty, *J. Am. Chem. Soc.* **118** (1996) 2307 (<https://doi.org/10.1021/ja9539608>)
11. R. A. Kumpf, D. A. Dougherty, *Science* **261** (1993) 1708 (<https://doi.org/10.1126/science.8378771>)
12. D. Zhu, B. E. Herbert, M. A. Schlautman, E. R. Carraway, *J. Environ. Qual.* **33** (2004) 276 (<https://doi.org/10.2134/jeq2004.2760>)
13. L. M. Salonen, M. Ellermann, F. o. Diederich, *Angew. Chem. Int. Ed.* **50** (2011) 4808 (<https://doi.org/10.1002/anie.201007560>)

14. M. Moradi, A. A. Peyghan, Z. Bagheri, M. Kamfiroozi, *J. Mol. Mod.* **18** (2012) 3535 (<https://doi.org/10.1007/s00894-012-1366-7>)
15. U. D. Priyakumar, M. Punnagai, G. P. Krishna Mohan, G. N. Sastry, *Tetrahedron* **60** (2004) 3037 (<https://doi.org/10.1016/j.tet.2004.01.086>)
16. L. Brocchieri, S. Karlin, *Proc. Natl. Acad. Sci. USA* **91** (1994) 9297 (<https://doi.org/10.1073/pnas.91.20.9297>)
17. P. W. Rose, B. Beran, C. Bi, W. F. Bluhm, D. Dimitropoulos, D. S. Goodsell, A. Prlic, M. Quesada, G. B. Quinn, J. D. Westbrook, J. Young, B. Yukich, C. Zardecki, H. M. Berman, P. E. Bourne, *Nucleic Acids Res.* **39** (2011) D392 (<https://doi.org/10.1093/nar/gkq1021>)
18. J. M. Word, S. C. Lovell, J. S. Richardson, D. C. Richardson, *J. Mol. Biol.* **285** (1999) 1735 (<https://doi.org/10.1006/jmbi.1998.2401>)
19. *Discovery Studio Visualizer, Release 2020*, Accelrys Software Inc., Accelrys Software Inc., San Diego, CA, 2020
20. V. R. Ribić, S. Đ. Stojanović, M. V. Zlatović, *Int. J. Biol. Macromol.* **106** (2018) 559 (<https://doi.org/10.1016/j.ijbiomac.2017.08.050>)
21. J. Hostaš, D. Jakubec, R. A. Laskowski, R. Gnanasekaran, J. Řezáč, J. Vondrášek, P. Hobza, *J. Chem. Theory Comput.* **11** (2015) 4086 (<http://dx.doi.org/10.1021/acs.jctc.5b00398>)
22. Schrödinger Release 2018-1: Jaguar, Schrödinger, LLC, New York, 2018
23. T. H. Dunning, *J. Chem. Phys.* **90** (1989) 1007 (<https://doi.org/10.1063/1.456153>)
24. T. Clark, J. Chandrasekhar, G. n. W. Spitznagel, P. V. R. Schleyer, *J. Comput. Chem.* **4** (1983) 294 (<https://doi.org/10.1002/jcc.540040303>)
25. A. D. Bochevarov, E. Harder, T. F. Hughes, J. R. Greenwood, D. A. Braden, D. M. Philipp, D. Rinaldo, M. D. Halls, J. Zhang, R. A. Friesner, *Int. J. Quantum Chem.* **113** (2013) 2110 (<https://doi.org/10.1002/qua.24481>)
26. K. E. Riley, J. A. Platts, J. Řezáč, P. Hobza, J. G. Hill, *J. Phys. Chem., A* **116** (2012) 4159 (<https://doi.org/10.1021/jp211997b>)
27. G. J. Jones, A. Robertazzi, J. A. Platts, *J. Phys. Chem., B* **117** (2013) 3315 (<https://doi.org/10.1021/jp400345s>)
28. S. Saebø, W. Tong, P. Pulay, *J. Chem. Phys.* **98** (1993) 2170 (<https://doi.org/10.1063/1.464195>)
29. A. Reyes, L. Fomina, L. Rumsh, S. Fomine, *Int. J. Quantum Chem.* **104** (2005) 335 (<https://doi.org/10.1002/qua.20558>)
30. R. M. Balabin, *J. Chem. Phys.* **132** (2010) 231101 (<https://doi.org/10.1063/1.3442466>)
31. P. J. Hay, W. R. Wadt, *J. Chem. Phys.* **82** (1985) 299 (<https://doi.org/10.1063/1.448975>)
32. Y. Deng, B. t. Roux, *J. Phys. Chem., B* **113** (2009) 2234 (<https://doi.org/10.1021/jp807701h>)
33. J. C. Gumbart, B. t. Roux, C. Chipot, *J. Chem. Theory Comput.* **9** (2013) 794 (<https://doi.org/10.1021/ct3008099>)
34. Z. Dosztányi, A. Fiser, I. Simon, *J. Mol. Biol.* **272** (1997) 597 (<https://doi.org/10.1006/jmbi.1997.1242>)
35. Z. Dosztányi, C. Magyar, G. Tusnady, I. Simon, *Bioinformatics* **19** (2003) 899 (<https://doi.org/10.1093/bioinformatics/btg110>)
36. H. Ashkenazy, E. Erez, E. Martz, T. Pupko, N. Ben-Tal, *Nucleic Acids Res.* **38** (2010) W529 (<https://doi.org/10.1093/nar/gkq399>)

37. B. Boeckmann, A. Bairoch, R. Apweiler, M. C. Blatter, A. Estreicher, E. Gasteiger, M. J. Martin, K. Michoud, C. O'Donovan, I. Phan, S. Pilbout, M. Schneider, *Nucleic Acids Res.* **31** (2003) 365 (<https://doi.org/10.1093/nar/gkg095>)
38. A. S. Mahadevi, G. N. Sastry, *Chem. Rev.* **113** (2013) 2100 (<https://doi.org/10.1021/cr300222d>)
39. M. M. Gromiha, *Biophys. Chem.* **103** (2003) 251 ([https://doi.org/10.1016/S0301-4622\(02\)00318-6](https://doi.org/10.1016/S0301-4622(02)00318-6))
40. B. P. Dimitrijević, S. Z. Borozan, S. Đ. Stojanović, *RSC Adv.* **2** (2012) 12963 (<https://doi.org/10.1039/C2RA21937A>)
41. S. Z. Borozan, B. P. Dimitrijević, S. Đ. Stojanović, *Comput. Biol. Chem.* **47** (2013) 105 (<https://doi.org/10.1016/j.compbiochem.2013.08.005>)
42. I. D. Mucić, M. R. Nikolić, S. Đ. Stojanović, *Protoplasma* **252** (2015) 947 (<https://doi.org/10.1007/s00709-014-0727-8>)
43. A. S. Mahadevi, G. N. Sastry, *Chem. Rev.* **116** (2016) 2775 (<https://doi.org/10.1021/cr500344e>)
44. D. Kim, E. C. Lee, K. S. Kim, P. Tarakeshwar, *J. Phys. Chem., A* **111** (2007) 7980 (<https://doi.org/10.1021/jp073337x>)
45. M. R. Davis, D. A. Dougherty, *Phys. Chem. Chem. Phys.* **17** (2015) 29262 (<https://doi.org/10.1039/C5CP04668H>)
46. G. R. Desiraju, T. Steiner, *The Weak Hydrogen Bond*, Oxford University Press, Oxford, 1999.



Rate coefficients for electron-impact dissociation of O_3^+ to singly charged fragments

DRAGOLJUB S. BELIĆ¹, MIRJANA M. VOJNOVIĆ¹, MIROSLAV M. RISTIĆ^{2*},
XAVIER URBAIN³ and PIERRE DEFRAНCE³

¹University of Belgrade, Faculty of Physics, P. O. Box 44, 11000 Belgrade, Serbia,

²University of Belgrade, Faculty of Physical Chemistry, P. O. Box 47, 11000 Belgrade,

Serbia and ³Université Catholique de Louvain, Institute of Condensed Matter and
Nanosciences, Chemin du Cyclotron 2, B-1348 Louvain-la-Neuve, Belgium

(Received 9 November, revised 11 December, accepted 13 December 2021)

Abstract: Rate coefficients for electron-impact dissociation of O_3^+ to the O^+ and O_2^+ fragments are calculated for the new, recommended cross section data set and for various collisional conditions. Two sets of the cross section data, measured recently by different experimental groups, are used. These cross sections differ significantly with each other, but are renormalized and optimized to the coherent data base. Rate coefficients for the ozone cation fragmentation are determined using the Maxwellian and the non-thermal electron energy distribution functions (EEDF). In the case of Maxwellian distribution, mean electron energies cover the range from zero up to 2 keV. Non-thermal electron energy distribution functions are adopted from the recent electron observations by the 3-D plasma and energetic particles experiment on the WIND spacecraft. The non-thermal rates are evaluated for the mean electron energies from 4 to 80 eV. The role of the possible contribution of electron-impact dissociation of O_3^+ to the ozone layer depletion has been emphasized.

Keywords: ozone cation; electron-molecule collisions; dissociative ionization, dissociative excitation.

INTRODUCTION

The problem of ozone layer depletion in the stratosphere is attracting significant attention of researchers, after the discovery of the Antarctic ozone hole.^{1,2} Various mechanisms contributing to the ozone molecule decomposition have been investigated in the past decades. A significant influence is attributed to the air pollutants, such as nitric oxides, as well as chlorine and bromine compounds.³ It has been recognized that the absorption of UV light leads to the ozone layer

* Corresponding author. E-mail: ristic@ffh.bg.ac.rs

Serbian Chemical Society member.

<https://doi.org/10.2298/JSC211109110B>

depletion, but some molecular reactions and collisions with atoms, ions and electrons present in the stratosphere are also found to play a role.^{4–6}

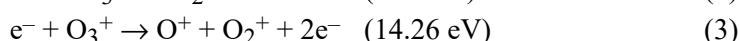
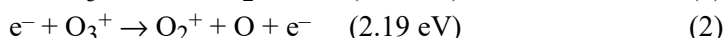
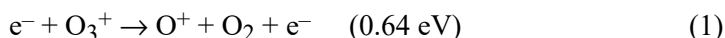
Electron-impact ionization of ozone has been studied experimentally,^{7,8} and also theoretically.⁹ These data are renormalized by the NIST Standard Reference Database.¹⁰ The renormalized cross section magnitude amounts $(3.8 \pm 0.5) \times 10^{-16}$ cm², at the maximum at 100 eV, with the threshold energy of 13.2 ± 0.5 eV. Visible and ultra violet (VUV) optical absorption and electron energy-loss spectroscopy of ozone have also been investigated and reviewed in detail.¹¹

The ozone cation O₃⁺ exists naturally in the atmosphere and is important for our understanding of ozone depletion as well.¹² The theoretical calculation of the electronic structure of the ozone cation is complex due to the strong electron correlations and a significant lacking of details of its potential energy surfaces. O₃⁺ is nonlinear and the bond distances and angles differ significantly for each electronic state. The three lowest doublet states are assigned X²A₁, A²B₂, and B²A₂ and their energies are all within 1 eV apart. The calculations show that the three lower quartet states are also close in energy, lying up to 2 eV above the ground state. The ozone cation is weakly bound and easily dissociates by photon absorption, electron collision, or recombination.

Electron-impact dissociative recombination of O₃⁺ has been investigated by the ion storage-ring method.¹³ This collision process is dominated at 0 eV by the three-body dissociation. The photo-dissociation of O₃⁺ yielding O⁺ or O₂⁺ fragments has also been studied intensively. It has been concluded that the formation of the O⁺ prevails in the visible light range.¹⁴

Electron-impact dissociation of O₃⁺ has recently been investigated in two separate experiments.^{15,16} The charged fragments, O⁺ and O₂⁺ were mass analyzed and the cross sections for their production were determined in a wide electron energy range.

In the present study, the above cited experimental results of O₃⁺ fragmentation are revisited. Some of the results are renormalized and the cross-section database is completed. In addition, the rate coefficients for corresponding processes, for Maxwellian and non-thermal electron energy distribution functions, are calculated and compared with each other. The following reactions are considered here:



The energies written in the parentheses represent the threshold energies for the given processes.¹⁵ Reactions (1) and (2) are dissociative excitation (DE) processes, while reaction (3) represents dissociative ionization (DI).¹⁶ In both exp-

eriments, only the charged fragments are detected, independently from each other. The reactions involving dissociation to three particles are not considered here.

Absolute cross sections for electron-impact dissociation of O_3^+ to the O^+ and to O_2^+ fragments have been measured first at ORNL, by Deng *et al.*¹⁵ An electron-ion crossed-beam method has been used for energies from about 3 to 100 eV. While the O_2^+ channel dominates the dissociation cross section over the entire electron energy range, a strong rise is also observed in the O^+ product channel, just above the threshold energy.

The cross sections for dissociation of O_3^+ to the O^+ fragments were also measured recently, at UCL (Louvain-la-Neuve), by Belić *et al.*¹⁶ This experiment also used a crossed-beam technique, but the results for dissociation producing the O^+ fragments disagree for a factor between 2 and 3, in a wide electron energy range, above 5 eV, the UCL results being larger than those of ORNL. This has been attributed to the broad O^+ fragments velocity and scattering angle distributions in the laboratory frame, causing a possible loss of the signal in the ORNL experiment. This effect is strongly affecting the DI signal leading to O^+ . It has been corrected in UCL experiment by performing careful magnetic field scans of the signal and by taking into account the transmission efficiency of the experiment. The correction procedure has been described in detail.¹⁶

The maximum of the O^+ cross section is found to be $3.6 \times 10^{-16} \text{ cm}^2$ at about 100 eV and has an average value of $3 \times 10^{-16} \text{ cm}^2$ in a wide energy range from 5 to 200 eV.¹⁶ Such a broad energy interval of high cross sections may result in a higher rate coefficient values for the considered process. Thus, we can raise the question of the importance of electron-impact dissociation of the ozone cation in the stratospheric layer, relative to the other competitive mechanisms. Furthermore, it may be possible that the electrons, originating from the Solar wind and penetrating in the stratosphere along the polar cusps, play an important role in the Ozone layer depletion. This possibility initiated this work and will be considered later in the text.

EXPERIMENTAL

Cross sections database

The cross sections, used here for the rate coefficient calculations, were measured by Deng and coworkers,¹⁵ and later by Belić *et al.*¹⁶ These are the only experimental results for electron-impact fragmentation of O_3^+ . In the ORNL experiment,¹⁵ both cross sections, for O^+ and O_2^+ fragments were measured.

In the UCL experiment,¹⁶ the cross sections are reported for the O^+ fragment production, only. An attempt to measure cross sections for the O_2^+ fragments failed, because enormous background count rate was present for this particular ion.

In the cited experiments, electron-impact simple ionization cross section of O_3^+ resulting in O_3^{2+} was found to be negligible. This finding is in agreement with the conclusion of Deng *et al.*¹⁵ We believe that the lifetime of the doubly charged ozone ion O_3^{2+} is shorter than the time scale of the experiments and that it dissociates before reaching the detector.

As in many other electron-ion dissociation experiments in the UCL laboratory, particular attention has been paid to the total detection of the product ions (see for example the proposed references).^{17–19} Due to the transfer of internal energy to the kinetic energy of the fragments, dissociation products exhibit both broad velocity distribution and a broad angular divergence in the laboratory frame. This often results in a partial loss of the signal. In order to compensate for this effect, careful analyzer magnetic-field scans of the signal have been performed for the selected electron energies (see for instance Fig. 1 in a publication by Belić *et al.*¹⁶). These scans are used: *i*) to normalize measurements to the absolute scale, *ii*) to determine total kinetic energy release (KER) distribution of the fragments, which illustrates Fig. 4 in a paper by Belić and coworkers,¹⁶ and consequently *iii*) to separate DE and DI contributions of the inclusive cross sections. In the present work, magnetic-field scans will be further used to estimate a new set of the cross section data for the O_2^+ fragment production *i.e.* to renormalize previous measurements of ORNL group. This is performed by taking into account proper transmission efficiency of the experiment, determined for the O^+ fragment and by applying it to the O_2^+ fragment. Our goal was to calculate and to compare resulting rate coefficients for O_3^+ fragmentation by electron impact, for various reaction channels.

Renormalization of the O_2^+ cross-sections

We have learned (in earlier study)¹⁶ that the difference between cross sections for O^+ fragment production in references^{15,16} results mainly from the loss of the DI contribution in ORNL experiment.¹⁵ Thus, similar effect can be expected for the O_2^+ fragments, as well. Furthermore, we have determined the DI cross section contribution for O^+ fragment¹⁶ to be dominant over DE for energies above 40 eV (see Fig. 3 in Belić *et al.*¹⁶). Consequently, the UCL group found the inclusive cross section for this fragment to be significantly higher in a wide energy range, compared to the results of ORNL group. Since the DI reaction (3) is dominant channel for the creation of both O_2^+ and O^+ fragments, we could expect similar situation for O_2^+ fragments. For that reason, we have made an attempt to renormalize the ORNL cross section results for the O_2^+ fragments production.

For this purpose, magnetic-field scans obtained for the O^+ fragments, *i.e.*, the total KER distributions of product fragments (see Fig. 4 in a UCL reference)¹⁶ are used. By applying Lorentz expression, these scans are first transformed to the center-of-mass velocity distribution of the O^+ fragments.¹⁷ Under the assumption of dominant DI contribution and based on the momentum conservation, initial velocity distributions of the O_2^+ fragments, in the center-of-mass frame, are determined. The results are further transformed to the fragment distributions in the laboratory frame. Because of the larger mass, they have lower velocity than O^+ fragments, but are occurring at the larger analyzer magnetic fields. These distributions are used for Monte Carlo simulation of the expected magnetic-field scans of the fragments, according to the procedure described before.^{18,19} Having these scans, the transmission efficiency for the O_2^+ fragments is determined to be between 30 and 42 %. The transmission factors are extrapolated to the considered electron energy range and are applied to the experimental cross sections published by Deng *et al.* for the O_2^+ fragments.¹⁵

In this way absolute cross sections for electron impact dissociation of O_3^+ producing the O_2^+ fragment, corrected for the experimental transmission and detection efficiency, are determined. They are shown in Fig. 1, together with the absolute cross sections for dissociation to the O^+ fragment.¹⁶ The O_2^+ cross sections are also presented in Table I and will be referred hereafter as recommended cross sections. The total charged fragments production cross section, also shown in Fig. 1, is the sum of these two, O^+ and O_2^+ cross sections.

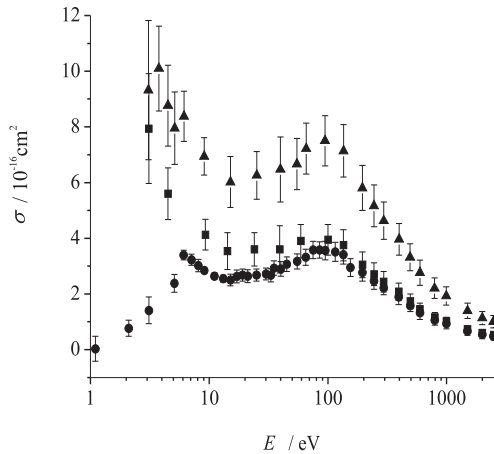


Fig. 1. Absolute cross sections for electron-impact dissociation of O_3^+ to O^+ (circles), O_2^+ (squares), and for total inclusive singly charged fragments production (triangles).

TABLE I. Recommended cross sections σ_r for electron-impact dissociation of O_3^+ yielding O_2^+ fragments, at various electron energies E

E / eV	$\sigma_r / 10^{-16} \text{ cm}^2$	$\Delta\sigma_r / 10^{-16} \text{ cm}^2$	E / eV	$\sigma_r / 10^{-16} \text{ cm}^2$	$\Delta\sigma_r / 10^{-16} \text{ cm}^2$
3.1	7.94	1.97	245.1	2.71	0.41
4.5	5.60	0.93	295.1	2.44	0.37
9.3	4.13	0.55	395.1	2.08	0.31
14.3	3.54	0.66	495.1	1.74	0.26
24.0	3.60	0.60	595.1	1.45	0.22
39.3	3.60	0.85	795.1	1.16	0.17
59.0	3.90	0.60	995.1	1.02	0.15
100.0	3.95	0.55	1495.1	0.73	0.11
135.1	3.75	0.56	1995.1	0.60	0.09
195.1	3.05	0.46	2495.1	0.53	0.08

Method of rate coefficient calculation

Rate coefficients have been calculated by using standard procedure,²⁰ given by the following expression:

$$K(\langle E \rangle) = \sqrt{\frac{2}{m}} \int_{E_{\text{th}}}^{\infty} \sigma(E) \sqrt{E} f_e(\langle E \rangle, E) dE \quad (4)$$

where $\langle E \rangle$ is the mean electron energy, $\sigma(E)$ is the cross section for considered process, E_{th} is the threshold energy and $f_e(\langle E \rangle, E)$ is the normalized electron energy distribution function (EEDF). Calculations have been performed by using numerical interpolation of experimental cross section data. In case of equilibrium conditions, the EEDF in (4) is given by the Maxwellian equation:

$$f_e(\langle E \rangle, E) = \frac{2}{\sqrt{\pi}} \left(\frac{3}{2\langle E \rangle} \right)^{3/2} \sqrt{E} e^{-3E/2\langle E \rangle} \quad (5)$$

For the non-Maxwellian, *i.e.*, non-equilibrium case, experimental EEDF-s for the mean electron energy values of 4.53, 6.4, 46.2 and 71.7 eV are used. They have been adopted from measurements of the non-thermal "super-halo" component of the Solar wind electrons per-

formed with the help of 3-D Plasma and energetic particles experiment on the WIND space-craft.²¹ In the present study, two different EEDF functions at 71.7 eV are used, including WIND and "super-halo" projects, giving essentially the same rate coefficients.

The solar wind is a stream of charged particles (plasma) emitted from the upper atmosphere of the Sun. It consists predominantly of electrons and protons in the energy range up to 0.5 to 10 keV.

The solar wind varies in density, temperature and speed over time and distance. Its particles can escape the Sun's gravity because of their high energy resulting from the high temperature of the corona. The consequences of this are solar wind and geomagnetic storms on Earth, and the light auroras at the poles.

High energy cross sections and contributions of the related processes

Generally, normalized EEDF becomes lower, but wider with increasing the mean electron energy. In both cases, Maxwellian and non-equilibrium, rates are dependent on the cross section magnitude and its shape, *i.e.*, they are related to the cross section and EEDF overlap at a given mean electron energy. This will be illustrated here for the O⁺ fragments. In UCL experiment,¹⁶ DE and DI contributions for this fragment are separated (see Fig. 3 in the cited work).¹⁶ The two cross sections are used to calculate Maxwellian rate coefficients for these particular processes. The results are compared in Fig. 2.

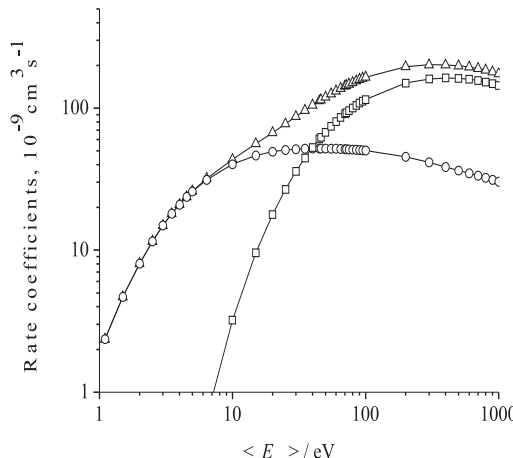


Fig. 2. Maxwellian rate coefficients for DE (circles), DI (squares) and inclusive cross-sections (triangles) for O⁺ fragment production.

The DE cross sections are higher than those for DI at low mean electron energy, below 40 eV. However, it turned out that corresponding rates at higher mean electron energies are up to a factor of 5 larger for DI than those for DE, Fig. 2. The total rate coefficients for O⁺ production reach $2 \times 10^{-7} \text{ cm}^3 \text{ s}^{-1}$ in a wide mean electron energy range, above 100 eV.

The comparison of these data is also performed with the results of rate coefficients calculated with corresponding cross sections for O⁺ fragments published by Deng *et al.*¹⁵ These rates are a factor of 3 lower than the present total inclusive rates shown in Fig. 2.

Similar, or even more pronounced effects are expected for non-thermal EEDF-s. Enhancements may be expected for processes which include high energy reactions, such as inner shell or multiple ionization.

Moreover, it should be pointed out that the Energetic electron precipitation (EEP) plays even more prominent role and affects the chemical composition of the polar mesosphere.²² It

leads to odd hydrogen (HO_x) production following ionization and ion chemical reactions, which are expected to contribute to the ozone balance in the mesosphere.

It has been shown,²³ using observations from three different satellite instruments, that EEP events strongly affect ozone at 60–80 km, leading to extremely large (up to 90 %) short-term ozone depletion. This impact is comparable to that of large, but much less frequent, solar proton events. On solar cycle timescales, it has been found that EEP causes ozone variations of up to 34 % at 70–80 km altitude. With such a magnitude, it is reasonable to suspect that EEP could be an important part of solar influence on the atmosphere and climate system.

RESULTS AND DISCUSSION

Maxwellian and non-thermal rate coefficients for electron impact dissociation of O_3^+ to the O^+ and O_2^+ fragments were calculated and are presented herein. The Maxwellian rates were determined in the mean electron energy range from 0 to 2 keV. The non-thermal rates were determined for the mean energies from 4 to 80 eV, for the experimental EEDF-s.²¹ These calculations were performed for the present recommended cross section data set (for the O^+ fragment of reference¹⁶ and for renormalized cross sections for the O_2^+ fragment, presented herein). Rate coefficients for the total singly charged fragments production, K_T , were obtained as the sum of these two results.

For comparison purposes, calculations are also performed using the cross sections for O^+ and O_2^+ measured directly and published by Deng *et al.*¹⁵ Rate coefficients for the total singly charged fragments production, K_T , were also obtained in this case.

Maxwellian rate coefficients

The results for the Maxwellian rate coefficients were calculated using Eqs. (4) and (5). They are presented in Table II, and also shown in Fig. 3. The lowest curve in Fig. 3, shown by circle symbols was obtained by using the cross section measurements of Belić *et al.* for O^+ .¹⁶ These results are denoted $K(\text{O}^+)$ in Table II. The data represented by squares in Fig. 3 were obtained using the recommended cross section results for O_2^+ , and they are marked $K(\text{O}_2^+)$ in Table II. The results denoted by K_T ($\text{O}^+ + \text{O}_2^+$) in Table II and by triangles in Fig. 3 represent the sum of these two results and are in fact the total inclusive rate for producing singly charged fragments by electron impact dissociation of O_3^+ . As could be noticed, the $K(\text{O}_2^+)$ results are higher over the whole range of considered mean electron energy than those for the O^+ fragments. This is expected bearing in mind that the cross sections for O_2^+ are higher for all energies than those for O^+ , particularly for the low energies near threshold, see Fig. 1.

The rates $K(\text{O}^+)$ and $K(\text{O}_2^+)$ have maximum values slightly above 2×10^{-7} $\text{cm}^3 \text{s}^{-1}$, at about 300 eV. The total rate K_T ($\text{O}^+ + \text{O}_2^+$) has a maximum value of 4.27×10^{-7} $\text{cm}^3 \text{s}^{-1}$ also at 300 eV. For the purpose of comparison, the ORNL cross-sections of Deng *et al.*,¹⁵ were extrapolated to the high energy side and all rates were calculated for the mean electron energies up to 2 keV. These rates

were determined for the O^+ and O_2^+ fragments, respectively. However, they were lower than $10^{-7} \text{ cm}^3 \text{ s}^{-1}$ over the whole energy range and are not presented herein. The sum of these two contributions for this data set had a maximum of $1.6 \times 10^{-7} \text{ cm}^3 \text{ s}^{-1}$ at about 250 eV and fell to a quarter of this value at 2 keV.

TABLE II. Maxwellian rate coefficients, $K / 10^{-7} \text{ cm}^3 \text{s}^{-1}$, for electron-impact dissociation of O_3^+ to O^+ , O_2^+ , and for the total inclusive production of singly charged fragments, K_T

E / eV	$K(O^+)$	$K(O_2^+)$	K_T	E / eV	$K(O^+)$	$K(O_2^+)$	K_T
1	0.02	0.052	0.062	200	1.95	2.17	4.12
2	0.08	0.23	0.28	250	2.00	2.22	4.21
3	0.15	0.37	0.52	300	2.01	2.23	4.27
4	0.21	0.46	0.68	350	2.02	2.23	4.25
5	0.26	0.53	0.79	400	2.04	2.22	4.23
6	0.30	0.57	0.89	450	2.00	2.21	4.21
7	0.34	0.62	0.97	500	1.98	2.20	4.17
8	0.37	0.65	1.04	550	1.96	2.17	4.14
9	0.40	0.68	1.09	600	1.94	2.15	4.09
10	0.43	0.71	1.15	650	1.92	2.12	4.05
20	0.67	0.92	1.59	700	1.90	2.10	3.99
30	0.87	1.11	1.98	750	1.88	2.08	3.95
40	1.02	1.27	2.32	800	1.85	2.04	3.89
50	1.21	1.43	2.60	850	1.83	2.02	3.94
60	1.33	1.54	2.83	900	1.80	1.98	3.78
70	1.42	1.63	3.04	950	1.77	1.95	3.73
80	1.51	1.72	3.22	1000	1.76	1.92	3.67
90	1.59	1.81	3.39	1500	1.48	1.63	3.09
100	1.66	1.85	3.50	2000	1.24	1.37	2.60
150	1.85	2.08	3.93				

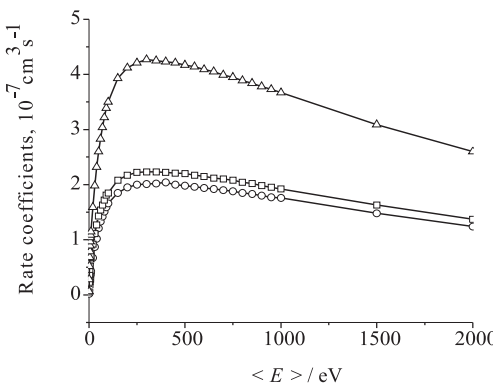


Fig. 3. Maxwellian rate coefficients for O_3^+ dissociation to O^+ (circles), O_2^+ (squares) and for the total inclusive production of singly charged fragments K_T (triangles). For explanation see the text.

The results for the present data set are more than a factor of two higher than the values obtained for the data set of Deng *et al.*,¹⁵ for all energies. This has a simple explanation. The cross sections used herein for the present data set are corrected to the loss of signal and are higher than in ORNL experiment.¹⁵ Of

particular interest is the fact that this lost signal originates mainly due to the DI contribution, which prevails in the higher incident electron energy range. Therefore, this results in a significant increase in the rate coefficients, relative to the previous data.¹⁵

Non-thermal rate coefficients

Non-Maxwellian (or non-thermal) rate coefficients are calculated for the same sets of cross section data, as above for the Maxwellian case. EEDF-s were available only for four mean electron energies in the range from 4.53 to 71.7 eV.²¹ The non-thermal rates obtained upon using these EEDFs in Eq. (4) were interpolated and extrapolated across the energy range from 4 to 80 eV, in order to make comparison with the Maxwellian rate coefficients.

The non-thermal rates for the present data set are listed in Table III and are also shown in Fig. 4, along with the Maxwellian ones. In the considered energy range, non-thermal rates do not reach their maxima. Their highest values for $\langle E \rangle = 80$ eV is $2.0 \times 10^{-7} \text{ cm}^3 \text{ s}^{-1}$ for $K(\text{O}^+)$, and $2.25 \times 10^{-7} \text{ cm}^3 \text{ s}^{-1}$ for $K(\text{O}_2^+)$. Thus, the total inclusive rate amounts to $4.25 \times 10^{-7} \text{ cm}^3 \text{ s}^{-1}$ at $\langle E \rangle = 80$ eV. This could be compared to the value of $3.22 \times 10^{-7} \text{ cm}^3 \text{ s}^{-1}$ obtained for the Maxwellian total inclusive rate coefficient (for the same mean electron energy), which is lower by some 25 %. Generally, the non-thermal rates are higher than the Maxwellian ones, for all reaction channels and for all electron energies.

TABLE III. Non-thermal rate coefficients, $K / 10^{-7} \text{ cm}^3 \text{ s}^{-1}$, for electron-impact dissociation of O_3^+ to O^+ , O_2^+ , and for the total inclusive production of singly charged fragments, K_T

E / eV	$K(\text{O}^+)$	$K(\text{O}_2^+)$	K_T	E / eV	$K(\text{O}^+)$	$K(\text{O}_2^+)$	K_T
4	0.38	0.67	1.07	25	1.10	1.32	2.40
5	0.43	0.71	1.15	30	1.24	1.45	2.70
6	0.46	0.74	1.22	35	1.36	1.56	2.91
7	0.50	0.78	1.29	40	1.48	1.67	3.14
8	0.54	0.81	1.36	45	1.59	1.78	3.35
9	0.58	0.84	1.42	50	1.68	1.87	3.55
10	0.61	0.87	1.49	55	1.76	1.96	3.70
12	0.68	0.94	1.62	60	1.83	2.03	3.87
14	0.75	1.00	1.75	65	1.88	2.09	3.96
16	0.82	1.06	1.88	70	1.94	2.15	4.08
18	0.88	1.12	2.00	75	1.99	2.20	4.17
20	0.94	1.18	2.12	80	2.00	2.24	4.25

For non-thermal EEDF-s, the results based on the ORNL cross-section measurements are lower than for the present set of data. The rate coefficient values are lower by even a factor of 2, for most of electron energies, and up to a factor of 3 for the high ones.

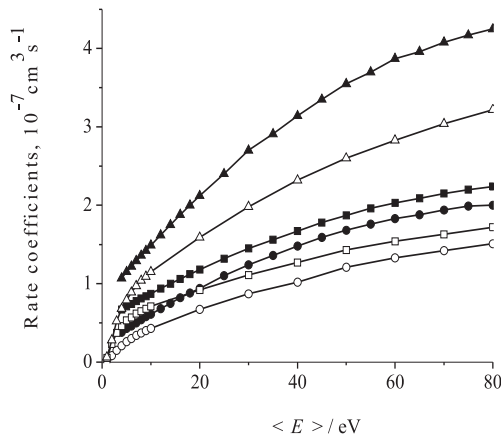


Fig. 4. Non-thermal rate coefficients (closed symbols) and Maxwellian rate coefficients (open symbols) for O_3^+ dissociation to O^+ (circles), O_2^+ (squares) and for the total inclusive singly charged fragments production K_T (triangles).

Comparison of Maxwellian and non-thermal rate coefficients

As already pointed out, due to the larger cross section values, the rate coefficients are higher for the present data set than for those based on the ORNL data. This was observed using both the Maxwellian and non-thermal EEDF-s. The reason for this is attributed to the loss of signals, *i.e.*, underestimated cross sections in the earlier data set, which were recuperated in the present data. This is clearly seen in particular for the high mean electron energies. Thus, the rate coefficient results based on the ORNL data will not be further considered herein and are not recommended for use in modeling the balance of ozone in the Earth's atmosphere.

Finally, we shall discuss the rate coefficient dependance on the used EEDF-s. For the purpose of comparison, we redirect reader's attention again to the Tables II and III. For all considered processes, the rate coefficients calculated by using available non-thermal EEDF-s are higher than for the case of Maxwellian EEDF. This is the consequence of the behavior of the cross sections. They have large values extended to relatively high electron energies, thus their overlapping integral with non-thermal EEDF-s is higher than with Maxwellian ones, in a wide energy range. Consequently, non-thermal rate coefficients are additionally magnified.

The effects of external electric or magnetic fields, or their combination, on the rate coefficients were not investigated in the present work. This obviously needs to be studied in detail, in future investigations.

CONCLUSIONS

Rate coefficients were calculated for electron-impact dissociation of O_3^+ to the O^+ and O_2^+ fragments. Experimental cross section results for O^+ fragments from Belić *et al.*¹⁶ and renormalized data for O_2^+ fragment from Deng *et al.*¹⁵ were used. Maxwellian and non-equilibrium EEDF-s were applied for the mean electron energies from threshold up to 2 keV. Significantly higher rate coefficients were observed for the present results than for those measured by the

ORNL group. Rate coefficients for non-equilibrium EEDFs were found to be higher by a factor of two than for the Maxwellian ones. Thus, the investigated processes were found likely to play an even more important role in the ozone cation dissociation, than had previously been expected.

This work demonstrates that the Solar wind electrons, penetrating in the Earth's stratosphere along the polar cusps, can make significant contribution in the Ozone layer depletion and should be included in future modeling.

Acknowledgements. This work was supported by the Fonds de la Recherche Scientifique – FNRS through IISN Contract No. 4.4504.10. The authors value the financial support of the Association Euratom-Belgian State. D.S.B. is grateful for support from Project No. 171016 from the Ministry of Education, Science and Technological Development of the Republic of Serbia.

И З В О Д

КОЕФИЦИЈЕНТИ БРЗИНЕ ЗА ДИСОЦИЈАЦИЈУ O_3^+ УДАРОМ ЕЛЕКТРОНА НА ЈЕДНОСТРУКО НАЕЛЕКТРИСАНЕ ФРАГМЕНТЕ

ДРАГОЉУБ С. БЕЛИЋ¹, МИРЈАНА М. ВОЈНОВИЋ¹, МИРОСЛАВ М. РИСТИЋ², XAVIER URBAIN³
и PIERRE DEFRAНCE³

¹Универзитет у Београду – Физички факултет, Студентски парк 16, Београд, ²Универзитет у Београду – Факултет за физичку хемију, Студентски парк 12–16, Београд и ³Université Catholique de Louvain, Institute of Condensed Matter and Nanosciences, Chemin du Cyclotron 2, B-1348 Louvain-la-Neuve, Belgium

Кофицијенти брзине за дисоцијацију O_3^+ ударом електрона на фрагменте O^+ и O_2^+ израчунати су за нови, препоручени скуп података ефективних пресека и за различите услове судара. Коришћена су два скупа ефективних пресека, које су недавно измериле различите експерименталне групе. Ови пресеци се међусобно значајно разликују, али су ренормирани и оптимизовани за кохерентну базу података. Кофицијенти брзине за фрагментацију катиона озона су одређени коришћењем Максвелове и неравнотежне функције расподеле енергије електрона. У случају Максвелове дистрибуције, средње енергије електрона покривају опсег од нула до 2 keV. Неравнотежне функције расподеле енергије електрона су усвојене из недавних посматрања електрона у 3-D експерименту са плазмом изведеном на свемирском броду WIND. Неравнотежни кофицијенти брзине су процењени за средње енергије електрона од 4 до 80 eV. Наглашена је улога могућег доприноса дисоцијацији O_3^+ електронским ударом у оштећењу озонског омотача.

(Примљено 9. новембра, ревидирано 11. децембра, прихваћено 13. децембра 2021)

REFERENCES

1. M. J. Molina, F. S. Rowland, *Nature* **249** (1974) 810 (<https://doi.org/10.1038/249810a0>)
2. J. C. Farman, B. G. Gardiner, J. D. Shanklin, *Nature* **315** (1985) 207 (<https://doi.org/10.1038/315207a0>)
3. V. Vaida, J. D. Simon, *Science* **268** (1995) 1443 (<https://doi.org/10.1126/science.268.5216.1443>)
4. J. A. Davies, W. M. Johnstone, N. J. Mason, P. Biggs, R. P. Wayne, *J. Phys., B* **26** (1993) L767 (<https://doi.org/10.1088/0953-4075/26/21/008>)

5. M. Allan, K. R. Asmis, D. B. Popović, M. Stepanović, N. J. Mason, J. A. Davies, *J. Phys., B* **29** (1996) 3487 (<https://doi.org/10.1088/0953-4075/29/15/020>)
6. C. J. Sweeney, T. W. Shyn, *Phys. Rev., A* **53** (1996) 1576 (<https://doi.org/10.1103/PhysRevA.53.1576>)
7. M. W. Siegel, *Int. J. Mass Spectrom. Ion Phys.* **44** (1982) 19 ([https://doi.org/10.1016/0020-7381\(82\)80036-3](https://doi.org/10.1016/0020-7381(82)80036-3))
8. K. A. Newson, S. M. Luc, S. D. Price, N. J. Mason, *Int. J. Mass Spectrom. Ion Process.* **148** (1995) 203 ([https://doi.org/10.1016/0168-1176\(95\)04300-A](https://doi.org/10.1016/0168-1176(95)04300-A))
9. Y.-K. Kim, W. Hwang, N. M. Weinberger, M. A. Ali, M. E. Rudd, *J. Chem. Physics* **106** (1997) 1026 (<https://doi.org/10.1063/1.473186>)
10. Y.-K. Kim, K. K. Irikura, M. E. Rudd, M. A. Ali, P. M. Stone, J. Chang, J. S. Coursey, R. A. Dragoset, A. R. Kishore, K. J. Olsen, A. M. Sansonetti, G. G. Wiersma, D. S. Zucker, M. A. Zucker, *NIST Standard Reference Database 107, Electron-Impact Cross Sections for Ionization and Excitation*, Vol. 107, 2005, p. 1, NIST, Gaithersburg (<http://www.nist.gov/pml/data/ionization/index.cfm>)
11. N. J. Mason, J. M. Gingell, J. A. Davies, H. Zhao, I. C. Walker, M. R. F. Siggel, *J. Phys., B* **29** (1996) 3075 (<https://doi.org/10.1088/0953-4075/29/14/019>)
12. G. de Petris, *Mass Spectrom. Rev.* **22** (2003) 251 (<https://doi.org/10.1002/mas.10053>)
13. V. Zhaunerchyk, W. D. Geppert, M. Larsson, R. D. Thomas, E. Bahati, M. E. Bannister, M. R. Fogle, C. R. Vane, F. Osterdahl, *Phys. Rev. Lett.* **98** (2007) 223201 (<https://doi.org/10.1103/PhysRevLett.98.223201>)
14. M. L. Vestal, G. H. Mauclaire, *J. Chem. Phys.* **67** (1977) 3767 (<https://doi.org/10.1063/1.435317>)
15. S. H. M. Deng, C. R. Vane, M. E. Bannister, M. Fogle, *Phys. Rev., A* **82** (2010) 062715 (<https://doi.org/10.1103/PhysRevA.82.062715>)
16. D. S. Belić, X. Urbain, P. Defrance, *Phys. Rev., A* **91** (2015) 012703 (<https://doi.org/10.1103/PhysRevA.91.012703>)
17. J. Lecointre, D. S. Belić, H. Cherkani-Hassani, J. J. Jureta, P. Defrance, *J. Phys., B* **39** (2006) 3275 (<https://doi.org/10.1088/0953-4075/39/16/011>)
18. D. S. Belić, X. Urbain, H. Cherkani-Hassani, P. Defrance, *Phys. Rev., A* **95** (2017) 052702 (<https://doi.org/10.1103/PhysRevA.95.052702>)
19. D. S. Belić, M. M. Ristić, H. Cherkani-Hassani, X. Urbain, P. Defrance, *Eur. Phys. J., D* **74** (2020) 100 (<https://doi.org/10.1140/epjd/e2020-100623-1>)
20. M. Ristić, G. B. Poparić, D. S. Belić, *Chem. Phys.* **331** (2007) 410 (<https://doi.org/10.1016/j.chemphys.2006.11.012>)
21. R. P. Lin, in *Proceedings of the CESRA Workshop*, 1996, Nouan le Fuzelier, France, Springer, Berlin, 1997, p. 93
22. P. T. Verronen, C. J. Rodger, M. A. Clilverd, S. Wang, *J. Geophys. Res.* **116** (2011) D07307 (<https://doi.org/10.1029/2010JD014965>)
23. M. E. Andersson, P.T. Verronen, C. J. Rodger, M. A. Clilverd, A. Seppälä, *Nature Commun.* **5** (2014) 5197 (<https://doi.org/10.1038/ncomms6197>).



Synthesis of the new lost foam refractory coatings based on talc

MARKO PAVLOVIĆ¹, JASMINA NIKOLIĆ^{2#}, LJUBIŠA ANDRIĆ³,
DEJAN TODOROVIĆ³, KATARINA BOŽIĆ^{4,5#} and SAŠA DRMANIĆ^{2**#}

¹*Kontrol Inspekt, Belgrade, Serbia*, ²*University of Belgrade, Faculty of Technology and Metallurgy, Belgrade, Serbia*, ³*University of Belgrade, Institute for Technology of Nuclear and Other Mineral Raw Materials, Belgrade, Serbia*, ⁴*University of Belgrade, Institute of Chemistry, Technology and Metallurgy, Department of Electrochemistry, Belgrade, Serbia* and ⁵*University of Belgrade, Institute of Chemistry, Technology and Metallurgy, Center of Excellence in Environmental Chemistry and Engineering, Belgrade, Serbia*

(Received 19 October, revised 14 December, accepted 16 December 2021)

Abstract: This paper is focused on the preparation procedures, using a talc-based filler, to improve the rheologic properties of the lost foam refractory coatings. Talc, with grain size of 40 µm, was mechanically activated in a vibration mill over the following times: 10, 20 and 30 min. Depending on the time required for the mechanical activation, the change in the filler grain size and shape was analysed along their effects on the talc-filled lost foam coating dispersion ability and stability. In order to characterize the filler, the following methods were used: X-ray diffraction, scanning electron microscopy and optic microscopy. The coating composition was tuned by choosing the suitable grain size and shape factor of the activated filler. In addition, different coating components (additives, solvent) were applied to alter the coating generation procedure. It was shown that the application of this type of the lost foam refractory coatings – water-based coatings – have a positive influence on quality of the aluminium alloy castings, which contributes to reducing the cost of cleaning and processing of the castings. Also, alcohol-based refractory coatings with talc-based activated fillers were tested and used to have the castings produced in the sand moulds.

Keywords: mechanical activation; talc-based fillers; rheologic properties of coating suspensions.

INTRODUCTION

Lost foam process is a new method for production of high quality low-cost castings. The technological possibilities for the lost foam casting process are examined and basic laws for the influence of numerous parameters on the process

* Corresponding author. E-mail: drmana@tmf.bg.ac.rs

Serbian Chemical Society member.

<https://doi.org/10.2298/JSC211019111P>

flow and castings quality are determined. The process includes a large number of insufficiently examined phenomena in connection with physicochemical and thermodynamic changes in the system: evaporative pattern–refractory coating–liquid metal–sand.^{1–3} The technological parameters important for the process to unfold and obtain high quality castings are: pattern density, granulometric contents of moulding sand (mould permeability), thermophysical features of coating materials, pouring temperature and pouring system.^{4,5}

Unlike sand mould casting, where liquid metal flows into the “mould cavity”, with the lost foam process, the patterns and pouring systems made of polymers are retained in the mould until a liquid metal has flown in (“full mould casting”).^{1,6–9} In contact with a liquid metal, polymer patterns degrade, evaporate and simultaneously the castings solidification takes place. As a consequence of the degradation and the evaporation of the polymer pattern, a large amount of liquid and gas products is released. These products are a frequent cause for castings’ defects. To obtain quality castings, it is necessary to apply highly permeable lost foam refractory coatings.^{10–17}

Basic role of the refractory coating is to form an efficient refractory barrier between the sand substrate and the liquid metal flow during the casting phase, and to control the solidification and the forming of the castings.¹¹ This provides a smooth and clean surface of castings, with no adhered sand or defects due to metal penetration into the mould (*e.g.*, rough surface, lumps, dents). The application of higher quality refractory coatings significantly can provide either reduction or elimination of the expensive foundry cleaning and mechanical operations, thus directly reducing production costs of a castings. The coating properties are strictly defined by standards; therefore, it is very important to make the right choice of coating, as well as its preparation and application procedures in the foundry working conditions.^{18,19}

Contemporary coatings, depending on their use, represent thermophysical mixtures of ceramic materials in a suspending medium which contains suspension bonding agents. The coating composition analyses show that the coating consists of a number of components of which the most important are: refractory filler, bonding agent, suspension stability agent, liquid carrier and the solvent.^{1,15,20–23}

Complexity of the casting solidification process is influenced by the insulation effect, governed by the lost foam refractory coatings. At the stage of filling the mould, when degradation and evaporation of polymer pattern take place, the refractory coating causes a temperature drop of the liquid metal. As soon as the mould is filled with liquid metal, *i.e.*, while polymer pattern is evaporating, the refractory coating, through the insulation effect, causes the decrease in the castings’ cooling and solidification rate. The endothermic degradation of the polymer pattern causes subcooling of the liquid metal and affects the formation of a fine structure of the

castings. If subcooling is considerably fast, a fine tiny-grained structure is formed on castings.^{1,7,13} The pattern degradation and the evaporation rate depend on polymer density, casting temperature, lost foam refractory coatings' permeability and sand mould permeability. Here described research paid particular attention to these factors.

For the development of the lost foam refractory coatings with the controlled rheologic properties, the influence of the mechanical activation process on the talc-based filler's properties was examined. The test preferentially referred to the change in filler grain size and shape, and afterwards to the dispersion quality and the stability of the coating suspension.^{24–30}

The composition and the production procedures for the lost foam refractory coatings, with a mechanically activated talc-based filler, were planned along with the research activities, and refer to the dependence of the castings structure and properties on the casting process parameters.

Talc is a magnesium hydrosilicate with the general formula $H_2Mg_2(SiO_3)_4$ or $Mg_6(OH)_4(Si_8O_{20})$ with the additions of Al_2O_3 , FeO , NiO and CaO . Talc was chosen to be the filler for lost foam coatings, owing to its following properties: Mohs hardness 1; density 2700–2800 kg/cm³; low heat conductivity coefficient, $\lambda = 3.5\text{--}4.0 \text{ W}/(\text{m K})$; low linear thermic expansion coefficient, $\alpha = 2.7 \times 10^6/\text{°C}$ (20–1000); high adherence and cladding ability to surfaces; high melting point, 1400–1550 °C; high inertia, *i.e.*, resistance to acids, alkalines and heat.^{16,31,32}

The influence of following parameters on the casting process is analyzed: casting temperature, mould permeability and the design of the pattern and pouring systems. The subject of research was the correlation between these parameters and the polymer pattern density, as well as the type and thickness of refractory coating layers.

EXPERIMENTAL

Talc-based filler synthesis

Talc used as filler was obtained with the use of combined preparation procedures from mineral raw materials; talc excavated at the site Studenica, Serbia, was crushed and leached. The particular attention was paid to the talc purification procedure, as well as to reduction of the Fe_2O_3 and CaO content as follows. The initial talc sample was of a heterogeneous chemical composition, Table I.

TABLE I. The initial composition of talc used for production of the filler T

Compound	SiO_2	MgO	Al_2O_3	Fe_2O_3	CaO	Na_2O+K_2O	LoI
Content, mass %	61.50	29.45	1.78	2.84	2.50	1.90	8.50

Talc purification was performed by means of leaching to reduce the Fe_2O_3 and CaO content. Talc was leached by hydrochloric acid (15 wt. %). The leaching was performed at a constant temperature ($t = 80 \text{ °C}$), in a three-neck bottle during 3.5 h of reflux. Calcite (green) precipitated as bottom solid, whereas talc concentrate (white) appeared as an upper layer. Car-

bon dioxide (CO_2) was produced during the leaching process, which lifts up the fine talc particles concentrate, lighter than calcite particles remaining at the bottom. Next, warm talc concentrate was rinsed by water, then filtered and dried. The same process was applied on calcite and intermediate product (talc–chlorite) which remain as final tailing. The talc samples produced were ground in a ceramic ball mill down to the limit grain size of 100 % – 40 μm . It was the initial grain size of the filler T; then, it was subjected to the mechanical activation process in a vibration mill over different times (min): 10, 20 and 30, with the filler sample codes: T_1 , T_2 and T_3 , respectively; Table II reports the grain size and shape data.

TABLE II. Talc-based refractory fillers after mechanical activation

Sample	Mechanical activation time, min	Grain size, μm	Grain shape factor
T_1	10	100% - 30	0.62
T_2	20	100% - 22	0.69
T_3	30	100% - 10	0.72

Characterization of filler T

To identify the composition and structure of the filler T, the method of X-ray diffraction analysis was applied. The XR diffractometer, model PW-1710 (Philips Analytical, Almelo, the Netherlands) was used; it involved a curved graphite mono-chromate meter and a scintillation counter. The intensities of the diffracted $\text{CuK}\alpha$ of the X-ray radiation (wavelength 1.54178 Å) were measured at room temperature with the 2θ intervals of 0.02° over the time of 1 s, within the 2θ range from 4 to 70°. The X-ray tube was under the voltage of 40 kV and the current of 30 mA, while the primary and the diffracted rays' slots were 1° and 0.1 mm.

The morphological and the quantitative chemical analysis was carried out by means of the scanning electronic microscope “Jeol” – model JSM 6610 LV (Jeol, Tokyo, Japan). In order to improve conductivity, the sample was coated with gold powder.

Refractory coating synthesis with activated fillers T_1 , T_2 and T_3

The talc samples produced after mechanical activation were used to produce both water and alcohol-based refractory coatings, Table III.

TABLE III. Talc-based refractory coatings composition

Component	Refractory coating		
	Type I	Type II	Type III
Refractory filler	T_2 (82–85 %)	T_2 (72–75 %) + T_3 (9–11 %)	T_2 (83–86 %)
Bonding agent	Bentonite 4–4.5 %; Bindal H 4–4.5 %	Bentonite 4.5–5 %; Bindal H 4.5–5 %	$(\text{C}_{20}\text{H}_{30}\text{O}_2)$ 3.5–4.5 % Dextrin 0.5–1 %
Additive	Suspension maintenance agent: carboxymethyl cellulose (CMC) 1–1.5 %	Suspension maintenance agent: carboxymethyl cellulose (CMC) 1.5–2 %	Bentone 25 1.5–2.5 %; phenolformaldehyde resins, 0.2–0.5 %
Solvent	Water	Water	Isopropylalcohol ($\text{C}_3\text{H}_8\text{O}$)
Density, kg m^{-3}	2000	2000	2000

The paper investigates refractory coatings based on activated talc filler for casting aluminium alloy castings in sand moulds. The sand moulds and cores were coated with a Type III

refractory coating. Also, Type I and Type II coatings for casting aluminium alloy castings by the lost foam process were investigated. These refractory coatings were used to coat polymer models. The coatings were tested in accordance with the standards for this type of refractory materials,^{18,19} and with respect to our previous works in this field,^{11,16,22,25,32} which also report the results of testing of the influence of mechanical activation on the structure and properties of talc.²⁶⁻³⁰ The sedimentation stability of the produced refractory coatings was tested at a temperature of 22 °C; thickness of the wet coating film layers was: 0.3, 0.6 and 0.9 µm. Refractory coatings were applied to polymer patterns through immersing and pouring procedures, while sand moulds were coated by means of brushes.

In order to obtain a homogeneous suspension of the coating, during application, light mixing was performed at a speed of 1 rpm. The water-based lost foam refractory coatings were air dried during 24 h. The alcohol-based coatings were burned to get dry.

Characterization of lost foam refractory coatings

In order to elucidate the filler and the binding agent's distributions, the lost foam refractory coating suspension was analysed on the polarized microscope for the transmitted light JENAPOL, manufactured by Carl Zeiss-Jena, Germany, with Microphoto System Studio PCTV; Pinnacle System, Mountain View, CA, USA. Measurements of the filler grain size and shape were carried out on 4000 grains, while the analysis was conducted by means of the software application package Ozaria 2.5 (interval 0–1), Vaga Lab, Belgrade, Serbia. The shape factor was: for 0 – corresponding to the position of the needle, for 1 – corresponding 158 to the circle. There is the following division according to the grain shape factor: from 0.0–0.2 159 – angular; from 0.2–0.4 – sub-angular; from 0.4–0.6 – sub-rounded; from 0.6–0.8 rounded and 160 from 0.8–1.0 – well rounded grain shape.

Properties of the refractory coatings obtained were examined in accordance with the standards.^{18,19} The test procedure is described in a previous paper.²³ The sedimentation stability of the suspension of the obtained coatings was tested by keeping the prepared coating samples for 24 h in a cylindrical vessel with a plug, with a volume of 10^{-4} m³ and a height of 0.28 m.

The test result is expressed in percentages: the volume in mL of transparent layer read is equal to the precipitation of solid particles in percent. Determination of the penetration of coatings into sand moulds was investigated using tubes made of moulding mixture. After applying the coating and drying, the tubes were broken and the depth of penetration of the coating in mm was measured at the fracture. The refractoriness of the filler was determined by a comparative test with bodies whose softening points at high temperatures are known. The symbol SK (Seger's pyramid) and the number that represents the code for the temperature.¹¹ Testing of the coating properties was performed by applying the prepared coatings on the surfaces of the test bodies made of moulded sand mixture and polystyrene. Coatings created in the described way should be easy to apply, adhere well to the surface, are not susceptible to leakage and creation of drops, bubbles, dry easily, without cracking and rubbing the dried layers of the coating.

To assess the quality of the obtained coatings, test castings of plate shape of dimensions 0.2 m × 0.05 m × 0.02 m were cast by casting in sand moulds and by the lost foam process. The casting alloy was AlSi12CuMg. Prior to casting, liquid casting was prepared by refining, degassing and modification processes. The refining and degassing process refers to the treatment of liquid metal with salts based on sodium and potassium chloride in order to remove impurities, inclusions and slag, as well as dissolved gases. To obtain a finer structure and better mechanical properties of castings, liquid metal is treated with structure grinding agents such as sodium, strontium, antimony, and phosphorus before pouring into moulds. Sodium was used in the experiment as a cheap modifier. The casting temperature was 778 °C. Sand moulds

are made of a moulding mixture based on quartz sand with a grain size of 0.17 mm, with 3 % bentonite and 0.15 % dextrin. The moulds for the lost foam process were made of dry quartz sand with a grain size of 0.26 mm. The polymer models in the experiment were made of polystyrene with a density of 19 kg/m³.

RESULTS AND DISCUSSION

Talc-based filler properties

Composition of the sample talc filler T, which was, after mechanical activation, used for production of refractory coatings, is shown in the Table I.

Fig. 1 shows XRD pattern of the talc samples with the dominant presence of talc in the initial sample. Fig. 2 shows SEM microphotograph of the initial talc sample before the mechanical activation. It is seen that the mineral was exclusively present in the proper foliar aggregates.

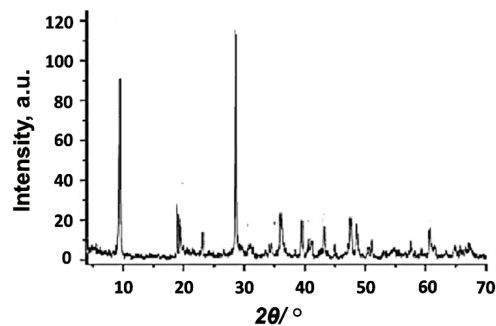


Fig. 1. XRD of talc samples before activation.

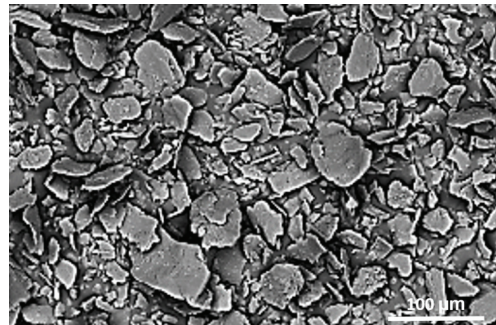


Fig. 2. SEM microphotograph of talc samples before activation.

Figs. 3 and 4 show XRD pattern and microstructure of the talc samples after activation (30 min).

Fig. 3 shows that the diffraction peaks got less intense, thus indicating the alteration of microstructure, amorphousness of the material treated, change of the filler grain size and shape (Table II), as well as the crystal defects.²⁵ During the mechanical activation, the structure was changed, the talc grain was crushed and rounded.

Figure 5 shows the histogram of the filler grain size distribution.

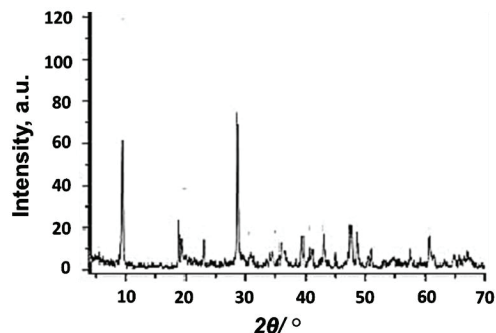


Fig. 3. XRD of talc samples after activation.

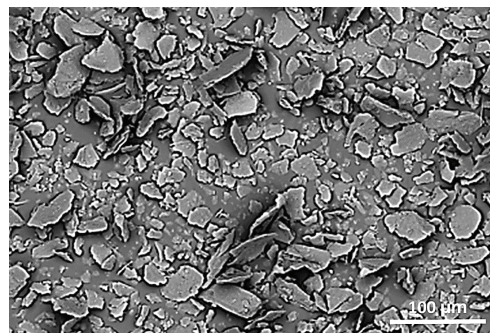


Fig. 4. SEM microphotograph of talc samples after activation.

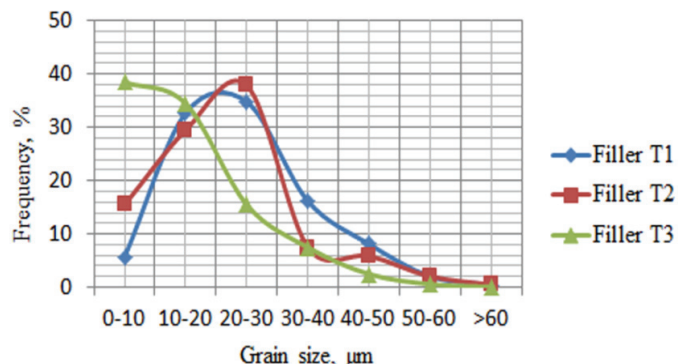


Fig. 5. Histogram of the filler grain size distribution.

Based on the data on the filler mean grain size, it may be expected that the lower-grained fillers will precipitate slower in suspension; they will keep their dispersed state longer and the coating suspension will homogenize more easily. Smaller grains have a larger active surface, they are more difficult to settle, which contributes to the improvement of sedimentation stability of the coating suspension.

Fig. 6 shows the histogram of the filler grain shape factor. Based on the data on the shape factor, the T₁, T₂ and T₃ filler grains are classified in the category of rounded grains (according to division for the grain shape factor of 0.6–0.8).

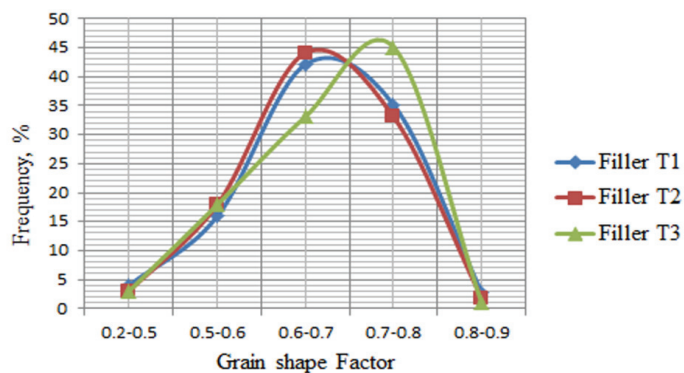


Fig. 6. Histogram of the filler grain shape factor.

Properties of refractory coatings with activated fillers

The microphotographies of suspension for all the 3 types of refractory coatings, with a talc-based activated filler (Table II), are shown in Figs. 7–9.

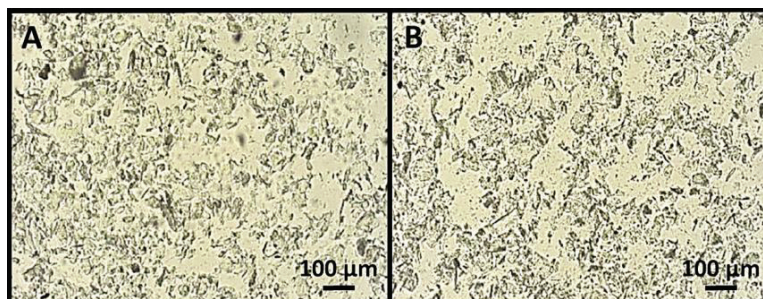


Fig. 7. Microphotographs of suspensions of the lost foam refractory coatings, Type I:
A – homogenous; B – diluted.

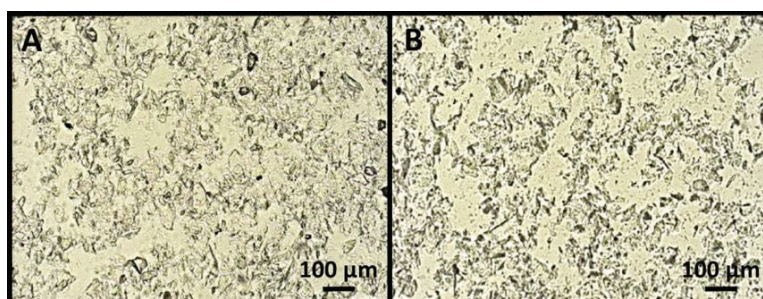


Fig. 8. Microphotographs of suspensions of the lost foam refractory coatings, Type II:
A – homogenous; B – diluted.

During the research referring to water-based coatings, Types I and II, a certain dissolution of the coating film was noticed on the surfaces of polymer

pattern, when a lower content of bentonite-based binding agent was used, up to 2.5 %, in reference to earlier works.²²

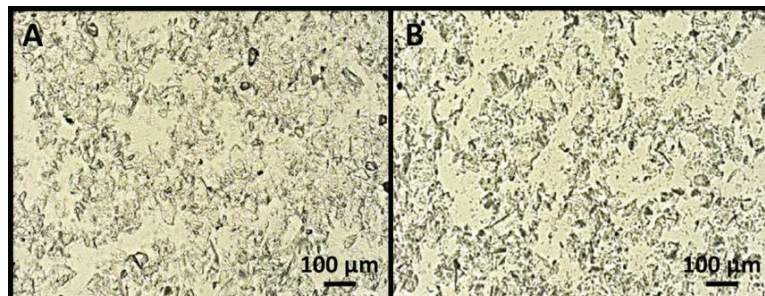


Fig. 9. Microphotographs of suspensions of the lost foam refractory coatings, Type III:
A – homogenous; B – diluted.

Furthermore, due to the mechanical activation, the filler grains got crushed, and increasing the amount of bentonite-based binding agent (to 4.5–5 %), led to a better coating layers adherence to the pattern surface. A of the coating, trade name Bindal H, was also introduced to the binding agent composition (in amount of 4.5–5 %), thus increasing the binding agent ability to get firmly adhered to the polymer pattern surface (Table III). Carboxymethyl cellulose (CMC), in amounts up to 1.5–2 %, was added as an additive in order to increase the coating suspension stability (Table III).

Type III alcohol-based coatings did not show any defects. By using both colophonium-based binding agents (up to 4.5 %) and the suspension maintaining agent Bentone 25 (organic type, up to 2.5 %), Table III) uniform and homogenous coating layers were formed on the surfaces of sand moulds and cores.

Table IV shows the technological properties of the refractory coatings produced: Types I–III.

TABLE IV. Comparison of technological properties of refractory coatings

Coating	Sedimentation (24 h) %	Penetration ^a mm	Drying	Refractoriness ^b	Layer thickness mm ²
Type I	5.5–5.7	≤1	Air-dried	SK 14/1410 °C	0.4–0.7
Type II	4.5	≤1	Air-dried	SK 14/1410 °C	0.4–0.5
Type III	5	≤2	Heat-dried	SK 14/1410 °C	0.3–0.8

^aPenetration coating suspension into the sand mould; ^bSeger's pyramid and the number that represents the code for the temperature

During the production of the Type I–III refractory coatings, it was observed that the coating suspensions with the density of 2000 kg/m³ got homogenized quickly and easy.

The use of a filler with various rounded grain sizes (Type II coating) led to a better mutual grain stack within the coating layers facilitating the filler grain – water-binding agent blend which contributed to the production of a highly permeable, thin (below 0.6 mm), homogenous and continuous film of coat on the pattern surface.

The application of the activated talc-based filler significantly improved the Type I–III coating suspension stability (sedimentation 4.5 - 5.7 %, Table IV).

Earlier research referring to talc-based coatings with grain size of 100 %, 40 μm ^{31,32} showed that the amount of precipitated matters was much higher (7–8 %).

In accordance with the standards,^{18,19} the results obtained for sedimentary suspension stability of all types of coatings were satisfactory, as well as the results obtained for the depth of their penetration into the sand mould (Table IV).

After the visual inspection of surface of the sand-produced castings (with the application of the Type III refractory coatings) and lost foam process (with application of the Type I and II refractory coatings), it was acknowledged that the surfaces were clean, smooth, and glossy with no visible surface defects like roughness or uneven spots. This will help reduce the cleaning and the mechanical operations applied for the castings, *i.e.* it will help make the production costs in cast houses lower.

CONCLUSIONS

The result of this research is the determination of the compositions of the water-based lost foam refractory coatings with the mechanically activated, talc-based filler (with grain size 10–22 μm). As for sand moulds and cores, the composition of the alcohol-based refractory coatings with talc-based activated filler (with grain size of 22 μm) was defined. As activated talc-based fillers with a smaller grain size were applied, the compositions of coatings were altered in terms of content of binding agent and additive, which helped them both improve sedimentary stability of coating suspension and utilization properties of the coatings.

The preparation procedures for the coating suspensions were defined to accomplish the pre-defined coating properties in terms of refractoriness, gas permeability, easy application and adherence to mould and pattern surfaces, easy adjustment of the coat layer thickness, no bubbles, no cracking, or erasure of the dried coat layers. The coating suspensions with density of 2000 kg/m³ presented high sedimentary stability (precipitated matters below 4.5 % during 24 h).

The results of examination of the quality of AlSi12CuMg castings, produced by the lost foam casting process, show that the following technological parameters have the significant influence on the castings quality: pattern density, thermo-physical characteristics of the refractory coating based on talc, shape and dimension the gating system, and particularly on the process flow and balance of the evaporative pattern–refractory coating–liquid metal–sand system. The application

of thinner layers (0.5 mm) of a water-based coating of Type I and II, as well as the application of polystyrene patterns with lower density (19 kg/m^3) have a positive influence on the surface quality and the structural and mechanical properties of castings made of aluminium alloys.

Talc-based filler has lower hardness; in order to increase the mechanical properties of the dried coat layers, the further research should focus on combined talc-based fillers with the addition of cordierite, zeolite or corundum, which could reduce distortion and defects of polymer patterns during the production of moulds in the lost foam process.

Acknowledgement. This work was supported by the Ministry of Education, Science and Technological Development of the Republic of Serbia (Contract No. 451-03-9/2021-316-14/200135, Contract No. 451-03-9/2021-14/200023, Contract No. 451-03-904/2021-16/6, Contract No. 451-03-9/2021-14/200026).

ИЗВОД

СИНТЕЗА НОВИХ "LOST FOAM" ВАТРОСТАЛНИХ ПРЕМАЗА НА БАЗИ ТАЛКА

МАРКО ПАВЛОВИЋ¹, ЈАСМИНА НИКОЛИЋ², ЉУБИША АНДРИЋ³, ДЕЈАН ТОДОРОВИЋ³,
КАТАРИНА БОЖИЋ^{4,5} и САША ДРМАНИЋ²

¹Конјирол инситекш, Београд, ²Универзитет у Београду, Технолошки-металуши факултет, Београд,

³Универзитет у Београду, Институт за технолођу нуклеарних и других минералних сировина,

Београд, ⁴Универзитет у Београду, Институт за хемију, технолођу и металургију, Центар за
електрохемију, Београд и ⁵Универзитет у Београду, Институт за хемију, технолођу и металургију,
Центар изузетних вредности за хемију и инжењерин животне средине, Београд

Истраживање је фокусирано на поступак припреме пуноца на бази талка у циљу побољшања реолошких својстава "lost foam" ватросталних премаза. Талк величине зрна од 40 μm механички је активиран у вибрационом млину у временима од 10, 20 и 30 min. У зависности од времена механичке активације, анализирана је промена величине и облика зрна пуноца заједно са њиховим утицајем на дисперзност и стабилност супензије премаза. За карактеризацију пуноца коришћене су следеће методе: рендгенска дифракционана анализа, скенинг електронска и оптичка микроскопија. Испитиван је утицај састава премаза избором подесне величине и облика зрна активираног пуноца на квалитет премаза. Осим тога, примењене су различите компоненте премаза и изменејен је поступак израде премаза. Показано је да је примена ове врсте "lost foam" ватросталних премаза на воденој основи имала позитиван утицај на квалитет одливака од легура алуминијума. Такође, тестирани су ватростални премази на бази алкохола са активираним пуноцем на бази талка који су коришћени за ливење одливака у калупе од песка.

(Примљено 19. октобра, ревидирано 14. децембра, прихваћено 16. децембра 2021)

REFERENCES

1. R. W. Monroe: *Expandable Pattern Casting*, AFS, Schaumburg, IL, 1994, pp. 66–77 (ISBN 0-87433-150-1)
2. W. D. Griffiths, P. J. Davies, *J. Mater. Sci.* **43** (2008) 5441 (<https://doi.org/10.1007/s10853-008-2844-2>)

3. M. Sands, S. Shivukumar, *J. Mater. Sci.* **38** (2003) 667 (<https://doi.org/10.1023/A:1021859523363>)
4. M. Karimian, A. Ourdjini, M. H. Idris, T. Chuan, H. Jafari, *Res. J. Appl. Sci.* **11** (2011) 3655 (<https://doi.org/10.3923/jas.2011.3655.3658>)
5. Z. Aćimović, Lj. Pavlović, Lj. Trumbulović, Lj. Andrić, M. Stamatović, *Mater. Lett.* **57** (2003) 2651 ([https://doi.org/10.1016/S0167-577X\(02\)01345-9](https://doi.org/10.1016/S0167-577X(02)01345-9))
6. K. H. Hass, S. Amberg-Schwab, K. Rose, G. Schottner, *Surf. Coat.* **111** (1999) 72 ([https://doi.org/10.1016/S0257-8972\(98\)00711-7](https://doi.org/10.1016/S0257-8972(98)00711-7))
7. Z. Aćimović-Pavlović, M. Đuričić, S. Drmanić, R. Đuričić, *Hem. Ind.* **64** (2010) 121 (<https://doi.org/10.2298/HEMIND100301011A>)
8. G. Šekularac, A. Terzić, J. Nikolić, S. Drmanić, M. Pavlović, Z. Aćimović, in *Proceedings of 44th International October Conference on Mining and Metallurgy*, 2012, Bor, Serbia, 2012, p. 281
9. M. Swartzlander, *Mod. Cast.* **82** (1992) 25)
10. T. Hübert, S. Svoboda, B. Oertel, *Surf. Coat.* **201** (2006) 487 (<https://doi.org/10.1016/j.surfcoat.2005.11.014>)
11. Z. Aćimović-Pavlović, A. Prstić, Lj. Andrić, V. Milošević, S. Miličević, in *Ceramic Coatings - Applications in Engineering*, F. Shi, Ed., InTech Open, London, 2012, pp. 261–286 (ISBN: 978-953-51-0083-6)
12. R. W. Davies, *J. ICME* **89** (1996) 287 (ISSN 0953-6035)
13. C. Viazzi, J. P. Bonino, F. Ansart, *Surf. Coat.* **201** (2006) 3889 (<https://doi.org/10.1016/j.surfcoat.2006.07.241>)
14. Lj. Andrić, M. Petrov, D. Radulović, V. Milošević, Z. Acimovic-Pavlovic, in *Proceedings of XX International Serbian Symposium on Mineral Processing*, 2006, Soko Banja, Serbia, 2006, p. 163
15. U. C. Nwaogu, N. S. Tiedje, *Int. J. Mater. Sci. Appl.* **2** (2011) 1143 (<https://doi.org/doi:10.4236/msa.2011.28155>)
16. M. Pavlović, Lj. Andrić, D. Radulović, Z. Čeganjac, in *Proceedings of 9th IOC*, 18–21 October, 2017, Bor Lake, Serbia, 2017, p. 53
17. Lj. Andrić, A. Terzić, Z. Aćimović-Pavlović, Lj. Pavlović, Milan Petrov, *Composites, B* **59** (2014) 181 (<https://doi.org/10.1016/j.compositesb.2013.12.003>)
18. Serbian Standard, *SRPS B.H9.102:1980, Foundry Means – Materials for mould and core dressing classification – Technical requirements – Testing Methods*, 1980
19. Serbian Standard, *SRPS EN 12890:2000/CEN/TC 190, “Founding – Patterns, Pattern Equipment and Core Boxes for the Production of Sand Moulds and Sand Cores”*, 2000
20. U. C. Nwaogu, T. Poulsen, R. Stage, C. Bischoff, N. S. Tiedje, *Surf. Coat. Technol.* **205** (2011) 4035 (<https://doi.org/10.1016/j.surfcoat.2011.02.042>)
21. Z. Aćimović-Pavlović, Lj. Pavlović, Z. Janjušević, M. Stamatović, *Sci. Sinter.* **32** (2000) 179
22. Z. Aćimović-Pavlović, A. Prstić, Lj. Andrić, *Chem. Ind. Chem. Eng. Q.* **13** (2007) 38 (<https://doi.org/10.2298/CICEQ0701038A>)
23. M. Pavlović, Lj. Andrić, D. Radulović, S. Drmanić, N. Đorđević, M. Petrov, *Sci. Sinter.* **51** (2019) 15 (<https://doi.org/10.2298/SOS1901015P>)
24. Z. Čeganjac, Z. Aćimović-Pavlović, Lj. Andrić, M. Petrov, S. Mihajlović, in *Proceedings of 3rd Balcan Metallurgical Conference*, Ohrid, Macedonia, 2003, pp. 24–27, 316

25. Lj. Andrić, A. Terzić, Z. Aćimović, Lj. Pavlović, M. Petrov, *Physicochem. Prob.* **50** (2014) 433 (<https://doi.org/10.5277/ppmp140202>)
26. J. Yvon, F. Villieras, L. Michot, *J. Min. Metall., A* **41** (2005) 1 (<https://scindeks.ceon.rs/article.aspx?artid=1450-59590501001Y>)
27. B. Fotoohi, *Master Thesis*, School of Chemical Engineering Interdisciplinary Research Centre (IRC) in Materials Processing, The University of Birmingham, Birmingham, 2010
28. D. Todorovic, M. Trumic, Lj. Andric, V. Milosevic, M. Trumic, *Physicochem. Prob.* **53** (2017) 321 (<https://doi.org/10.5277/ppmp170126>)
29. J. Zivojinovic, V. Pavlovic, D. Kosanovic, S. Markovic, J. Krstic, V. Blagojevic, V. Pavlovic, *J. Alloys Compd.* **695** (2017) 863 (<https://dx.doi.org/10.1016/j.jallcom.2016.10.159>)
30. M. Yekeler, U. Ulusoy, C. Hicyilmaz, *Powder Tech.* **140** (2004) 68 (<https://dx.doi.org/10.1016/j.powtec.2003.12.012>)
31. M. Pavlović, L. Andrić, D. Radulović, M. Petrov, in *Proceedings of XVII 407 Balkan Mineral Processing Congress*, 2017, Antalya, Turkey, 2017, p. 607
32. Lj. Andrić, Z. Aćimović-Pavlović, N. Pavlović, V. Milošević, S. Miličević, *CERAM* **38** (2012) 2913 (<https://doi.org/10.1016/j.ceramint.2011.11.067>).



Microextraction of lanthanum using a rotating microchannel extractor

SANXING LI, GAOXIANG CHEN, CHUNXIN FAN and JIANHONG LUO*

Department of Chemical Engineering, Sichuan University, Chengdu, Sichuan 610065, China

(Received 23 August, revised 29 September, accepted 6 October 2021)

Abstract: This work introduced a novel microchannel extractor. The extraction system was intended to extract lanthanum nitrate aqueous solution with 2-ethylhexyl phosphoric acid-2-ethylhexyl ester (EHEHPA). Different feeding methods and inner rotors were explored first. The results showed that parallel feeding and inner rotors engraved with spiral stripes were more favorable for extraction. Next, the effect of various factors on the extraction was explored, including the aqueous phase pH, rotational inner rotor speed (R) and the fluid volumetric flow rate (Q). The results showed that these factors are closely related to the extraction. Finally, the experiment was verified by CFD numerical simulation, the simulation result was consistent with the experiment. In this device, active mixing was introduced into the microchannel extraction, which significantly improved the extraction efficiency. Under certain conditions, the extraction efficiency of this device exceeded stirring extraction equilibrium. Moreover, the extraction in the device is faster than with conventional stirring extraction. These advantages provide a possibility for highly efficient extraction of rare earth elements.

Keywords: micro-extraction; La (III); mass transfer; simulation.

INTRODUCTION

Rare earth elements (REEs) are an important non-renewable resource and play an irreplaceable role in high-tech materials. They are widely used in chemical engineering, metallurgy, electronic equipment and other fields.^{1,2} The demand for REEs is also increasing, so the research on extracting and separating them is important. Lanthanides are widely used in many fields because of their luminescence, electronics, and magnetism.³ As one of the most abundant REEs, lanthanum and its compounds are widely used in batteries, catalysts, and so on.⁴

Solvent extraction has the advantages such as: simple equipment, high selectivity, and is renewable.^{5,6} It is widely used in chemical, metallurgy, and other

* Corresponding author. E-mail: luojianhong@scu.edu.cn
<https://doi.org/10.2298/JSC210823080L>

fields.⁷ The separation techniques based on solvent extraction have been widely used to produce high-purity single rare earth solutions or compounds.⁸ However, the conventional equipment like stirring contactors,⁹ packed extraction columns,¹⁰ packed bed columns,¹¹ mixing settlers,¹² etc. can no longer meet the production requirements because of their large area, and a time consuming process. Therefore, it is necessary to develop new equipment. Microchannel extraction is a new direction to improve extraction. Compared with traditional extractors, the specific surface area for a droplet in microchannel is significantly larger. Microchannel extraction has the advantages of large total mass transfer coefficient, short reaction time, safety, etc.¹³ So, it has been a topic of interest for almost 20 years.¹⁴ There have been many reports on micro-extractor, such as tubular microchannel extractor with T-junction,¹⁵ Y-junction serpentine micro-extractor,¹³ hollow fiber contactor¹⁶ and so on. However, two phases are no longer mixed after entering those microreactors. It can be defined as passive mixing. As there are few studies on active mixing micro-extractors, inspired by Nakase *et al.*,^{17,18} our research lab has designed a rotating microchannel extractor.

EXPERIMENTAL

Materials

Kerosene and EHEHPA are purchased from Luoyang Zhongda Chemical Co., Ltd. They are used as diluent and extractant, respectively. After pre-experimental tests, the volume ratio of kerosene to EHEHPA is chosen as 95:5. Lanthanum nitrate (AR) is purchased from Tianjin Oboke Chemical Co., Ltd. Ascorbic acid (AR) and Sudan III (AR) is purchased from Chengdu Jinshan Chemical Reagent Co., Ltd. Hydrochloric acid (AR) is purchased from Sichuan Xilong Science Co., Ltd. Arsenazo (III) is purchased from East China Normal University Chemical Plant (Shanghai). Deionized water is produced by Aquapro water making machine (ABZ1-1001-P) in laboratory. The concentration of lanthanum reserve solution is 510.52 mg L⁻¹.

Experimental equipment and procedure

The schematic diagram of the experimental equipment is shown in Fig. 1.

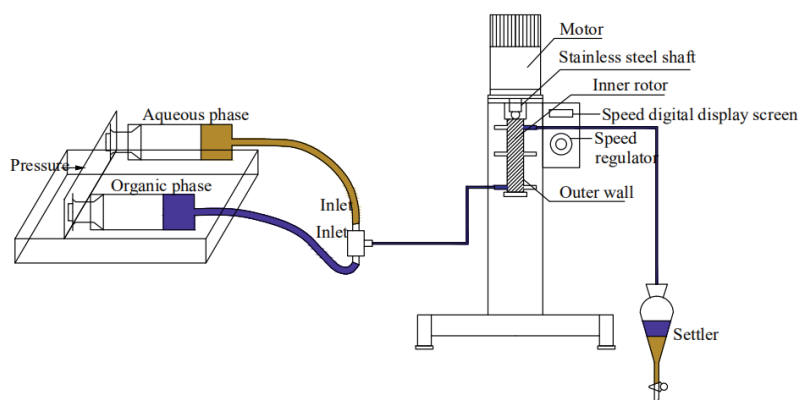


Fig. 1. Schematic drawing of the experimental equipment.

The detailed structure of the extractor is shown in Fig. 2.

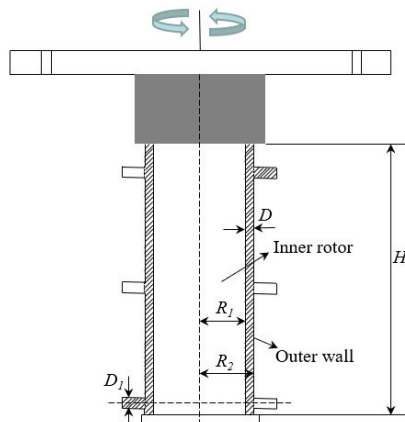


Fig. 2. The detailed structure of extractor.

Radius of inner rotor (R_1) is 9.45 mm; radius of outer cylinder (R_2) is 9.8 mm; making the microchannel width (D) 0.35 mm. The height of fluid region (H) is 200 mm; diameter of inlet/outlet (D_1) is 2.5 mm. The gap between the inner rotor and outer cylinder comprises the microchannel, which is within the standard of microchannel equipment.^{14,19} The inner rotor is connected to a motor for rotation. When the two phases enter the microchannel, they are mixed by the rotation of the inner rotor. This form of active mixing is efficient for mass transfer.²⁰ The outer cylinder is made of hydrophilic acrylic, while the inner rotor is made of hydrophobic polytetrafluoroethylene (PTFE). The design causes the aqueous phase to flow towards the outer wall and the organic phase to flow towards the inner rotor, thereby avoiding emulsification. The inner rotor is replaceable.

There are seven different inner rotors, including a smooth inner rotor (Fig. 3; #0), three inner rotors engraved with cross stripes (Fig. 3; #1, #2 and #3), and three inner rotors engraved with spiral stripes (Fig. 3; #4, #5 and #6).

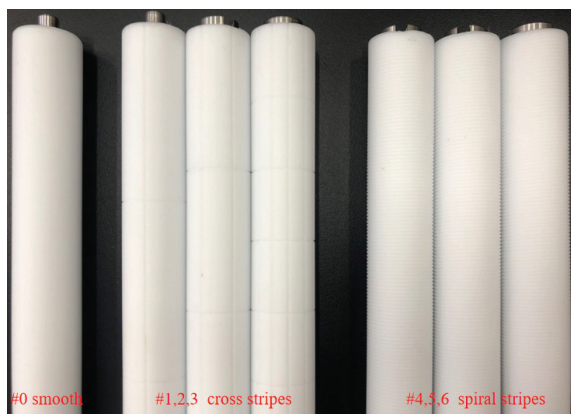


Fig. 3. Different kinds of inner rotors.

All engraved shapes are equilateral triangles, with a height of 0.25 mm, and equidistant. The cross stripes are three horizontal stripes and three vertical stripes (#1), four horizontal

stripes and six vertical stripes (#2), and nine horizontal stripes and twelve vertical stripes (#3). The pitch on the inner rotors with spiral stripes are 1 mm. The difference between them is the helix angle; their details are shown in Fig. 4.

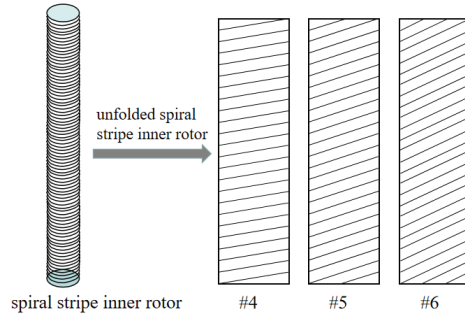


Fig. 4. Schematic diagram of the unfolded spiral stripe inner rotors.

First, different feeding methods and inner rotors were explored. On this basis, the effect of the remaining three factors on extraction was researched. The experiment was run at atmospheric pressure and room temperature. The volume ratio of the two phases (O/A) is 1:1.

Physical properties and analysis

The viscosity of organic phase ($\mu_o = 2.36 \times 10^{-3}$ Pa·s) and aqueous phase ($\mu_{aq} = 9.07 \times 10^{-4}$ Pa·s) are measured with an Ubbelohde viscometer. The surface tension between aqueous phase and organic phase is 22.47 mN m⁻¹, which is measured with an automatic surface tension-meter (BZY-201, Shanghai Fangrui Instrument Co., Ltd.). The two-phase immiscible fluid flow in the microchannel are observed by a high-speed CCD camera (FASTCAM Mini Wx100, Japan Photron). The concentration of La (III) is measured with an ultraviolet spectrophotometer (UV-3100PC, Shanghai Science and Technology Co., Ltd.).

RESULTS AND DISCUSSION

The equations given below are used to analyze the experimental results:

Eq. (1) is used to calculate the percentage extraction:

$$E = 100 \frac{c_{aq,in} - c_{aq,out}}{c_{aq,in}} \quad (1)$$

The overall volumetric mass transfer coefficient ($K_L \alpha$) reflects the mass transfer performance of an extractor. As the component is transferred through the phase interface from one phase to the other, the logarithmic-mean concentration difference (LMCD) was employed to determine the overall volumetric mass transfer coefficient:²¹

$$\Delta_{LMCD} = \frac{(c_{aq,in}^* - c_{aq,in}) - (c_{aq,out}^* - c_{aq,out})}{\ln \left[(c_{aq,in}^* - c_{aq,in}) / (c_{aq,out}^* - c_{aq,out}) \right]} \quad (2)$$

Using LMCD, the average value of the mass transfer flux can be calculated as follows:

$$N = K_L \Delta_{LMCD} \quad (3)$$

$$N = \frac{Q_{\text{aq}}(c_{\text{aq,out}} - c_{\text{aq,in}})}{V\alpha} \quad (4)$$

Incorporating Eqs. (3) and (4), the overall volumetric mass transfer coefficient ($K_L\alpha$) for the extraction process is defined as follows:^{13,21-23}

$$K_L\alpha = \frac{Q}{H\pi(R_2^2 - R_1^2)} \ln \left[\frac{c^{*}_{\text{aq,out}} - c_{\text{aq,in}}}{c^{*}_{\text{aq,out}} - c_{\text{aq,out}}} \right] \quad (5)$$

Eq. (6) is used to calculate the velocity at the inlet and outlet of the fluid:

$$u = \frac{4(Q_{\text{aq}} + Q_o)}{\pi D_l^2} \quad (6)$$

Before evaluating the performance of the device, a conventional stirring extraction experiment was run. When the extraction reached equilibrium, it took 90 s, and $E = 79.61\%$.

Effect of feeding method

The extractor has three inlets and three outlets, as shown in Fig. 2. Different feeding methods were tested using corresponding inlets and outlets, blocking the others with water stop clips. Different feeding methods changed the fluid flow state in the microchannel, affecting the mass transfer. Six different feeding methods were designed, as shown in Fig. 5.

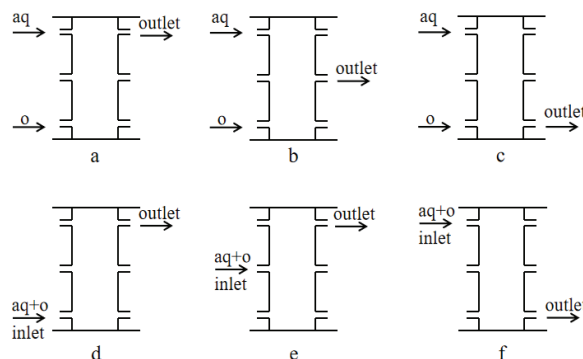


Fig. 5. Different feeding methods. (aq: aqueous phase; o: organic phase).

For a, b and c, the idea was that the density of aqueous phase was greater than organic phase. Feeding from above makes the aqueous phase flow downward. Similarly, the organic phase flows upward to achieve a countercurrent flow. For d, e and f, a parallel feeding method was used. All outlets were designed to ensure that the fluid stays in the microchannel longer.

Methods d, e and f performed significantly better than methods a, b and c, as shown in Fig. 6. The flow patterns of all methods are shown in Fig. 7.

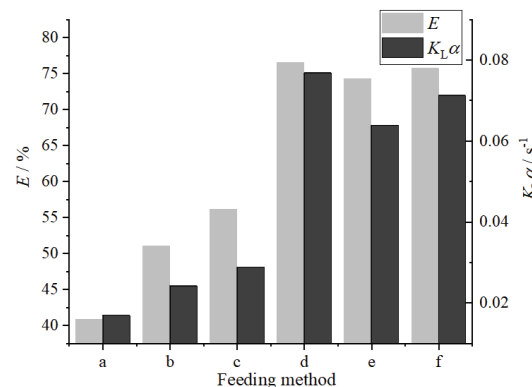


Fig. 6. Variation of E and $K_{L\alpha}$ with feeding method. Conditions: inner rotor is #0, $Q_{\text{aq}} = 3 \text{ mL min}^{-1}$, $R = 400 \text{ rpm}$.

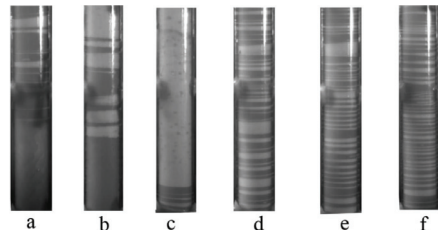


Fig. 7. Flow patterns of different feeding methods. Conditions: inner rotor is #0, $Q_{\text{aq}} = 3 \text{ mL min}^{-1}$, $R = 400 \text{ rpm}$.

The dark part was the organic phase dyed with Sudan III, and the aqueous phase was the transparent part without dyeing. In method a, because fluid is discharged from above, the rising organic phase can only contact the initially deposited aqueous phase, and the subsequent aqueous phase is not fully extracted before being discharged. In method b, fluid is discharged from the middle, causing the upper part to be filled with the aqueous phase and the lower part filled with the organic phase, while the two phases were mixed briefly around the outlet. In method c, fluid was discharged from the bottom, the residence time was short, the organic phase could not flow upward as expected, and it was discharged before being fully extracted. For these reasons, feeding methods a, b and c did not perform well. In methods d, e, and f, parallel flow causes the two phases to be fed together and discharged together so that they mix well and disperse evenly. Moreover, the flow distance of the parallel flow is longer, causing it to perform significantly better. Based on the results, feeding method d was chosen for the next experiment.

Effect of inner rotor surface smoothness

There are seven inner rotors, as shown in Fig 3. The effect of inner rotor surface smoothness on extraction was explored. The results are shown in Fig. 8.

The engraved inner rotors are conducive to extraction. This phenomenon can be explained in three ways. First, because the engravings are equilateral triangles, the engraved inner rotor has a larger wetted area than the smooth one. The increased wetted area is conducive to liquid-liquid contact mass transfer. Second,

the rough engravings allow the fluid to be dispersed and mixed, thereby increasing the surface renewal of the droplet. Third, the engravings increase the turbulence of the fluid. These changes had a positive effect on the extraction. The inner rotors engraved with spiral stripes perform better than those engraved with cross stripes because they have a larger wetted area (mentioned before as the first explanation).

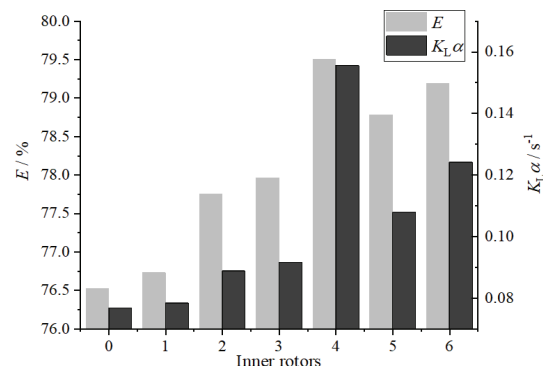
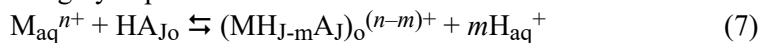


Fig. 8. Variation of E and $K_L\alpha$ with inner rotor surface smoothness. Conditions: feeding method is d, $Q_{aq} = 3$ mL min⁻¹, $R = 400$ rpm.

Effect of aqueous phase pH

EHEHPA is an acidic extractant and contains dissociable H^+ , its mechanism for extracting metal cations is consistent with the cation exchange mechanism. The mechanism is roughly expressed as follows:



The subscripts aq and o represent the aqueous and organic phases, respectively. J represents the number of polymerizations of the extractant, and m is the number of solvent molecules of EHEHPA in the extraction complex.

The apparent equilibrium constant K can be expressed as follows:

$$K = \frac{c_{(MH_{J-m}A_J)_0^{(n-m)+}} c_{H_{aq}}^{+m}}{c_{M_{aq}}^{n+} c_{HA_{J_0}}} \quad (8)$$

The distribution coefficient of metal ions in solution can be expressed as follows:

$$D = \frac{c_{(MH_{J-m}A_J)_0^{(n-m)+}}}{c_{M_{aq}}^{n+}} \quad (9)$$

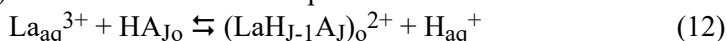
pH definition is as follows:

$$pH = -\log c_{H^+} \quad (10)$$

Combining Eqs. (8)–(10), Eq. (11) can be obtained:

$$\log D = \log (Kc_{(HA)J_0}) + mpH \quad (11)$$

To explore the mechanism the experiment was run in the pH range from 1.5 to 2.5. The linear relationship between $\log D$ and pH is shown in Fig. 9a. The slope of this line is 1.09681 ± 0.09847 , which is close to 1, indicating that the number of solvent molecules of the extracted complex in the organic phase is equal to 1 ($m = 1$).²⁴ Therefore, when pH ranges from 1.5 to 2.5, the mechanism of extracting La (III) with EHEHPA can be expressed as follows:



The effect of pH, in a larger range, on extraction was explored next. The results are shown in Fig. 9b. As the pH of aqueous phase increases from 1.5 to 5.1 (with 5.1 being the initial pH of aqueous phase), E does as well. The change in trend is the same as the mechanism above. As the pH increases, E increases slowly. When the pH is about 3.5, E begins to stabilize.

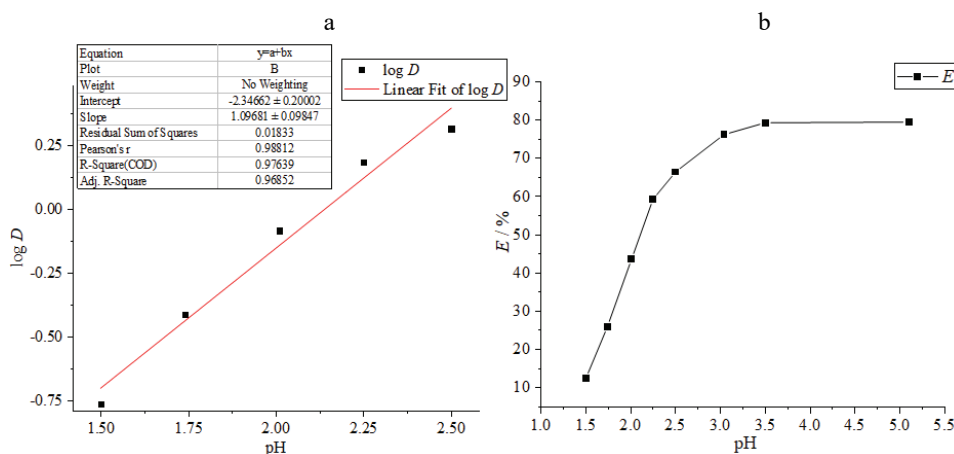


Fig. 9. Research on pH. a) Extraction distribution coefficient ($\log D$) versus the pH; b) variation of E with the pH of aqueous phase. Conditions: feeding method is d, inner rotor is #4, $R = 400$ rpm, $Q_{\text{aq}} = 3 \text{ mL min}^{-1}$.

Effect of inner rotor speed

The experiment was done without rotating at first, and then the speed of the inner rotor was set from 50 to 600 rpm to explore the effect of active mixing on the extraction, Fig. 10.

Without rotation $E = 57.60 \%$ and $K_L \alpha = 3.040 \times 10^{-2} \text{ s}^{-1}$. E reaches 75.93 % and $K_L \alpha$ reaches $7.265 \times 10^{-2} \text{ s}^{-1}$ at a speed of 50 rpm. Compared to the passive mixing without rotation, the active mixing produced by rotating the inner rotor greatly improves extraction. When the inner rotor is at rest, the fluid track is 200 mm long from bottom to top. The schematic diagram of force on the fluid when the inner rotor rotates is shown in Fig. 11.

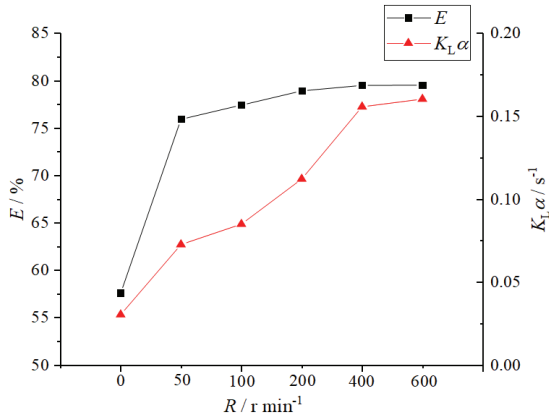


Fig. 10. Variations of E and $K_{L\alpha}$ with inner rotor speed. Conditions: feeding method is d, inner rotor is #4, $Q_{\text{aq}} = 3 \text{ mL min}^{-1}$.

F_1 represents the upward force on the fluid, which mainly comes from the liquid that subsequently enters the microchannel, F_2 represents the centrifugal force, G represents gravity, and F is the total force on the fluid. As F is inclined upward, the fluid spirals up in the microchannel, and its flow pattern is shown in Fig. 12.

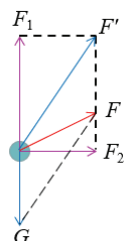


Fig. 11. The schematic diagram of force on the fluid.

The length of this motion track is greater than 200 mm. A longer motion track increases the contact area, and active mixing increases the turbulence of the fluid.

When the inner rotor is at rest, the two phases are not dispersed well and aggregate into large blocks, as shown in Fig. 12.

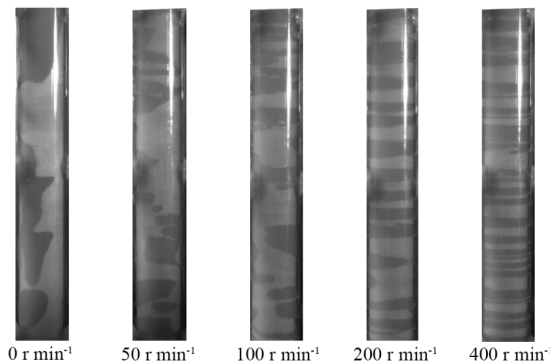


Fig. 12. Flow patterns of different inner rotor speed. Conditions: feeding method is d, inner rotor is #4, $Q_{\text{aq}} = 3 \text{ mL min}^{-1}$.

When the inner rotor rotates, the two phases gradually become increasingly dispersed as the speed increases. Dispersion is conducive to mass transfer, causing the extraction efficiency to increase. As the rotation speed reaches 200 rpm, the dispersion gradually becomes stable, and the extraction efficiency is relatively stable.

This is because centrifugal force determines the size of the droplet in the microchannel. The higher rotation speed causes the smaller droplet size, and the organic droplets are more easily dispersed in the aqueous phase. However, there is a limit to this relationship; as the rotation speed increases and the droplet size decreases to a certain level, it cannot be reduced. Therefore, even if the rotation speed continues to increase, the mass transfer cannot increase significantly, and the extraction efficiency remains stable.

Effect of fluid volumetric flow rate

Changing the fluid volumetric flow rate while keeping other conditions unchanged was tested. Fig. 13 shows the effect of the fluid volumetric flow rate on E . As Q_{aq} increases from 0.5 to 5.0 mL min^{-1} , E decreases.

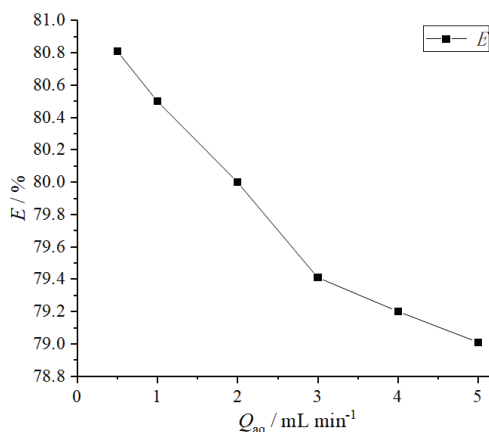


Fig. 13. Variation of E with fluid volumetric flow rate. Conditions: feeding method is d, inner rotor is #4, $R = 400$ rpm.

Fig. 14 shows, as the flow rate increases, the fluid becomes more dispersed, which helps mass transfer. This happens because increasing Q helps to renew the phase interface. However, the extraction efficiency is reduced as the residence time of the fluid decreases. The magnitude of the reduction in residence time outweighs the increase in the mass transfer rate, causing the overall extraction efficiency to be reduced.

It is worth noting that when Q_{aq} is reduced to a certain level, such as 0.5 mL min^{-1} , the extraction efficiency of the extractor exceeds the equilibrium value of stirring extraction. This happens for two reasons. One, when Q is small, the residence time is extended. As they stay for a long time, the different densities of the

two phases are separated. As a result, there are several intermittent fluid accumulation bands during the slow rise of the fluid, as shown in Fig. 14 (0.5 mL). Each time the fluid passes through an accumulation band, an extraction is completed. In other words, it creates a situation like multi-stage extraction. On the other hand, the fluid forms a thin liquid film at a low flow rate, which is conducive to mass transfer.

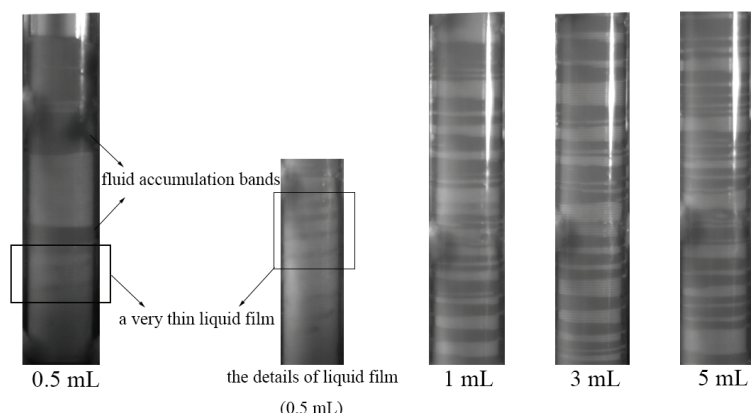


Fig. 14. Flow patterns at different volumetric flow rate conditions: feeding method is d, inner rotor is #4, $R = 400$ rpm.

CFD simulation of flow pattern

After the experiment, CFD numerical simulation was carried out. The software used was SolidWorks 2020 to build the model, IECM CFD 19.2 to draw the mesh and ANSYS Fluent 19.2 to simulate the fluid flow. The mesh is unstructured, and the number is about 3.52 million.

All simulations use double-precision transient solver. The volume of fluid method (VOF) is used to model the two-phase interface. The transient simulation uses the explicit VOF method, and the time step of the volume fraction equation is limited by the maximum Courant number.⁷ The multi-reference Frame (MRF) model is used to model the device, that is the microchannel divided into two areas, one is the area a near the inner rotor, the other is the area b near the acrylic outer cylinder. The fluid in the area a is mainly moved by the rotation of the inner rotor, and the fluid in the area b moves with the fluid in the area a. In the simulation, the time step is controlled at 10^{-5} – 3×10^{-5} s. Momentum is discretized by a second order upwind method. During the calculation process, the Courant number is kept below 5 by adjusting momentum to ensure the convergence of result.

The simulation result is shown in Fig. 15, and the result is basically consistent with the fluid flow pattern captured by the high-speed camera.

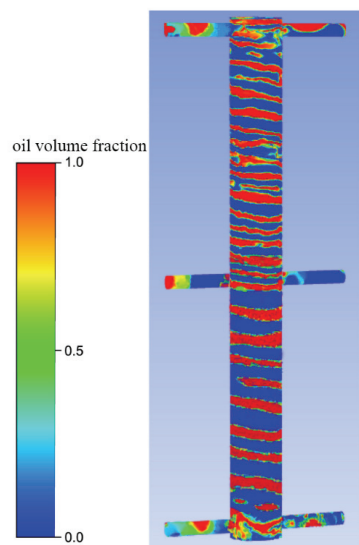


Fig. 15. Simulation result of fluid flow pattern in outer cylinder side Conditions: feeding method is d, inner rotor is #4, $Q_{\text{aq}} = 3 \text{ mL min}^{-1}$, $R = 400 \text{ rpm}$.

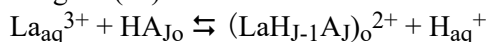
CONCLUSION

In this work, a novel rotating microchannel extractor was used to extract La (III). The introduction of active mixing generated by the rotation of the inner rotor caused the microchannel extraction device to perform excellently. First, the feeding methods and the inner rotors were researched. Next, the effects of aqueous phase pH, inner rotor speed and fluid volumetric flow rate on extraction were investigated. Finally, the experiment was verified by CFD numerical simulation. The experimental results obtained are as follows:

1. Active mixing increases the fluid's turbulence and the surface renewal rate of the mixed-phase. Active mixing significantly improves the extraction in the microchannel.

2. For this novel extractor, the best feeding method is d, a parallel feeding method involving feeding in the bottom and discharging from the top. The best inner rotor is spiral tube #4. The increase in inner rotor speed and the aqueous phase pH is beneficial to extraction. Conversely, an increase in fluid volumetric flow rate is not conducive to extraction.

3. When the pH of the aqueous phase ranges from 1.5 to 2.5, the reaction mechanism for extracting La (III) with EHEHPA can be described as:



4. The extraction in this device is faster than the conventional stirring extraction. When the residence time of the device is 25.38 s, $E = 79.01 \%$, which has basically reached the extraction equilibrium, while stirring extraction takes 90 s.

5. The numerical simulation results are consistent with the phenomena observed in the experiment, which further supports the experiment.

6. When the fluid volumetric flow rate is low, the extraction efficiency of the extractor exceeds the equilibrium value of stirring extraction. It provides a possibility for highly efficient extraction of rare earth elements.

Acknowledgements. We gratefully acknowledge financial support from the National Natural Science Foundation of China (21776181), Sichuan University innovation spark project (2018SCUH0012), Science and Technology Plan Project of Sichuan Province (2021YFG0285) and Chinese National Key Research and Development Plan (2018YFC1900203-03).

ИЗВОД

МИКРОЕКСТРАКЦИЈА ЛАНТАНА ПОМОЋУ РОТИРАЈУЋЕГ МИКРОКАНАЛНОГ ЕКСТРАКТОРА

SANXING LI, GAOXIANG CHEN, CHUNXIN FAN и JIANHONG LUO

Department of Chemical Engineering, Sichuan University, Chengdu, Sichuan 610065, China

У овом раду описан је нови микроканални екстрактор. Екстракциони систем је коришћен за екстракцију воденог раствора лантан-нитрата коришћењем 2-етилхексил-естра 2-етилхексил-фосфорне киселине (ЕНЕНРА). У експериментима су испитивани различити начини увођења напојних смеша, као и различити типови унутрашњих ротора. Испитивања су показала да се најбољи резултати постижу приликом паралелног увођења напојних смеша и коришћењем унутрашњих ротора са спиралним жљебовима. Такође је испитиван утицај процесних параметара, као што су pH вредност раствора, број обртаја унутрашњег ротора (R) и запремински проток флуида (Q) на ефикасност процеса. Резултати су показали да сви ови фактори значајно утичу на процес екстракције. Експериментални резултати су верификовани CFD нумеричком симулацијом. У овом уређају се врши активно мешање струја у микроканалном екстрактору, што значајно доприноси повећању ефикасности процеса. Под одређеним условима извођења, ефикасност екстракције је већа од равнотежне екстракције у класичном уређају са мешалицом. Такође, екстракција у овом уређају се одвија већом брзином у односу на класичан уређај. Ове предности омогућавају коришћење микроканалног екстрактора за извођење високо-ефикасне екстракције елемената из групе ретких земаља.

(Примљено 23. августа, ревидирано 29. септембра, прихваћено 6. октобра 2021)

REFERENCES

1. R. K. Jyothi, T. Thenepalli, J. W. Ahn, P. K. Parhi, K. W. Chung, J. Y. Lee, *J. Clean Prod.* **267** (2020) 122048 (<http://dx.doi.org/10.1016/j.jclepro.2020.122048>)
2. A. Soukeur, A. Szymczyk, Y. Berbar, M. Amara, *Sep. Purif. Technol.* **256** (2021) 117857 (<http://dx.doi.org/10.1016/j.seppur.2020.117857>)
3. V. V. Belova, M. M. Martynova, Y. V. Tsareva, V. E. Baulin, D. V. Baulin, *J. Mol. Liq.* **293** (2019) 111568 (<http://dx.doi.org/10.1016/j.molliq.2019.111568>)
4. R. Panda, M. K. Jha, J. Hait, G. Kumar, R. J. Singh, K. Yoo, *Hydrometallurgy* **165** (2016) 106 (<http://dx.doi.org/10.1016/j.hydromet.2015.10.019>)
5. W. Xiang, S. Liang, Z. Zhou, W. Qin, W. Fei, *Hydrometallurgy* **171** (2017) 27 (<http://dx.doi.org/10.1016/j.hydromet.2017.04.007>)

6. C. Shi, D. Duan, Y. Jia, Y. Jing, *J. Mol. Liq.* **200** (2014) 191 (<http://dx.doi.org/10.1016/j.molliq.2014.10.004>)
7. R. Ma, C. Fan, Y. Wang, J. Luo, J. Li, Y. Ji, *Chem. Eng. Process.* **151** (2020) 107916 (<http://dx.doi.org/10.1016/j.cep.2020.107916>)
8. F. Xie, T. A. Zhang, D. Dreisinger, F. Doyle, *Miner. Eng.* **56** (2014) 10 (<http://dx.doi.org/10.1016/j.mineng.2013.10.021>)
9. P. A. Quadros, C. M. S. G. Baptista, *Chem. Eng. Sci.* **58** (2003) 3935 ([http://dx.doi.org/10.1016/S0009-2509\(03\)00302-6](http://dx.doi.org/10.1016/S0009-2509(03)00302-6))
10. A. M. Dehkordi, *Ind. Eng. Chem. Res.* **40** (2001) 681 (<http://dx.doi.org/10.1021/ie000279s>)
11. R. P. Verma, M. M. Sharma, *Chem. Eng. Sci.* **30** (1975) 279 ([http://dx.doi.org/10.1016/0009-2509\(75\)80078-9](http://dx.doi.org/10.1016/0009-2509(75)80078-9))
12. M. N. Kashid, I. Gerlach, S. Goetz, J. Franzke, J. F. Acker, F. Platte, D. W. Agar, S. Turek, *Ind. Eng. Chem. Res.* **44** (2005) 5003 (<http://dx.doi.org/10.1021/ie0490536>)
13. Y. He, K. Chen, C. Srinivasakannan, S. Li, S. Yin, J. Peng, *Chem. Eng. J.* **354** (2018) 1068 (<http://dx.doi.org/10.1016/j.cej.2018.07.193>)
14. K. Wang, G. Luo, *Chem. Eng. Sci.* **169** (2017) 18 (<http://dx.doi.org/10.1016/j.ces.2016.10.025>)
15. G. Orsi, M. Roudgar, E. Brunazzi, C. Galletti, R. Mauri, *Chem. Eng. Sci.* **95** (2013) 174 (<http://dx.doi.org/10.1016/j.ces.2013.03.015>)
16. D. N. Ambare, S. A. Ansari, M. Anitha, P. Kandwal, D. K. Singh, H. Singh, P. K. Mohapatra, *J. Membr. Sci.* **446** (2013) 106 (<http://dx.doi.org/10.1016/j.memsci.2013.06.034>)
17. M. Nakase, R. Makabe, K. Takeshita, *J. Nucl. Sci. Technol.* **50** (2013) 287 (<http://dx.doi.org/10.1080/00223131.2013.772445>)
18. M. Nakase, H. Kinuhata, K. Takeshita, *J. Nucl. Sci. Technol.* **50** (2013) 1089 (<http://dx.doi.org/10.1080/00223131.2013.835248>)
19. C. Xu, T. Xie, *Ind. Eng. Chem. Res.* **56** (2017) 7593 (<http://dx.doi.org/10.1021/acs.iecr.7b01712>)
20. P. Erfle, J. Riewe, H. Bunjes, A. Dietzel, *Micromachines* **10** (2019) 220 (<http://dx.doi.org/10.3390/mi10040220>)
21. Q. Li, P. Angeli, *Chem. Eng. Sci.* **143** (2016) 276 (<http://dx.doi.org/10.1016/j.ces.2016.01.004>)
22. S. Yin, J. Pei, J. Peng, L. Zhang, C. Srinivasakannan, *Hydrometallurgy* **175** (2018) 64 (<http://dx.doi.org/10.1016/j.hydromet.2017.10.027>)
23. J. Chang, F. Jia, C. Srinivasakannan, K. A. Mumford, X. Yang, *Chem. Eng. Process.* **137** (2019) 54 (<http://dx.doi.org/10.1016/j.cep.2019.02.001>)
24. S. Dai, J. Luo, J. Li, X. Zhu, Y. Cao, S. Komarneni, *Ind. Eng. Chem. Res.* **56** (2017) 12717 (<http://dx.doi.org/10.1021/acs.iecr.7b01888>).



Distribution and provenance of heavy metals in sediments of the Vrbas River, Bosnia and Herzegovina

SANJA PRŽULJ¹, ANA RADOJIČIĆ², MILICA KAŠANIN-GRUBIN³,
DUŠICA PEŠEVIĆ¹, SANJA STOJADINOVIC³, BRANIMIR JOVANIĆEVIĆ^{4#}
and GORICA VESELINOVIĆ^{3*}

¹University of Banja Luka, Faculty of Natural Sciences and Mathematics, Dr. Mladena Stojanovića 2, 78000 Banja Luka, Bosnia and Herzegovina, ²Mining Institute Ltd. Belgrade, Batajnički put 2, 11080 Belgrade Zemun, Serbia, ³University of Belgrade, Institute of Chemistry, Technology and Metallurgy (ICTM), Njegoševa 12, 11000 Belgrade, Serbia and ⁴University of Belgrade, Faculty of Chemistry, Studentski trg 12–16, 11000 Belgrade, Serbia

(Received 8 June, revised 1 September, accepted 3 September 2021)

Abstract: Heavy metals are naturally occurring elements, but they are regarded as significant environmental pollutants due to their high density and high toxicity even at low concentrations. The aim of this paper is the evaluation of the pollution level of heavy metals in the river and riverbank sediments, as well as the estimation of their origin and spatial differences along the course of the Vrbas River through Banja Luka. The concentrations of metals have been assessed using the Inductively coupled plasma – optical emission spectrometry and Advanced mercury analyzer for mercury determination. The anthropogenic impact on heavy metal concentration in sediments was estimated by the calculating of pollution indices: geoaccumulation index (I_{geo}), contamination factor (C_f), pollution load index (PLI) and potential ecological risk index (E_r). Obtained results indicate that there is no statistically significant spatial difference in metal concentration, indicating that heavy metals in sediments have a constant source. The anthropogenic impact expressed by the values of pollution indices showed that sites are generally uncontaminated by Co, Cr and V and moderately contaminated by Zn, Cu and Ni. On the contrary, lead, mercury and cadmium pose the highest ecological risk. The anthropogenic source of Pb, Hg and Cd is industry, municipal waste and the combustion of fossil fuels. The obtained results demonstrate the high ecological risk and the need for environmental monitoring, with the aim to support an efficient strategy to reduce local pollution and contamination of the investigated system.

Keywords: pollution indices; anthropogenic impact; river sediments.

* Corresponding author. E-mail: gorica.veselinovic@ihtm.bg.ac.rs

Serbian Chemical Society member.

<https://doi.org/10.2298/JSC210608070P>

INTRODUCTION

The Vrbas River is an important river ecosystem in Bosnia and Herzegovina with a length of 250 km and catchment areas of 5,900 km². Before reaching Banja Luka, it passes through a canyon and numerous gorges, which are, from 1955, protected by the Law on the Protection of Natural Values. The Vrbas River, as a right tributary of the Sava, belongs to the Black Sea basin. Along the entire course, this river flows through many towns and villages, but the main anthropogenic influence comes from Banja Luka, one of the largest cities in Bosnia and Herzegovina.

The presence of microelements, dominantly heavy metals, is undoubtedly one of the most important indicators of environmental quality and assessing their content in river sediments is an imperative for estimating the environmental risk.¹ Heavy metals are naturally occurring elements, but they are regarded as significant environmental pollutants due to high density and high toxicity even at low concentrations. They might remain permanently present in the environment due to the fact that they cannot be degraded or biodegraded, and in that way they affect metabolic processes of flora and fauna, which identifies them as high category pollutants.² The occurrence of heavy metals in waters, sediments and biota can indicate the presence of natural sources (weathering of rocks, atmospheric precipitate and wind erosion) or anthropogenic activities (urbanization itself, agricultural and urban activities, industrial discharge, mining, transport).^{3–6} Rivers, which approximately deliver 20 billion metric tons of transported sediment to oceans every year, play a key role in Earth surface processes, marine sedimentation and biogeochemical cycles in oceans.⁷ Thus, rivers have an essential role in the acceptance and the transportation of heavy metals, which can accumulate in the sediments through complex physical and chemical adsorption mechanisms, depending on the nature of the sediment matrix and the adsorbed components.⁸ Hence, the water sediments are a highly dynamic part of river systems, not tied to a particular area and are transported through countries in the same river basin. The quality of sediment affects the downstream areas. In particular, the presence of contaminants, such as heavy metals, threatens the ecological and chemical status of waterways and other water bodies (affecting the living organisms, the water resources and the water management), which are the focal point of the European Water Framework Directive,⁹ where the Vrbas River belongs as well.

Due to the expanding frequency of the anthropogenic activities, which results in an increase in the concentration of heavy metals in surface sediments and soil, various factors, such as geoaccumulation index (I_{geo}) – quantitative measure of the extent of metal pollution in the studied sediments, contamination factor (C_f) – the enrichment in metals in relation to the background concentrations of each metal in sediments, pollution load index (PLI) – the level of pol-

lution or potential ecological risk index (E_r) – the degree of heavy metal pollution in sediments, according to the toxicity of heavy metals and the response of the environment, were introduced to assess the origin of these elements.^{5,7,8,10–12}

The aim of this paper is the evaluation of the pollution level of heavy metals in the river and riverbank sediments, as well as the estimation of their origin, and the spatial differences along the course of the Vrbas River in Banja Luka city.

EXPERIMENTAL

Details about the study area and sampling are given in the Supplementary material to this paper.

Content of heavy metals

Concentrations of heavy metals were determined on sediment fraction size <63 µm, which was obtained by the wet-sieving method. The following heavy metals were determined in 16 river sediments and 16 riverbank sediments: Cd, Co, Cr, Cu, Ni, Pb, V, Zn, and Hg. All the chemicals used for analysis were of analytical reagent grade and deionized water with resistivity 18.2 MΩ cm obtained from a Milli-Q system (Elga Purelab Ultra). The sediment samples were prepared by weighing 0.5 g of sample into PFA vessels and adding 9 ml HNO₃ (65 %), 3 ml HF (48 %) and 2 ml HCl (37 %) and digested according to the standard procedure for closed-vessel acid digestion of siliceous and organically based matrices (EPA Method 3052). After the digestion, the solutions were cooled, then filtered and diluted with deionized water to the total volume of 50 mL in volumetric flasks.

The blank sample contained all reagents in the same amounts as used in sample processing and was run through the complete procedure. Each sample was analyzed in duplicate. The certified reference material Sewage Sludge 2 (CRM 029-50G, Fluka Analytical) was used to validate the method. The quality of data was also checked through recovery experiments by spiking several samples with a known concentration of standards. The results showed an acceptable agreement with the certified values. The recovery values were in the acceptable range (80–110 %) for each element.

The calibration of each element was performed by preparing 5 standard solutions in the range of 0.01 to 1.0 mg L⁻¹. A stock solution was the multi-element plasma emission calibration standard (Accu standard). The values of linear correlation coefficients were $R > 0.99$ for each element. The detection limit (LOD) was determined as a triple value of the standard deviation obtained from ten measurements of the low concentration standard.

For heavy metal determination, an inductively coupled plasma-optical emission spectrometer Varian 730-ES (ICP-OES) with CCD detector was used, which provides true simultaneous measurement and full wavelength coverage from 167 to 785 nm. The operational parameters used in this paper were: power 1.15 kW; plasma flow 15 L min⁻¹; nebulizer pressure 200 kPa; replicate read time 5 s; stabilization delay 15 s; sample delay time 30 s; pump rate 30 rpm; rinse time 10 s; fast pump on. The selected elemental wavelengths for determination were as follows: Zn: 206.200, Cu: 327.393, Ni: 231.604, Pb: 220.353, Cr: 267.716, Cd: 214.480, V: 292.401 and Co: 228.616 nm.

For mercury determination, LECO AMA254 advanced mercury analyzer – atomic absorption spectrometer, specifically designed to determine total mercury content in various solids and liquids – without sample pre-treatment or sample pre-concentration, was used. The sample measured weights ranged from 0.025 to 0.080 g. The operational parameters used in this study were: drying time 60 s, decomposition time 200 s, cuvette clear time 45 s, dosing delay time 0 s, auto select cell selection, metric for calculations peak area.

Evaluation of anthropogenic impact on heavy metal concentration in sediments

Estimation of the anthropogenic impact of the toxic metal enrichment implies a comparison of the obtained metal concentration in the sample with its concentration in the background sample. The background sample represents the sample that was not exposed to the anthropogenic impact. In this study the following average metal concentrations in the Earth's continental crust (Taylor)¹³ were used as background values: $c_{\text{Cd}} = 0.2$, $c_{\text{Co}} = 25$, $c_{\text{Cr}} = 100$, $c_{\text{Cu}} = 55$, $c_{\text{Ni}} = 75$, $c_{\text{Pb}} = 12.5$, $c_{\text{V}} = 135$, $c_{\text{Zn}} = 70$ and $c_{\text{Hg}} = 0.08 \text{ mg kg}^{-1}$.

Geoaccumulation index was calculated according to Müller¹⁴ as follows:

$$I_{\text{geo}} = \log_2 \left(\frac{M_s}{1.5B_M} \right) \quad (1)$$

M_s presents the concentration of the obtained metal in the sample and B_M the geochemical background concentration of the same metal.¹⁴ According to the calculated values of the geoaccumulation index, the anthropogenic impact on the metal content in the observed sample can be classified into seven categories, from zero value to seven, according to the increasing metal contamination.¹⁵

For the formulation of the potential ecological risk index and the pollution load index, it is required to define the contamination factor (C_f) as the ratio of the concentration of each metal individually and its background concentration, as follows:

$$C_f = \frac{M_s}{M_B} \quad (2)$$

where M_s presents the concentration of the metal in the sample and M_B metal concentration in the background sample.¹⁶ The n^{th} root of the multiplicated contamination factors of all present metals in the obtained sample represents the formulation of the pollution load index.¹⁶⁻¹⁸ For the first time, *PLI* was defined by Tomlinson,¹⁹ as follows:

$$PLI = \sqrt[n]{C_{f1}C_{f2} \cdots C_{fn}} \quad (3)$$

where index numbers in contamination factors represent different toxic metals in samples. For a *PLI* value less than 1, it is assumed that no heavy metal contamination has occurred, respectively for values greater than 1 for the observed sample, it is considered that the exposure to toxic metals pollution by anthropogenic influence was present.¹⁹

In 1980's one more descriptive approach of the anthropogenic impact on the metal concentration was revealed by Hakanson,²⁰ called an index of potential ecological risk (E_r). In mathematical formulation, it is a multiplication of contamination factor (C_f) and toxic response factor (T_f), as follows:

$$E_r^i = C_f^i T_r^i \quad (4)$$

A toxic response factor is a constant number, its value depends on the nature of the metal, and it is known in the literature. A total potential ecological risk index (R) presents the sum of all potential ecological risk indexes for each toxic metal present in the sample individually, mathematically formulated as follows:

$$R = \sum E_r^i \quad (5)$$

Evaluation of anthropogenic impact on the toxic metal concentration in the observed sample is made by following ranges: for the E_r values lower than 40 (R values lower than 94, respectively), the ecological risk for the analyzed sample is considered as low; for E_r in the range of 40 to 80 (R values in the range from 94 to 188, respectively), the risk is rated as a medium; if the E_r value is in the range from 80 to 160 (R values in the range from 188 to 376),

the potential ecological risk is significant, and at the end, for the E_r values larger than 160 (R values larger than 376), the potential ecological risk is very high.^{20,21}

Statistical analyses

The results were quantitatively described using the descriptive statistics. An independent *t*-test which determines whether there are differences between groups, was used in this study for the comparison between heavy metal composition of river and riverbank sediments. The coefficient of variation is used to determine the variation within groups, and in this case it was used for finding a difference between the concentrations of a certain element at different locations. The coefficient of variation shows the extent of variability of data in a sample in relation to the mean of the population. The data with coefficient of variation higher than 1 are considered to be high variance whereas those with a *CV* lower than 1 are considered to be low-variance. The factor analysis (rotation method: Varimax with Kaiser Normalization) was used to reduce a large number of variables into fewer numbers of factors which were employed to determine which heavy metals might have the same source. Statistical analysis was performed by IBM SPSS Statistics 20.

RESULTS AND DISCUSSION

The concentrations of heavy metals, determined in 16 river sediments (RS) and 16 riverbank sediments (BS) sampled at eight locations during the summer of 2020 along the Vrbas River in Banja Luka, are given in Table I. The riverbank sediments were deposited during the last flood (May 2014), and the river sediments are constantly deposited and transported by the Vrbas River.

The average concentration of studied metals in water followed a decreasing order of Hg < Cd < Co < Pb < Ni < Cu < V < Cr < Zn. The range of concentration are: c_{Cd} , <0.05–2.13; c_{Co} , 13.13–36.73; c_{Cr} , 61.01–197.40; c_{Cu} , 47.68–426.00; c_{Ni} , 50.31–256.23; c_{Pb} , 21.85–272.00; c_{V} , 55.60–153.12; c_{Zn} , 112.47–489.00, c_{Hg} , 0.13–1.43 mg kg⁻¹.

The independent *t*-test results revealed no statistically significant difference between the river and the riverbank samples (Table S-I of the Supplementary material), indicating that the sediments are exposed to the same source of heavy metals. Furthermore, the low coefficient of variation indicates that the concentrations of heavy metals are similar among locations (*CV* < 1; Table II). Although the sampling size is small, this result confirms the constant source of heavy metals.

The factor analysis helped to reduce the dimensionality of the metal contamination from 9 original variables to 3 factors (Table II). These new variables accounted for 84.4 % of the total variance. The factor analysis showed that there are three groups that have similar mechanisms of transport and accumulation within the sediments: Factor 1 accounted for Co, Cr, Ni, and Hg, Factor 2 Cu, Pb and Zn, and Factor 3 Cd and V.

The I_{geo} values for Co, Cr and V below 0 classify the investigated sediments as uncontaminated (Fig. 1; Table S-II). The only positive value is 0.13 for Cr at location 5 (close to the Incel Bridge). Most sites are uncontaminated or uncontaminated to moderately contaminated with Cu and Ni, with a slightly higher

value for Cu ($I_{\text{geo}} = 1.02$) at the site near the thermal power plant. The majority of samples are uncontaminated to moderately contaminated or moderately contaminated with Zn and Pb, except for a higher I_{geo} value for lead ($I_{\text{geo}} = 2.23$), again at site 6, near the power plant. The vast majority of samples are moderately contaminated with Hg (I_{geo} in range 1–2), with the exception of $I_{\text{geo}} = 2.51$ at site 2 (promenade) in which is moderate to strongly contaminated.

TABLE I. The concentrations of heavy metals (mg kg⁻¹) in riverbank and river sediments; BS – riverbank sediment; RS – river sediment; a and b – sample duplicates

Sample site	Metal									
	Cd		Co		Cr		Cu		Ni	
	a	b	a	b	a	b	a	b	a	b
BS 1	1.35	2.12	13.74	16.68	84.20	101.72	82.70	73.81	80.37	77.99
RS	1.55	<1	16.85	13.13	86.87	61.01	188.00	69.05	77.80	50.31
BS 2	1.80	1.90	18.45	18.36	101.74	98.46	78.60	71.33	91.98	74.88
RS	1.56	1.40	17.55	14.48	107.34	75.51	122.60	82.96	93.85	63.83
BS 3	1.93	1.44	15.48	17.91	110.64	104.26	95.70	77.11	90.80	76.62
RS	1.36	1.24	14.79	18.50	91.60	79.49	88.24	119.11	79.44	73.43
BS 4	1.59	1.29	20.92	23.74	134.02	117.03	64.40	55.85	157.00	138.48
RS	1.22	1.64	22.65	27.79	121.09	158.27	71.23	90.00	150.00	207.00
BS 5	1.78	1.18	25.52	22.09	180.74	107.43	59.70	52.88	235.00	128.23
RS	1.80	1.35	31.51	36.68	176.37	183.35	59.72	94.55	260.00	256.23
BS 6	1.64	1.73	15.80	20.03	89.20	84.77	141.00	74.96	76.70	84.21
RS	1.22	1.29	17.59	14.44	101.00	65.78	47.68	426.00	89.20	59.96
BS 7	1.81	1.24	22.50	28.05	133.71	129.76	83.53	56.42	150.00	141.13
RS	1.21	1.67	16.98	36.73	104.57	197.40	91.68	66.90	109.00	180.71
BS 8	1.47	1.21	15.48	17.86	90.50	78.70	96.53	93.26	80.13	69.67
RS	1.57	1.56	30.56	29.62	170.56	134.44	57.50	79.36	195.00	155.82
Sample site	Pb		V		Zn		Hg			
	a	b	a	b	a	b	a	b		
BS 1	33.52	35.13	95.25	117.69	192.06	141.74	0.35	0.28		
RS	43.40	22.21	90.67	66.63	355.12	168.99	0.96	0.28		
BS 2	36.34	33.29	116.91	114.01	171.04	163.37	0.34	0.28		
RS	40.50	30.67	116.00	80.32	233.28	226.96	0.69	1.43		
BS 3	32.02	40.92	116.89	120.83	174.82	176.88	0.34	0.32		
RS	32.22	47.84	103.00	84.64	272.41	258.29	0.77	0.46		
BS 4	21.85	23.04	96.85	88.76	134.50	112.47	0.14	0.52		
RS	23.10	29.30	92.40	114.00	126.38	172.00	0.59	0.58		
BS 5	24.71	23.10	124.00	82.90	167.89	113.41	0.17	0.13		
RS	24.80	77.85	114.00	112.77	217.89	249.29	0.23	0.18		
BS 6	29.83	40.57	80.30	86.36	261.24	201.31	0.46	0.16		
RS	26.40	272.00	90.60	55.60	120.10	489.00	0.43	0.54		
BS 7	27.52	33.44	110.00	110.16	176.92	140.00	0.36	0.25		
RS	25.10	30.13	88.20	153.12	197.51	143.27	0.38	0.36		
BS 8	31.10	49.20	75.30	81.19	254.31	233.07	0.51	0.61		
RS	23.80	54.34	141.00	111.71	133.09	171.95	0.17	0.18		

TABLE II. Results of factor analysis (FA) after Varimax rotation and coefficient of variation (CV) for concentration of heavy metals in the Vrbas River sediments

Element	Factor analysis			Coefficient of variation
	1	2	3	
Cd			0.951	0.09
Co	0.940			0.24
Cr	0.916			0.25
Cu		0.955		0.34
Ni	0.934			0.43
Pb		0.936		0.47
V			0.643	0.12
Zn		0.902		0.15
Hg	-0.502			0.30

The most severe is the anthropogenic impact of cadmium on the Vrbas River sediments collected in the City of Banja Luka. In each sample, the calculated values of I_{geo} for Cd (2.08–2.29) show a moderately to strongly contaminated environment. Cd is closely related to industrial activities in the upstream areas.²²

According to the values of contamination factor,²⁰ the analyzed sediment samples mostly have a low degree of contamination with V and Co, or they are moderately contaminated with Cr, Ni, Cu, and Zn. However, in some samples, they have a considerable degree of contamination, e.g., in the case of Cu and Zn near the thermal power plant, or Zn at sampling points 1 and 3, which are impacted by frequent traffic and number of sewage outlets (Fig. 1; Table S-III). The C_f values for lead represent a moderate to considerable contamination for all sampling sites, except thermal power plant ($C_f = 7.03$) where the level of contamination is very high. All sampling sites are considerably contaminated with mercury, except the samples from site 2 near the promenade, with a very high degree of contamination. The contamination factor values for Cd ($C_f > 6$) imply a very high degree of contamination at all locations (Fig. 1; Table S-III).

The calculated pollution load index (PLI) values of metals in sediment are in the range 1.79–2.27 (Table S-III), confirming that the deposition of the urban stretch of the Vrbas River is polluted ($PLI > 1$), which might be due to urban activities.

The most significant value of the C_f that contributes to the PLI values are the values of contamination factors for Cd, Pb and Hg.

The potential ecological risk (E_r) regarding the content of the Cd and Pb in observed sediments is estimated as very high. These values are significantly higher than minimal values that pose a high ecological risk (Table III).

Although the statistical difference between heavy metal concentrations at different locations does not exist ($CV < 1$), certain trends can be observed (Table II). The correlations obtained by the factor analyses (Table II) have proved that the elevation of certain elements coincides with some specific locations. For

example, Cd and Hg have the highest concentrations at location 2, Pb, Cu, Zn at location 6 and Co, Cr and Ni at locations 5, 7 and 4. This further implies the same source of correlated elements.

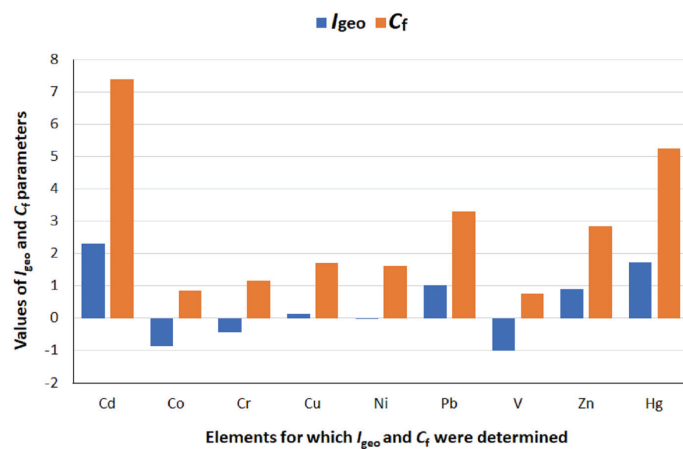


Fig. 4. Geoaccumulation index (I_{geo}) and contamination factor (C_f) for average heavy metal concentrations measured in the Vrbas River sediments (classes of contamination related to I_{geo} values: <0 uncontaminated, 0–1 uncontaminated to moderately contaminated, 1–2 moderately contaminated, 2–3 moderately do strongly contaminated, 3–4 strongly contaminated, 4–5 strongly to extremely strongly, >5 extremely contaminated; C_f values: <1 low degree, 1–3 moderate degree, 3–6 considerable degree, >6 very high degree).

The highest Pb, Cu and Zn concentrations, and consequently the highest pollution indices at location 6, can be due to the effect from point and non-point sources, such as leaded gasoline, municipal runoffs and atmospheric deposition.^{24,25} The elevated concentrations of Pb and Cu might also be originating from urban and industrial wastes.²⁶ Also, traffic pollution and road dust could be responsible for the high heavy metal concentrations, including Cu and Pb.²³

The pollution from Cd is due to anthropogenic sources, such as fertilizers and pesticides used in agricultural and industrial activities.^{22,27} Mercury can be a significant sediment contaminant in environmental systems not always obviously originating from a local point source, which can also be related to atmospheric deposition,²⁸ but most often originates from the anthropogenic emission sources of mercury, mostly from solid wastes (municipal and medical) incineration.²⁹

PLI is decreasing in the following order of locations: 5 > 6 > 8 > 7 > 2 > 3 > > 4 > 1. Since *PLI* can provide the understanding about the quality of the environment and also provides valuable information to the decision-makers on the pollution status of the area,²⁵ these results indicated that the sediments in the lower and middle stretch of the urban part of the Vrbas sediments are under higher risk (*R*) of pollution than the upper stretch. The total potential ecological

risk index also indicated that the middle and lower stretch is under the highest potential ecological risk ($5 > 6 > 7 > 4 > 8 > 3 > 2 > 1$).

TABLE III. Potential ecological risk index (E_r) and total potential ecological risk index (R) ranges for heavy metals measured in river and riverbank sediments

Element	1	2	3	4	5	6	7	8
	E_r							
Cd	38.09	50.00	44.90	46.40	46.69	39.98	44.53	43.64
Co	75.50	86.05	83.35	114.24	146.81	87.40	130.33	116.90
Cr	166.90	191.53	193.00	249.08	328.75	181.71	282.72	237.10
Cu	516.95	444.36	475.20	375.74	337.28	834.45	373.16	408.31
Ni	358.09	405.68	400.36	747.76	1112.14	442.61	726.05	625.78
Pb	167.83	176.00	191.25	143.53	188.00	439.16	145.24	198.05
Zn	214.43	198.58	220.54	158.33	186.94	245.85	164.32	198.01
Hg	18.70	27.40	18.90	10.70	14.60	16.00	13.50	14.70
	R							
	2019.29	2113.64	2159.20	2332.77	2910.61	2673.91	2456.69	2353.98
Classes of contamination related to the values of the potential ecological risk indexes and literature values of toxic response factors used for E_r calculations ^{20,23}								
Element	T_r	E_r		R		Risk		
Cd	30^{20}	< 40		< 94		Low ecological risk		
Co	5^{23}	40 – 80		94 – 188		Medium ecological risk		
Cr	2^{20}	80 – 160		188 – 376		Significant ecological risk		
Cu	5^{19}	> 160		> 376		Very high ecological risk		
Ni	5^{20}							
Pb	5^{20}							
Zn	1^{20}							
Hg	40^{20}							

CONCLUSION

The concentrations of heavy metals determined in 16 river sediments and 16 riverbank sediments sampled at eight locations along the Vrbas River in Banja Luka city during the summer of 2020 indicate that there is neither a statistically significant difference in metal concentration between river and riverbank samples, nor the statistically significant difference between heavy metal concentrations between selected locations. Although there are no statistically significant differences between heavy metal concentrations among locations, some trends are observed. Cadmium and Hg have the highest concentrations at location 2, Pb, Cu, Zn at location 6 and Co, Cr and Ni at locations 5, 7 and 4. This further implies the same source of correlated elements. The anthropogenic impact, expressed by values of pollution indices, showed that sites are generally uncontaminated by Co, Cr and V and moderately contaminated by Zn, Cu and Ni. On the contrary, lead, mercury and cadmium pose the highest ecological risk. The anthropogenic source of Pb, Hg and Cd is industry, municipal waste and the combustion of fos-

sil fuels. The obtained results demonstrate the high ecological risk and need for environmental monitoring, supporting the development of an efficient strategy to reduce the local pollution and contamination of the investigated system.

SUPPLEMENTARY MATERIAL

Additional data and information are available electronically at the pages of journal website: <https://www.shd-pub.org.rs/index.php/JSCS/article/view/10834>, or from the corresponding author on request.

Acknowledgement. The study was supported by the Ministry of Education, Science and Technological Development of the Republic of Serbia (Grants No. 451-03-9/2021-14/200026, 451-03-9/2021-14/ 200168 and 451-03-9/2021-14/200358).

ИЗВОД

ПРИМЕНА ИНДЕКСА ЗАГАЂЕЊА У ОДРЕЂИВАЊУ ПРОСТОРНИХ И ВРЕМЕНСКИХ РАЗЛИКА У КОНЦЕНТРАЦИЈИ ТЕШКИХ МЕТАЛА У СЕДИМЕНТИМА РЕКЕ ВРБАС, (БАЊА ЛУКА, БОСНА И ХЕРЦЕГОВИНА)

САЊА ПРЖУЉ¹, АНА РАДОИЧИЋ², МИЛИЦА КАШАНИН-ГРУБИН³, ДУШИЦА ПЕШЕВИЋ¹,
САЊА СТОЈАДИНОВИЋ³, БРАНИМИР ЈОВАНЧИЋЕВИЋ⁴ и ГОРИЦА ВЕСЕЛИНОВИЋ³

¹Универзитет у Бањој Луци, Природно-математички факултет, Др Младена Стојановића 2, 78000
Бања Лука, Босна и Херцеговина, ²Рударски Институт г.о.о. Београд, Батајнички шум 2, 11080
Београд Земун, ³Универзитет у Београду, Институт за хемију, технологију и међалуреју
(ИХТМ), Његошева 12, 11000 Београд и ⁴Универзитет у Београду, Хемијски факултет,
Службени штаб 12–16, 11000 Београд

Тешки метали су елементи природног порекла, али се сматрају значајним полу-
тантима животне средине због велике густине и токсичности, чак и при малим концен-
трацијама. Циљ овог рада је процена нивоа загађености речних и приобалних седи-
мената тешким металима, као и процена њиховог порекла и просторне расподеле дуж
toka реке Врбас кроз Бањалуку. Концентрације тешких метала одређивање су помоћу
индуктивно спрегнуте плазме – оптичке емисионе спектрометрије и наменског живиног
анализатора. Антропогени утицај на концентрацију тешких метала у седиментима про-
цењен је израчунавањем различитих индекса загађења: индекса геоакумулације (I_{geo}),
фактора контаминације (C_f), индекса оптерећења загађењем (PLI) и индекса потенци-
јалног еколошког ризика (E_r). Добијени резултати указују да не постоје статистички зна-
чајне просторне разлике у концентрацији метала, што указује на то да тешки метали у
испитиваним седиментима имају константан извор. Антропогени утицај изражен у вред-
ностима индекса загађења показао је да су локације генерално незагађене кобалтом,
хромом и ванадијумом, а умерено загађене цинком, бакром и никлом. С друге стране,
кадмијум, жива и олово представљају највећи еколошки ризик. Антропогени извори
ових метала су индустрија, комунални отпад и сагоревање фосилних горива. Добијени
резултати показују висок еколошки ризик и потребу за мониторингом животне средине,
подржавајући развој ефикасне стратегије за смањење локалног загађења и загађења
испитиваног подручја.

(Примљено 8. јуна, ревидирано 1. септембра, прихваћено 3. септембра 2021)

REFERENCES

1. S. Šrbac, M. Kašanin-Grubin, N. Vasić, *Environ. Geochem. Health* **40** (2017) 1 (<https://doi.org/10.1007/s10653-017-0053-0>)
2. V. Masindi, K. L. Muedi, *Heavy metals* **10** (2018) 115 (<https://doi.org/10.5772/intechopen.76082>)
3. J. Nouri, A. H. Mahvi, G. R. Jahed, A. A. Babaei, *Environ. Geol.* **55** (2008) 1337 (<https://doi.org/10.1007/s00254-007-1081-3>)
4. H. Gao, J. Bai, R. Xiao, P. Liu, W. Jiang, J. Wang, *Stoch. Env. Res. Risk, A* **27** (2013) 275 (<https://doi.org/10.1007/s00477-012-0587-8>)
5. S. Sakan, G. Dević, D. Relić, I. Andelković, N. Sakan, D. Đorđević, *Environ. Earth Sci.* **73** (2015) 6625 (<https://doi.org/10.1007/s12665-014-3886-1>)
6. Q. Zhuang, G. Li, L. Zhiyong, *Catena* **170** (2018) 386 (<https://doi.org/10.1016/j.catena.2018.06.037>)
7. M. Kašanin-Grubin, L. Hagemann, G. Gajica, S. Šrbac, B. Jovančićević, N. Vasić, A. Šajnović, S. Djogo Mračević, J. Schwarzbauer, *Environ. Geochem. Health* **42** (2020) 693 (<https://doi.org/10.1007/s10653-019-00403-6>)
8. A. Tnoumi, M. Angelone, G. Armiento, R. Caprioli, C. Crovato, M. De Cassan, M.R. Montereali, E. Nardi, L. Parrella, M. Proposito, F. Spaziani, B. Zourarah, *Earth* **2** (2021) 16-31. (<https://doi.org/10.3390/earth2010002>)
9. *Contaminated Sediments in European River Basins – European Sediment Research Network*, SedNet. (2004) EVK1-CT-2001-20002 (www.SedNet.org)
10. K.M. Mohiuddin, Y. Ogawa, H.M. Zakir, K. Otomo, N. Shikazono, *Int. J. Environ. Sci. Technol.* **8** (2011) 723 (<https://doi.org/10.1007/BF03326257>)
11. Ž. Vuković, D. Vuković, M. Radenković, S. Stanković, *J. Serb. Chem. Soc.* **77** (2012) 381 (<https://doi.org/10.2298/JSC110217169V>)
12. S. Šrbac, A. Šajnović, Lj. Budakov, N. Vasić, M. Kašanini-Grubin, P. Simonović, B. Jovančićević, *Chem. Ecol.* **30** (2014) 169 (<https://doi.org/10.1080/02757540.2013.841893>)
13. Taylor, S. R. (1964) *Geochim. Cosmochim. Acta* 28 (1964) 1273 ([https://doi.org/10.1016/0016-7037\(64\)90129-2](https://doi.org/10.1016/0016-7037(64)90129-2))
14. G. Müller, *Umsch. Wiss. Tech.* **79** (1979) 778
15. M. Barbieri, *J. Geol. Geophys.* **5** (2016) 1 (<http://dx.doi.org/10.4172/2381-8719.1000237>)
16. M. B. Sulaiman, K. Salawu, A. U. Barambu, *J. Appl. Sci. Environ. Manage.* **23** (2019) 187 (<https://doi.org/10.4314/jasem.v23i1.28>)
17. S. Šrbac, M. K. Grubin, N. Vasić, *Environ. Geochem. Health* **40** (2018) 1247 (<https://doi.org/10.1007/s10653-017-0053-0>)
18. G. Suresh, P. Sutharsan, V. Ramasamy, R. Venkatachalapathy, *Ecotoxicol. Environ. Safety* **84** (2012) 117 (<https://doi.org/10.1016/j.ecoenv.2012.06.027>)
19. D. L. Tomlinson, J. G. Wilson, C. R. Harris, D. W. Jeffrey, *Helgoländer Meeresunters.* **33** (1980) 566 (<https://doi.org/10.1007/BF02414780>)
20. L. Hakanson, *Water Res.* **14** (1980) 975 ([https://doi.org/10.1016/0043-1354\(80\)90143-8](https://doi.org/10.1016/0043-1354(80)90143-8))
21. H. N. Zhu, X. Z. Yuan, G. M. Zeng, M. Jiang, J. Liang, C. Zhang, J. Yin, H. J. Huang, Z. F. Liu, H. W. Jiang, *Trans. Nonferrous Met. Soc. China* **22** (2012) 1470 ([https://doi.org/10.1016/S1003-6326\(11\)61343-5](https://doi.org/10.1016/S1003-6326(11)61343-5))
22. B. Wu, G. Wang, J. Wu Q. Fu, C. Liu, *PLoS ONE* **9** (2014) 102101 (<https://doi.org/10.1371/journal.pone.0102101>)
23. Z. Yang, Y. Wang, Z. Shen, J. Niu, Z. Tang, *J. Hazard. Mater.* **166** (2009) 1186 (<https://doi.org/10.1016/j.jhazmat.2008.12.034>)

24. N. Shikazono, K. Tatewaki, K.M. Mohiuddin, T. Nakano, H.M. Zakir, *Environ. Geochem. Health* **34** (2012) 13 (<https://doi.org/10.1007/s10653-011-9409-z>)
25. S. Islam, K. Ahmed, M. Raknuzzaman, H. Al- Mamun, M.K. Islam, *Ecol. Indic.* **48** (2015) 282 (<https://doi.org/10.1016/j.ecolind.2014.08.016>)
26. K. M. Mohiuddin, K. Otomo, Y. Ogawa, N. Shikazono, *Monit. Assess.* **184** (2012) 265 (<https://doi.org/10.1007/s10661-011-1966-1>)
27. F. Cevik, M.Z. Lugal Göksu, O.B. Derici, O. Fındık, *Environ. Monit. Assess.* **152** (2009) 309 (<https://doi.org/10.1007/s10661-008-0317-3S>)
28. Heim and J. Schwarzbauer, *Environ. Chem. Lett.* **11** (2013) 255 (<https://doi.org/10.1007/s10311-013-0409-3>)
29. H. Astatkie, A. Ambelu, E. Mengistie, *Front. Earth Sci.* **9** (2021) (<https://doi.org/10.3389/feart.2021.658737>).



SUPPLEMENTARY MATERIAL TO
**Distribution and provenance of heavy metals in sediments of the
Vrbas River, Bosnia and Herzegovina**

SANJA PRŽULJ¹, ANA RADOJIĆIĆ², MILICA KAŠANIN-GRUBIN³,
DUŠICA PEŠEVIĆ¹, SANJA STOJADINOVIĆ³, BRANIMIR JOVANIĆEVIĆ⁴
and GORICA VESELINOVIC^{3*}

¹*University of Banja Luka, Faculty of Natural Sciences and Mathematics, Dr. Mladena Stojanovića 2, 78000 Banja Luka, Bosnia and Herzegovina*, ²*Mining Institute Ltd. Belgrade, Batajnički put 2, 11080 Belgrade Zemun, Serbia*, ³*University of Belgrade, Institute of Chemistry, Technology and Metallurgy (ICTM), Njegoševa 12, 11000 Belgrade, Serbia* and ⁴*University of Belgrade, Faculty of Chemistry, Studentski trg 12–16, 11000 Belgrade, Serbia*

J. Serb. Chem. Soc. 87 (4) (2022) 519–530

STUDY AREA

The Vrbas River springs at 1715 m above sea level, and flows into the Sava River as its right tributary at 90 m above sea level. The 90 % of the Vrbas basin relief is mountain-hilly, while the lower area of the basin, the remaining 10 %, represents the river plain.¹ This 10 % of river plain, parts of the middle and lower course of the Vrbas River are exposed to floods during high water levels. One of the most threatened municipalities by the Vrbas outflow is Banja Luka, along with the countryside at the confluence with the Sava River.² The study area includes the part of the Vrbas flow that passes through the Banja Luka city (Fig. S-1), located in a valley at an altitude of 164 m in the northwestern part of Bosnia and Herzegovina at the crossing between the Dinaric Mountains in the South and the Pannonian Basin in the North. While the Vrbas River flows through the city centre, the confluence with its tributary, Vrbanja is in the immediate urban area.

The climate of Banja Luka is typically temperate continental, with moderately cold winters and warm summers. Climatological and hydrological datasets of temperature values, precipitation, and flows collected at Banja Luka's meteorological station and hydrological station "Delibašino Selo" were analyzed on a seasonal and annual basis (Figs. S-2 and S-3).

During the period 1961–2020, the average annual temperature was 11.2 °C, and there was a positive linear trend in the average annual temperature with a noticeable increase of 0.46 °C per decade in the last 30 years. The consequences of climate change are reflected in the distribution of precipitation during the year, and they are more pronounced by seasons than on an annual basis. As a consequence of these changes, the pluviometric regime was also disturbed (Fig. S-3).

With the increased precipitation and its greater seasonal variability, as well as the increased contribution of heavy rains to the total precipitation, the risk of floods in the north-

*Corresponding author. E-mail: gorica.veselinovic@ihtm.bg.ac.rs

eastern part of Bosnia and Herzegovina increased. The most catastrophic floods in recorded history were in May 2014. During this period, the maximum water level was recorded at the Delibašino Selo hydrological station at 816 cm (Fig. S-3), while the extraordinary level of flood protection at that measuring point was 370 cm. In the last 20 years, floods were recorded in 2001 (water level maximum 677 cm) and 2019 (water level maximum 630 cm), in addition to the one mentioned in 2014.²

Sampling

Total of 32 sediment samples were collected at eight sites along the course of the Vrbas River in the city of Banja Luka during summer 2020. Four samples, two river and two riverbank sediments, were collected at locations which were selected based on the vicinity of potential sources of anthropogenic pollution (Fig. S-1 of the Supplementary material). Locations 1 and 3 represent sites near bridges with frequent traffic and high number of sewage outlets. Sampling site 2 is on the promenade, where the possible pollution source is the nearby sewage outlet. The sites marked with numbers 4 and 5 represent the samples collected in the largest tributary of the Vrbas River, Vrbanja, and they are in the vicinity of Incel Bridge and former Incel, nowadays Celex Company, which is producing cellulose and paper. The sampling point 6 is in the vicinity of the thermal power plant, and therefore also close to the sewage outlet. Close of the sampling site 7 is the Banja Luka Brewery and the bridge - the main road. The “Vitaminka” is a food industry in the vicinity of sampling point 8. The collected samples were placed in a clean polyethylene bag, transported to the laboratory and conserved at 4 °C in the dark until analysis.

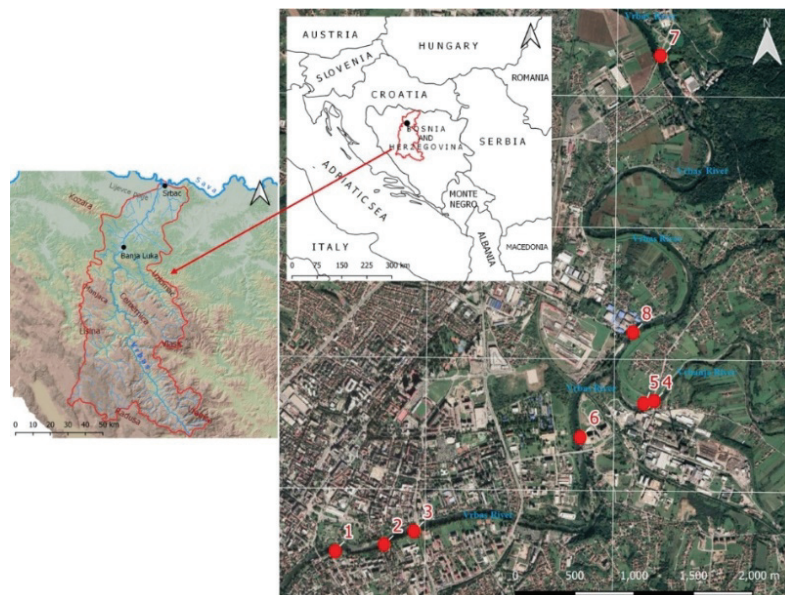


Fig. S-1. Map of the Vrbas watershed on the left; map of Banja Luka city with labeled sampling locations along the Vrbas River on the right (Inset: position of Bosnia and Herzegovina in Europe).

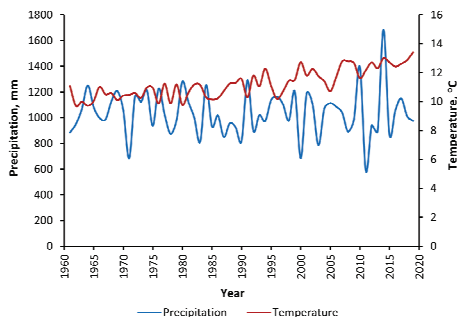


Fig. S-2. Average precipitation and temperature values at the Vrbas River (1961-2020) – Banja Luka meteorological station.

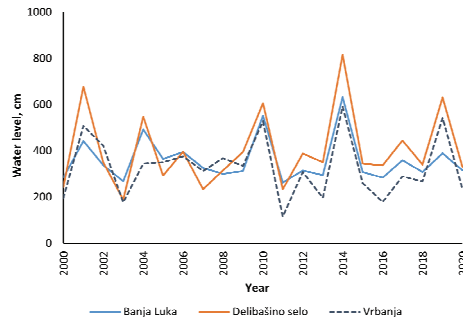


Fig. S-3. Maximum water levels at the Vrbas River (2000-2020) – Hydrological stations “Banja Luka”, “Delibašino selo” and “Vrbanja”.

Twenty-eight municipalities with approximately 464,000 inhabitants, which is about 15 % of the population of Bosnia and Herzegovina, with the Banja Luka as the most densely populated part, are located in the Vrbas drainage basin.^{3,4} The results of the 2013 census of population and housing units showed Banja Luka as the second biggest city in Bosnia and Herzegovina with a population of 180,053.⁴

The anthropogenic impact of the urbanized part of the Vrbas drainage basin is assumed to cause permanent pollution, which originates mainly from industrial activities, discharge of community sewage, illegal waste disposal, and agriculture. A large number of different economic activities are related to Banja Luka, which is the main factor in the emergence of greater anthropogenic pressure on the water quality of the Vrbas River and its tributaries in the lower part of the basin.² The anthropogenic impact on the Vrbanja River, one of the largest tributaries, is undeniable, primarily by the municipal wastewater, as well as by the industrial wastewater, and the examination of its impact is also significant.

TABLE S-I. independent t-test for heavy metal concentrations measured in river and riverbank sediment samples ($n = 32$)

Element	t-value	p-value
Cd	2.183	0.047
Co	-0.997	0.336
Cr	-0.643	0.531
Cu	-1.524	0.15
Ni	-0.758	0.461
Pb	-1.235	0.237
V	0.02	0.984
Zn	-1.788	0.095
Hg	-1.856	0.085

TABLE S-II. Geoaccumulation index (I_{geo}) ranges for heavy metal concentrations measured in river and riverbank sediments

Element	I_{geo}								Average value
	1	2	3	4	5	6	7	8	
Cd	2.08	2.47	2.32	2.37	2.38	2.15	2.31	2.28	2.29
Co	-1.31	-1.12	-1.17	-0.71	-0.35	-1.10	-0.52	-0.68	-0.87
Cr	-0.85	-0.65	-0.64	-0.27	0.13	-0.72	-0.09	-0.34	-0.43
Cu	0.33	0.11	0.20	-0.13	-0.29	1.02	-0.14	-0.01	0.13
Ni	-0.65	-0.47	-0.49	0.41	0.98	-0.35	0.37	0.15	-0.01
Pb	0.84	0.91	1.03	0.61	1.00	2.23	0.63	1.08	1.04
V	-1.13	-0.92	-0.93	-1.06	-0.88	-1.39	-0.81	-0.99	-1.01
Zn	1.03	0.92	1.07	0.59	0.83	1.23	0.65	0.92	0.90
Hg	1.96	2.51	1.98	1.16	1.60	1.74	1.49	1.61	1.76

Classes of contamination related to the values of the geoaccumulation indexes.⁵

Class	I_{geo}	
0	< 0	Uncontaminated
1	0 – 1	Uncontaminated to moderately contaminated
2	1 – 2	Moderately contaminated
3	2 – 3	Moderately to strongly contaminated
4	3 – 4	Strongly contaminated
5	4 – 5	Strongly to extremely strongly contaminated
6	> 5	Extremely contaminated

TABLE S-III. Contamination factor (C_f) and Pollution Load Index (PLI) ranges for heavy metal concentrations measured in river and riverbank sediments

Element	1	2	3	4	5	6	7	8	Average value
	C_f								
Cd	6.35	8.33	7.48	7.73	7.78	6.66	7.42	7.27	7.38
Co	0.60	0.69	0.67	0.91	1.17	0.70	1.04	0.94	0.84
Cr	0.83	0.96	0.96	1.25	1.64	0.91	1.41	1.19	1.14
Cu	1.88	1.62	1.73	1.37	1.23	3.03	1.36	1.48	1.71
Ni	0.95	1.08	1.07	1.99	2.97	1.18	1.94	1.67	1.61
Pb	2.69	2.82	3.06	2.30	3.01	7.03	2.32	3.17	3.30
V	0.69	0.79	0.79	0.72	0.81	0.57	0.85	0.76	0.75
Zn	3.06	2.84	3.15	2.26	2.67	3.51	2.35	2.83	2.83
Hg	5.84	8.56	5.91	3.34	4.56	5.00	4.22	4.59	5.25

PLI

1.79 2.00 1.95 1.88 2.27 2.17 2.02 2.04 1.79

Classes of contamination related to the values of the contamination factors⁶

C_f	PLI value ⁶	
	< 1	PLI value ⁶
< 1	Low degree of contamination	<1 Unpolluted condition
1 – 3	Moderate degree of contamination	>1 Polluted condition
3 – 6	Considerable degree of contamination	
> 6	Very high degree of contamination	

REFERENCES

1. S. Kostadinov, R. Tošić, D. Hrkalović, S. Nikolić N. Sudar, M. K. Solomun, S. Bundalo, *Vodoprivreda* **51** (2019) 211 (UDK: 631.432/627.51)
2. D. Pešević, *The ENVIRONMENT* **4** (2016) 23 (http://environment.gef.bg.ac.rs/files/PDF%20vol4No1_2016/5_Pesovic%20-%20FINAL.pdf)
3. UNDP (2019) Technology transfer for climate resilient flood management in Vrbas river Basin Project supported by UNDP in Bosnia and Herzegovina, available at: (https://info.undp.org/docs/pdc/Documents/BIH/PIMS%205241_SCCF_BH_UNDP_Pro_doc%2026%20Feb%20final%20LPACed.pdf) (accessed: 15. 5. 2021)
4. Census 2013 in Bosnia and Herzegovina (<http://www.statistika.ba/?show=12&id=20010>) (accessed 15. 5. 2021)
5. S. Islam, K. Ahmed, M. Raknuzzaman, H. Al- Mamun, M.K. Islam, *Ecol. Indic.* **48** (2015) 282 (<https://doi.org/10.1016/j.ecolind.2014.08.016>)
6. Z. Yang, Y. Wang, Z. Shen, J. Niu, Z. Tang, *J. Hazard. Mater.* **166** (2009) 1186 (<https://doi.org/10.1016/j.jhazmat.2008.12.034>).



Internet pages for asynchronous online and face-to-face learning about solutions and dissolution

LIDIJA R. RALEVIC[#], BILJANA I. TOMASEVIC^{*#} and DRAGICA D. TRIVIC[#]

University of Belgrade – Faculty of Chemistry, Studentski trg 12–16, Belgrade, Serbia

(Received 4 August, revised and accepted 10 August 2021)

Abstract: In the last decades online communication has become an important part of the realization of the educational process. In the conditions caused by the Covid-19 pandemic it has become particularly significant since in most cases it was necessary to switch to some forms of online teaching-learning. This paper presents the results of a research study conducted as a pedagogical experiment with parallel groups. The aim of this research study was to compare the effects of the application of internet pages for independent online asynchronous learning outside the school environment (group A) and face-to-face learning realized by a teacher at school (group B). The content of the internet pages was created in order to enable the acquisition of the concepts of solutions and dissolution. The effects of the approaches applied were studied based on the student achievement in a post-test (immediately upon learning about the concepts of solutions and dissolution) and in a delayed post-test (a year after the acquisition of these concepts). The participants in this research study were 187 primary school students, who participated in the pedagogical experiment when they were in the seventh grade, while they were in the eighth grade when they did the delayed post-test. The results showed that there was not a statistically significant difference between the overall achievements of the students who learnt about the concepts of solutions and dissolution by independent asynchronous online learning and face-to-face learning at school. This implies that the similar results can be achieved with asynchronous online learning as with face-to-face learning when the conditions do not allow school-based education.

Keywords: e-teaching; digital materials; submicroscopic level; educational video.

* Corresponding author. E-mail: bsteljic@chem.bg.ac.rs
[#] Serbian Chemical Society member.
<https://doi.org/10.2298/JSC210804060R>

INTRODUCTION

Various approaches and teaching/learning methods used for achieving educational goals/outcomes are continuously developed and proposed. Online learning is one of the methods used to organize teaching/learning which has shown an increasing potential for the improvement of the educational process in the last decades. Online learning is distance learning based on online communication with the application (distribution) of digital teaching materials. Due to the Covid-19 pandemic, teaching methods within which social contact among students at school is avoided, which reduces the risk of contracting the disease, have become particularly significant.¹ Faced with this novel situation, over 160 countries switched to online teaching/learning.²

Online learning can be divided into synchronous and asynchronous. Synchronous online learning includes real-time communication between the teachers and students *via* various communication media. The main advantages of this method are the possibility of obtaining an instant feedback³ and increased student motivation due to their obligation to be directly involved in the teaching process.⁴ Asynchronous online learning is time-independent communication, which supports work relation among learners and teachers when participants cannot be online at the same time.⁵ One of the most available options is sending questions to the teacher *via* e-mail.¹ This has proven to be very significant in asynchronous learning since students avoid asking their teacher questions for various reasons, for example, in order to avoid drawing other students' attention. Students find asynchronous learning convenient due to the freedom of choice regarding the time and place when they access the learning material, learning dynamics and independence in doing the activities.⁶ For these reasons, students find asynchronous online learning more satisfactory than synchronous online learning.¹ During the Covid-19 pandemic, there were situations when students were not able to participate in the organized synchronous online instruction. In these situations it was really important to enable them asynchronous instruction, for example, by posting a link to an educational video which served as a learning material.⁷

Apart from images, an educational video can also contain textual and audio information. Videos with an audio component have a greater potential for achieving learning outcomes compared to the ones accompanied only by textual explanations.^{8,9} On the other hand, students remember better the information introduced through an educational video than the information introduced through a text or an audio, with or without images.¹⁰ This is due to the fact that students pay more attention to the information introduced through video material than to the information introduced through a text or an audio recording.¹¹ With video materials it is possible to adjust the viewing dynamics to the tempo of information processing by stopping the video and watching it again, playing it again, slowing it down and speeding it up.^{12,13} The research results have shown that multiple viewing of

educational videos distributed to students via the YouTube platform has contributed to the improvement of their achievements by approximately 13 %.¹⁴

Some research studies have shown positive effects of asynchronous learning accompanied by the use of digital materials such as, for example, educational videos, while the results of some other research studies have shown that, as far as effectiveness is concerned, this approach does not differ from face-to-face approach.¹⁵ This is explained by the fact that asynchronous learning fails to engage students' higher-order cognitive skills to a sufficient degree.^{16,17} With asynchronous learning students can have difficulties with using the technology and understanding the content of the learning materials, but they can also experience a lack of motivation for this kind of learning or a lack of concentration.¹⁸ The aim of this research study is to compare the effects of learning when internet pages, with digital materials about Solutions and Dissolution, are used in asynchronous online learning with the effects of learning within a class period held by a teacher at school.

EXPERIMENTAL

Based on the aim of this research study, the following null hypothesis was formulated: There is no statistically significant difference between the achievements of the seventh-grade students in Solutions and Dissolution after the application of internet pages for independent asynchronous online learning and the achievements of the seventh-grade students after face-to-face learning at school.

The proposed hypothesis was tested in a pedagogical experiment with parallel groups.

The sample

The pedagogical experiment was conducted with 187 seventh-grade students (aged 13–14) from two primary schools in the territory of Belgrade. The schools were selected based on the equipment available for the application of ICT (computers, projectors and a good internet connection), necessary for the realization of the pedagogical experiment. All seventh-grade students from the selected schools were included in the sample. The students were randomly divided into two groups: group A ($N = 94$) and group B ($N = 93$), formed by two classes from each school. The consent for conducting the pedagogical experiment was obtained from the management of both schools. The cooperation agreements were signed by the Dean of the University of Belgrade – Faculty of Chemistry, and the school principals. Written consents for the participation of students in this research study were obtained from the students' parents/guardians. The parents/guardians and students were informed in detail about the aim of the research study, the method of its realization and students' roles in the research study. It was pointed out that the participation is on a voluntary basis and data confidentiality was guaranteed. It was explained to the students that they would not be rewarded for their participation in the research study and that there would be no consequences if they decided to withdraw from the research study. Students could withdraw from the research study at any moment.

Design and procedure

The research study was organized during the lesson on Solutions and Dissolution, the first one within the thematic unit Solutions according to the chemistry curriculum for the

seventh grade of primary school. Understanding the contents about Solutions and Dissolution depends on understanding the concepts from the curricular thematic unit The Structure of Substance. A description of the activities done with each group of students (A and B) in the pedagogical experiment is provided in Table I.

TABLE I. The plan for the pedagogical experiment implementation

Activity	Group A activities	Group B activities
1.	Pre-test	Pre-test
2.	Asynchronous online learning by independently accessing the internet pages on Solutions and Dissolution, outside the school	Face-to-face learning by the application of the internet pages on Solutions and Dissolution, at school with teacher guidance
3.	Post-test	Post-test
4.	Delayed post-test	Delayed post-test

At the beginning of the research study both groups were tested by a pre-test, which tested the groups' previous knowledge. Students from Group A were given a link for accessing the internet pages for independent asynchronous online learning and instructions on how to access the internet pages before their next chemistry lesson.

Students from Group B learned about Solutions and Dissolution using the same internet pages at school, with teacher guidance. The internet pages used as a teaching material were created in line with the outcomes defined by the seventh grade chemistry curriculum. The teaching material on the internet pages was prepared with the aim of enabling students to understand the process of dissolving at the submicroscopic (particles) level. The content of the internet pages was presented in the textual, visual (images, video recordings and animations) and audio format (narration). The introductory part of the content about Solutions and Dissolution was given in the textual form, while the other parts were given in the form of educational videos. As a key segment of the internet pages, the educational videos included animations which showed the process of dissolution of an ionic substance and a non-polar substance at submicroscopic level, accompanied by the narration by the author/researcher. Video 1 shows the dissolution of an ionic substance in a polar solvent. Video 2 shows the dissolution of a non-polar substance in a non-polar solvent.

Apart from being shown the content of the same internet pages, the students from Group B learnt about Solutions and Dissolution by listening to their teacher talk on this topic during the chemistry class period. After the class period, the students from Group B did not have an opportunity to access the internet pages. During the 35-min lesson students listened to their teacher's lecture which included watching educational videos with the explanations which accompanied the digital material. After that, the teacher checked students' understanding of the process of dissolving ionic and non-polar substances through a ten-minute conversation with the students. In the next chemistry class period, students from both groups did a post-test. The time available for the completion of the post-test was 45 minutes. A year after the post-test, the groups made up of the same students were tested again. The delayed testing was conducted in order to measure retained learning about Solutions and Dissolution in each group a year after they had learnt about these concepts.

Instruments

In order to collect data in this research study two tests for knowledge assessment were designed and administered to all students. Both tests were paper-pen tests. The pre-test was used to check students' knowledge of the concepts within the thematic unit The Structure of Substance, key to understanding the concepts of Solutions and Dissolution.¹⁹ The pre-test had six questions with eight items altogether: three open-ended (short-answer) and five closed-ended (multiple-choice questions). The questions included the following content: the types of chemical bonds in compounds, chemical formulae of compounds, types of particles in the crystal of an ionic compound and the dipole.

The same test was used for the purpose of post-testing and delayed-testing. The test contained eight questions with ten items altogether. Six questions were closed-ended questions (two questions, each with two items, were alternate-choice questions; four questions were multiple-choice questions). Two questions in the test were open-ended (essay-type) questions. Four questions tested students' understanding of the dissolution of an ionic substance in a polar solvent. In the test this process was presented by an illustration at the submicroscopic level. The other four questions in the test checked the students' understanding of the process of dissolving a non-polar substance in a non-polar solvent. An illustration showing this process at the submicroscopic level was given in this part of the test as well. During post-testing, the educational videos about the dissolution of ionic and non-polar substances, which had been used as teaching material on the internet pages, were played the whole time. The students were expected to identify the type of chemical bonding in the solutes and the solvents based on the illustrations given within the questions in the tests and the educational videos played. Students were also asked to describe the formation of each solution at the submicroscopic level, considering the type of chemical bond in the solute and in the solvent.

Video 1 contained the information necessary for responding to items 1a, 1b, 2, 3 and 4 of the test. Video 2 contained the information necessary for responding to items 5a, 5b, 6, 7 and 8.

The tests were reviewed by the experts in the field of chemical education, who were not involved in their design, in order to assess their validity with respect to the defined aim of the research and the hypothesis. The two chemistry teachers who enabled the realization of the research study and the members of the Department of Chemical Education, the University of Belgrade – the Faculty of Chemistry, examined the content of the tests, upon which the necessary revisions of the tests were made.

RESULTS AND DISCUSSION

The results obtained in the tests are presented below.

The distribution of the results in the pre-test, post-test and delayed post-test

The maximum score which students could achieve in the pre-test was 8 points, while it was 10 points in the post-test and delayed post-test. The characteristics of the distribution of the scores of both student groups are presented in Table II. The following data are presented: the number of students in each group (N), the minimum (Min) and maximum (Max) number of correct answers in each test, the mean ($Mean$), the standard deviation (SD), the contribution of correct answers (C), the skewness value and the kurtosis value. The mean score of Group A in the pre-test (5.11) was higher than the mean score of Group B (4.83). In the post-test, Group B (5.54) was more successful than Group A (5.20). The mean

score achieved by Group A in the delayed post-test (4.45) was higher than the mean score achieved by Group B (4.35).

TABLE II. Descriptive statistics of student achievement in the pre-, post- and delayed post-test

Testing	Group	N	Number of correct answers				C / %	Skewness	Kurtosis
			Min	Max	Mean	SD			
Pre-test	A	94	1	8	5.11	1.72	63.8	0.013	-0.655
	B	93	0	8	4.83	2.16	60.4	-0.338	-0.033
Post-test	A	94	1	8	5.20	1.61	52.0	-0.226	-0.351
	B	93	2	8	5.54	1.46	55.4	-0.162	-0.477
Delayed post-test	A	94	2	8	4.45	1.52	44.5	0.590	-0.079
	B	93	2	8	4.35	1.28	43.5	0.283	0.018

The skewness and kurtosis values were used as the criterion for assessing the normality of the distribution of the obtained results. The obtained values range from -1 to +1, which indicates that the data have a normal distribution. Based on this, it was decided to apply the independent-samples *t*-test in order to determine whether there was a statistically significant difference between the means in Groups A and B. The obtained data are presented in Table III.

TABLE III. The value of the *t*-test for the results of Groups A and B

Value	Pre-test	Post-test	Delayed post-test
<i>t</i>	0.97 ^a	-1.49 ^a	0.45 ^a
<i>p</i>	0.33 ^b	0.14 ^b	0.66 ^b

^aConfidence interval - less than 95 %; ^b*p*-value – more than 0.05

The value obtained by the *t*-test shows that there is no statistically significant difference between the mean scores achieved by Groups A and B in the pre-test. Based on this, it was concluded that both groups of students were at the same level regarding their previously acquired knowledge. There were no statistically significant differences between the mean scores achieved by Groups A and B in the post-test and the delayed post-test. It can be concluded based on the obtained results that the application of the internet pages on Solutions and Dissolution for independent asynchronous online learning outside the school environment contributes to similar achievements as face-to-face learning with the same internet pages in the school environment with teacher guidance. These results are consistent with previous research studies, which have shown the same students' scores after online and face-to-face course in inorganic chemistry²⁰ and after introductory chemistry lectures and laboratories.²¹

Student achievement in the pre-test questions

Table IV shows the number of correct answers (frequency, *F*) expressed as the contribution of correct answers given by the students from both groups to the

pre-test items. The values of the *t*-test, used for assessing the statistical significance of the difference and the *p*-values (*p*) are presented.

TABLE IV. The pre-test results in Groups A and B

Item	Group A		Group B		<i>t</i> -test A-B	<i>p</i>
	<i>F</i>	Contribution, %	<i>F</i>	Contribution, %		
1	69	73.4	65	69.9	0.53 ^a	0.597 ^b
2a	30	31.9	27	29.0	0.43 ^a	0.671 ^b
2b	37	39.4	25	26.9	1.82 ^a	0.070 ^b
2c	36	38.3	30	32.3	0.86 ^a	0.390 ^b
3	68	72.3	63	67.7	0.68 ^a	0.495 ^b
4	85	90.4	82	88.2	0.50 ^a	0.620 ^b
5	89	94.7	81	87.1	1.81 ^a	0.073 ^b
6	66	70.2	76	81.7	-1.85 ^a	0.066 ^b

^aConfidence interval - less than 95 %; ^b*p*-value – more than 0.05

In Group A, the contribution of correct answers to individual pre-test items ranged from 31.9 to 94.7 %, while it ranged from 26.9 to 88.2 % in Group B. The students from Group A were less successful than the students from Group B at only one item (item 6). The results obtained by the *t*-test did not show a statistically significant difference between the contributions of correct answers in the groups for any of the pre-test items. This confirmed that the students from Group A and Group B had similar previous knowledge of the concepts from the thematic unit The Structure of Substance.

Student achievement in the post-test and delayed post-test questions

Table V shows the number of correct answers (frequency, *F*) and the contribution of correct answers to the items of the post-test and delayed post-test in both groups.

TABLE V. The results of the post-test and delayed post-test in Groups A and B; number of correct answers (*F*) and the contribution of correct answers (*CA*)

Item	Post-test					Delayed post-test						
	Group A		Group B		<i>t</i> -test A-B	<i>p</i>	Group A		Group B		<i>t</i> -test A-B	<i>p</i>
	<i>F</i>	CA / %	<i>F</i>	CA / %			<i>F</i>	CA / %	<i>F</i>	CA / %		
1a	87	92.6	89	95.7	-0.91	.363	63	67.0	66	71.0	-0.58	.562
1b	84	89.4	91	97.8	-2.40 ^a	.018	83	88.3	86	92.5	-0.96	.336
2	45	47.9	38	40.9	0.96	.337	28	29.8	26	28.0	0.28	.784
3	36	38.3	34	36.6	0.24	.807	31	33.0	20	21.5	1.77	.079
4	6	6.4	0	0.0	2.52 ^a	.013	0	0.0	1	1.1	-1.0	.316
5a	82	87.2	80	86.0	0.24	.809	61	64.9	75	80.6	-2.45 ^a	.015
5b	82	87.2	86	92.5	-1.18	.238	74	78.7	76	81.7	-0.51	.609
6	26	27.7	42	45.2	-2.52 ^a	.013	45	47.9	31	33.3	2.04 ^a	.043
7	41	43.6	55	59.1	-2.14 ^a	.034	31	33.0	24	25.8	1.07	.284
8	0	0.0	0	0.0	0	-	2	2.1	0	0.0	1.41	.159

^aThe difference in the contributions of correct answers by Groups A and B statistically significant at the level *p* < 0.05

It also shows the values obtained by the *t*-test, which was used to assess the statistical significance of the difference between the contributions of correct answers achieved in Groups A and B, as well as the *p*-values for the given values of the *t*-test.

In the post-test, the contribution of correct answers to individual items ranged from 0 to 92.6 % in Group A, and from 0 to 97.8 % in Group B. The students in Group A had the larger number of correct answers to four items, while the students in Group B had the larger number of correct answers to five items. A statistically significant difference between the contributions of correct answers given by Groups A and B was found for four post-test items. The students in Group A were statistically significantly more successful at one post-test item (item 4). The students from Group B were statistically significantly more successful at three items (1b, 6 and 7).

The results of the post-test show that, after seeing Videos 1 and 2 (the content of the internet pages), over 86 % of the students were able to differentiate between the models of the solute particles and the models of the solvent particles. In one of the four items which related to differentiating between the ions of the solute and the molecules of the polar solvent and between the molecules of a non-polar substance and non-polar molecules of the solvent, the students from Group B achieved a statistically significantly higher contribution of correct answers. In this item, students were asked to identify the models showing polar molecules of the solvent (item 1b). During the learning process, the students from Group B watched the models of the presented solvent particles (Video 1) while listening to their teacher who explained the models showing the particles. In this case, watching and listening to the content turned out to be more effective than watching and reading.²²

A slightly higher contribution of students from Group A identified the ionic bond in the dissolved substance, but a statistically significantly higher contribution of students from Group B identified the non-polar covalent bond in the solute molecules (item 7). Since students from Group B were more successful at recognizing the type of particles which make up the solute (item 6), they were expectedly more successful at identifying the type of chemical bond in the solute molecules. Explaining the dissolution process at the submicroscopic level presented the biggest problem for both groups. The process of dissolving both ionic and non-polar covalent compounds was presented using particle models. The explanation of the dissolution of an ionic substance in a polar solvent was provided by only 6 students from Group A (item 4). None of the students provided an explanation of the dissolution of a non-polar covalent substance in a non-polar solvent. It can be concluded, based on the obtained results, that the largest number of students could differentiate between the solute and solvent particles in the watched educational videos, but fewer than half of the students named the types

of particles and the type of chemical bond in the solute based on the models. The representations of ion models and models of polar and non-polar molecules did not contribute to a better understanding of the dissolution process at the submicroscopic level. These results are consistent with the previous research studies which had shown that students found it difficult to interpret and explain observations of phenomena and to relate them to the models of submicroscopic level of matter.²³ Therefore, it is always necessary to develop learning practices in chemistry which emphasise representations of the submicroscopic level.

The contribution of correct answers to the individual items in the delayed post-test ranged from 0 to 88.3 % in Group A and from 0 to 92.5 % in Group B. The total number of correct answers was lower in both groups in the delayed post-test compared to the post-test. In the delayed post-test, students were also most successful at differentiating between the models of solute and solvent particles (the contribution of correct answers was higher than 65 %). In both groups, less than one third of students could successfully identify the type of solute and solvent particles. Both groups were more successful at identifying the type of particle in the case of a non-polar solute than in the case of an ionic solute. There were more correct answers to both items in Group A, but the difference is statistically significant for the identification of the particles of the non-polar covalent substance. The students from Group A were more successful than the students from Group B at identifying the type of chemical bonding in the solutes. It can be observed for Group A that the contribution of students who correctly named the ionic bond is higher than the contribution of students who identified an ion as the type of solute particle. In the delayed post-testing, none of the students from Group A explained the process of dissolution of a polar substance in a polar solvent. The situation is slightly different with the explanation of the dissolution of a non-polar substance. Two students from Group A explained the dissolution process and none of the students from Group B. The insight into the retention of the acquired knowledge based on the delayed post-test results indicates that the watched videos enabled more than two thirds of the students to be successful at differentiating the model of solute particles from the model of solvent particles. Group A was more successful at identifying the type of particles and chemical bond in the solute, while both groups were more successful at identifying the type of particle and chemical bond in the case of a non-polar substance.

The presented results show that the digital material, created for the acquisition of the concepts of Solutions and Dissolution and posted on the internet pages, can be used both in the conditions of regular school education and for independent asynchronous online learning. Online distribution of digital materials for independent learning can be an additional method within the usual realization of the teaching process, but the fact that it can be used as a particularly use-

ful teaching method when face-to-face teaching is not possible, as was the case in the conditions caused by the Covid-19 pandemic, is particularly significant.

CONCLUSION

The conducted research study is a pilot study of the effects of the internet pages with contents about Solutions and Dissolution on the seventh-grade students' achievements when the pages are used for independent asynchronous online learning (student group A) and when they are used in the class with explanations provided by the teacher (student group B). According to the pre-test results, Groups A and B were at the same level as far as their previous knowledge was concerned. The post-test and delayed post-test results showed that there was not a statistically significant difference between the overall achievements of the students who had studied independently asynchronously online and the ones who had studied in the face-to-face instruction. These results confirmed the proposed null hypothesis that the seventh-grade students' achievements in Solutions and Dissolution do not statistically significantly differ after the application of the internet pages for independent asynchronous online learning outside their school and face-to-face learning at school. In both groups, the achievements in the delayed post-test were lower than in the post-test. There was not a statistically significant difference between the mean values achieved by the groups in the delayed post-test. This indicates that the retention of knowledge acquired by asynchronous online learning is similar to the retention of knowledge acquired with teacher guidance. Even though the difference between the achievements of the two groups is not statistically significant, it is important to point out that Group A, which experienced asynchronous online learning, had a worse score than Group B in the post-test, while it had a slightly better score in the delayed post-test. This suggests the stability of the knowledge acquired by independent asynchronous online learning.

Apart from the overall results, the results achieved in individual items of the post-test and the delayed post-test were analyzed for both kinds of learning immediately upon learning and a year after learning. It was established that the application of educational videos (Videos 1 and 2), in which the dissolution processes are presented through the models of solute and solvent particles, had enabled the largest number of students to identify the models of solute and solvent particles. Better achievements of the students from Group B in these items indicate that additional teacher narration with explanations (which were given through images and texts in the educational videos) had enabled students to better identify the presented models of particles. A relevant implication of this research is that in the preparation of the material/videos for asynchronous online learning, textual explanations should also be given in the audio format. Compared to identifying the models of solute and solvent particles, a smaller number of students

correctly identified the types of solute particles and the type of chemical bond in the solute and the solvent. In the delayed post-test both groups were more successful at identifying the type of particle and chemical bond in the case of the dissolution of a non-polar covalent substance. The results achieved within individual items in both groups show that students find it difficult to explain the process of dissolution by relating it to the models at submicroscopic level of matter. One way of dealing with these difficulties could be a wider and constant application of the representations of the submicroscopic level in the chemistry teaching/learning practice.

The results obtained within this research study are important for the situations when it will be necessary to make decisions about the methods of chemistry teaching/learning due to various circumstances. Since the learning outcomes were equivalent for both teaching/learning approaches we have investigated, the application of the independent asynchronous online learning outside the school environment can be recommended in the conditions when it is not possible to organize face-to-face learning with teacher guidance in school classes. In the context of the current limitations to the realization of face-to-face teaching/learning due to the coronavirus pandemic, this conclusion has an immediate and current application. Furthermore, it is relevant for some future situations in which, for various reasons, it might be estimated that pedagogic teacher-student interaction at school environment is not possible. The main limitation of this research study is the size of the sample. The number of students participating in the research study is not sufficient to make generalizations. The choice of schools which participated in the research study was influenced by the IT equipment available since it was essential for conducting the pedagogical experiment. In addition to this, the duration of the study is relatively short and limited to the realization of one lesson. The future research studies should focus on the comparison of the investigated approaches when some other chemistry contents are introduced and elaborated. It should be pointed out that students from Group A were new to independent online asynchronous learning as a teaching/learning method. In their learning experience prior to the conducted research study, the students had never participated in any activities which included the above-mentioned approach, so a certain adjustment was probably necessary. Meanwhile, students at all educational levels have gained new experience of online teaching/learning. This experience will help overcome some potential problems in conducting new research studies which will aim at comparing the efficiency of online and face-to-face teaching/learning.

Acknowledgement. Ministry of Education, Science and Technological Development of Republic of Serbia Contract number: 451-03-9/2021-14/ 200168.

И З В О Д

ИНТЕРНЕТ СТРАНИЦЕ ЗА АСИНХРОНО “ON-LINE” УЧЕЊЕ И УЧЕЊЕ У УЧИОНИЦИ
О РАСТВОРИМА И РАСТВАРАЊУ

ЛИДИЈА Р. РАЛЕВИЋ, БИЉАНА И. ТОМАШЕВИЋ и ДРАГИЦА Д. ТРИВИЋ

Универзитет у Београду – Хемијски факултет, Студентски јар 12–16, Београд

Последњих деценија on-line комуникација је постала важан део у реализацији образовног процеса. Под условима Covid-19 пандемије то је било значајно јер се у највећем броју случајева морало прећи на неке од облика on-line наставе/учења. У раду су представљени резултати истраживања, спроведеног као педагошки експеримент са паралелним групама. Циљ овог истраживања је био да се упореде ефекти примене интернет страница за самостално on-line асинхроно учење ван школе (група А) и наставе/учења коју реализује наставник у школи (група Б). Садржај интернет страница припремљен је за усвајање појмова раствори и растварање у седмом разреду основне школе. Ефекти примењених приступа испитивани су на основу постигнућа ученика на пост-тесту (непосредно након учења) и на одложеном пост-тесту (годину дана након примењених приступа). У истраживању је учествовало 187 ученика који су у педагошком експерименту учествовали као ученици седмог разреда основне школе, а потом на одложеном пост-тесту као ученици осмог разреда. Резултати су показали да не постоји статистички значајна разлика између укупних постигнућа ученика који су појмове раствор и растварање усвајали путем самосталног асинхроног on-line учења и наставе/учења коју у школи реализује наставник. То имплицира да је могуће под условима који не дозвољавају организовање наставе у школи, асинхроним онлајн учењем постићи резултате сличне резултатима наставе у школи.

(Примљено 4. августа, ревидирано и прихваћено 10. августа 2021)

REFERENCES

1. M. W. Lee, *J. Chem. Educ.* **97** (2020) 2834 (<https://doi.org/10.1021/acs.jchemed.0c00881>)
2. F. J. de O. Araújo, L.S. A. de Lima, P. I. M Cidade, C. B. Nobre, M. L. R. Neto, *Psychiatry Res.* **288** (2020) 112977 (<https://doi.org/10.1016/j.psychres.2020.112977>)
3. B. O'Rourke, U. Stickler, *Lang. Learn. High. Educ.* **7** (2017) 1 (<https://doi.org/10.1515/cercles-2017-0009>)
4. N. S. Chen, H. C. Ko, Kinshuk, T. Lin, *Innov. Educ. Teach. Int.* **42** (2005) 181 (<https://doi.org/10.1080/14703290500062599>)
5. S. Hrastinski, *Educause Quarterly* **31** (2008) 51 (<https://er.educause.edu/-/media/files/article-downloads/eqm0848.pdf>)
6. M. D. Casselman, K. Atit, G. Henbest, C. Guregyan, K. Mortezaei, J. F. Eichler, *J. Chem. Educ.* **97** (2020) 27 (<https://doi.org/10.1021/acs.jchemed.9b00767>)
7. C. E. McCusker, R. Mohseni, *J. Chem. Educ.* **97** (2020) 2913 (<https://doi.org/10.1021/acs.jchemed.0c00743>)
8. P. Ginns, *Learn. Inst.* **15** (2005) 313 (<https://doi.org/10.1016/j.learninstruc.2005.07.001>)
9. R. E. Mayer, C. Pilegard, in *The Cambridge Handbook of Multimedia Learning*, R. Mayer, Ed., Cambridge University Press, Cambridge, 2014, p. 316 (<https://doi.org/10.1017/CBO9781139547369.016>)
10. J. H. W. Van der Molen, T. H. A. Van der Voort, *Hum. Commun. Res.* **26** (2000) 3 (<https://doi.org/10.1111/j.1468-2958.2000.tb00747.x>)

11. S. Alley, C. Jennings, N. Persaud, R.C. Plotnikoff, M. Horsley, C. Vandelanotte, *Front. Public Health* **2** (2014) 13 (<https://doi.org/10.3389/fpubh.2014.00013>)
12. P. A. Chandler, *Learn. Instr.* **14** (2004) 353 (<https://doi.org/10.1016/j.learninstruc.2004.06.009>)
13. R. E. Mayer, P. Chandler, *J. Educ. Psychol.* **93** (2001) 390 (<https://doi.org/10.1037/0022-0663.93.2.390>)
14. J. Rose, R. Pennington, D. Behmke, D. Kerven, R. Lutz, J. E. B. Paredes, *J. Chem. Educ.* **96** (2019) 2632 (<https://doi.org/10.1021/acs.jchemed.9b00234>)
15. J. Paul, F.A. Jefferson, *Front. Comput. Sci.* **1** (2019) 7 (<https://doi.org/10.3389/fcomp.2019.00007>)
16. M. D. Dixson, *JoSoTL* **10** (2010) 1 (<https://files.eric.ed.gov/fulltext/EJ890707.pdf>)
17. M. E. Villanueva, E. Camilli, A. C. Chirillano, J. A. Cufré, M. C. de Landeta, L. N. Rigacci, V. M. Velasco, A. F. Pighin, *J. Chem. Educ.* **97** (2020) 2719 (<https://doi.org/10.1021/acs.jchemed.0c00664>)
18. M. Shapiro, D. M. Solano, J. J. Bergkamp, A. Gebauer, E. Gillian, K. M. Lopez, H. Santoke, L. E. Talbert, *J. Chem. Educ.* **97** (2020) 2526 (<https://doi.org/10.1021/acs.jchemed.0c00788>)
19. M. M. Cooper, L. M. Corley, S. M. Underwood, *J. Res. Sci. Teach.* **50** (2013) 699 (<https://doi.org/10.1002/tea.21093>)
20. H. T. Nennig, K. L. Ida'rraga, L. D. Salzer, A. Bleske-Rechek, R. M. Theisen, *Chem. Educ. Res. Pract.* **21** (2020) 168 (<https://doi.org/10.1039/C9RP00112C>)
21. E. K. Faulconer, J. C. Griffith, B. L. Wood, S. Acharyya, D. L. Roberts, *Chem. Educ. Res. Pract.* **19** (2018) 392 (<https://doi.org/10.1039/C7RP00173H>)
22. R. Mayer, in *The Cambridge Handbook of Multimedia Learning*, R. Mayer, Ed., Cambridge University Press, Cambridge, 2014, p. 43 (<https://doi.org/10.1017/CBO9781139547369>)
23. A. Berg, D. Orraryd, A. Jahic Pettersson, M. Hulten, *Chem. Educ. Res. Pract.* **20** (2019) 710 (<https://doi.org/10.1039/C8RP00288F>).